



HAL
open science

Multi-scale study of the phenomena of reconstitution of powders from agroressources

Tristan Fournaise

► **To cite this version:**

Tristan Fournaise. Multi-scale study of the phenomena of reconstitution of powders from agroressources. Food engineering. Université de Lorraine, 2022. English. NNT: 2022LORR0100 . tel-03880686

HAL Id: tel-03880686

<https://hal.univ-lorraine.fr/tel-03880686>

Submitted on 1 Dec 2022

HAL is a multi-disciplinary open access archive for the deposit and dissemination of scientific research documents, whether they are published or not. The documents may come from teaching and research institutions in France or abroad, or from public or private research centers.

L'archive ouverte pluridisciplinaire **HAL**, est destinée au dépôt et à la diffusion de documents scientifiques de niveau recherche, publiés ou non, émanant des établissements d'enseignement et de recherche français ou étrangers, des laboratoires publics ou privés.



**UNIVERSITÉ
DE LORRAINE**

**BIBLIOTHÈQUES
UNIVERSITAIRES**

AVERTISSEMENT

Ce document est le fruit d'un long travail approuvé par le jury de soutenance et mis à disposition de l'ensemble de la communauté universitaire élargie.

Il est soumis à la propriété intellectuelle de l'auteur. Ceci implique une obligation de citation et de référencement lors de l'utilisation de ce document.

D'autre part, toute contrefaçon, plagiat, reproduction illicite encourt une poursuite pénale.

Contact bibliothèque : ddoc-theses-contact@univ-lorraine.fr
(Cette adresse ne permet pas de contacter les auteurs)

LIENS

Code de la Propriété Intellectuelle. articles L 122. 4

Code de la Propriété Intellectuelle. articles L 335.2- L 335.10

http://www.cfcopies.com/V2/leg/leg_droi.php

<http://www.culture.gouv.fr/culture/infos-pratiques/droits/protection.htm>



Thèse

**Présentée et soutenue publiquement pour l'obtention du
titre de DOCTEUR DE L'UNIVERSITE DE LORRAINE**

Mention : Procédés Biotechnologiques et Alimentaires

Par Tristan FOURNAISE

Sous la direction de Pr. Claire GAIANI

et Dr. Jérémy PETIT

**Étude multiéchelle des phénomènes de reconstitution
de poudres issues d'agroressources**

**Multiscale study of the phenomena of reconstitution
of powders issued from agroressources**

Soutenue publiquement le 4 juillet 2022

Membres du jury :

Directrice de thèse :

Pr. Claire GAIANI

Université de Lorraine, Nancy

Co-directeur de thèse :

Dr. Jérémy PETIT

Université de Lorraine, Nancy

Président du jury et rapporteur :

Dr. Guillaume DELAPLACE

INRAE, Université de Lille

Rapporteur :

Dr. Marco RAMAIOLI

INRAE, Université de Paris-Saclay

Examineurs :

Dr. Jennifer BURGAIN

Université de Lorraine, Nancy

Dr. Julien DUPAS

Nestlé, Lausanne

Remerciements

Ce travail de recherche a été réalisé au sein du Laboratoire d'Ingénierie des Biomolécules (LIBio).

Je remercie le laboratoire pour m'avoir accueilli et donné les moyens de réaliser ce travail durant mes trois années de thèse.

Je remercie chaleureusement mes encadrants, tout d'abord Claire GAIANI pour m'avoir accepté en tant que doctorant, qui m'a fait profiter de son expérience et de son expertise dans la recherche. Sans oublier Jérémy PETIT qui a été bien plus qu'un encadrant un véritable ami, je le remercie pour sa disponibilité et ses précieux conseils.

J'adresse mes remerciements aux membres de mon jury de thèse qui ont accepté de prendre le temps d'évaluer ces trois années de travail réunies dans ce mémoire.

Je tiens à remercier toutes les personnes qui m'ont permis de réaliser l'ensemble de mes manipulations au laboratoire, tout d'abord le personnel technique les Carole, Loubiana, Aurélie, Blandine, Myriam et Sylvie qui ont veillé au jour le jour au bon fonctionnement du laboratoire. Sans elles, je n'aurais rien pu faire. D'autre part aux enseignants-chercheurs Florentin et Jennifer qui ont passé du temps avec moi sur des machines récalcitrantes ou encore Jordane et Stéphane qui ont passé du temps à réfléchir avec moi sur la mise en place de protocole d'analyse. Je remercie encore une fois Jennifer pour son aide précieuse sur le travail portant sur l'AFM. Je n'oublie pas tous ceux qui ont pu me glisser un conseil en passant ou donner une piste de réflexion.

Je remercie Philippe MARCHAL, Véronique FALK, et Thibault ROQUES-CARMES pour m'avoir accueilli et aidé lors de mes venues dans leur laboratoire (Laboratoire Réactions et Génie des Procédés - LRGP).

Merci à Roger SCHÜTZ pour son temps, sa disponibilité, qui m'aura permis d'avancer et de gagner un temps précieux.

Finalement, j'adresse un remerciement à ma famille, mes amis qui ont toujours été là, en me soutenant directement ou indirectement. Ils ont été un élément indispensable à ma réussite.

Table des matières

Remerciements	3
Table of figures	7
Table of tables	14
I. Introduction.....	16
1.1. Contexte.....	16
1.2. Organisation et originalité de la thèse	17
1.2.1. Caractérisation de l’aptitude à la reconstitution d’un grand nombre de poudres (échelle macroscopique)	20
1.2.2. Caractérisation de la surface des poudres aux échelles micro- et nanoscopiques.....	20
1.2.3. Développement de modèles descriptifs et prédictifs pour la reconstitution des poudres.....	21
1.3. Valorisation scientifique.....	22
1.3.1. Publications	22
1.3.2. Chapitre de livre	23
1.3.3. Communications orales	23
II. State of the art	24
2.1. Food powder structure	25
2.1.1. Powder manufacturing processes	25
2.1.2. Powder physicochemical properties.....	33
2.2. Powder functional properties.....	48
2.2.1. Gelation	48
2.2.2. Foamability.....	49
2.2.3. Antioxidant activity.....	49
2.2.4. Flowability	50
2.2.5. Reconstitutability	51
2.2.6. Powder reconstitution improvement	54

2.3.	Analytical methods for reconstitution monitoring and modelling of powder reconstitution steps	64
2.3.2.	Monitoring of powder reconstitution and characterization of reconstitution steps.....	64
2.3.3.	Descriptive and predictive modelling of powder reconstitution	69
III.	Material and methods	76
3.1.	Investigated powders	76
3.1.1.	Commercial powders.....	76
3.1.2.	Coated powders	79
3.2.	Physicochemical characterization.....	79
3.2.1.	Particle size and shape distributions.....	79
3.2.2.	Aerated density.....	80
3.2.3.	Glass transition temperature transition.....	80
3.2.4.	Bulk chemical properties.....	80
3.2.5.	Surface characterization	82
3.3.	Powder reconstitution behavior	85
3.3.1.	Wettability evaluation	85
3.3.2.	Monitoring of reconstitution kinetics.....	87
3.4.	Modelling of powder reconstitution	88
3.4.1.	Descriptive modelling of powder reconstitution kinetics	88
3.4.1.3.	Predictive modelling of powder reconstitution time	97
3.5.	Statistical analysis.....	99
IV.	Results and discussion.....	100
4.1.	Main powder physicochemical characteristics influencing their reconstitution behavior	100
4.1.1.	Impact of particle size distribution and lipid content on powder reconstitution.....	100
4.1.2.	Powder reconstitution kinetics monitored by conductivity.....	108

4.1.3.	Surface composition of the thirty-six food powders	110
4.1.4.	Principal component analysis linking physicochemical properties, manufacturing process, and reconstitution behavior of the thirty-six food powders	111
4.1.5.	Conclusion.....	113
4.2.	Coating of whey protein isolate with sugars: surface modification and wettability	115
4.2.1.	Determination of coating duration	115
4.2.2.	Impact of sugar nature on wettability of coated whey protein isolate powders	119
4.2.3.	Impact of a humid environment on sucrose-coated whey protein isolate powder.....	130
4.2.4.	Conclusion.....	136
4.3.	Descriptive modelling of food powders reconstitution kinetics followed by laser granulometry.....	137
4.3.1.	Application of the two-step fitting approach of the descriptive reconstitution model: example of instant mash	137
4.3.2.	Influence of physicochemical properties on powder reconstitution steps.....	141
4.3.3.	Conclusion.....	148
4.4.	Development of an empirical predictive model for powder reconstitution time.....	150
4.4.1.	First approaches.....	150
4.4.2.	Improvement of prediction accuracy.....	161
4.4.3.	Conclusions of the predictive modelling of the reconstitution time	167
V.	Conclusion and perspectives	169
5.1.	Conclusion	169
5.2.	Perspectives	171
VI.	References.....	174

Table of figures

Figure 1. Organisation générale de la thèse.	19
Figure 2. Enrobage par des sucres d'une poudre de protéines solubles du lait présentant un mouillage lent et caractérisation de la poudre enrobée à différentes échelles : macroscopique, microscopique et atomique.....	21
Figure 3. Links between material physical state (solid or liquid), production process, and physicochemical properties of powders.	25
Figure 4. Grinding systems based on: A- crushing (hammer mill; Blazy et al., 2006) and B- mechanical shear (colloid mill; Gao et al., 2020).....	26
Figure 5. Vibrating sieve (Crawford and Quinn, 2017).	27
Figure 6. Principles of dry mixing (Cuq et al., 2013): A - rotative mixing, B - blade mixing, and C - static mixing.	28
Figure 7. Single drum-dryer with feed applicator rollers (Moore, 1995).....	29
Figure 8. Principle of spray-drying supplied with a cyclone separator (Santos et al., 2017)..	30
Figure 9. Principle of freeze-drying: representation of water thermodynamic transformations on the pressure-temperature diagram. A: initial conditions, B: freezing, C: beginning of pressure reduction (application of partial vacuum), and D: heating, leading to water sublimation (Ratti, 2013).....	31
Figure 10. Crystallization processes (Biscans, 2013): A- evaporative crystallizer and B- reactor crystallizer.	32
Figure 11. Determination of the relative proportions of lipids and proteins in whole milk powder by CLSM coupled with image analysis (Claire Gaiani's personal data).	33
Figure 12. Examples of volume-weighted (left), specific surface area-weighted (middle), and number-weighted (right) particle size distributions of the same sample of whey protein isolate powder.....	35
Figure 13. A- Interparticular spaces and B- closed and open pores (Onwulata, 2005).....	37
Figure 14. Example of CLSM associated with image analysis to determine pores in whole milk powder (Claire Gaiani's personal data).....	38
Figure 15. Principle of atomic force microscopy (Burgain, 2013).	40
Figure 16 : 2D (A) and 3D (B) pictures of skim (1) and whole (2) milk powders (Murrieta-Pazos et al., 2011).	41
Figure 17. Observation range of microscopies (Burgain et al., 2017).	41

Figure 18 : Examples of force–distance curves recorded for hard (a) and soft (b) surfaces (Kasas et al., 2013).....	42
Figure 19. Summary of the relevant results in terms of physicochemical properties from macro- to nano-scale for fruit powders, adapted from Gaudel et al. (2022).	43
Figure 20. Differences between surface and bulk chemical compositions of spray-dried skim and whole milk powders (Murrieta-Pazos et al., 2012).	46
Figure 21. Surface composition on dry basis deduced from XPS analysis of spray-dried skim, semi-skim, and whole milk powders with or without prior aeration of feed concentrate. For each component separately, bars topped with different letters were significantly different according to Tukey's HSD test ($p < 0.05$; $n = 2$) (Fournaise et al., 2020).	47
Figure 22. Reconstitution steps (wetting, sinking/swelling, dispersion, and solubilization) of a powder in a solvent (adapted from Forny et al., 2011).	51
Figure 23. Principle of top-spray fluidized bed coating (Dewettinck and Huyghebaert, 1999).	57
Figure 24. Principle of bottom-spray fluidized bed coating (Dewettinck and Huyghebaert, 1999).....	58
Figure 25. Principle of tangential-spray fluidized bed coating (Dewettinck and Huyghebaert, 1999).....	59
Figure 26. Chemical structure of lecithins, where R1 and R2 designate two fatty acids (Van Nieuwenhuyzen, 1976).....	60
Figure 27. Chemical structure of polysorbates (Kerwin, 2008).	60
Figure 28. Chemical structure of maltodextrins, where n ranges between 2 and 20.....	61
Figure 29. Chemical structure of some monosaccharides (left: glucose; middle: fructose; right: galactose).....	62
Figure 30. Chemical structure of two disaccharides (left: sucrose; right: lactose).....	62
Figure 31. A- powder samples prepared by compaction into pellets and B- sputtering on double-sided tape.....	86
Figure 32. Experimental apparatus employed for the sessile drop method, adapted from Roques-Carnes et al., (2013).....	86
Figure 33. Experimental setup used for reconstitution experiments and schema of the geometrical characteristics of the A200 impeller and the cylindrical reactor (h:d:H:D of 1:1:3:3 with $H = D = 150$ mm and $h = d = 50$ mm) (Fournaise et al., 2021b).	87
Figure 34. Example of reconstitution curve of instant mashed potatoes powder.....	88
Figure 35. Raw conductivity curve of milk protein concentrate.	89

Figure 36. Normalized conductivity curves of milk protein concentrate.....	90
Figure 37. Reconstitution curves obtained by monitoring or reconstitution assays with laser granulometry, with temporal axis in logarithmic scale. (A) instant mashed potatoes powder (first reconstitution type); (B) T45 flour (second reconstitution type); (C) small couscous (third reconstitution type); (D) instant coffee (fourth reconstitution type); (E) MPI (fifth reconstitution type). Error bars indicate standard deviations obtained with three replicates of reconstitution assays; some, inferior to the marker size, are not visible.	92
Figure 38. Surface atomic compositions (left) and carbon bond ratios (right) of instant coffee, ground instant coffee, skim milk, and whole milk powders.	107
Figure 39. Bulk and surface compositions of skim and whole milk powders.....	108
Figure 40. A- Effect of median particle size and B- fat content on powder reconstitution kinetics.	109
Figure 41. Classification of investigated powders into three groups (more hydrophobic, intermediate, and more hydrophilic) from C/O ratio and C-C bonds / C-other atom bonds ratio at particle surface.	111
Figure 42. Correlation scores obtained from PCA for the thirty-six investigated powders. .	112
Figure 43. Classification of the thirty-six investigated powders deduced from PCA (loading scores).....	113
Figure 44. Overview of the main factors influencing powder reconstitution.	114
Figure 45. Particle size distributions (in volume) of native, control, and sucrose-coated whey protein isolate powders.....	117
Figure 46. Evolution of wetting time and proportion of added sucrose of sucrose-coated whey protein isolate powders with the coating time.....	118
Figure 47. Influence of added sucrose on wetting time of sucrose-coated whey protein isolate powders.	119
Figure 48. Particle size distributions (in volume) and SEM pictures of whey protein isolate powders fluidized without air A- Air-60, with water B- Water-60 and coated with different sugars for 60 min. C- Sucrose-60, D- Lactose-60, E- Glucose-60, F- Fructose-60, and G- Galactose-60. 1: $\times 200$ magnification, 2: $\times 1\ 500$ magnification, and 3: $\times 5\ 000$ magnification.	121
Figure 49. C/O ratio of whey protein isolate powders coated for 60 min with different sugars and native WPI and sugars. Means with different superscripted letters in the same column were significantly different according to Tukey's HSD test ($p < 0.05$; $n = 2$).	123

Figure 50. Differential scanning calorimetry spectra of whey protein isolate powders coated with different sugars for 60 min. A: Sucrose-60; B: Lactose-60; C: Glucose-60; D: Fructose-60; and E: Galactose-60).	124
Figure 51. A- Wetting time by FIL method, B- contact angle of whey protein isolate powders fluidized without (Air-60) or with water (Water-60) and coated with different sugars for 60 min. Letters in the same column were significantly different according to Tukey's HSD test ($p < 0.05$; $n = 9$).	126
Figure 52. Surface topography of whey protein isolate powders fluidized with water (Water-60) and coated with different sugars for 60 min.	128
Figure 53. Measurement principle of coating thickness of whey protein isolate powders fluidized with water (Water-60) and coated with different sugars for 60 min. Three dimensional images show the black line where thickness was measured. Yellow parts of the diagrams correspond to uncoated (smooth) areas, and blue parts to coated (rough) areas.	129
Figure 54. Particle size distributions of whey protein isolate powders coated with sucrose for 60 min at relative humidities between 10 and 60 %	132
Figure 55. Evolution of the wetting time with the increase in relative humidity.	132
Figure 56. Young's modulus maps and diagrams of sucrose-coated whey protein isolate powders (sucrose-60) equilibrated at various relative humidities, A- 10 % RH, B- 20 % RH, C- 40 % RH, and D- 60 % RH.	134
Figure 57. Evolution of the surface appearance with the increase of the relative humidity, A- sucrose-60 10 % RH, B- sucrose-60 20 % RH, C- sucrose-60 40 % RH, D- sucrose-60 60 % RH, 1: $\times 2\ 000$ magnification, and 2: $\times 3\ 000$ magnification. Blue arrows indicate the location of patches.	135
Figure 58. Hypothesis about the mechanism of wetting for whey protein powder coated with sugar.	136
Figure 59. Separate fitting of the swelling step of the (first type) reconstitution profile of instant mash using Equation 24 . Error bars indicate standard deviations obtained with three replicates of reconstitution assays; some, inferior to the marker size, are not visible.	138
Figure 60. Separate fitting of the dispersion and solubilization steps of the (first type) reconstitution profile of instant mash using Equation 25 .	139
Figure 61. Descriptive reconstitution model for instant mash obtained by fitting with Equation 23 ; swelling and dispersion times; swelling, dispersion, and solubilization rates.	140

Figure 62. Descriptive reconstitution model, swelling, dispersion, and solubilization times and rates of powders of the first reconstitution type: (A) instant mash, (B) casein, and (C) polenta 1.0 mm..... 141

Figure 63. Descriptive reconstitution model, dispersion time, as well as dispersion and solubilization rates of powders of the second reconstitution type: (A) T55 flour, (B) T45 flour, (C) cocoa fat- alka-, and (D) cocoa fat+ alka+..... 142

Figure 64. Descriptive reconstitution model, swelling, dispersion/solubilization times and rates of small couscous (third reconstitution type). 143

Figure 65. A- Comparison of predicted and experimental values of reconstitution times for the multilinear model obtained with unnormalized physicochemical parameters using **Equation 28**. B- focus on reconstitution times between 0 and 1 200 s. Colors correspond to the powder classification according to wetting and reconstitution behavior deduced from section 4.1.4.: green, good behavior (short wetting and short reconstitution), yellow: decent behavior (long wetting and short reconstitution), orange: mediocre behavior (short wetting and long reconstitution), and red: poor behavior (long wetting and long reconstitution)..... 151

Figure 66. A- Comparison of predicted and experimental values of reconstitution times for the monome model obtained with unnormalized physicochemical parameters using **Equation 29**. B- focus on reconstitution times between 0 and 1 200 s. Colors correspond to the powder classification according to wetting and reconstitution behavior deduced from section 4.1.4.: green, good behavior (short wetting and short reconstitution), yellow: decent behavior (long wetting and short reconstitution), orange: mediocre behavior (short wetting and long reconstitution), and red: poor behavior (long wetting and long reconstitution)..... 152

Figure 67. A- Comparison of predicted and experimental values of reconstitution times for the exponential model obtained with unnormalized physicochemical parameters using **Equation 30**. B- focus on reconstitution times between 0 and 1 200 s. Colors correspond to the powder classification according to wetting and reconstitution behavior deduced from section 4.1.4.: green, good behavior (short wetting and short reconstitution), yellow: decent behavior (long wetting and short reconstitution), orange: mediocre behavior (short wetting and long reconstitution), and red: poor behavior (long wetting and long reconstitution)..... 153

Figure 68. A- Comparison of predicted and experimental values of reconstitutions times for the multilinear model obtained with normalized physicochemical parameters using **Equation 28**. B- focus on normalized reconstitution times between 0 and 25 % s. Colors correspond to the powder classification according to wetting and reconstitution behavior deduced from section 4.1.4.: green, good behavior (short wetting and short reconstitution), yellow: decent

behavior (long wetting and short reconstitution), orange: mediocre behavior (short wetting and long reconstitution), and red: poor behavior (long wetting and long reconstitution). 157

Figure 69. A- Comparison of predicted and experimental values of reconstitutions times for the monome model obtained with normalized physicochemical parameters using **Equation 29**. B- focus on normalized reconstitution times between 0 and 25 % s. Colors correspond to the powder classification according to wetting and reconstitution behavior deduced from section 4.1.4.: green, good behavior (short wetting and short reconstitution), yellow: decent behavior (long wetting and short reconstitution), orange: mediocre behavior (short wetting and long reconstitution), and red: poor behavior (long wetting and long reconstitution)..... 158

Figure 70. A- Comparison of predicted and experimental values of reconstitutions times for the exponential model obtained with normalized physicochemical parameters using **Equation 30**. B- focus on normalized reconstitution times between 0 and 25 %. Colors correspond to the powder classification according to wetting and reconstitution behavior deduced from section 4.1.4.: green, good behavior (short wetting and short reconstitution), yellow: decent behavior (long wetting and short reconstitution), orange: mediocre behavior (short wetting and long reconstitution), and red: poor behavior (long wetting and long reconstitution)..... 159

Figure 71. A- Comparison of predicted and experimental values of reconstitutions time for the PLSR model obtained with normalized physicochemical parameters. B- focus on normalized reconstitution times between 0 and 25 %. Colors correspond to the powder classification according to wetting and reconstitution behavior deduced from section 4.1.4.: green, good behavior (short wetting and short reconstitution), yellow: decent behavior (long wetting and short reconstitution), orange: mediocre behavior (short wetting and long reconstitution), and red: poor behavior (long wetting and long reconstitution)..... 160

Figure 72. Comparison of exponential and power laws for the dependency of reconstitution times to the physicochemical parameters to be used in the predictive model; examples of the C/O ratio and D50. 161

Figure 73. A- Comparison of predicted and experimental values of reconstitutions times for the model combining power laws and exponentials obtained with normalized physicochemical parameters using **Equations 29 and 30**. B- focus on normalized reconstitution times between 0 and 25 %. Colors correspond to the powder classification according to wetting and reconstitution behavior deduced from section 4.1.4.: green, good behavior (short wetting and short reconstitution), yellow: decent behavior (long wetting and short reconstitution), orange: mediocre behavior (short wetting and long reconstitution), and red: poor behavior (long wetting and long reconstitution)..... 163

Figure 74. A- Comparison of predicted and experimental values of reconstitutions times for the model combining power laws and exponentials obtained with the extended set of normalized physicochemical parameters using **Equations 33**. B- focus on normalized reconstitution times between 0 and 25 %. Color corresponds to the powder classification according to wetting and reconstitution behavior deduced from chapter 4.1.4.: green, good behavior (short wetting and short reconstitution), yellow: decent behavior (long wetting and short reconstitution), orange: mediocre behavior (short wetting and long reconstitution), and red: poor behavior (long wetting and long reconstitution)..... 167

Table of tables

Table 1. Advantages and drawbacks of the main methods of powder reconstitution monitoring (W: wetting, S: swelling, D: dispersion, R: reconstitution).	67
Table 2. Chemical composition and manufacturing processes of investigated powders.	77
Table 3. Proteins, lipids, carbohydrates (fibers excluded), fibers, and minerals content ranges*, median particle size, as well as C/O and C-C/other C bonds ratios at the particle surface for investigated powders.	102
Table 4. Water activity, water content, wetting time, reconstitution time, and Hill model parameters (k and n) of investigated powders.	105
Table 5. Wetting and reconstitution times, as well as Hill model parameters (time constant k and power n) and coefficient of determination (R^2) of normalized conductivity curve fitting by Hill model for investigated milk and coffee powders.	109
Table 6. Granulometric parameters of native, control, and sucrose-coated whey protein isolate powders obtained at different processing times in the fluid-bed coater.	116
Table 7. Physicochemical properties of native sucrose and native, control, and sucrose-coated whey protein isolate powders.	118
Table 8. Wetting time of native sucrose and native, control, and sucrose-coated whey protein isolate powders, as well as native sucrose.	119
Table 9. Granunometric parameters of whey protein isolate powders in native state, fluidized without (Air-60) or with water (Water-60), and coated with different sugars for 60 min.	120
Table 10. Physicochemical properties of whey protein isolate powders fluidized without (Air-60) or with water (Water-60) and coated with different sugars for 60 min.	122
Table 11. Glass transition temperature of sucrose, lactose, glucose, fructose, and galactose (Haque et al., 2006; Y. Roos, 1995; Tita-Goldstein, 2013).	125
Table 12. Solubility of sucrose, lactose, glucose, fructose, and galactose (Haque et al., 2006; Roos, 1995; Tita-Goldstein, 2013).	127
Table 13. Wetting properties of whey protein isolate powders fluidized with water (Water-60) and coated with different sugars for 60 min determined by capillary rise.	128
Table 14. Particle and coated layer roughnesses of whey protein isolate powders fluidized with water (Water-60) and coated with different sugars for 60 min.	129
Table 15. Coating thickness of whey protein isolate powders coated for 60 min with different sugars.	130

Table 16. Granulometric characteristics, water content, and wettability of whey protein isolate powders coated with sucrose for 60 min under various conditions of air relative humidity from 10 to 60 %	131
Table 17. Modelled initial, maximal, and final median particle sizes; model parameters and coefficient of determination; swelling, dispersion, and solubilization durations and rates; reconstitution time of investigated powders of the first (instant mash, casein, and polenta 1.0 mm), second (T55 flour, T45 flour, cocoa fat- alka-, and cocoa fat+ alka+), and third reconstitution types (small couscous).	144
Table 18. Pearson’s correlation coefficients between powder physicochemical properties (bulk and surface chemical compositions, granulometric characteristics) and reconstitution characteristic parameters (swelling, dispersion, and solubilization durations and rates; reconstitution time issued from the descriptive modelling approach).	146
Table 19. Normalized input data (predictors) and reconstitution time (dependent variable) used for the determination of predictive models.	155
Table 20. Coefficients of determinations of exponential and power law regressions for the dependency of reconstitution times to the physicochemical parameters to be used in the predictive model (green: higher R ² , red: lower R ²).	162
Table 21. Extra powder physicochemical properties used for predictive modelling.	164
Table 22. Extra normalized powder physicochemical properties used for predictive modelling.	165
Table 23. Coefficients of determinations of exponential and power law regressions for the dependency of reconstitution times to the additional physicochemical parameters to be used in the predictive model (green: higher R ² , red: lower R ²).	166

I. Introduction

1.1. Contexte

Les matériaux issus d'agroressources sont utilisés sous la forme de poudres par de nombreux industriels en particulier dans les domaines cosmétique, agroalimentaire ou pharmaceutique. Dans le secteur agroalimentaire par exemple, on trouve sous forme de poudres de nombreux produits bruts (aussi appelés ingrédients), comme les farines, les cacao ou les épices ; ou des produits transformés, comme les soupes instantanées ou les poudres laitières. Elles peuvent provenir de la déshydratation d'un liquide par différentes techniques, telles que le séchage par atomisation, la lyophilisation, le séchage à tambour rotatif, le séchage à bande, la cristallisation, etc., ou de la réduction de taille d'un solide par broyage, concassage, attrition, etc. (Karam et al., 2016 ; Schuck et al., 2012 ; Waiss et al., 2020). Ainsi, selon le type et les conditions de procédé utilisés, la taille, la forme, la densité, la composition chimique de la particule ou encore la composition de surface sont susceptibles d'être différentes, ce qui peut impacter leurs propriétés fonctionnelles (reconstitution, écoulement, etc.) (Burgain et al., 2016; Deotale et al., 2020 ; Roos et al., 2020 ; Yuan et al., 2019). C'est la raison pour laquelle il est souvent nécessaire de mettre en œuvre de nombreuses techniques analytiques pour caractériser la qualité des poudres, ainsi que leurs applications potentielles (Burgain et al., 2016b ; Forny et al., 2011 ; Gaiani, 2006 ; Mitchell et al., 2020).

La reconstitution ou réhydratation d'une poudre peut être définie par quatre étapes consécutives : le mouillage, l'immersion/gonflement, la dispersion et la solubilisation. Le mouillage de la poudre est le phénomène résultant du remplacement de la phase gazeuse par de l'eau à la surface de la poudre. La mouillabilité est principalement déterminée par le temps de diffusion capillaire de l'eau dans la poudre, cela conduit donc à une immersion totale ou partielle de cette dernière dans l'eau (Forny et al., 2011 ; Schuck et al., 2012). L'immersion/gonflement sont définis comme le temps nécessaire pour que les particules ou les agglomérats de particules s'immergent (Jiang et al., 2013). Puis, dans un second temps, leur gonflement est dû à une pénétration de l'eau par capillarité dans les particules et/ou agglomérats grâce à la présence de pores intra- ou interparticulaires. Ce phénomène se produit sous l'effet de forces de capillarité, cette étape n'est pas systématique et dépend de plusieurs facteurs, notamment la composition chimique. Ainsi, les polymères et macromolécules (protéines, amidons, fibres, etc.) interagissent avec l'eau ce qui conduit à un déploiement de ces derniers faisant ainsi gonfler les particules ou les agglomérats (Bonacucina et al., 2009 ; Conti et al., 2006 ; Cuq et al., 2011). Ensuite, vient la dispersion, qui est définie comme la capacité d'une poudre à se disperser dans

l'eau. Une fois que les particules ou les agglomérats de particules sont immergés, avec ou sans gonflement, ils se désagrègent progressivement et/ou se dispersent en particules individuelles. La dispersion se produit lorsque les forces exercées par le solvant pour séparer les particules les unes des autres dépassent les forces de cohésion interparticulaires (Freudig et al., 1999 ; O'Mahony and McSweeney, 2016 ; Schuck et al., 2012). La solubilisation est la quatrième et dernière étape de la reconstitution (O'Mahony and McSweeney, 2016). Elle entraîne la disparition complète de la structure granulaire (Freudig et al., 1999 ; Gaiani et al., 2007 ; Marabi et al., 2008). Les poudres issues d'agroressources forment généralement des solutions hydrocolloïdales suite à la dissolution des composés solubles (sucres, minéraux, etc.) et la mise en suspension des composés insolubles (lipides, micelles de protéines, fibres insolubles, etc.) (Forny et al., 2011 ; Mitchell et al., 2020 ; O'Mahony and McSweeney, 2016 ; Schuck et al., 2012a).

Les études approfondies sur les mécanismes de reconstitution des poudres alimentaires ont été réalisées sur un nombre très limité de poudres, principalement les poudres laitières, les cacao, les céréales (blé, maïs, etc.) et les gommes (gomme arabique, gomme de xanthane, etc.) (Boucheham et al., 2019 ; Burgain et al., 2016b ; Di Battista et al., 2015 ; Galet et al., 2004 ; Hla and Hoge Kamp, 1999). Il apparaît qu'une compréhension fine de ces mécanismes et une recherche plus approfondie sont plus que nécessaires. En effet, ces dernières années, l'utilisation et le développement de nouvelles poudres pour répondre aux besoins des consommateurs et des industriels ont énormément augmenté. Au vu de la grande variété de poudres existant actuellement sur le marché et de leur complexité structurale ou encore biochimique, les connaissances actuelles restent limitées et insuffisantes pour comprendre l'ensemble des mécanismes de reconstitution. Ainsi, des connaissances fines sur les propriétés physicochimiques des poudres sont encore nécessaires pour améliorer la compréhension des phénomènes de reconstitution des poudres. La complexité des poudres et des procédés de reconstitution industriels (par exemple, la reconstitution d'une poudre présentant une composition de surface hétérogène ou dans un fluide à rhéologie complexe) n'est pas encore bien appréhendée avec les approches actuelles.

1.2. Organisation et originalité de la thèse

Jusqu'à présent, les études menées sur la reconstitution des poudres se focalisaient sur un nombre de poudres restreint et visaient l'amélioration et/ou l'optimisation de cette fonctionnalité à des fins de valorisation industrielle, ou une meilleure compréhension des mécanismes impliqués dans les différentes étapes de la reconstitution selon un point de vue plus

fondamental en utilisant des modèles d'étude comme des billes de verre ou des approches basées sur une particule unique (Diersch et al., 2010 ; Duarte et al., 2009 ; Sweijen et al., 2017). L'originalité de ce travail de thèse repose sur une approche multiéchelle (macro-, micro- et nanoscopique) de l'étude d'un grand nombre de poudres alimentaires d'origines diverses et couvrant une grande variété de propriétés physicochimiques et de comportements de reconstitution.

Le manuscrit de thèse est focalisé sur quatre questions scientifiques :

- Quelles sont les principales propriétés physicochimiques (composition, structure, etc.) des poudres alimentaires influençant leur reconstitution et comment impactent-elles les différentes étapes de la reconstitution ?
- Comment les caractéristiques de surface des poudres influencent-elles l'étape du mouillage dépendamment des interactions entre la surface des particules et l'eau ?
- Est-il possible de caractériser le comportement d'une poudre lors des différentes étapes de la reconstitution à l'aide de modèles mathématiques décrivant la cinétique des phénomènes observés ?
- Est-il possible de prédire le temps de reconstitution d'une poudre à partir de ses propriétés physicochimiques à l'aide de modèles mathématiques ?

Afin de pouvoir répondre à ces quatre questions scientifiques, le travail de thèse a été divisé en trois grandes approches (**Figure 1**). Premièrement la caractérisation des propriétés physicochimiques et de reconstitution d'un grand nombre de poudre. Puis une focalisation sur l'étape de mouillage afin de mieux comprendre les liens entre les propriétés de surface et le mouillage d'une poudre. Et finalement l'exploitation des cinétiques de reconstitutions dans l'optique de développer des modèles descriptifs et prédictifs de la reconstitution des poudres.

Caractérisation de l'aptitude à la reconstitution d'un grand nombre de poudres

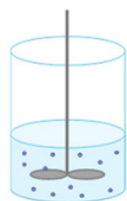
Etapes de réhydratation

Mouillage

Gonflement

Dispersion

Solubilisation



→ Cinétiques de réhydratation en réacteur instrumenté et granulomètre laser

→ Mouillage des poudres



→ Caractérisations des propriétés physicochimiques des poudres

→ Caractérisation des propriétés physicochimiques influençant le mouillage et le temps de reconstitution

→ Développement d'une classification en fonction des propriétés de mouillage et de reconstitution

Classification des poudres

Bonne

Correcte

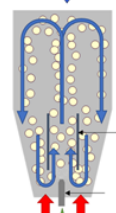
Médiocre

Mauvaise

Caractérisation de la surface des poudres aux échelles micro- et nanoscopiques

Modification de la surface d'une poudre

Enrobage avec des sucres (bon mouillage)



Protéines sériques (mauvais mouillage)

Protéines sériques enrobées avec des sucres (bon mouillage)

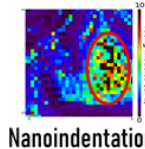
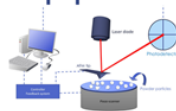
Échelle macroscopique

Caractérisation du mouillage

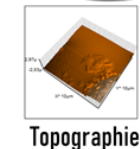


Échelle microscopique

Microscope à force atomique



Nanoindentation

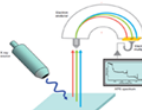


Topographie

Échelle atomique

Spectrométrie photoélectronique X (XPS)

Composition atomique de surface

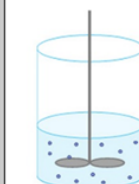


Développement de modèles descriptifs et prédictifs pour la reconstitution des poudres



→ Cinétiques de réhydratation en granulomètre laser

→ Caractéristiques physicochimiques des poudres



→ Cinétiques de réhydratation en réacteur instrumenté

Modèle semi-empirique descriptif des cinétiques de reconstitution en granulomètre laser

Modèle empirique de la prédiction du temps de réhydratation

Figure 1. Organisation générale de la thèse.

1.2.1. Caractérisation de l'aptitude à la reconstitution d'un grand nombre de poudres (échelle macroscopique)

Trente-six poudres alimentaires ont été sélectionnées pour représenter le plus de diversité possible en termes de composition (teneurs en eau, lipides, protéines, glucides – dont sucres et fibres, minéraux), de propriétés structurales (structure amorphe, vitreuse...) et de procédés de fabrication (séchage par atomisation, lyophilisation, broyage, etc.) pour obtenir des profils de reconstitution variés (Fitzpatrick et al., 2016 ; Mitchell et al., 2015).

Cette première partie du travail de thèse s'est appuyée sur des méthodes classiques de caractérisation de la reconstitution des poudres (Gaiani, 2006 ; Burgain et al., 2016 ; Fournaise et al., 2020 ; Mitchell et al., 2020, 2015) déjà employées au sein du laboratoire, notamment la granulométrie et la conductimétrie.

Le premier objectif de cette partie a été de discriminer les poudres par analyse en composantes principales (ACP) selon leurs caractéristiques physicochimiques et structurales, ainsi que leur procédé de fabrication. Ensuite, le second objectif a été de déterminer les facteurs principaux impliqués dans la reconstitution des poudres et leurs impacts sur l'aptitude à la reconstitution et au mouillage. Les poudres ont ainsi été classées selon leurs aptitudes au mouillage et à la reconstitution en quatre catégories : bonne (mouillage rapide et reconstitution courte), correcte (mouillage lent et reconstitution courte), médiocre (mouillage rapide et reconstitution longue) et mauvaise (mouillage lent et reconstitution longue).

1.2.2. Caractérisation de la surface des poudres aux échelles micro- et nanoscopiques

La surface des particules de poudre joue un rôle déterminant dans la reconstitution notamment lors de l'étape du mouillage. Les propriétés physicochimiques de la surface (hydrophobicité, porosité, état structurel amorphe/vitreux...) et la morphologie des particules sont déterminantes dans la mouillabilité des poudres (Angelopoulou et al., 2021a ; Burgain et al., 2016b ; Ji et al., 2017 ; Kelly et al., 2015 ; Kim, 2008 ; Mitchell et al., 2019).

Pour étudier l'impact des propriétés de surface sur le mouillage, une poudre d'isolat de protéines solubles pour laquelle le mouillage est l'étape limitante de la reconstitution (catégorie de reconstitution correcte : mouillage lent et reconstitution courte) a été sélectionnée. Sa surface a été modifiée par enrobage avec différents sucres (saccharose, lactose, glucose, fructose et galactose) pour améliorer la mouillabilité de la poudre et comprendre les mécanismes d'interaction entre l'eau et sa surface. Ainsi, l'impact de la nature des sucres (mono- ou disaccharides), de leurs propriétés (température de transition vitreuse, point de fusion, solubilité dans l'eau, etc.), de leur localisation à la surface des particules, de l'épaisseur de l'enrobage et

de la quantité ajoutée ont permis de mieux comprendre les mécanismes régissant la première étape de reconstitution des poudres. Pour cela, les particules ont été étudiées aux échelles macro-, micro- et nanoscopique (**Figure 2**).

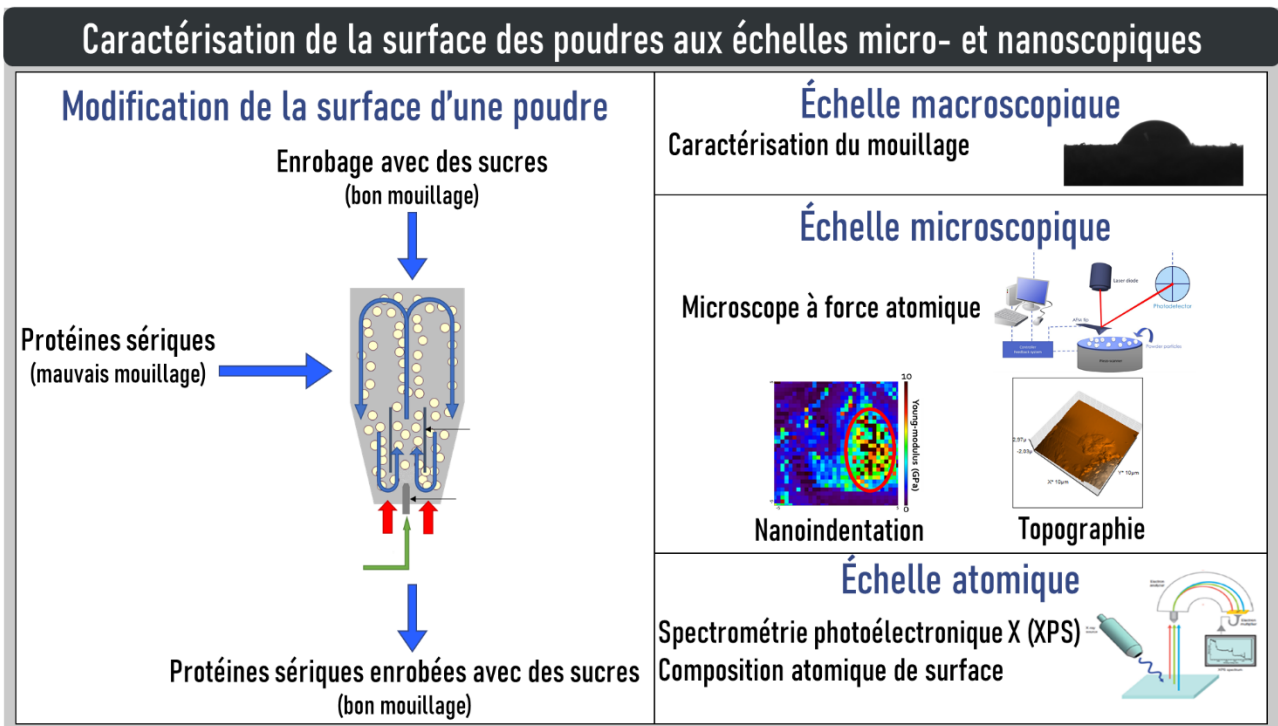


Figure 2. Enrobage par des sucres d'une poudre de protéines solubles du lait présentant un mouillage lent et caractérisation de la poudre enrobée à différentes échelles : macroscopique, microscopique et atomique.

1.2.3. Développement de modèles descriptifs et prédictifs pour la reconstitution des poudres

La première étape a été d'identifier, grâce au développement d'un modèle empirique descriptif des cinétiques de reconstitution obtenues par suivi conductimétrique, les principales caractéristiques (propriétés physicochimiques et structurales, ainsi que procédé de fabrication) des particules ayant une influence majeure sur leur aptitude à la reconstitution. Des méthodes d'analyse statistique (ANOVA, test des étendues de Tukey, etc.) ont été utilisées pour déterminer les caractéristiques prédominantes dans l'aptitude à la reconstitution en les liant aux temps de mouillage et de reconstitution expérimentaux de trente-six poudres.

Dans un second temps, un modèle semi-empirique décrivant les cinétiques de reconstitution suivies par granulométrie laser a été élaboré. Il a consisté à représenter l'évolution de la taille médiane de particules lors des principales étapes de la reconstitution (du gonflement à la solubilisation) sous forme de réponses indicielles d'ordre 1, ce qui a permis d'accéder à des informations cinétiques sur chacune des étapes de reconstitution considérées.

Le développement de cette méthode de modélisation descriptive a permis de répondre à deux enjeux importants : disposer d'un modèle qui soit à la fois applicable à des poudres ayant des comportements de reconstitution variés, permettant de décrire l'ensemble de la reconstitution avec une équation unique, et dont les paramètres du modèle ont un sens physique en lien avec les cinétiques des étapes de la reconstitution. Jusqu'à présent, les modèles utilisés se focalisaient uniquement sur l'une des étapes de la reconstitution, telles que le gonflement ou la dispersion/solubilisation (Dokoumetzidis et Macheras, 2006 ; Richard, 2012 ; Siepmann et Peppas, 2001 ; Sweijen et al., 2017 ; Zheng and Lu, 2011). Le modèle descriptif semi-empirique obtenu a permis par des méthodes statistiques (coefficients de Pearson) d'identifier l'impact des paramètres physicochimiques de 8 poudres sur les durées et vitesses des différentes étapes de la reconstitution (les cinétiques obtenues pour les autres poudres n'ayant pas pu être modélisées au vu de leur instantanéité ou de leur complexité). Ceci a permis de confirmer les conclusions tirées précédemment des cinétiques de reconstitution obtenues par suivi conductimétrique.

Pour terminer, un modèle visant à prédire, à partir des propriétés physicochimiques des poudres les plus influentes, le temps de reconstitution des poudres dans les conditions de référence utilisées dans les expérimentations menées lors de la première année a été développé en employant des modèles empiriques de forme classique (régression multilinéaire, modèle monôme) ou des améliorations de ceux-ci (modèles basés sur une normalisation des propriétés physicochimiques, modèle hybride combinant lois puissances et exponentielles). La difficulté de cette étape a résidé dans le choix pertinent des caractéristiques physicochimiques prises en compte pour le large panel constitué des trente-six poudres considérées.

1.3. Valorisation scientifique

1.3.1. Publications

- **Fournaise, T.,** Petit, J., & Gaiani, C. (2021). Main powder physicochemical characteristics influencing their reconstitution behavior, *Powder Technology*, 383, 65–73. Doi.org/10.1016/j.powtec.2021.01.056
- **Fournaise, T.,** Gaiani, C., & Petit, J. (2022). Descriptive modelling of food powders reconstitution kinetics followed by laser granulometry, *Chemical Engineering Science*, 251, 117440. Doi.org/10.1016/j.ces.2022.117440

1.3.2. Chapitre de livre

- Roos, Y.H., Afrassiabian, Z., Saleh, K., Famelart, M.-H., Audebert, A., Gulzar, M., Croguennec, T., Burgain, J., **Fournaise, T.**, Gaiani, C., Scher, J., Petit, J., Martins, E., Rodrigues, R.C., Schuck, P., Perrone, Í.T., Machado, S.G., Carvalho, A.F., & Roos, Y.H. (2020), Powder properties and influencing factors, in: *Drying in the Dairy Industry*. CRC Press. ISBN: 9781351119504

1.3.3. Communications orales

- **Fournaise, T.**, Burgain J., Petit, J. (2019), Impact of formulation on the reconstitution properties of spray-dried dairy powders, 9th International Granulation Workshop Lausanne (Suisse).
- **Fournaise, T.**, Petit, J., & Gaiani, C. (2020), Annual General Meeting of IFPRI (International Fine Particle Research Institute).
- **Fournaise, T.**, Petit, J., & Gaiani, C. (2021), Annual General Meeting of IFPRI (International Fine Particle Research Institute).

II. State of the art

Powders are part of our daily life and they are increasingly employed in various industries, such as construction materials, food, pharmaceuticals, or cosmetics (Ajayi and Amin, 2021; Barbosa et al., 2012; Sauer et al., 2013; Schuck et al., 2012). The food industry is one of the largest consumers and producers of powders based on organic materials. The primary objective of the powder form resides in reducing the size of stocks to facilitate transport and improving the duration of preservation (Schuck et al., 2012). The second objective is to improve the functional properties of an ingredient or a raw material, among which reconstitutability, flowability, aptitude for gelation, preservation ability, etc.

These functionalities depend on the manufacturing process and conditions. A large number of processes have been developed, such as grinding, drying, or crystallization (Bhandari et al., 2013; Biscans, 2013; Karam et al., 2016; Schuck et al., 2012). The production process directly influences the physicochemical properties of powders, such as chemical composition, internal structure, particle size distribution, morphology, surface composition, and mechanical properties (Burgain et al., 2016b; Hogg, 2008; Lowell and Shields, 1991; Murrieta-Pazos et al., 2012; Witt et al., 2007).

To better understand the impact of the different physicochemical properties on powder functional properties, a large number of studies was performed to develop analytical techniques for the characterization of powder properties (Crowley, 2016; Crowley et al., 2014; Mitchell et al., 2020). This permitted to improve knowledge on the links between powder production processes, physicochemistry, and functionalities and to focus scientific research on the enhancement of powder functionalities (Fournaise et al., 2020; Hammes et al., 2015; Ji et al., 2015; Li et al., 2017). These studies have made it possible to develop descriptive and predictive models for certain functionalities such as reconstitutability or flowability (Dokoumetzidis and Macheras, 2006; Ma et al., 2019; Richard, 2012; Siepmann and Peppas, 2001).

In this thesis, the state of the art is divided in three parts. The first part deals with food powder structure and physicochemical properties according to the main manufacturing processes. Then, the second part of the state of the art describes the main powder functionalities (gelation, flowability, reconstitutability, etc.) and the different approaches for powder reconstitution enhancement. The last part of the state of the art lists the main analytical methods for the monitoring of powder reconstitution and different approaches to develop descriptive or predictive modelling of the kinetics of food powder reconstitution.

2.1. Food powder structure

2.1.1. Powder manufacturing processes

Various manufacturing processes exist for the production of powders, depending on the nature of material to be powdered. In particular, powder manufacturing processes markedly differ for solid and liquid matrices. Consequently, obtained powders may exhibit significant differences in physicochemical and functional properties. **Figure 3** summarizes the main powder production processes dependently from material origin (animal or vegetal) and physical state (solid or liquid).

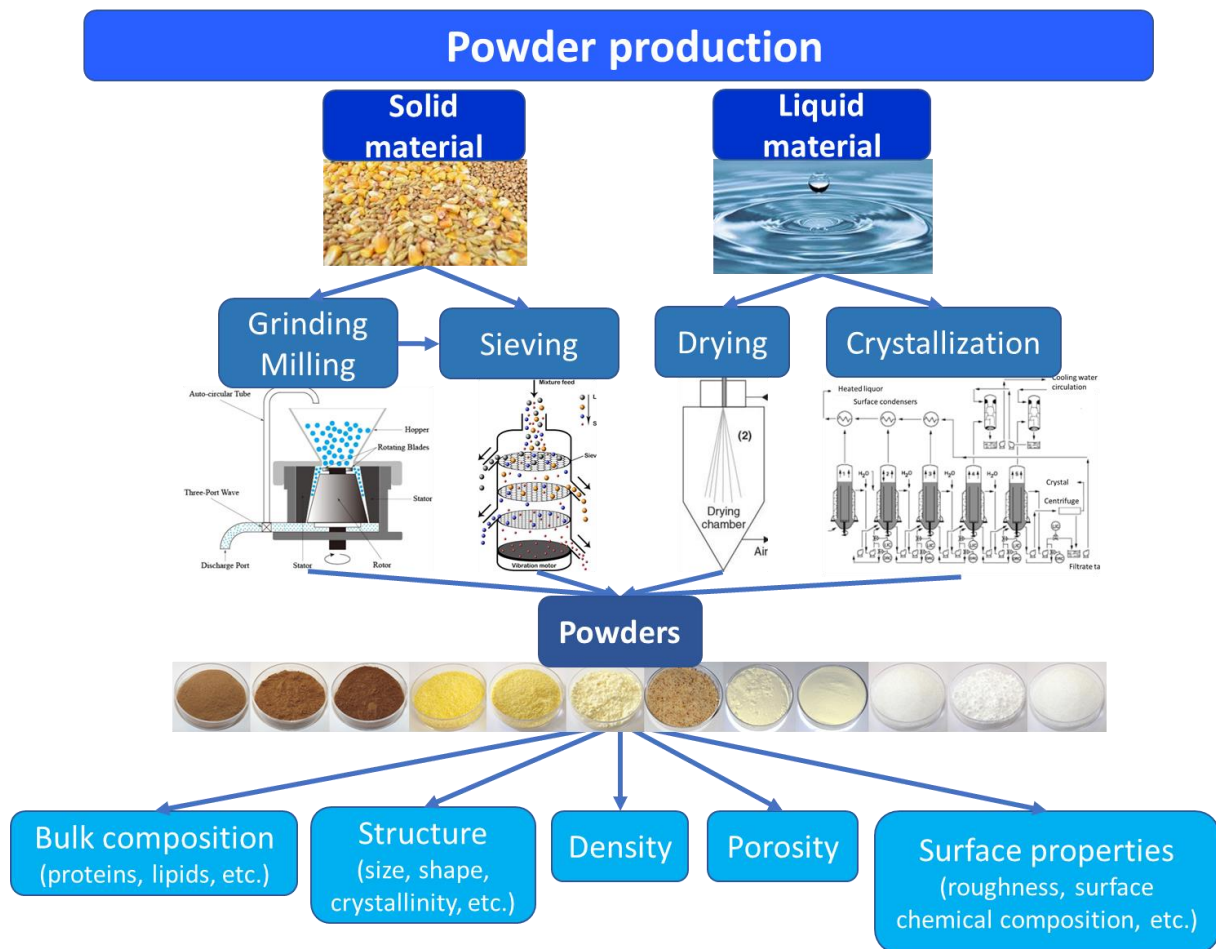


Figure 3. Links between material physical state (solid or liquid), production process, and physicochemical properties of powders.

2.1.1.1. Powder production from solid material

2.1.1.1.1. Grinding

Grinding is a widely-used process to produce powders such as flours (grounded cereal grains) (Blazy et al., 2006). It consists in breaking solid material pieces by crushing or mechanical shear (**Figure 4**), which results in size reduction. Crushing consists in impacting the solid material by mechanical forces (**Figure 4A**) with a hammer or by projection. Mechanical shear designates the application of shear stresses by compressing the solid against a moving surface (**Figure 4B**). Grinding mainly influences particle size and shape distributions, but it also affects the structural state of the solid material and chemical composition, in particular at the surface of formed particles. Grinding process conditions are more influential on particle size distribution characteristics, whereas the chemical composition (contents in starch, fibers, and proteins) of the solid material to be ground significantly affects particle shape properties (Blazy et al., 2006; Cuq et al., 2011; Mohamad Saad et al., 2009; Waiss et al., 2020). Friction-induced heating of the solid material induces a loss of water and volatile molecules, as well as the development of Maillard reaction (Andueza et al., 2003; Deli et al., 2019; Karam et al., 2016; Qiu et al., 2005; Waiss et al., 2020). Moreover, the grinding of crystalline parts of the solid material induces their transition to an amorphous form due to heat transfer and water evaporation (Nakai et al., 1977; Otsuka et al., 1999).

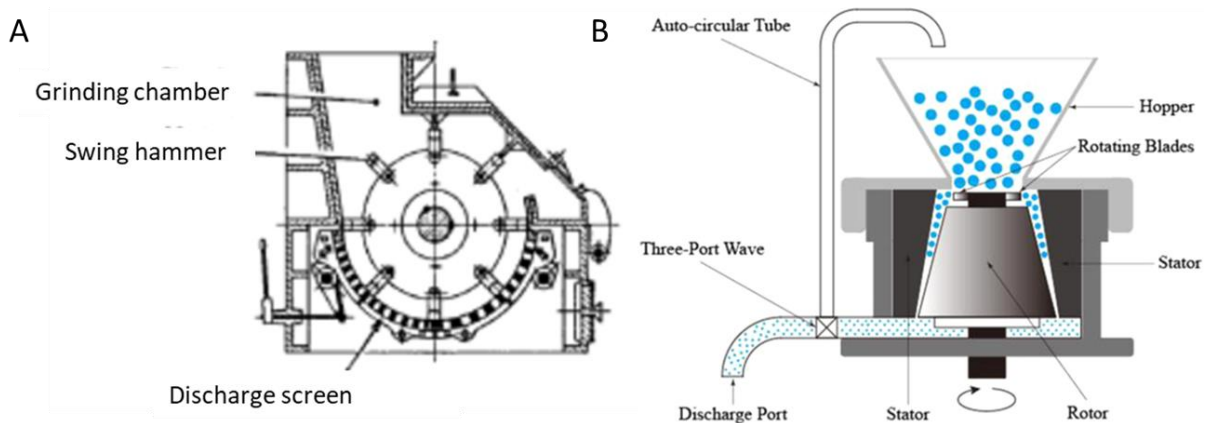


Figure 4. Grinding systems based on: A- crushing (hammer mill; Blazy et al., 2006) and B- mechanical shear (colloid mill; Gao et al., 2020).

2.1.1.1.2. Sieving

Sieving can be used to discriminate powders into granulometric classes differing in particle size distribution (**Figure 5**). The separation between the different classes is achieved by size exclusion when particles are forced to pass through sieves of decreasing mesh size by vibration of the equipment. When applied to ground materials, granulometric classes resulting from sieving often have different chemical composition, as larger particles are expected to come from solid material parts that are harder to grind (Becker et al., 2016; Doesthale et al., 1979; Liu et al., 2015; Waiss et al., 2020; Zaiter et al., 2016), such as those richer in fibers for instance.

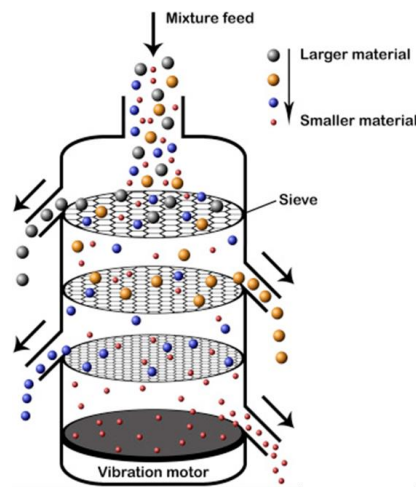


Figure 5. Vibrating sieve (Crawford and Quinn, 2017).

2.1.1.1.3. Powder mixing

The mixing of dry powders is a process designed to homogenize powder batches or formulations, like flours, sugars, instant soups, bakery mixes, cocoa, etc. Powder mixing is achieved by application of external energy causing the relative motion of particles. This is generally performed with a blade passing through the powder bed, by rotating a drum containing the powder, gravity, or combinations of these principles (**Figure 6**). The efficiency of powder mixing processes is impaired on one hand by powder cohesion coming either from van der Waals interactions, electrostatic forces, or stickiness due to presence of fat or amorphous sugars at particle surface, and on the other hand by particle segregation due to the Brazil nut effect (under motion, the large particles of a powder tend to move toward the top of the powder bed as smaller particles have the possibility to move in the interparticular spaces between large particles, especially under them, which blocks the larger particle from moving to the bottom),

which is highly linked to the heterogeneity of particle size distribution (Cuq et al., 2013; Fournaise et al., 2020; Liao et al., 2012).

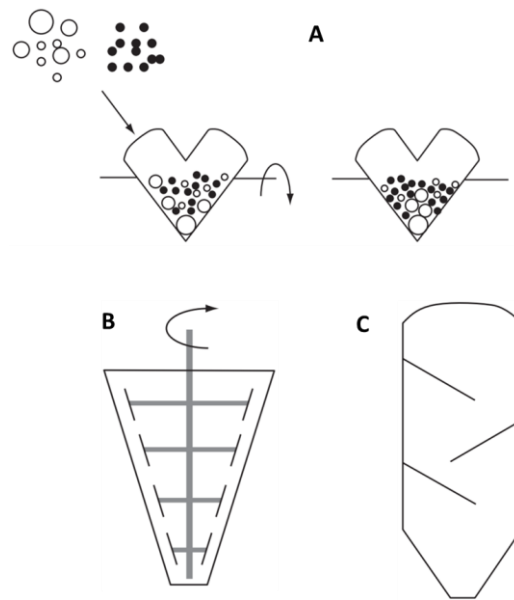


Figure 6. Principles of dry mixing (Cuq et al., 2013): A - rotative mixing, B - blade mixing, and C - static mixing.

2.1.1.2. Powder production from liquid material

2.1.1.2.1. Drying processes

Various kinds of drying processes have been developed to transform liquids into powders: e.g., drum-dryer, spray-dryer, and freeze-dryer. Drying is obtained by water removal either by evaporation or boiling, depending on applied temperature and pressure.

- Drum-drying

Drum-drying is one of the first-developed drying technique. First, the liquid or paste to be dried is spread into a fine layer at the surface of a heated rotating drum (**Figure 7**). Heat transfer to the product causes quick drying by water evaporation and resulting powder is collected by scraping with a blade (Caparino et al., 2012; Courtois, 2013). This high heat treatment leads to particles exhibiting a cooked flavor and a significant coloration due to Maillard reactions, a high level of free fat, a high density, a low porosity, a large size, and a flake shape (Caparino et al., 2012; Courtois, 2013; Nindo and Tang, 2007). Drum-drying is mainly used for instant mashed potatoes or chocolate powders. Due to the loss of organoleptic quality, this technique is not adapted to dairy powders for milk reconstitution applications but

useful for the production of ingredients for the bakery and chocolate industries (Caparino et al., 2012; Karthik et al., 2017; Nindo and Tang, 2007).

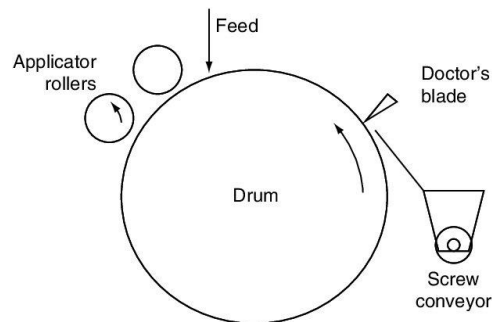


Figure 7. Single drum-dryer with feed applicator rollers (Moore, 1995).

- Spray-drying

Spray-drying is largely used in the food industry as it allows preserving product organoleptic quality while achieving good production rates. To optimize spray-drying efficiency, the liquid to be dried is previously concentrated by evapoconcentration. Spray-drying is performed in three main steps (**Figure 8**):

- first, the liquid is sprayed by an atomizer: it is injected into the drying chamber through a pressure nozzle or after flowing at the surface of a rotating wheel atomizer, leading to the formation of a continuous spray (fine droplets suspended in air).

- then, sprayed droplets are dried by surrounding heated air; their high specific surface favors heat and mass transfer leading to water evaporation. This results in the formation of dry particles.

- last, the powder is separated from the cooled and moisture-enriched drying gas, with a cyclone separator or using bag filters, and collected (Petit et al., 2015; Santos et al., 2017; Schuck et al., 2012).

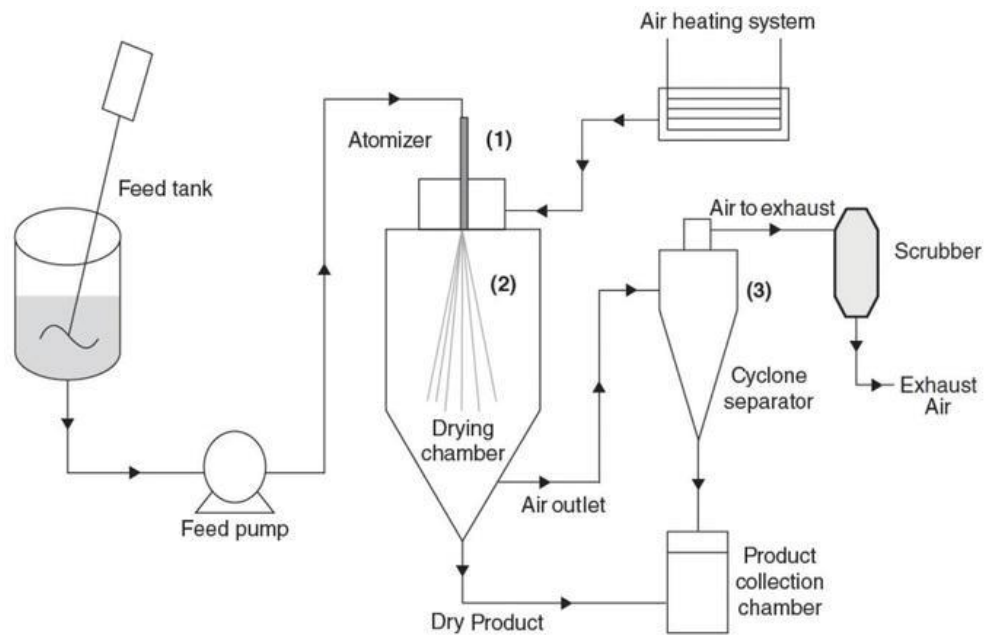


Figure 8. Principle of spray-drying supplied with a cyclone separator (Santos et al., 2017).

During the initial stage of spray-drying, differential compound migration takes place in the sprayed droplets of concentrate: proteins and lipids move to the droplet surface owing to their surface-active properties and buoyancy, respectively. For skim milk powders, protein diffusion to the surface occurs until reaching saturation. For whole milk powders, lipids, saturating the surface more quickly and making it hydrophobic, limit proteins diffusion toward the droplet surface (Kelly et al., 2015; Shrestha et al., 2007a). The high levels of milk proteins and lipids limit the presence of lactose and minerals at air-liquid interfaces (Kelly et al., 2015). That is why minerals and lactose are preferentially found at the heart of particles. However, a higher temperature drying air limits the possibility of compound migration within the droplet and thus reduces the composition gradient between particle bulk and surface (Shrestha et al., 2007). Surface lipids make powders more sensitive to oxidation and sticking, while particles surface composed of proteins and lactose decreases the possibility of powder oxidation and promotes reconstitutability and flowability (Kim et al., 2002; Kim et al., 2005; Vignolles et al., 2007). The rapidity of the drying mechanism leads to a high proportion of amorphous sugar in spray-dried powders, as it is the case for lactose in dairy powders (Makower and Dye, 1956; Windhab, 1999). Spray-drying leads to particles of rather spherical shape in comparison with other drying techniques. Using high temperature drying air may induce the quick solidification of droplet surface, forming a crust that keeps the spherical shape of droplet/particles during the drying mechanism (Kim et al., 2002). Subsequent water evaporation leads to particles containing a vacuole (occluded air), decreasing the apparent density and increasing the porosity

of particles (Caparino et al., 2012; Nindo and Tang, 2007). The pretreatment of the concentrate to be dried can modify spray-dried powder structure: for example, aeration of whole milk concentrate prior to spray-drying was hypothesized to result in particles containing internal pores covered by lipids, thus decreasing lipid content at particle surface (Fournaise et al., 2020). Other food powders can be produced by spray-drying, for example fruit juice powders (Phisut, 2012; Yousefi et al., 2011). Due to their high content in low molecular weight sugars (glucose, fructose, and sucrose), fruit juice powders are very hygroscopic and have a low glass transition temperature, which may be responsible for stickiness problems (Muzaffar et al., 2015). In order to improve the stability of these powders and reduce their stickiness, carrier agents (maltodextrins, gum Arabic, etc.) are often added before spray-drying (Bhandari et al., 1993; Jiang et al., 2013; Phisut, 2012).

- Freeze-drying

The freeze-drying process is based on water sublimation at reduced pressure (Ratti, 2013). First, the liquid product is frozen; then, the frozen liquid is put under partial vacuum; last, the product is heated at around 40 °C, which induces its sublimation (**Figure 9**).

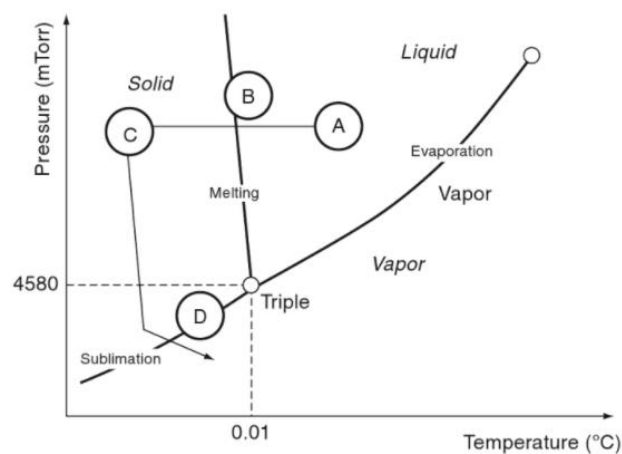


Figure 9. Principle of freeze-drying: representation of water thermodynamic transformations on the pressure-temperature diagram. A: initial conditions, B: freezing, C: beginning of pressure reduction (application of partial vacuum), and D: heating, leading to water sublimation (Ratti, 2013).

This powder production process is reserved to high-value products, owing to its very high cost and low production rate, as at industrial scale it can only be carried out by batches. The low temperature required for sublimation at reduced pressure allows a better conservation

of organoleptic properties (color and flavor) and limits heat-induced denaturation of proteins and vitamins in comparison with drum- and spray-drying (Aguilera, 2005; Ratti, 2013). Freeze-drying results in powders of highest porosity and lowest density among drying processes (Aguilera, 2005; Ratti, 2008).

2.1.1.2.2. Crystallization

Amorphous sugars are deleterious for long storage due to their high hygroscopicity which leads to powder sticking or caking. For powdered products of high sugar content, it may be interesting to use a crystallization process which allows reorganization of molecular structure of the dry matter, reaching a most stable state named crystalline state (Biscans, 2013; Mathlouthi and Genotelle, 1998; Windhab, 1999). Two main types of crystallization techniques are encountered. On one hand, crystallization can be induced in sub-saturated liquids either by water evaporation leading to an increase in the dry matter content of the liquid up to saturation, or by decreasing the saturation concentration by adiabatic cooling (**Figure 10A**). With these techniques, the size and shape of formed crystals depend on the agitation mobile and the guide tube of the centrifuge system. On the other hand, crystallization can be the result of a chemical reaction between two solutions. The addition and mixing of reagents is then controlled in a stirred reactor supplied with a recirculation tube (**Figure 10B**) (Biscans, 2013).

The main impact of the increase in the degree of crystallization of powders consists in the decrease in the freezing point (Makower and Dye, 1956; Mathlouthi and Genotelle, 1998; Windhab, 1999).

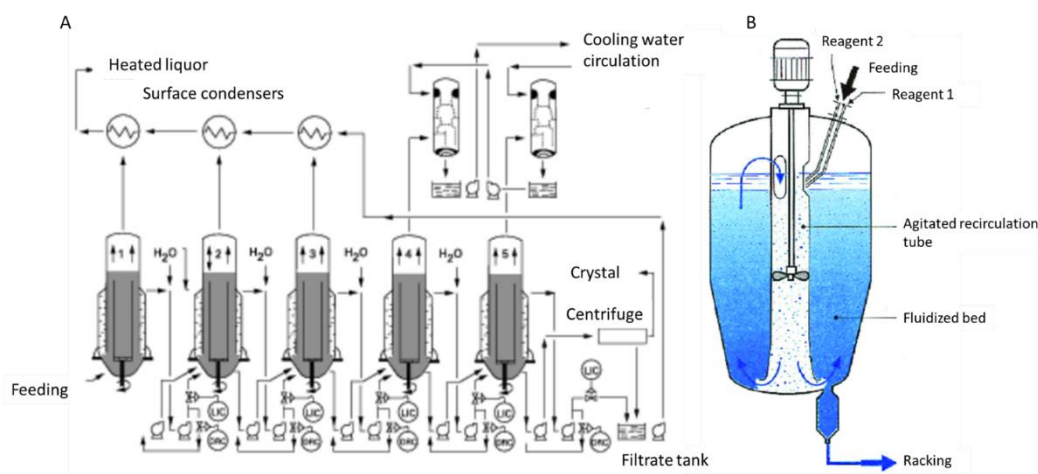


Figure 10. Crystallization processes (Biscans, 2013): A- evaporative crystallizer and B- reactor crystallizer.

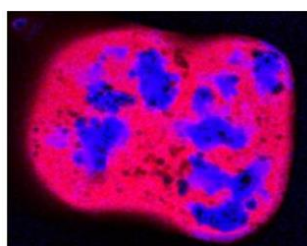
The use of a wide variety of powder manufacturing processes (grinding, drying, crystallization, etc.) and the great variability in raw materials (physical state, origin, etc.) induce a large range of physicochemical (chemical composition, particle size and shape distributions, surface properties, etc.) and functional properties (reconstitutability, flowability, gelation, etc.) of food powders.

2.1.2. Powder physicochemical properties

2.1.2.1. *Chemical composition and structure*

The chemical composition (which can be expressed in dry or wet basis) of a powder issued from agroresources consists in the contents in proteins, lipids, carbohydrates, minerals, and water averaged for the whole particles constituting the powder. It is usually evaluated by standard methods (ADPI, 2002; AFNOR, 2005; George and Latimer, 2019). Chemical composition is an important property impacting powder functionalities like reconstitutability, flowability, and gelation ability (Fournaise et al., 2020; Sharma et al., 2012). The chemical composition is greatly dependent on the nature of the raw material used for powder production (animal or vegetal).

More complex techniques are available to determine the location of chemical components in particles. For example, the distribution of components such as lipids or proteins within particles can be determined by confocal laser scanning microscopy (CLSM), which is a technique permitting to acquire three dimensional images of particles by assembling successive pictures of single focal planes (Burgain, 2013; Stancovski and Badilescu, 2014). Emitted fluorescence induced by laser excitation can be used to identify different compounds such as lipids, proteins, or lactose in whole milk powders (**Figure 11**) or bacteria for example (Burgain, 2013; McKenna, 1997).



Lipids: blue (39 %)
Proteins: red (61%)

Figure 11. Determination of the relative proportions of lipids and proteins in whole milk powder by CLSM coupled with image analysis (Claire Gaiani's personal data).

Fourier-transform infrared spectroscopy (FTIR), another analytical technique which allows the determination of the chemical composition, is based on spectral analysis (Dankar et al., 2018). It has been employed to characterize the modification of potato starch induced by additives, namely agar-agar, soybean lecithin, sodium alginate, and glycerol. Additives induce molecular modification of starches by disrupting the OH bonds, which alters starch conformation (Dankar et al., 2018). FTIR analyzes have been used to characterize the denaturation of caseins and whey proteins (Gaiani et al., 2011; Hussain et al., 2012). FTIR is generally complemented by Raman spectroscopy, which is more sensitive. Raman spectroscopy, based on the analysis of the inelastic scattering of photons by matter called the Raman effect, allows the determination of chemical bonds and the identification of molecular structure of organic and inorganic compounds. This method has been used to show that heat treatment modifies rice starch structure by forming more digestible aggregates (Wang et al., 2018). FTIR analyzes also allow the study of the state of matter (crystalline or amorphous) of powders (Jensen et al., 2005; Kumar et al., 2000).

X-ray diffraction is a technique for characterizing crystallized parts of solid material, then it is suitable for the determination of the structural state of powders. It is based on the determination of the diffraction angle of X-ray beams upon interaction with sample atoms. Obtained spectra presents peaks at diffraction angles specific of sample components (Burgain et al., 2017; Werner, 1952). This analytical technique can be used to identify the presence of sugar crystals within powders, such as crystallized lactose in the case of dairy powders (Forbes et al., 1998; Naini et al., 1998). The structural state of the material (amorphous or crystalline) greatly impacts on the functional properties of powders. Differential scanning calorimetry (DSC) permits the measurement of enthalpy changes associated with thermal transitions and thus allows the determination of several physicochemical properties such as the glass transition temperature (T_g), melting temperature, etc. Low molecular weight sugars have a low T_g (close to the ambient temperature) and thus powders rich in sugars, such as fruit juice powders are particularly sensitive to caking during production and storage (Phisut, 2012; Roos, 1995; Shrestha et al., 2007b). Many studies on fruit juice powders have been conducted with a view to increase their T_g and improve their storage stability using polymers additives with a high molecular weight (maltodextrin, Arabic gum, etc.). For a 60/40 maltodextrin/orange juice mixture, it has been evidenced that the T_g was increased at 86.4 °C which permitted to ensure better stability during storage, while the main components of orange juice powder have a T_g between 14-31 °C (Shrestha et al., 2007b). It has been demonstrated that a T_g higher than 40 °C

makes it possible to avoid reaching the sticking point of powders at room temperature for powders containing maltodextrins (Gianfrancesco, 2009).

2.1.2.2. Particle size and shape distributions

The measurement of the particle size distribution of a powder represents the evaluation of spatial dimensions of sample particles. It can be performed by indirect and direct methods, such as sieving, sedimentometry, optical microscopy, laser diffraction, and image analysis (Allen and Roux, 1988; Merkus, 2009; Sun et al., 2019).

The particle size of powders is generally described as volume-weighted size distributions, in which the contribution of each particle to the particle size distribution is proportional to its volume. In this case, the frequency of each granulometric classes, i.e. the volume proportion of all particles of the size class, is called volume density. Particle size distributions may also rarely be weighted with particle specific surface area or number (**Figure 12**) (Hogg, 2008; Witt et al., 2007). Based on particle size distribution, characteristic granulometric parameters can be calculated, such as D_{10} , D_{50} , and D_{90} , where D_x represents the diameter for which x % of the particles have a smaller size. The width of the particle size distribution can be evaluated with the span, deduced from D_{10} , D_{50} , and D_{90} using **Equation 1** (Grossman and Cline, 1957).

$$span = \frac{D_{90} - D_{10}}{D_{50}} \quad \text{Equation 1}$$

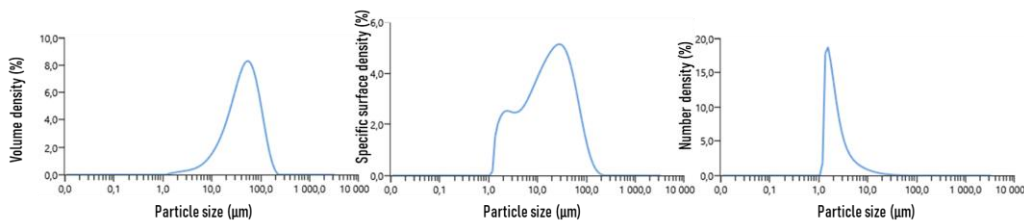


Figure 12. Examples of volume-weighted (left), specific surface area-weighted (middle), and number-weighted (right) particle size distributions of the same sample of whey protein isolate powder.

Sieving is the oldest size characterization method. The sample is separated in different granulometric classes with sieves of various mesh sizes and each granulometric class is weighed. This permits to calculate the mass proportion of granulometric classes, which is assumed to correspond to their volume density (Allen and Roux, 1988; Laguna et al., 1999). Sieving efficiency and duration are extremely dependent from particle shape, sample amount, as well as powder cohesion and friability (Allen and Roux, 1988; Frančišković-Bilinski et al.,

2003; Laguna et al., 1999). Also, this technique leads to rather imprecise results owing to the low number of employed sieves.

Sedimentometry allows calculation of particle size from the velocity at which particles fall in a liquid or gaseous fluid using the Stokes equation (Allen and Roux, 1988). Validity conditions of this method require that particles should be spherical, smooth, and rigid; measurement should be performed by ensuring that fall velocity is reached; and the fluid should be homogeneous and dense enough to obtain low sedimentation speeds which allow neglecting the effects of inertia on particle motion (Allen and Roux, 1988; Shein et al., 2006).

Laser diffraction analysis consists in the determination of particle size from the diffraction angle of a laser beam when passing through a dispersion of particles in a liquid or gaseous fluid in the measurement cell. It allows size measurement of small particles until about 0.2 μm . Optical microscopy allows the observation and measurement of particle size and shape by manual count or image analysis. This method requires preparation to ensure particle separation and sampling of a representative particle population (Allen and Roux, 1988). Measurement of particle size is realized by means of an ocular graticule allowing the dimensioning of the observation field (Allen and Roux, 1988; Martins et al., 2020). For a measurement to be considered accurate (inferior to 2 % standard deviation for particle size), it is necessary to analyze a minimum of 96 fields and 625 particles, and their size should exceed 2.3 μm . However, this method should be considered precise only for particles over 2.3 μm (Allen and Roux, 1988).

Image analysis is another direct technique allowing the determination of particle size. It consists in acquiring high frequency images of a dispersion of particles in a liquid or gaseous fluid passing through a measurement cell and analyzing them with a software to deduce particle size but also shape characteristics. The determination of particle size by image analysis is restricted to particles superior to 1 μm by the resolution of employed camera (Merkus, 2009; Shein et al., 2006). Also, the determination of shape properties (e.g., sphericity, convexity, aspect ratio) is made possible for particle larger than 10 μm due to the limitation of the number of pixels covered by the particle (Merkus, 2009; Shein et al., 2006; Witt et al., 2007).

2.1.2.3. Density and porosity

Density is generally defined as the ratio of mass to volume. For powders, different measurement methods exist, leading to various definitions of powder density either based on the material constituting particles, individual particles, or the whole powder bed and dependent

from the way by which the powder sample has previously been prepared, as the operations of pouring, conditioning, compaction, etc. are known to affect the spatial arrangement of particles within the powder bed. Interparticular spaces as well as open and closed pores play a central role in the definition of the different densities (**Figure 13**). Interparticular spaces designate the air-filled spaces between the particles in the powder bed (**Figure 13 A**). Open pores represent the pores connected to the surface of particles and closed pores are totally surrounded by solid parts of particles (**Figure 13 B**) (Barbosa-Cánovas and Juliano, 2005; Lowell and Shields, 1991; Onwulata, 2005).

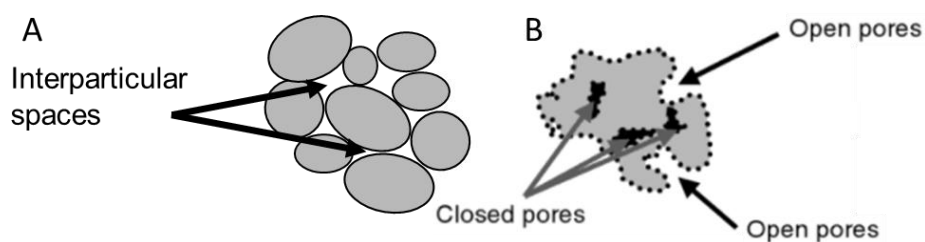


Figure 13. A- Interparticular spaces and B- closed and open pores (Onwulata, 2005).

At the particle scale, two definitions of density are found in the powder field (Barbosa-Cánovas and Juliano, 2005; Lowell and Shields, 1991; Onwulata, 2005):

- The true density of powders corresponds to the density of the solid material constituting powder particle, it depends on powder chemical composition only. Interparticular spaces, open and closed pores are excluded from the volume considered in the definition of true density.
- The apparent density of powders is equal to the mass of particles divided by their volume, closed and open pores included, but interparticular spaces excluded. The apparent density can be measured by pycnometry, which consists in the determination of the volume of displaced gas or liquid after immersion of a given particle mass (Onwulata, 2005).

At the powder bed scale, several powder densities can be defined according to the method of volume determination:

- The aerated density, also called conditioned density, is determined by using the powder bed volume measured after conditioning (i.e., powder homogenization);
- The tapped density is calculated from the volume of the powder bed after a given number of taps of the powder sample, or after application of vibration during a given duration;
- The compacted density, the volume of the powder bed is measured after compaction, i.e. application of a given value of normal stress;

- The loose density is obtained from the powder bed volume after free pouring in a measurement cell without conditioning;
- For the aerated bulk density, the volume is measured after fluidization of the powder bed.

Powder densities mainly depend on the production process and the chemical composition that control the formation of open and closed pores, as well as the particle size and shape distributions which are directly linked to interparticular spaces. Among functionalities, powder densities impact more significantly on flowability and reconstitutability (Barbosa-Cánovas and Juliano, 2005; Onwulata, 2005; Schuck et al., 2012).

Particle porosity is defined by the ratio between volumes of open pores and particles including open and closed pores. It can be measured with mercury porosimetry or bed voidage method. The bed voidage method is based on the difference of bulk density before and after mixing the powder bed with an extremely fine powder that fills open pores and interparticular spaces (Barbosa-Cánovas and Juliano, 2005; Lowell and Shields, 1991; Schuck et al., 2012a). The porosity has a marked impact on technofunctional properties (Lowell and Shields, 1991).

CLSM allows the observation of the inner structure of a particle, in particular open and closed pores (**Figure 14**) (Kosasih et al., 2016; Paramita et al., 2010).

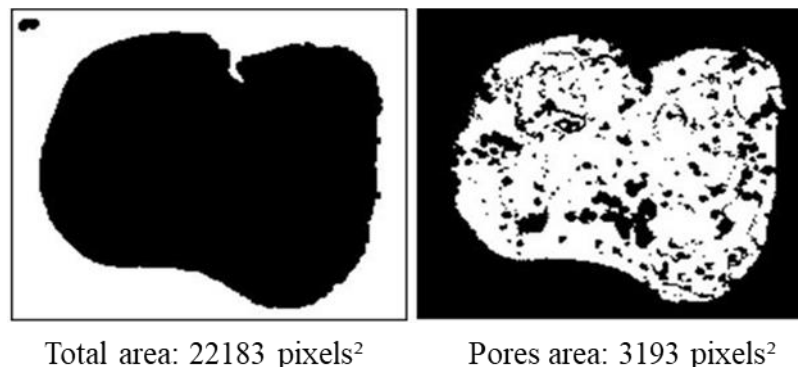


Figure 14. Example of CLSM associated with image analysis to determine pores in whole milk powder (Claire Gaiani’s personal data).

This technique has been used in formulation to determine the impact of additives (gelatin, decaglycerin monolaurate, or ethanol) on the internal structure of particles composed of matodextrin and gum Arabic. The additives have the effect of increasing the formation of closed pores (Paramita et al., 2010). CLSM also permitted to evidence the increase in closed

pores for whole milk powders when using carbonation as pretreatment prior to drying, but also the evolution of particle physical structure during storage (Kosasih et al., 2016).

Finally, transmission electron microscopy permits to acquire two dimensional pictures at higher definition. It requires an ultrathin cut of sample particle, because it is based on the analysis of the electron beam transmitted through the sample (Burgain et al., 2017; Lie-Piang et al., 2021). This technique has been used in studies aimed at characterizing the internal structure of casein micelles in raw milk or after reconstitution (Karlsson et al., 2007; Knudsen and Skibsted, 2010; Lie-Piang et al., 2021).

2.1.2.4. Powder surface characterization

2.1.2.4.1. Surface imaging

- *Scanning electron microscopy*

Scanning electron microscopy (SEM) permits to acquire two dimensional high-definition pictures with a high magnification. The sample is scanned by a focused electron beam under high partial vacuum, and the secondary electrons emitted by the sample are detected. which permits to build an image of the surface and the shape of particles from contrast variations (Burgain, 2013; Klang et al., 2013).

The limitation of this technique comes from the sample preparation step. First, the sample needs to have a low water content, then sometimes the sample has to be dried before analysis which may induce alteration of powder surface structure. The second concern is that sample coating is needed to conduct the electron beam, with carbon or gold for low- or high-resolution analysis, respectively. The coating needs to be as fine as possible to avoid missing topographical information relative to sample surface (Fournaise et al., 2020; Klang et al., 2013).

An improved method of SEM has been developed to allow the analysis of hydrated samples and avoid the necessity of conductive coating: Environmental Scanning Electron Microscopy (ESEM). ESEM resolution is lower than SEM but it can be used for the observation of particles in hydrated conditions. Measurements can be made in the absence of water vapor pressure up to the dew point (Donald et al., 2000; Klang et al., 2013; Stokes et al., 1998).

- *Atomic force microscopy*

Atomic force microscopy (AFM) is currently a rising star in the food powder surface analysis field, mainly for its resolute capacity (on the order of fractions of a nanometer) 1000 times better than the optical diffraction limit. AFM is a versatile tool compared to other surface analysis techniques as it is possible to record topographic images and/or to perform force

measurements. The major difference between AFM and optical microscopy or electron microscopy is that AFM does not use lenses or beam irradiation. The information is gathered by touching the surface with a mechanical probe. Therefore, AFM does not suffer from a limitation in spatial resolution due to diffraction and aberration, the measurements can be performed in controlled environment and vacuum is not required and finally, sample staining or coating is not necessary (Burgain et al., 2017).

Application of AFM to food powders allows to study single particle surface topography and roughness, surface chemistry and nanomechanics. With AFM, a small sample surface is scanned by a tip staying in contact with the sample or tapping the sample surface (**Figure 15**). A laser beam is focused on the cantilever to record the 3D position with a photodiode detector.

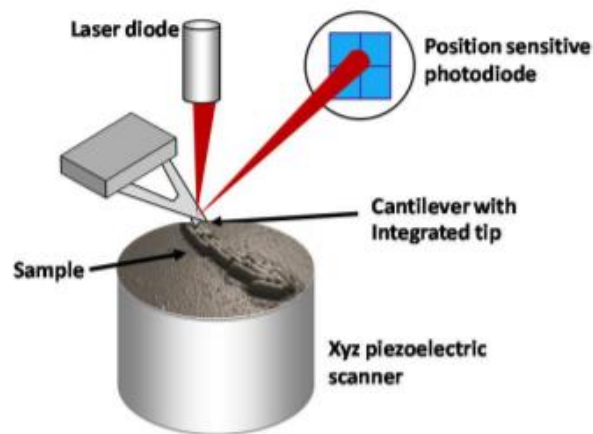


Figure 15. Principle of atomic force microscopy (Burgain, 2013).

This technique can be used to create high-definition 2D and 3D pictures of particle surface and measure surface roughness (**Figure 16**). The strength of AFM regarding food powders lies in its ability to highlight very fine structures such as small patches at powder surface which cannot be evidenced by SEM or ESEM due to the required coating or the degradation of sample surface caused by the electron beam (Andre et al., 2010; Burgain, 2013; Klang et al., 2013).

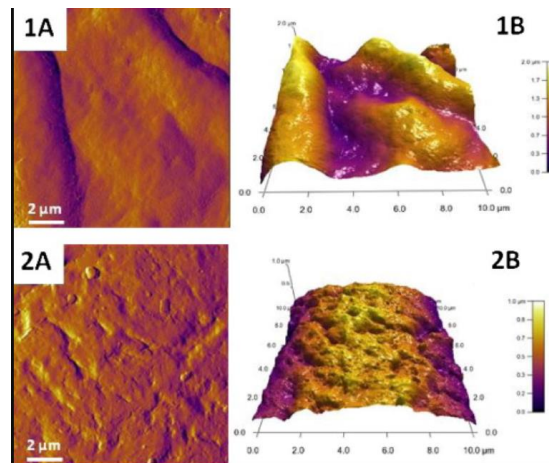


Figure 16 : 2D (A) and 3D (B) pictures of skim (1) and whole (2) milk powders (Murrieta-Pazos et al., 2011).

The AFM has recently been applied to the analysis of food powders and used to improve the knowledge on particle surface of skim and whole milk powders (Burgain et al., 2017) or on proteins from various origins (soy, wheat, dairy, etc.) with a view to determine the impact of the production process (Shi et al., 2019). Also, the increase in surface roughness during long-term storage of dairy powders has been evidenced by AFM (Burgain et al., 2016b, 2017; Klang et al., 2013).

The dimensional limitations of microscopic techniques have been summarized by Burgain et al. (2017) in **Figure 17**. Optical microscopy allows the observation of particles from millimetric to micrometric scales. For smaller particle sizes, only electronic and atomic microscopies allow the measurement from micrometric to nanometric scales.

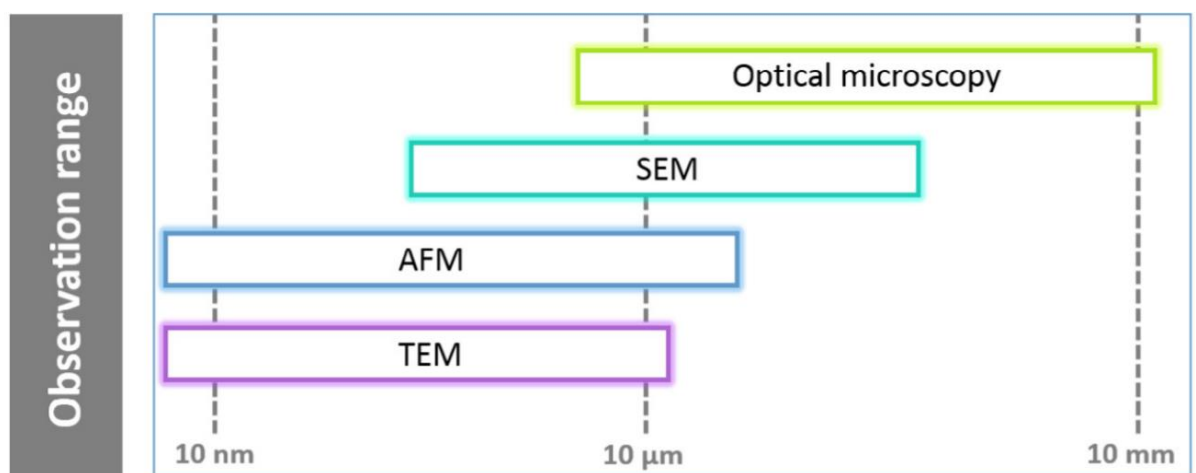


Figure 17. Observation range of microscopies (Burgain et al., 2017).

2.1.2.4.2. Surface physicochemical properties

AFM can be used in force spectroscopy mode to measure the interaction force between tip and sample. This mode permits to characterize sample surface elasticity by the calculation of Young's modulus (Burgain et al., 2017; Gaboriaud and Dufrêne, 2007; Shi et al., 2019). This measurement is carried by nanoindentation to evaluate surface elasticity. Elasticity is related to the ability of the surface of a solid material to be deformed under application of a normal stress. In nanoindentation mode, AFM analysis is performed by penetrating the sample surface with the tip (**Figure 18**) and the Young's modulus, which described the elasticity of a solid material, is calculated from the force-distance curve with the Hertz model (Burgain et al., 2017; Hertz, 1882; Klang et al., 2013).

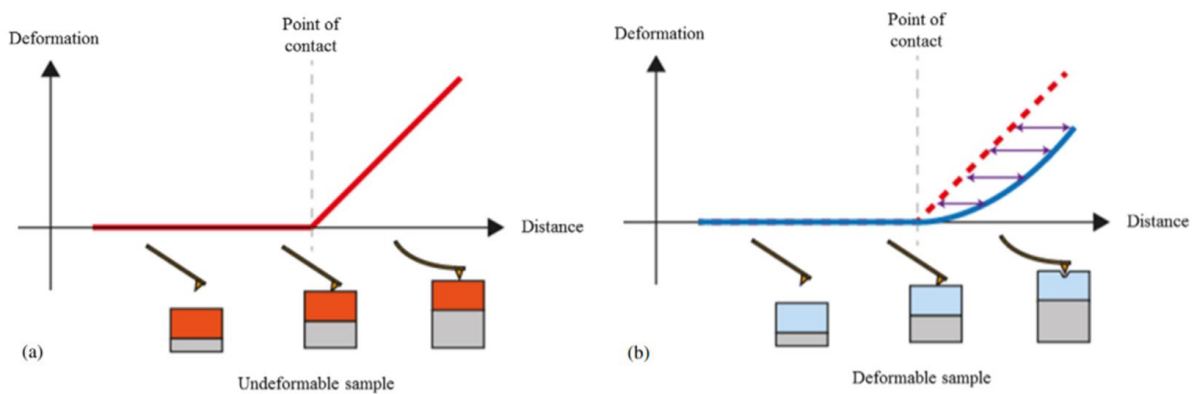


Figure 18 : Examples of force–distance curves recorded for hard (a) and soft (b) surfaces (Kasas et al., 2013).

AFM analyses of food powders (nanoindentation and imaging) are fairly recent. First nanoindentation measurements concerned particles of crystallized sugars : Young's moduli of 3 – 7 and 33 – 38 GPa were respectively obtained for lactose and sucrose particles (Perkins et al., 2007; Ramos and Bahr, 2007). AFM nanoindentation of the surface of micellar casein powder highlighted the link between surface elasticity increase and reconstitutability impairment during storage: fresh and aged micellar casein powders had Young's moduli around 0.2 and 20 GPa, respectively, showing that powder aging induces surface hardening, which was related to the alteration of the structuration of micellar caseins at particle surface following their agglomeration (Burgain et al., 2016b).

More recently, a study on fruit powders evidenced a strong impact of storage temperature and humidity on particle surface properties using AFM. Decreased roughness and stiffness were linked to a lower reconstitutability as above a glass transition temperature (T_g), a viscous layer around the particle limited water entrance (closed porosity during swelling)

which was described as the limiting step in the global reconstitution process (**Figure 19**) (Gaudel et al., 2022).

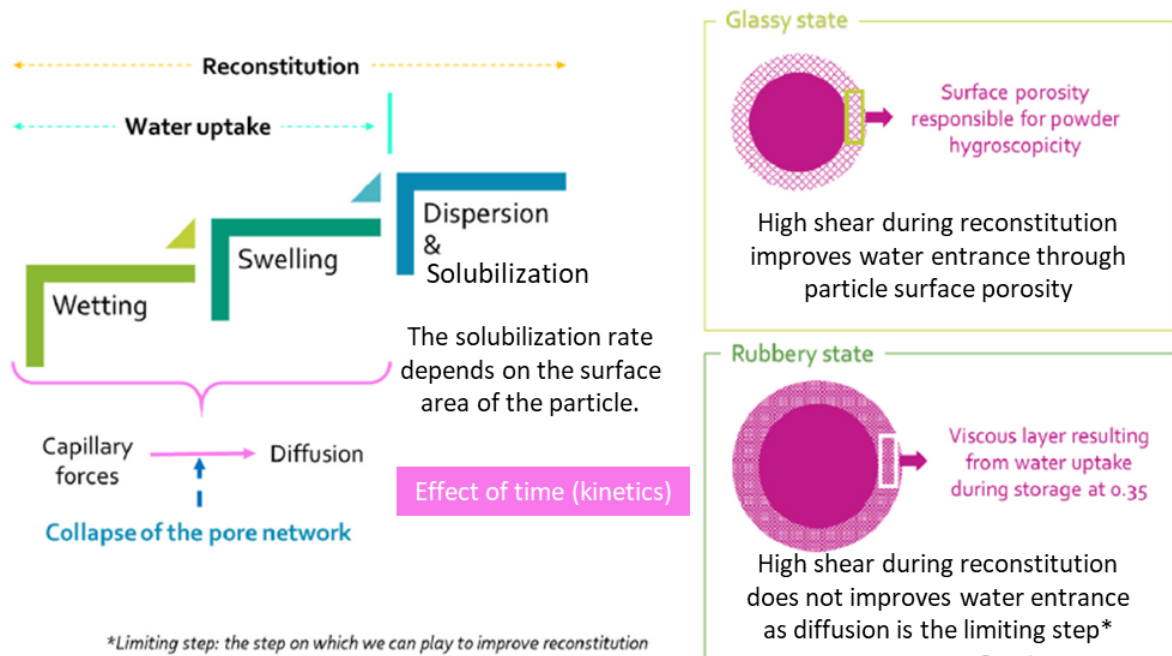


Figure 19. Summary of the relevant results in terms of physicochemical properties from macro- to nano-scale for fruit powders, adapted from Gaudel et al. (2022).

2.1.2.4.3. Surface chemical composition

Surface chemical composition influences functional properties of powders, especially reconstitutability and flowability (Kim et al., 2002). In chemical force microscopy (CFM) mode, tips are functionalized by grafting with biomolecules or bacteria, which allows the identification of their specific interactions with the surface of particles. CFM has been employed to create hydrophobic maps of particle surfaces and identify protein-protein interactions or specific adhesive interactions between bacteria and dairy proteins located at powder surface. This allows improving the knowledge about mechanical, biophysical, and biochemical properties of particle surface (Burgain, 2013; Burgain et al., 2016b, 2017; Gaboriaud and Dufrêne, 2007; Noy et al., 1997).

Time-of-flight secondary ion mass spectrometry is a technique providing atomic and molecular quantification of particle surface (3 – 5 nm). Its principle consists in focusing a pulsed beam of primary ions on the surface to be analyzed in order to produce secondary ions from the first monoatomic layers of the sample (Nicholas et al., 2020). This technique has already been used to follow the evolution of the surface of milk protein or cocoa powders during storage

(Burgain et al., 2016a; Jacquot et al., 2016) and study surface composition of coated powders along with the proportion of covered surface (Nicholas et al., 2020).

X-ray photoelectron spectroscopy (XPS) has initially been used in the food powder field by Fäldt et al. (1993). XPS allows the determination of the atomic surface composition of the 10-nm outer layer of solid samples. Sample surface is excited by a photon beam, which releases photoelectrons that are then detected by an energy analyzer. The deconvolution of obtained spectra allows identifying the atomic composition and the type of chemical bonds between atoms (Fäldt et al., 1993; Kim et al., 2002; Kim et al., 2005). For food powders, it is mainly used to determine the surface composition in carbon, oxygen, nitrogen, and other minor components (phosphorus, sulfur, calcium, manganese, etc.) (Kim et al., 2002; Kim, 2008; Nawaz et al., 2016). The ratios between surface contents in carbon and oxygen and between carbon-oxygen bonds and other carbon bonds have been positively correlated to surface hydrophobicity (Kim, 2008). Therefore, contrary to AFM in CFM mode for which the measurement area is small (square of few micrometers side), XPS is not a local analysis due to the large measurement area ($300\ \mu\text{m} \times 700\ \mu\text{m}$). Thus, XPS applied to powders provides global results for a large number of particles (Fäldt et al., 1993). For dairy powders, the atomic surface composition can be converted into macrocomponents (proteins, lipids, lactose, and minerals) surface composition from atomic compositions of pure components. Unfortunately, this method seems hard to extend to other kinds of food powders, owing to the requirement of well-distinct XPS signatures of macrocomponents (Gaiani, 2006; Nikolova et al., 2015).

Energy-dispersive X-ray spectroscopy (EDX) allows the measurement of surface composition for a maximum analysis depth of $5\ \mu\text{m}$. An electron beam scans the sample surface and induces the formation of X-rays that are collected by a detector. Obtained spectrum is then interpreted to determine surface atomic composition. The combination of EDX and XPS analyses made it possible to determine the gradient between surface and bulk macrocomponents (proteins, lipids, lactose, and minerals) composition of whole and skim milk powders (Benjakul and Karnjanapratum, 2018; Murrieta-Pazos et al., 2012; Shetty and Shivani, 2020).

2.1.2.5. Process impact on powder physicochemical properties

The powder production process, in relation with the nature of the raw material (solid or liquid, animal or vegetal) to be powdered, has a direct impact on powder physicochemical properties such as physical properties (particle size and morphology distributions) and bulk and surface chemical compositions.

2.1.2.5.1. Process impact on powder structure

Drum-drying leads to the formation of flakes varying in particle size according to the thickness of the product deposited on the surface of the dryer: a thicker layer induces the formation of larger flakes (Caparino et al., 2012; Courtois, 2013; Kalogianni et al., 2002).

The particle size distribution of powders produced by crystallization depends on the crystallization time. For example, in the case of sugar powders, a shorter crystallization time induces the formation of small crystals (caster sugar), whereas a longer time leads to larger crystals (granulated sugar) (Biscans, 2013; Mathlouthi and Genotelle, 1998).

Spray-drying induces the formation of rather spherical powders following the mechanisms of droplet drying. Particle size distribution of spray-dried powders mainly depends on nozzle or rotating wheel geometry, spraying conditions, and concentrate physicochemical properties (viscosity, density), as the size of resulting spray-dried particles is highly correlated to the size of sprayed droplets (Petit et al., 2015; Santos et al., 2017; Schuck et al., 2012). Droplet size is markedly dependent from the type of nozzle: bi-fluid nozzles generally result in smallest droplets than single-fluid nozzles in comparable spraying conditions. The feed flowrate of the concentrate impacts on the size of sprayed droplets: the higher the flowrate, the smaller the droplets. A difference in air-liquid velocity also induces the formation of smaller droplets because of the higher friction forces. Last, a concentrate with a high dry matter content (thus having high density and viscosity) induces the formation of larger droplets (Mandato et al., 2012; Petit et al., 2015; Schuck et al., 2012). The drying air temperature influences particle shape: a high temperature induces the formation of particles with a smooth surface, while a low temperature induces the shrinkage of the surface of dairy and fruit juice powders (Kim et al., 2003; Phisut, 2012).

The particle size distribution of powders produced by single-effect spray-drying is generally monomodal, whereas grinding processes often result in heterogenous solid fragments and bi- or polymodal size distributions (Boucheham et al., 2019; Waiss et al., 2020). Grinding

is generally followed by sieving to allow powder discrimination in monomodal granulometric classes (Deli et al., 2019; Waiss et al., 2020).

2.1.2.5.2. Process impact on powder bulk and surface compositions

Particles issued from crystallization processes generally have a homogenous chemical composition, because the chemical reaction of crystal formation is selective and leads to a certain degree of purification. Refined sugars or salts are composed of a single compound for instance (Biscans, 2013; Mathlouthi and Genotelle, 1998; Windhab, 1999).

Other powder production processes result in powders of heterogeneous chemical composition. For instance, proteins, lipids, sugars, and minerals are not regularly distributed within particles of dairy powders produced by spray-drying (Murrieta-Pazos et al., 2012): bulk and surface compositions generally differ, depending on spray-drying conditions and chemical composition of the concentrate to be dried, due to the migration of the components in sprayed droplets. Murrieta-Pazos et al. (2012) highlighted differences between surface and bulk compositions of whole and skim milk powders using XPS and EDX for surface composition up to two different depths, and classical chemical methods for bulk composition (**Figure 20**).

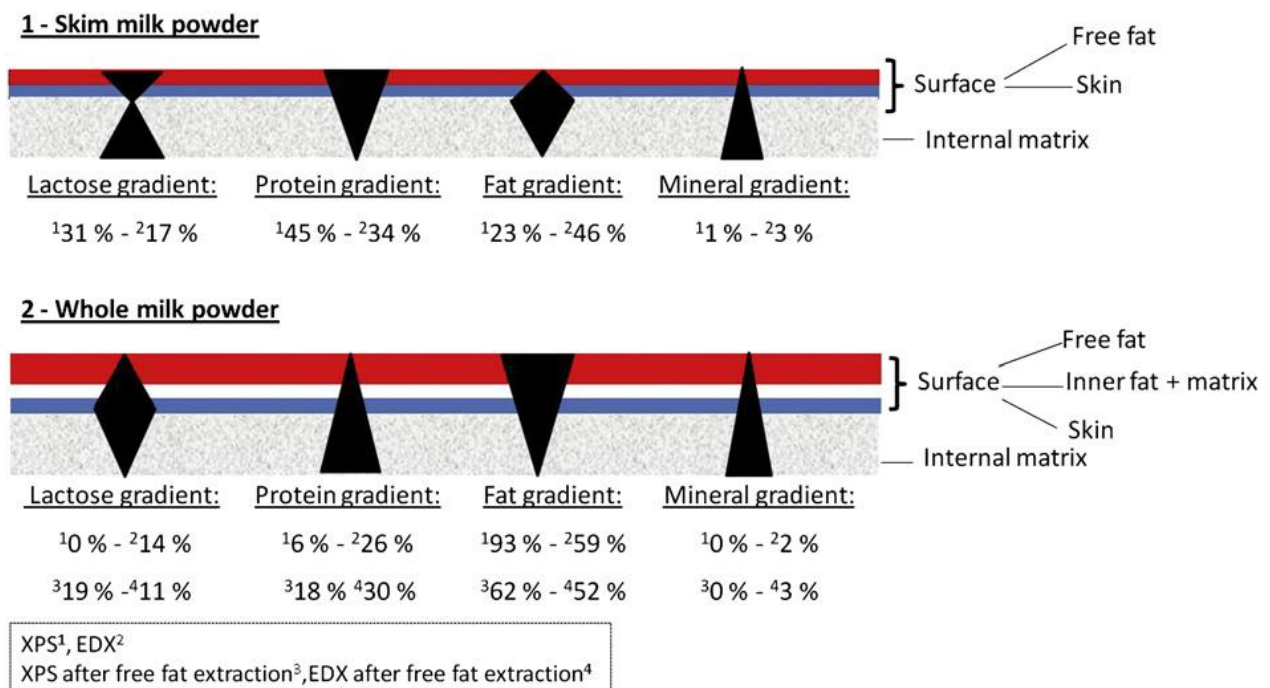


Figure 20. Differences between surface and bulk chemical compositions of spray-dried skim and whole milk powders (Murrieta-Pazos et al., 2012).

The use of pretreatments such as air incorporation into the concentrate before spray-drying modifies the surface chemical composition of whole or semi-skim milk powders (**Figure 21**). It was hypothesized that droplets coming from aerated feed concentrates may have a higher proportion of occluded air (i.e. closed pores). Thus, due to buoyancy and hydrophobicity, lipids may be found either at the embedded air/water interfaces or at droplet surface, leading to lower lipid content of particle surface (Fournaise et al., 2020).

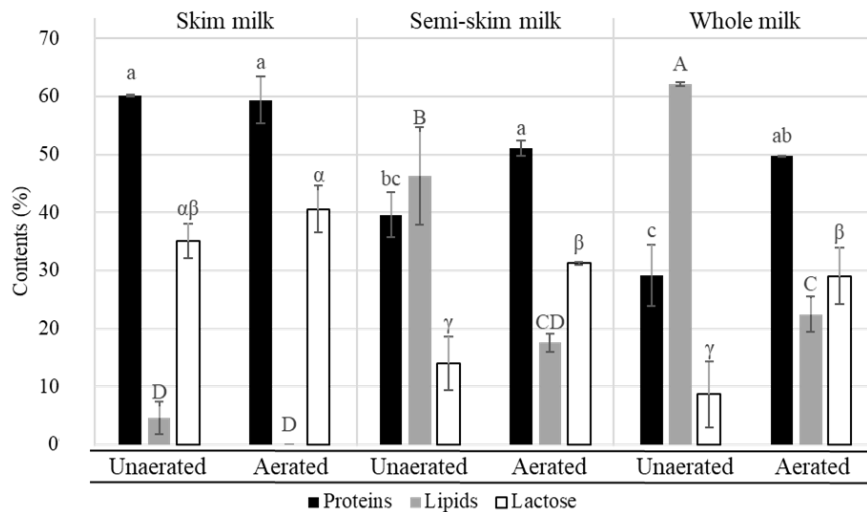


Figure 21. Surface composition on dry basis deduced from XPS analysis of spray-dried skim, semi-skim, and whole milk powders with or without prior aeration of feed concentrate. For each component separately, bars topped with different letters were significantly different according to Tukey's HSD test ($p < 0.05$; $n = 2$) (Fournaise et al., 2020).

Surface contents in macrocomponents and hydrophobicity are extremely important for powder functionalities, as particle surface is in direct contact with other particles, equipment walls, or water. Thus, surface composition controls powder cohesion, adhesion, and water interaction properties, which are fundamental for flow and reconstitution properties (Fournaise et al., 2020; Kim et al., 2002; Kim, 2008; Kim et al., 2005).

It was highlighted that sieving powders obtained by grinding of plants or cereals induces differences in chemical composition of granulometric classes (Deli et al., 2019; Gnagne, 2017; Ndangui et al., 2010; Waiss et al., 2020). The finest fractions are generally richer in proteins, lipids, and minerals, whereas the largest particles contain more fibers and carbohydrates. It has been shown that bran of plants or cereals are harder to grind, leading to particles of greater size (Becker et al., 2016; Silva et al., 2011; Zaiter et al., 2016). Grinding conditions impact on powder water content: in fact, high-speed grinding induces friction of the solid material to be ground leading to temperature increase and subsequent water evaporation (Waiss et al., 2020).

Powder production processes and processing conditions specifically influence particle size and shape distributions. The origin of the raw material (animal or vegetal, liquid or solid) coupled with the impact of the processes influence the bulk and surface chemical composition (homogeneous or heterogeneous composition of particles of different size, composition gradients within single particles). These results in a large variability of powder physicochemical properties, which in turn results in a wide range of powder functional properties.

2.2. Powder functional properties

The various applications of food powders have led to define many functional properties in relation with their end-use: gelation or texturation, antioxidant activity, foamability, flowability, reconstitutability, preservation of nutritional quality during storage, etc. (Cayot and Lorient, 1997; Fournaise et al., 2020, 2021a; Neves et al., 2019; Scheidegger et al., 2013; Silva and O'Mahony, 2017).

2.2.1. Gelation

Food product texture is a very important attribute of organoleptic properties. Addition of powdered ingredients during food production process is often used to improve gelation or foaming properties and contribute to modulate food product texture (Cayot and Lorient, 1997; Sharma et al., 2012). Powder gelation properties are of utmost importance in the dairy industry for the production of yogurt and cheese. Protein powders are added to milk to control its gelation (which is related to denaturation and modifications of chemical structure of proteins caused by various mechanisms such as acidification, enzymatic hydrolysis, and/or heating) and textural properties of resulting dairy products (Cayot and Lorient, 1997; English, 1981; Lankveld, 1984; Sharma et al., 2012). Gelation ability and texturation are also important in the bakery industry; in this case, it is related to gelatinization and swelling power of starches, pea isolate, or chickpea flour (Miñarro et al., 2012). Polysaccharides such as xanthan gum or carrageenans are employed to enhance gel resistance (elasticity and hardness) and stability. Moreover, these polysaccharides are resistant to heating or freezing, unlike starch, making them particularly interesting in the food industry (Miller-Livney and Hartel, 1997; Yuan et al., 2019).

2.2.2. Foamability

Foaming properties of powders are employed for instant beverages (coffee, cappuccino, etc.) or desserts (ice cream, whipped cream, foam, etc.) (Deotale et al., 2020; Li et al., 2018; Sharma et al., 2012). Proteins or surfactants, through their surface-active properties, have the ability to stabilize water-liquid interfaces. Foam formation can result from two production methods: on one hand, gas (air, carbon dioxide, nitrogen, etc.) can be incorporated in the formulated food product by intense mixing or bubbling (Amagliani and Schmitt, 2017; Li et al., 2018; Weaire and Phelan, 1996); on the other hand, gas can be encapsulated in powdered ingredients, leading to gas release upon powder reconstitution when formulating the food product (Deotale et al., 2020; Illy and Navarini, 2011; Pugh, 2016). After foam generation, proteins or surfactants have the natural propension to migrate to water-air interfaces, leading to stabilization of the foam, thus limiting bubble coalescence and/or liquid drainage susceptible to destabilize the foam (Taisne, 1997). Other compounds may help stabilizing foams by increasing the viscosity of the liquid phase, such as polysaccharides (xanthan gum, carrageenans, etc.) or proteins (Dickinson, 2010; Mohanan et al., 2020).

2.2.3. Antioxidant activity

Antioxidant activity is an important functionality of powdered ingredients both for preservation purposes and formulation of food supplements. It is closely related to powder chemical composition. For example in dairy powders, some proteins like lactoferrin and bovine serum albumin are antioxidant due to their chelation ability and their content in amino acids such as tyrosine and cysteine that are able to reduce reactive oxygen species owing to their thiol groups (Scheidegger et al., 2013). Besides, dairy powders have sometimes been used as a solid matrix able to encapsulate antioxidant compounds (Neves et al., 2019; Waghmare, 2020). In this case, encapsulation of bioactive compounds can be viewed as a way to increase the antioxidant activity of powdered dairy ingredients. Other powders have noticeable antioxidant properties, especially plant-based powders issued from fruits and vegetables (Salehi and Aghajanzadeh, 2020). The main antioxidant compounds found in this kind of powders are anthocyanins, flavonoids, proanthocyanidins, and phenolic acids (Camire et al., 2007; Park and Chung, 2014; Salehi and Aghajanzadeh, 2020).

2.2.4. Flowability

The flowability of a powder designates the ability of individual particles to move independently from each other, which is notably related to powder compressibility and cohesion (Silva and O'Mahony, 2017). Powder flowability is very dependent on particle size and shape distributions, powder apparent density, and electrostatic interactions: particles of large size, having highly spherical shapes, and/or high density often flow better, and electrostatic interactions are unfavorable to flowability as they tend to increase powder cohesion. A high proportion of fine particles ($< 90 \mu\text{m}$) impairs flowability (Fournaise et al., 2020 ; Kim et al., 2005 ; Schuck et al., 2012). In addition, heterogeneous particle sizes often lead to the filling of the space between large particles by small ones, which increases interparticular friction and therefore decreases powder flowability. Particle shape also impacts on flowability, because at the same particle size, particles with a smooth surface and spherical shape flow more easily. Therefore, spray-dried whey protein powders, which have a more regular shape than spray-dried casein powders, have better flow properties (Silva and O'Mahony, 2017). Air trapped in particles decreases the apparent density and thus impairs flowability. For spray-dried particles, a low solid content of the feed concentrate, generally resulting in its low viscosity, induces the formation of particles with a large amount of occluded air and then numerous closed pores and a low powder apparent density (Crowley et al., 2014; Fournaise et al., 2020). Powder chemical composition, and more particularly surface composition, also has a huge influence on flow properties (Kim et al., 2005). A high water content induces a decrease in flowability, as a wet particle surface is generally stickier (Teunou and Fitzpatrick, 1999). Surface lipids are known to strongly reduce powder flowability, by making particles sticky at room temperature, which promotes adhesion of the particles to the surfaces with which they come into contact due to the low fusion temperature of lipids (Kim, 2008; Petit et al., 2017; Shrestha et al., 2007a). Increasing the lipid content also increases cohesion by creating hydrophobic interactions between particles, further reducing powder flowability (Silva and O'Mahony, 2017). Therefore, it is preferable to reduce powder lipid content as much as possible and select processing conditions so as to put lipids in crystalline form (Sharma et al., 2012). The use of additives such as flow agents by the reduction of cohesion or moisture absorbers (silicon dioxide, modified starches, etc.) can improve powder flowability (Schuck et al., 2012).

2.2.5. Reconstitutability

Powder reconstitution is of utmost relevance for industrial applications, considering that most powdered ingredients are reconstituted or extracted before use. Literature put in evidence the existence of four main reconstitution steps: wetting, sinking/swelling (which often occur simultaneously), dispersion (including breaking of lumps and agglomerates, along with fragmentation of individual particles), and solubilization (**Figure 22**). The main scientific obstacle is that these steps can hardly be isolated. Indeed, several reconstitution steps overlap at different time scales (Schubert, 1993) and the entire reconstitution mechanism is still complicated to state (Forny et al., 2011; Gaiani et al., 2006; Mitchell et al., 2015).

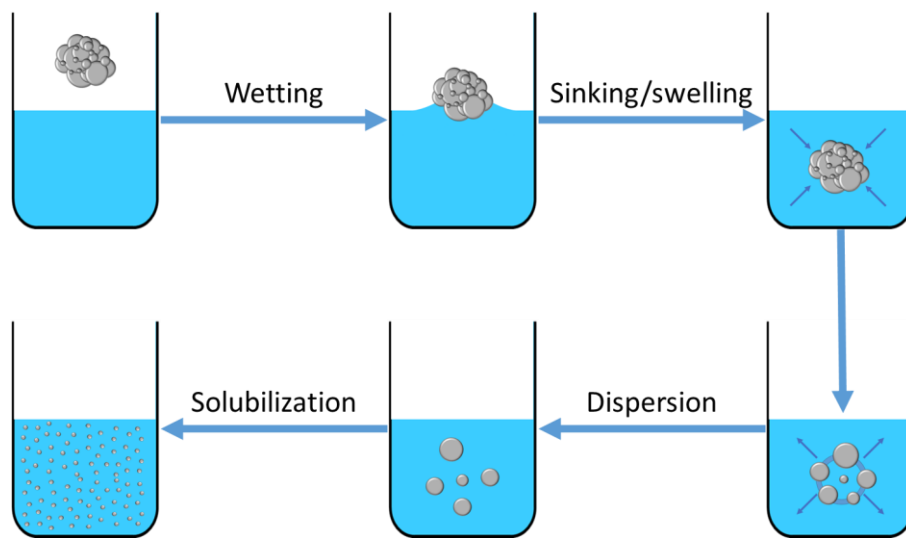


Figure 22. Reconstitution steps (wetting, sinking/swelling, dispersion, and solubilization) of a powder in a solvent (adapted from Forny et al., 2011).

2.2.5.1. *Wetting*

Powder wetting is the phenomenon defined by the replacement of the gaseous phase by water at the powder surface. It can be experimentally determined by using standard methods of the International Dairy Federation (IDF, 1987) developed for milk powders. Previous studies evidenced that powder wetting is more efficient for large particles (at least over 90 μm) or agglomerated powders (Fournaise et al., 2020, 2021a; Hogeekamp and Schubert, 2003; Schuck et al., 2012; Richard, 2012). High porosity and spherical particles also have a good wetting behavior (Hla and Hogeekamp, 1999; Ji et al., 2015). In addition to physical properties, chemical composition also has a great influence on powder wettability. For instance, high lipid or protein contents makes powder surface hydrophobic, leading to poor wettability and large contact angle measurement. Powder wettability can be related to the contact angles between particles and

liquid surface, as small contact angles are correlated to a good wettability (Young, 1805; Nijdam and Langrish, 2006; Schuck et al., 2012; Crowley, 2016; Wu et al., 2020). On the contrary, hydrophilic components located at powder surface like carbohydrates, sugars, or surfactants enhance its wettability (Hammes et al., 2015; Ji et al., 2017, 2015; Wu et al., 2020). The structural state of sugars is known to influence the wetting step. In fact, amorphous sugars at particle surface facilitate its interaction with water due to the formation of a largest number of hydrogen bonds with water and the absorption of water in their bulk. On the contrary, water can only adsorb at the surface of crystalline sugars by weak interaction forces and it does not immediately penetrate into their bulk, which results in well poorer wettability than amorphous sugars (Angelopoulou et al., 2021b; Puri et al., 2010; Szakonyi and Zelkó, 2012).

2.2.5.2. Sinking and swelling

Sinkability is defined as the ability of particles or particle agglomerates to sink below the water surface (Jiang et al., 2013). Sinking mainly depends on particle size distribution, porosity, and apparent density: as a general rule, large and/or high-density particles enhance sinking. However, large particles of high porosity (low density) exhibit higher sinking rate than small and low porosity (high density) particles, as sinking is favored by water capillary diffusion into inter- and intraparticle pores (Caric and Milanovic, 2002; Ji et al., 2017; Mitchell et al., 2019; Ong et al., 2021). Cohesive powders often sink in the form of lumps (cluster of dry particles trapped inside a viscous layer formed upon liquid-particle interaction) (Mitchell et al., 2015). The ability of powders to sink is also related to surface tension, buoyancy, liquid-particle contact angle, particle mass and density force. For example, if the contact angle exceeds a critical value, particle weight is not sufficient to overcome the effects of surface tension and buoyancy which are opposed to particle sinking, which results in the floating of particles and a poor wettability (Ong et al., 2019, 2021). The sinking can be improved by pouring powder in a liquid at high flow rate, owing to the increased particle velocity and kinetic energy upon impact with liquid surface (Ong et al., 2021). Additionally, particle swelling may occur depending on the chemical composition of particles, and this phenomenon can also result in the formation of lumps for cohesive powders (Forny et al., 2011; Jiang et al., 2013). Indeed, upon interaction with water, polymers of macromolecules (for food powders: mainly, proteins, starch, and fibers) contained in particles disentangle, resulting in a softening of the particle outer layers and an increase in their size, leading to particle size increase (Bonacucina et al., 2009; Conti et al., 2006; Cuq et al., 2011; Forny et al., 2011). Fibers and starches are known to induce significant swelling due to their hydrophilic behavior, contrarily

to proteins which are more hydrophobic and thus have a low swelling rate (Eastman and Moore, 1984; Gaiani et al., 2007; Kravtchenko et al., 1999; Lamberti et al., 2004; Parker et al., 2000).

2.2.5.3. *Dispersion*

Dispersibility is defined as the ability of a powder to disperse into water. Powder dispersion consists in two simultaneous mechanisms: desagglomeration which designates the disintegration of lumps and agglomerates into individual particles, and attrition which corresponds to the release of particle fragments by water-induced breaking (Fang et al., 2011; Forny et al., 2011; Mimouni et al., 2010). Both dispersion mechanisms lead to size reduction and specific surface area increase, further facilitating interactions of the solid matrix with water. Particle dispersion occurs when the cohesion between particle components (mainly by van der Waals interactions and hydrogen bonds) is overwhelmed by shear forces exerted by the liquid. Powders rich in proteins and/or lipids are known to be cohesive due to the hydrophobicity of these compounds (Cuq et al., 2011; Freudig et al., 1999; O'Mahony and McSweeney, 2016; Schuck et al., 2012). The dispersion rate is enhanced for high porosity, low density, or lowly cohesive particles (Fournaise et al., 2020; Goalard et al., 2006; O'Mahony and McSweeney, 2016).

2.2.5.4. *Solubilization*

Solubilization is often considered as the determinant reconstitution step as it is the final one (O'Mahony and McSweeney, 2016). The solubilization step encompasses the dissolution of soluble components and the homogenization of insoluble components in the liquid. This leads to the complete loss of particle structure and the final reconstituted product consists in a suspension of insoluble components in a solution of soluble ones (Gaiani et al., 2007; Marabi et al., 2008; O'Mahony and McSweeney, 2016). Complete powder solubilization leads to a homogeneous solution without insoluble particles, which is an important criterion for the consumer. The chemical composition is crucial for powder solubility. The presence of proteins is known to decrease the solubilization rate, as interactions between them should be broken before proteins may be solubilized. Also, it has been observed that intermicellar interactions of caseins significantly decrease the solubilization rate (Fang et al., 2011). Besides, fibers generally contribute to increase the solubilization rate, as soluble fibers are extremely hydrophilic and thus prone to solubilize, whereas insoluble fibers and starches are not susceptible to solubilize, which shortens the whole solubilization time (Gaiani et al., 2007; Kravtchenko et al., 1999; Yousefi et al., 2011). Powder solubilization is generally delayed by the presence of hydrophobic molecules at the particle surface (Lee et al., 2006). Based on

diffusive models, it can be stated that small particles may solubilize faster, owing to their higher specific surface area (Dokoumetzidis and Macheras, 2006; Nernst, 1904).

The identification of reconstitution steps (wetting, sinking/swelling, dispersion, and solubilization) highlighted the impact of physicochemical properties of the powders, such as particle size and shape distributions, bulk and surface chemical compositions, or density on the reconstitution. The identification of the reconstitution steps and the comprehension of the mechanisms of reconstitution made it possible to start many studies have tried to improve reconstitutability by focusing on the wetting, dispersion, and solubilization steps.

2.2.6. Powder reconstitution improvement

Reconstitution improvement is challenging for industrials, as the demand for powders that reconstitute quickly is increasing among consumers. Several approaches are employed to improve powder reconstitution through the choice of adequate pre- or posttreatments in the production process and modifications of product formulation by using additives. This part focuses on the main methods to improve the reconstitution.

2.2.6.1. *Processes used to improve powder reconstitutability*

Several methods have been developed to improve the wetting, dispersion, and solubilization steps by pretreatments (sonication, cavitation, etc.), formulation, or powder modification after production (agglomeration, coating, etc.) (Chandrapala et al., 2014; Dewettinck and Huyghebaert, 1999; Hla and Hoge Kamp, 1999; Knudsen and Skibsted, 2010; Lallbeeharry et al., 2014; Li et al., 2018; Oestergaard, 2016; Wu et al., 2020)

2.2.6.1.1. Pretreatments before powder production

In order to improve the reconstitution of dairy protein powders, application of shear stress to liquid concentrate prior to spray-drying using mechanical pretreatments (sonication, high pressure homogenization, or cavitation) has been studied. These pretreatments result in the diminution of concentrate viscosity and modification of protein assemblies: dissociation of whey/casein aggregates, dissociation of aggregates of denatured whey proteins, and/or solubilization of micellar caseins. The lower viscosity of the concentrate before spray-drying induces the formation of smaller particles (Chandrapala et al., 2014, 2012, 2011; Iordache and Jelen, 2003; Li et al., 2018). Smaller particles are known to impair wetting but improve solubilization.(Chandrapala et al., 2014, 2012; Fournaise et al., 2020; Li et al., 2018).

Chemical approaches such as carbonation associated with concentrate ultrafiltration are also employed to modify protein structure in dairy concentrates prior to spray-drying. The injection of carbon dioxide decreases the pH of dairy concentrates and modifies the interactions between proteins, more especially by modifying bounds between caseins and minerals. The content in minerals, in particular calcium phosphates, can be reduced by ultrafiltration in order to improve dairy powder reconstitutability. Indeed, the decrease in calcium phosphate content increases powder solubility by increasing casein micelle solubility (Marella et al., 2015; Sikand et al., 2013). Reducing the lipid content makes it possible to improve the reconstitution of the powders, for this pretreatment such as skimming of the concentrate before drying can easily reduce the lipid content (Schuck et al., 2012; Stocco et al., 2015).

2.2.6.1.2. Post-treatments of powders

Three main processes can be used to modify powders with a view to improve their reconstitutability: dry mixing, agglomeration, and coating (Angelopoulou et al., 2021b; Dewettinck and Huyghebaert, 1999; Dhanalakshmi et al., 2011; Schuck et al., 2012).

- Dry mixing

Dry mixing consists in mixing the powder for which reconstitution improvement is desired with a powder having excellent reconstitutability. This technique is very common in the food industry, for cocoa or whole milk powders for instance, because it is inexpensive and simple to set up, as described in section 1.1.1.3. (Cuq et al., 2013). Dry mixing with sugars makes it possible to improve powder wetting mainly, but also dispersion and solubilization to a lesser extent, because sugars located at the surface of powders are reconstituted quickly, thus favoring the contact between powders to be reconstituted and water. Micronized lactose can be used to cover the surface of whole or skim milk particles, facilitating powder wetting and sinking (Angelopoulou et al., 2021b, 2021a; Ben Abdelaziz et al., 2014).

- Agglomeration

Particle agglomeration is known to be efficient to improve powder wettability, dispersion, and solubilization. Indeed, the agglomeration process induces an increase in particle size and a modification of porosity and apparent density leading to an improvement of the wetting or sinking steps (Dhanalakshmi et al., 2011; Schuck et al., 2012). Powder agglomeration can be achieved by dry or wet granulation.

Dry granulation

Dry agglomeration can be achieved by two processes first, pressure agglomeration consists in compaction of particles resulting in the formation of a tablet. The main advantage of pressure granulation is the low cost of the equipment and the fact that it does not require any addition of a liquid binder, thus avoiding modification of the bulk composition. Pressure granulation is based on interparticular cohesion: the compaction first forces particles to rearrange in order to leave the least interparticular spaces, then breaks some particles, and finally induces consolidation of the structure of formed tablet (Dhanalakshmi et al., 2011; Snow et al., 1999).

Thermal agglomeration (heat sintering) consists in the heating of particles up to the melting point of compounds located at particle surface. At this temperature, sintering occurs: viscous bridges build between particles, resulting in powder agglomeration; then, the powder sample is cooled down under stirring in order to solidify bridges between particles constituting the aggregates (Dhanalakshmi et al., 2011; Omobuwajo et al., 2000).

Wet granulation

Wet agglomeration is based on the addition of a liquid binder “rewetting” the particles, making their surface sticky. The binder solution can be water, a solution of the same composition as the particles, or a binder with specific properties intended to improve powder reconstitution or flowability. Agglomeration increases the size and the number of pores of particles, which promotes wetting and dispersion (Barbosa-Cánovas and Juliano, 2005; Dhanalakshmi et al., 2011; Goldszal and Bousquet, 2001; Henry, 2013).

It can be performed in high-shear mixers, where the binder solution is sprayed on particles stirred in a mixing tank, or in fluidized bed agglomerators, where the spraying of a binder solution is carried out on particles fluidized by heated air. Binder spraying on particles to be agglomerated results in the spreading of binder droplets at particle surface, which makes it sticky. Then, particle collision makes them adhere to each other, resulting in the formation of larger particles which are dried by the heated fluidizing air (Dhanalakshmi et al., 2011; Gong et al., 2007). A similar agglomeration technique is performed in multi-effect spray-dryers, where the particles once dry are reinjected in the spray of droplets to induce their agglomeration (Schuck et al., 2012).

- Coating

Coating is another technique which allows the modification of particle surface using fluidized bed processes (**Figures 23, 24, and 25**); this is either used for encapsulation or reconstitution improvement purposes. Coating processes consist in the spraying of a liquid solution in a fluidized powder bed, which results in the deposition of a liquid layer at the surface of particles that is dried by the hot fluidized air.

Top-spray coating

The first developed coating technology was top-spray fluidized bed coating, in which the coating solution is sprayed with a vertical nozzle oriented toward the bottom of the equipment (**Figure 23**). The top-spray technology does not allow controlling the travelling time of sprayed droplets from the nozzle to particle surface, which causes an imperfect coating of particles due to droplet evaporation before their spreading at particle surface (Dewettinck and Huyghebaert, 1999, 1998; Jones, 1988).

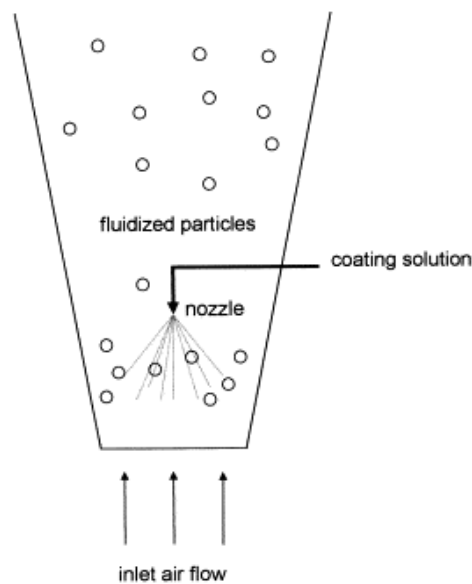


Figure 23. Principle of top-spray fluidized bed coating (Dewettinck and Huyghebaert, 1999).

Bottom-spray coating

The bottom-spray fluidized bed coating process (also called Wurster process) permits to improve the control of the coating process due to the recirculation of particles in the solution spray through the Wurster tube, resulting in the application of a fine layer of coating solution at particle surface (**Figure 24**). Also, with this equipment, the evaporation of the solution before its spreading at particle surface is reduced (Dewettinck and Huyghebaert, 1999; Mehta and Jones, 1985).

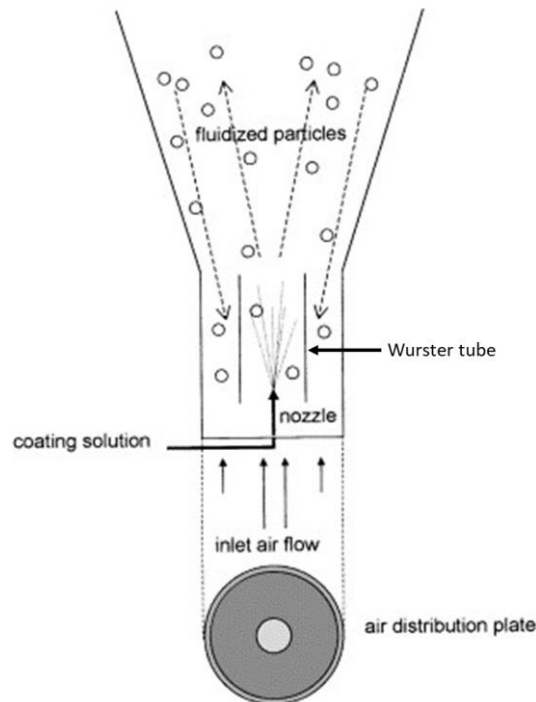


Figure 24. Principle of bottom-spray fluidized bed coating (Dewettinck and Huyghebaert, 1999).

Tangential-spray coating

The tangential-spray fluidized coating (also called rotary fluidized bed coating; **Figure 25**), permits to obtain a similar particle coverage efficiency as the bottom-spray fluidized bed coating without the necessity to use a Wurster tube (Dewettinck and Huyghebaert, 1999; Torres-Martinez et al., 2007).

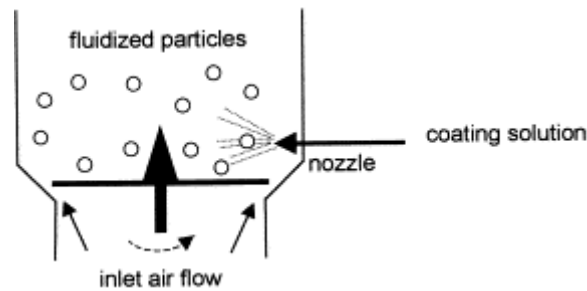


Figure 25. Principle of tangential-spray fluidized bed coating (Dewettinck and Huyghebaert, 1999).

Owing to the high cost of the coating process, it has first been used in the pharmaceutical industry (Dewettinck and Huyghebaert, 1999; Sauer et al., 2013; Thierry et al., 2007). Now, this process is employed to improve wetting of food powders such as dairy (skim milk powder and milk or whey protein isolates) or rice powders by coating with sugars (e.g., lactose, sucrose), maltodextrins, or lecithins (Dewettinck and Huyghebaert, 1999, 1998; Hammes et al., 2015; Ji et al., 2015; Li et al., 2017; Palamanit et al., 2016; Szulc and Lenart, 2013). Improvement of powder wettability is the result of the hydrophilicity of compounds deposited at particle surface (Ji et al., 2017, 2015; Szulc and Lenart, 2013). In addition, coating reduces surface porosity and particles are sometimes slightly agglomerated which further improves powder wettability by improving their water contact angle, thus facilitating the wetting step (Angelopoulou et al., 2021a; Ji et al., 2017, 2015; Szulc and Lenart, 2013; Turchiuli et al., 2013).

2.2.6.2. Additives for reconstitution improvement

2.2.6.2.1. Additives

There is a multitude of additives in the food industry dedicated to the improvement of powders functional properties, and more especially for reconstitutability enhancement. These additives can be divided into two main categories: surfactants and polysaccharides (disaccharides, sugars, etc.).

- Surfactants

Surfactants, such as lecithins or polysorbates, are molecules with the ability to reduce the surface tension between particle and a liquid interface, owing to their amphiphilic behavior, which results in an improvement of particle wetting and sinking (Kerwin, 2008; Rydhag and Wilton, 1981; Van Nieuwenhuyzen, 1976; Wu et al., 2020).

Lecithins are phosphatidylcholines, a group of phospholipids, which are composed of phosphoric acid, choline, glycerol esters, and two fatty acids. The fatty acid part depends on the origin, either animal or vegetable, for example egg white or soybean, respectively (**Figure 26**) (Scholfield, 1981; Van Nieuwenhuyzen, 1976).

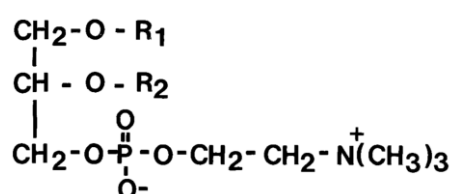


Figure 26. Chemical structure of lecithins, where R1 and R2 designate two fatty acids (Van Nieuwenhuyzen, 1976).

In the food industry, lecithins are used as stabilizers in emulsions or to improve the interaction with water of powders rich in lipids or proteins (Hammes et al., 2015; Ji et al., 2017; Lu et al., 2003; Rydhag and Wilton, 1981; Wendel, 2000). They can also be used as viscosity reducers leading to improvement of powder dispersion (Van Nieuwenhuyzen, 1976).

Polysorbates, also known by the trade name Tween®, are fatty acid esters of polyoxyethylene sorbitan (**Figure 27**), it is a surfactant used in the dairy and ice cream industry to stabilize emulsions (Kerwin, 2008).

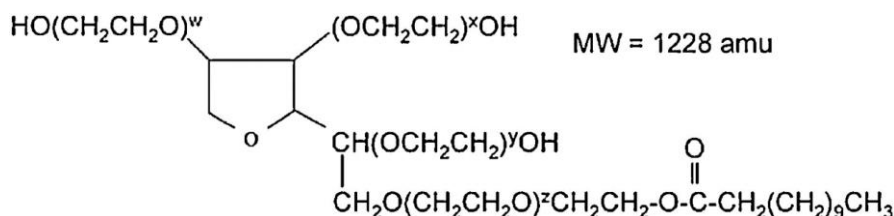


Figure 27. Chemical structure of polysorbates (Kerwin, 2008).

- Polysaccharides and sugars

Maltodextrins are a class of additives largely used in the food industry for their good solubility in water. They are polysaccharides of chemical formula $C_{6n}H_{(10n+2)}O_{(5n+1)}$ with n ranging from 2 to 20 (**Figure 28**).

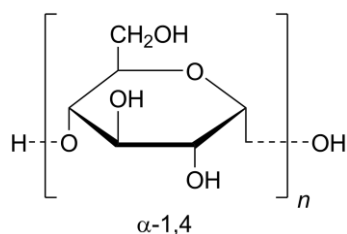


Figure 28. Chemical structure of maltodextrins, where n ranges between 2 and 20.

They are issued from starch hydrolysis by acids or the combination of acids and enzymes (Hobbs, 2009; Linden and Lorient, 1999). The level of starch hydrolysis is expressed by the dextrose equivalent (DE). A high DE means a high level of hydrolysis, resulting in a low molecular weight (Linden and Lorient, 1999; Nurhadi et al., 2016). The physicochemical properties of maltodextrins such as glass transition temperature, melting point, water sorption, water plasticization, or relaxation enthalpy directly depend on the DE. For example, the transition temperature varies from 140 °C for a DE of 20 to 180 °C for a DE of 5. Maltodextrins are specifically used in the powder field to increase the glass transition temperature, agglomerate particles, improve powder wettability, or reduce particle stickiness (Caliskan and Nur Dirim, 2013; Li et al., 2017; Potes et al., 2012; Turchiuli et al., 2013). The ability of maltodextrins to increase the glass transition temperature is particularly used for powders rich in amorphous sugars: for example, it has been demonstrated to reduce lactose crystallization in dairy powders which is favorable to their reconstitution (Li et al., 2017; Nurhadi et al., 2016; Roos and Karel, 1991).

- Sugars

Sugars, i.e. monosaccharides and disaccharides, are also employed as additives to improve powder reconstitution. Monosaccharides are isomers sharing the same chemical formula ($C_6H_{12}O_6$). The same is true for disaccharides ($C_{12}H_{22}O_{11}$), which are constituted by the association of two monosaccharides (Preedy, 2012). Isomers differ in physicochemical properties such as water solubility at saturation, melting point, sweetening power, glass transition temperature, rotary power, etc. (Brown and Pickering, 1897; Preedy, 2012; Roos,

1995, 2013). Disaccharides have higher glass transition temperatures than monosaccharides (Brown and Pickering, 1897; Preedy, 2012).

Glucose is a monosaccharide in pyran form (α -D-glucopyranose) with a glass transition temperature of 31 °C and a water solubility of 0.90 g/mL (Horton et al., 1994; Roos, 1995). Fructose is an isomer of glucose in furan form (β -D-fructofuranose) which is less stable, resulting in a lower glass transition temperature of 5 °C. Its water solubility is equal to 3.75 g/mL (Horton et al., 1994; Roos, 1995). Galactose is a monosaccharide in pyran form (α -D-galactopyranose) with a glass transition temperature of 30 °C and a water solubility of 0.68 g/mL (Roos, 1995; Tita-Goldstein, 2013) (**Figure 29**).

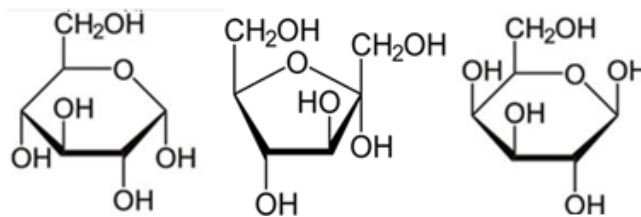


Figure 29. Chemical structure of some monosaccharides (left: glucose; middle: fructose; right: galactose).

Sucrose is a disaccharide (α -D-glucopyranosyl-(1 \rightarrow 2)- β -D-fructofuranoside) composed of glucose and fructose linked by a glycosidic bond α (1 \rightarrow 2). Its glass transition temperature and water solubility equal 74 °C and 2.02 g/mL, respectively (Horton et al., 1994; Simperler et al., 2006).

Lactose is a disaccharide (β -D- galactopyranosyl(1 \rightarrow 4)D-glucopyranose) composed of galactose and glucose linked by a β (1 \rightarrow 4) galactosidic bond, with a glass transition temperature of 100 °C and a water solubility of 0.22 g/mL (Haque et al., 2006; Roos, 1995; Tita-Goldstein, 2013) (**Figure 30**).

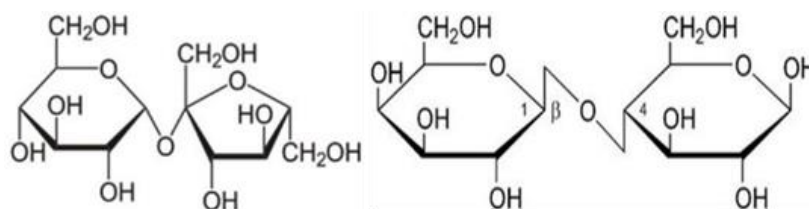


Figure 30. Chemical structure of two disaccharides (left: sucrose; right: lactose).

2.2.6.2.2. Mode of action of additives

Reconstitution can be enhanced by the incorporation of additives directly in product formulation prior to powder production or by powder coating with additives. Mostly used additives are high molecular weight hydrophilic polymers (e.g., maltodextrin, gum Arabic, starches, sodium carboxymethylcellulose, methylcellulose, hydroxypropylmethylcellulose), amphiphilic molecules (lecithins), and sugars (such as lactose or sucrose) (Hammes et al., 2015; Li et al., 2017; Wan et al., 1992; Yousefi et al., 2011; Li et al., 2017; Neves et al., 2019).

Surfactants have two modes of action depending on their location in the particle. When distributed in the whole particle bulk like for spray-dried particles, the emulsifying action of these compounds makes it possible to improve powder wetting and dispersion upon reconstitution by the reduction of surface tension (Hammes et al., 2015; Van Nieuwenhuyzen, 1976). However, when surfactants are coated at the surface of particles, it only improves powder wettability by reducing surface tension during the wetting steps, but does not improve the other reconstitution steps such as dispersion and solubilization (Lallbeeharry et al., 2014; Li et al., 2017; Wu et al., 2020).

Malto-oligosaccharides and sugars have also different modes of action depending on their location in the particles. When distributed in the whole particle bulk, they tend to improve powder wettability and the solubility owing to their hydrophilicity which facilitates water/particle interactions (Atalar and Yazici, 2019; Caliskan and Nur Dirim, 2013; Li et al., 2017; Turchiuli et al., 2013). Like surfactants, coating with sugars only improves the wetting step (Ben Abdelaziz et al., 2014; Ji et al., 2015; Szulc and Lenart, 2013; Wee et al., 2020). The physical structure (amorphous or crystalline) of sugars at the surface of coated particles has a great impact on the wetting and sinking steps. It was found that amorphous sugars improve wetting more than crystalline sugars (for lactose), but it is the opposite for the sinking step (Angelopoulou et al., 2021a, 2021b). The faster wetting of the amorphous state has been attributed to its greater hydrophilicity. Its delaying effect on sinking compared to the crystalline state was explained by a local increase in viscosity, resulting a slow capillary penetration of water into particles (Angelopoulou et al., 2021a, 2021b).

Two main approaches have been used to improve powder reconstitutability. On one hand, innovative processes have been developed to modify physicochemical properties of the raw material (pretreatments) or the particles (posttreatments), such as cavitation, sonication, agglomeration, etc, with a view to enhance their reconstitutability. On the other hand, additives can either be incorporated in the powder formulation or at the surface of particles by coating. Despite recent advances on the impact of coating on the interactions between particle surface and water during the first stages of reconstitution, further studies are still necessary to have a complete understanding of the phenomena occurring for the enhancement of powder reconstitutability.

2.3. Analytical methods for reconstitution monitoring and modelling of powder reconstitution steps

Despite the consensus on the identification of reconstitution steps, the determination of their kinetics still remains a challenge. Indeed, for some powders, wetting and dispersion steps may be almost instantaneous, precluding the possibility to determine their kinetics owing to limitations in acquisition frequency of analytical equipments. Also, some of the reconstitution steps may overlap (for instance, when the particle outer layer begins to solubilize before that dispersion or even swelling steps may have been finished), making it difficult to deconvolute the respective influences of each step (Forny et al., 2011).

2.3.2. Monitoring of powder reconstitution and characterization of reconstitution steps

Quick standard methods have been developed to characterize the aptitude of instant powders, especially dairy ones, to realize specific reconstitution steps (**Table 1**) (IDF, 1987; Schuck et al., 2012). These methods require adaptations to be used for other kind of powders (Deli et al., 2019; Fournaise et al., 2020). However, even if these methods are useful to evaluate powder reconstitutability, they do not allow to determine the kinetics of the whole reconstitution or each of its steps in given reconstitution conditions. Other techniques make it possible to characterize particular reconstitution steps (**Table 1**), such as wetting step with the sessile drop method which deals with the determination of the contact angle between a powder compact and a drop of solvent and then provides an indication of wettability (Galet et al., 2010; Janssen et al., 2006) or the capillary rise method, intended to measure the ability of solvents to rise through a powder bed by capillary forces and thus to determine powder surface energies that are also related to wettability (Goldszal and Bousquet, 2001).

Many direct and indirect approaches are available to identify powder reconstitution steps and characterize their kinetics during reconstitution assays performed in stirred tanks. The direct methods are able to follow the evolution of powder physicochemical properties upon reconstitution, such as particle size distribution, whereas indirect methods are designed to follow the evolution of physicochemical properties of the reconstitution medium, such as turbidity or viscosity (AFNOR, 2005; Bonacucina et al., 2009; Galet et al., 2004; Goalard et al., 2006; IDF, 1987; Li et al., 2013; Marabi et al., 2008).

2.3.2.1. Direct methods

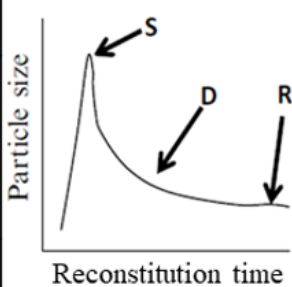
With direct methods, particle size is tracked once powder has sunk into the liquid until the end of its solubilization; the typical reconstitution profile obtained with direct methods is represented in **Table 1**. Classical methods for particle size monitoring in liquid solution are laser diffraction and image analysis (swelling, dispersion and solubilization steps or the erosion of insoluble particles). Laser diffraction analysis has a better resolution than image analysis. Both methods are limited by similar acquisition frequencies: few seconds are needed for each measure. Image analysis methods have the advantage to allow the simultaneous characterization of particle shape (Cannova et al., 2018; Karam et al., 2017, 2016; Merkus, 2009; Perez et al., 2017; Sun et al., 2019). The focused beam reflectance measurement (FBRM) is a technique based on the measurement of the chord length distribution, which is indirectly related to particle size, shape, number, and dispersion (Höpfner et al., 2010). The advantage of this method is the possibility to follow powder reconstitution in situ (in a mixing vessel) at high powder/water ratio (Fang et al., 2012, 2010; Mitchell et al., 2020). FBRM is adapted to follow dispersion and solubilization of lumps, aggregates, and particles (Fang et al., 2011; Mitchell et al., 2020).

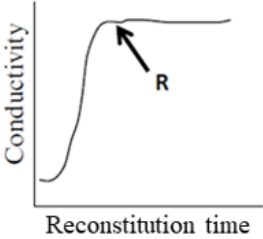
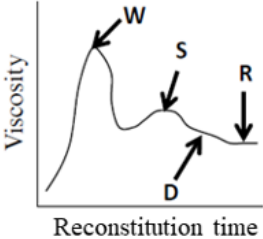
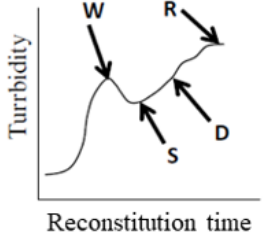
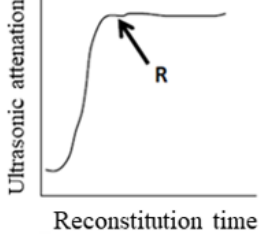
2.3.2.2. Indirect methods

Indirect methods are intended to follow physicochemical properties of the liquid suspension/solution during a reconstitution assay. The increase in ionic strength subsequent to powder component solubilization can be detected by conductimetry; unfortunately, reconstitution steps cannot be separated with this method. It still permits to determine the time needed to reach the end of the solubilization step, namely the reconstitution time (Crowley, 2016; Meyer et al., 2006; Mitchell et al., 2020). Turbidimetry evaluates the intensity of light transmitted through the sample which is related to the size and number of suspended particles. It can then be used to indirectly follow the reconstitution steps from wetting to solubilization, nevertheless its sensitivity is limited at high optical concentration, also called obscuration (cf.

Table 1) (Crowley, 2016; Hussain et al., 2012). Last, the evolution of dynamic viscosity of the suspension can be followed with a rheometer, which allows both working with a high powder-water ratio and identifying reconstitution steps (wetting, swelling, dispersion, and solubilization; **Table 1)** (Crowley, 2016; Gaiani, 2006; Rao, 2010).

Table 1. Advantages and drawbacks of the main methods of powder reconstitution monitoring (W: wetting, S: swelling, D: dispersion, R: reconstitution).

Methods	Measurement	Wetting	Swelling/ sinking	Dispersion	Solubilization	Reconstitution profile adapted from Crowley, 2016	Advantages and drawbacks	References
Normalized methods	Empirical	X	X	X	X	/	<ul style="list-style-type: none"> Empirical methods Require adaptations for non-instant powders 	Deli et al., 2019; George and Latimer, 2019; Fournaise et al., 2020
Sessile drop	Direct	X				/	<ul style="list-style-type: none"> Requires a smooth sample surface, i.e., the preparation of powder tablet 	Young, 1805; Janssen et al., 2006
Capillary rise	Direct	X				/	<ul style="list-style-type: none"> Repeatability impaired by the variability caused by sample preparation 	Galet et al., 2010; Sing and Williams, 2012
Laser diffraction	Direct		X	X	X		<ul style="list-style-type: none"> Accurate for small particle size Limited by low acquisition frequency and to low obscuration 	Mori et al., 2007; Merkus, 2009; Cannova et al., 2018; Jeantet et al., 2010
Image analysis	Direct		X	X	X		<ul style="list-style-type: none"> Allows shape characterization Limited by low acquisition frequency and to low obscuration Inaccurate for small particle size 	Mimouni et al., 2009; Perez et al., 2017; Sun et al., 2019; Richard et al., 2012
FBRM	Direct		X	X	X		<ul style="list-style-type: none"> High acquisition frequency Easy to implement Does not directly measure the particle size 	Kail et al., 2008; Fang et al., 2011; Mitchell et al., 2020

Conductimetry	Indirect		X	X	X		<ul style="list-style-type: none"> • Easy to implement • Requires the release of ions from powders • Does not allow the characterization of the wetting step 	Marabi et al., 2008; Mitchell et al., 2015; Crowley, 2016; Mitchell et al., 2020
Rheology	Direct	X	X	X	X		<ul style="list-style-type: none"> • Suitable for high powder/water ratio • Allows the identification of all reconstitution steps 	Ennis et al., 1998; Gaiani, 2006; Crowley, 2016; Rao, 2010
Turbidimetry	Indirect	X	X	X	X		<ul style="list-style-type: none"> • Allows the identification of all reconstitution steps • Suitable for low powder/water ratios only due to limitations of optical concentration 	Herri et al., 1999; Gaiani, 2006; Hussain et al., 2012; Crowley, 2016
Ultrasonic device	Indirect		X	X	X		<ul style="list-style-type: none"> • Allows the identification of gas release by powders • Does not allow the characterization of the wetting step 	Meyer et al., 2006; Povey et al., 2013; Crowley, 2016; Richard et al., 2012

2.3.3. Descriptive and predictive modelling of powder reconstitution

The development of descriptive models aiming at characterizing the kinetics of the reconstitution steps (wetting, sinking/swelling, dispersion, and solubilization) can be carried out from the reconstitution profiles acquired by monitoring techniques. Once kinetics of reconstitution steps can be characterized, predictive models can be investigated in order to link the kinetic parameters, especially durations, of reconstitution and its steps to powder physicochemical properties (bulk and surface chemical compositions, particle size and shape distribution, density, etc.) and reconstitution conditions (liquid temperature, stirring speed, geometry of the mixing tank, etc.).

2.3.3.1. *Empirical descriptive modelling of powder reconstitution kinetics*

In the literature, several models have been developed for the description of reconstitution kinetics of powders coming from various fields (food, pharmaceutical, cosmetics, etc.). These models were based on the monitoring of powder reconstitution by turbidimetry, conductimetry, or granulometry.

The major drawback of turbidimetry and conductimetry for the monitoring of powder reconstitution is that they are indirect methods which cannot be used to characterize the kinetics of all reconstitution steps. Turbidimetry is intended to evaluate the loss of intensity of transmitted light due to the scattering of particles suspended in a solvent (i.e. the change in absorbance of the suspension). It is indirectly related to the (insoluble) particle number and size distribution and cannot provide direct information on the kinetics of the various reconstitution steps, as it does not give direct access to the evolution of the physical characteristics of the particle population upon powder reconstitution. Conductimetry concerns the measure of solution conductivity and can then be used to follow the concentration increase of soluble powder components in a solvent upon powder reconstitution, which is related to the solubilization step only: conductimetry cannot provide information on the kinetics of powder wetting, sinking/swelling, and dispersion steps.

For these reasons, developed descriptive models for the fitting of reconstitution kinetics followed by turbidimetry and conductimetry were exclusively empirical and could only be used to characterize powder reconstitution in its globality (i.e. to identify the end of the solubilization step).

Turbidimetry curves obtained upon powder reconstitution have been fitted by first-order indicial response (**Equation 2**) (Galet et al., 2009).

$$X(t) = X_{\infty} \times (1 - e^{-\alpha t}) \quad \text{Equation 2}$$

With:

- X (-): normalized turbidity;
- X_{∞} (-), normalized turbidity reached at the final stage of the reconstitution;
- t (s), time;
- α (s^{-1}), “dispersion” kinetic rate.

Descriptive models dealing with component release from a matrix are generally not able to distinguish dispersion and solubilization steps. These models are based on the evolution of the concentration or the mass of dissolved solid, or the mass of remaining dry matter in particles (**Equations 3 and 4**).

$$C = \frac{M}{V} \quad \text{Equation 3}$$

With:

- C (kg/m^3), concentration of particle dry matter dissolved in the solvent at time t ;
- M (kg), mass of particle dry matter dissolved in the solvent at time t ;
- V (m^3), the volume of the solution.

$$M = W_0 - W \quad \text{Equation 4}$$

With:

- W_0 (kg), initial particle dry matter mass;
- W (kg), remaining particle dry matter mass at time t .

Peppas model is a simple empirical model (**Equation 5**) suitable to describe swelling and solubilization in a single kinetic model. The model parameter K mainly integrates the influence of powder size, shape, and physical structure, whereas the exponent n is more related to the dominant reconstitution mechanism, varying in the case of spherical particles from $n = 0.43$ for diffusion-controlled reconstitution to 0.85 for swelling-controlled reconstitution (Richard, 2012; Siepmann and Peppas, 2001).

$$\frac{M}{W_0} = K \times t^n$$

Equation 5

With:

- K (s^{-n}), model parameter expressing the kinetic rate;
- n (-), exponent related to the dominant reconstitution mechanism.

Another well-known semi-empirical model for the description of powder reconstitution curves is the Weibull function (**Equation 6**) (Richard, 2012; Zheng and Lu, 2011).

$$\frac{M}{W_0} = 1 - e^{-a \times t^b}$$

Equation 6

With:

- a (s^{-b}), first Weibull model parameter;
- b (-), second Weibull model parameter.

The Hopfenberg model is particularly interesting to describe the evolution of dissolved mass during the solubilization step as it takes in account the diminution of the area of water/particle interface using a shape factor (**Equation 7**) (Hopfenberg, 1976; Richard, 2012).

$$\frac{M}{W_0} = 1 - \left(1 - \frac{k_0 \times t}{\rho_0 \times d}\right)^s$$

Equation 7

With:

- k_0 ($kg/m^2/s$), mass transfer coefficient;
- ρ_0 (kg/m^3), particle apparent density;
- d (m), particle radius;
- s (-), shape factor: $s = 1$ for a disc, $s = 2$ for a cylinder, and $s = 3$ for a sphere.

The main issue with such semi-empirical models used to describe the reconstitution resides in the difficulty to link physical phenomena to model parameters (Richard, 2012; Zheng and Lu, 2011).

2.3.4. *Semi-empirical descriptive modelling of powder reconstitution kinetics*

Semi-empirical reconstitution models are based on physics equations, such as diffusion of a solid in a solution. They still necessitate the fitting of reconstitution curves and thus the determination of model parameters, but they are more appropriate for linking them to reconstitution phenomena and identifying the limiting reconstitution mechanism.

First, dispersion and solubilization of monocomponent powders were simultaneously considered through a diffusion model with the Noyes-Whitney equation (**Equation 8**) (Dokoumetzidis and Macheras, 2006; Noyes and Whitney, 1897), a first-order differential equation leading to a model for concentration in the form of a first-order indicial response. The limitation of this approach comes from the fact that it neglects the decrease in water/particle interface area (i.e. particle surface area) during solubilization (Richard, 2012), which is expected to lower the solubilization rate as the reconstitution progresses; in other words, k depends on C in a complex way that is not explicated in this equation. Thus, k should be fitted, leading to an averaged solubilization rate only representative for given experimental conditions.

$$\frac{dC}{dt} = k \times (C_s - C) \quad \text{Equation 8}$$

With:

- k (s^{-1}), solubilization rate,
- C_s (kg/m^3), saturating concentration of the compound in the solvent.

To improve the descriptive modelling approach using the Noyes and Whitney equation, Hixon and Crowell developed a model taking into account the particle size reduction upon reconstitution, leading to a decrease of particle surface area (**Equation 9**) (Hixon and Crowell, 1931).

$$-\frac{dW}{dt} = k_L \times A_0 \times \left(\frac{W}{W_0}\right)^{2/3} \times (C_s - C) \quad \text{Equation 9}$$

With:

- k_L (m/s), volumetric flux of the compound in the solvent;
- A_0 (m^2), initial area of water/particle interface (i.e. particle surface area);

- C_s (kg/m³), saturating concentration of the compound in the solvent.

Some improvements of the Hixon and Crowell model have been made by Wang and Flanagan (2002, 1999) by introducing the influence of particle size, porosity, and concentration gradient of the compound within the particle.

The Higuchi model, initially developed for the release of a component from matrix systems such as ointments, was adapted to describe the release of a component in a solvent (**Equation 10**) (Higuchi, 1961; Siepmann and Peppas, 2001).

$$\frac{M}{A} = \sqrt{D \times (2C_0 - C_s) \times C_s \times t} \quad \text{with } C_0 \gg C_s \quad \text{Equation 10}$$

With:

- A (m²), area of water/matrix system interface (i.e. total particle surface area in the case of powder);

- D (m²/s), mass diffusivity of the compound in the solvent;

- C_0 (kg/m³), compound concentration in the matrix system (such as ointment or powder);

- C_s (kg/m³), saturating concentration of the compound in the solvent.

2.3.3.2. Theoretical approaches for predictive modelling of powder reconstitution kinetics

Theoretical models focused on a single reconstitution step only have been developed based on physical characteristics (such as particle size) of monocomponent. Swelling of a single particle of super absorbent polymers (long hydrophilic chains of acrylic acid polymer) can be modelled using a physical approach (Diersch et al., 2011, 2010; Sweijen et al., 2017). The swelling of single particle is predicted by numerical methods which allows the determination of the swelling rate. The predictive model is based on mass transfer by diffusion based on Fisher's reaction-diffusion equation (Cabr e and Roquejoffre, 2009), in which coupled water diffusion and absorption result in an increase in particle density and size (Cabr e and Roquejoffre, 2009; Sweijen et al., 2017).

To the author's knowledge, no purely theoretical predictive model was developed for multicomponent powders such as food powders, presumably owing to the complexity of their structure and composition, along with multiplicity of reconstitution behaviors of their components.

2.3.3.3. *Empirical approaches for predictive modelling of powder reconstitution kinetics*

The prediction of reconstitution behavior of food powders from their physicochemical properties seems to have never been published. The majority of studies aim at improving reconstitutability by modelling the impact of reconstitution process conditions with a view to increase reconstitution efficiency for industrial purposes (Mitchell et al., 2015, 2020; Richard, 2012). The following modelling methods (PLSR, etc.) have never been used for predicting the reconstitution time of powders, however these models may be interesting for the development of a predictive model for reconstitution time of powders according to their physicochemical properties (Huffel and Lemmerling, 2013; Mevik and Cederkvist, 2004; Siepmann and Peppas, 2001; Van Huffel and Vandevallé, 1991; Woodbury, 2002; Zheng and Lu, 2011).

In order to link a great number of data relative to complex phenomena in which numerous variables could have a significant influence, several statistical approaches employed in various fields such as thermodynamics, analytical chemistry, or chemometrics have been developed.

Principal component analysis (PCA), an exploratory multivariate data analysis method, was initially developed by Pearson in 1901 (Jolliffe, 2005; Pearson, 1901). Its main objectives are to identify the groups of samples that share similar characteristics and the degree of correlation between sample characteristics. The PCA, which allows evidencing the parameters having the most influence on sample characteristics (i.e. inducing the most variability of sample characteristics), is often the first step for data analysis before proceeding with a multivariate approach to build a predictive model for sample characteristics (Geladi and Linderholm, 2020; Jolliffe, 2005).

Also, partial least squares regression (PLSR) is a multivariate technique used to develop predictive models. It generally requires performing a PCA to identify the main factors influencing a phenomenon, these factors are then used in the PLSR. Model parameters are calculated to maximize the covariance between two matrices: X, the matrix of predictor variables (known data), and Y is the matrix of dependent variables (experimental results) (Wold et al., 2001; Zheng and Lu, 2011).

Last, inverse modelling can also be used to develop a model to link predictor variables and dependent variables by least square regression (Huffel and Lemmerling, 2013; Van Huffel and Vandevallé, 1991; Woodbury, 2002). This technique is mainly used in the physics field, more specifically for heat flow modelling (Özisik and Orlande, 2021).

Many analytical techniques have been developed to monitor reconstitution kinetics. They all have advantages and drawbacks and are complementary to each other.

Descriptive models have been developed from experimental data to describe swelling or dispersion/solubilization based on empirical or semi-empirical models.

Until now, no universal predictive model has allowed the prediction of the reconstitution time of the powders. However, numerical models based on complex physical phenomena allow the prediction of swelling on monocomponent powders.

III. Material and methods

3.1. Investigated powders

3.1.1. Commercial powders

The reconstitution assays were carried out with thirty-six powders varying in chemical composition (water, lipid, protein, carbohydrate, and mineral contents), physical properties (particle size distribution, shape, porosity and density), structural properties (amorphicity/crystallinity), and manufacturing processes (spray-drying, drum-drying, freeze-drying, crystallization) (**Table 2**). This powder variety was considered with a view to study various types of reconstitution profiles. In order to get more data on the impact of particle size distribution on reconstitution, polenta and instant coffee were ground with an ultra-centrifugal mill (ZM 200, Retsch, France) using sieves with holes of 0.08 and 1.0 mm diameter at a low rotation frequency of 8 000 rpm in order to limit the heating of the grinding system as much as possible (Waiss et al., 2020).

Table 2. Chemical composition and manufacturing processes of investigated powders.

Powder sample name	Commercial name	Supplier (country)	Manufacturing process	Chemical composition (g/100 g on wet basis)					
				Proteins content	Lipids content	Carbohydrates content, sugars and fibers excluded	Sugars content	Fibers content	Minerals content
Polenta R (raw)	Polenta	Leclerc (France)	Grinding	7.7	2.0	77.5	6.8	2.8	0.01
Instant coffee R (raw)	Instant coffee	Carte d'Or (France)	Freeze-drying	21.1	6.2	42.6	0.0	8.2	9.2
Granulated sugar	Granulated sugar	Daddy (France)	Crystallization	0	0	0	100	0	0
Caster sugar	Caster sugar	Daddy (France)	Crystallization	0	0	0	100	0	0
Icing sugar	Icing sugar	Daddy (France)	Crystallization	0	0	0	99.9	0	0
Flour T45	T45 flour	Tablier Blanc (France)	Grinding	13.1	1.3	69.6	6.6	6.0	0.03
Flour T55	T55 flour	Leclerc (France)	Grinding	13.1	1.3	69.8	6.7	6.0	0.03
Cocoa 12F A-	12 % fat not alkalized cocoa	Bensdorp (U.S.A.)	Grinding	25.4	12.2	20.6	0.6	38.2	2.11
Cocoa 12F A+	12 % fat lightly alkalized cocoa	Bensdorp (U.S.A.)	Grinding	25.4	12.2	20.5	0.6	38.1	2.11
Cocoa 12F A+++	12 % fat highly alkalized cocoa	Bensdor. (U.S.A.)	Grinding	25.3	12.2	20.4	0.6	38.0	2.10
Cocoa 23F A+	23 % fat lightly alkalized cocoa	Bensdorp (U.S.A.)	Grinding	21.5	25.4	17.5	0.4	32.9	1.54
Pea fiber	Pea fiber	KG. GmbH & Co.. (Netherlands)	Grinding	10.0	0	30.2	4.8	49.9	3.00
SMP	Skim milk powder	Lactalis (France)	Spray-drying	33.5	1.5	0	55.2	0	8.38
SMPG	Granulated skim milk powder	Lactalis (France)	Spray-drying	33.5	1.5	0	55.2	0	8.38
WMP	Whole milk powder	Lactalis (France)	Spray-drying	31.7	23.9	0	37.7	0	5.97
MPI	Milk protein isolate	Ingredia (France)	Spray-drying	89.1	1.6	0	1.0	0	6.74
WPI	Whey protein isolate	Ingredia (France)	Spray-drying	89.2	1.0	0	5.7	0	2.61

MCP	Micellar casein powder	Ingredia (France)	Spray-drying	86	1.6	0	2.1	0	8.81
Hazelnut	Hazelnut powder	Leclerc (France)	Grinding	13.2	67.2	1.8	8.1	8.5	0.00
Instant mash	Instant mashed potatoes	Pom'Lisse (France)	Drying and grinding	8.1	0.6	78.3	2.5	8.4	0.08
Coarse salt	Coarse salt	Salinor (France)	Crystallization	0	0	0	0	0	99.98
Fine salt	Fine salt	Salinor (France)	Crystallization	0	0	0	0	0	99.98
Baking soda	Baking soda	La Baleine (France)	Crystallization	0	0	0	0	0	90.54
Couscous F	Fine couscous powder	Comptoir du Grain (France)	Grinding	13.2	2.0	76.3	3.2	2.6	0.04
Couscous M	Medium couscous powder	Comptoir du Grain (France)	Grinding	13.2	2.0	76.1	3.2	2.6	0.04
Acerola	Acerola cherry juice	SARL Européenne Extraction et Séchage (France)	Spray-drying	16.4	0	16.3	49.0	16.74	0.66
Xanthan gum	Xanthan gum	Louis François (France)	Drying	0	0	0	0	97.2	0
Agar agar	Agar agar	Louis François (France)	Drying	0	0	0	0	97.9	0
Pectin	Pectin	Louis François (France)	Drying	0	0	0	0	98.7	0
Yeast extract 1	Normal nucleotide extract	Unilever (Netherlands)	Drying	59.1	0.5	17.9	2.3	0	19.48
Yeast extract 2	High nucleotide extract	Unilever (Netherlands)	Drying	59.1	0.5	17.9	2.3	0	19.48
Onion	Onion powder	Unilever (Netherlands)	Drying	10.8	1.1	40.0	39.8	6.1	0.06
Lactose	Lactose powder	Sigma-Aldrich (France)	Drying	0	0	99.9	0	0	0

3.1.2. Coated powders

Whey proteins isolate (PRODIET 90 S, Ingredia, France) was coated with solutions prepared from sugar powders: sucrose (granulated sugar, Daddy, France), lactose (Sigma-Aldrich, Germany), glucose (Fisher Scientific, Germany), fructose (β Sigma-Aldrich, Germany), and galactose (Alfa Aesar, USA).

Coated powders were produced by a bottom-spray fluid bed coater (Mini-Glatt, Glatt GmbH, Deutschland) using the Wurster process. Coating solutions at 3 % dry extract (w/w) were prepared by reconstitution of sugars (sucrose, lactose, glucose, fructose, or galactose). Prior to coating, 200 g whey powder was heated at 50 °C by fluidization with an air relative pressure fixed at 0.2 bar during 10 min. After that, the coating assays were performed by injecting the coating solution at 0.8 g/s with a peristaltic pump (Fisherbrand variable-flow peristaltic pumps, Fisher Scientific) through the bi-fluid nozzle supplied with air at 0.5 bar relative pressure during 15, 30, 45, and 60 min for sucrose and 60 min only for other sugars. Control powders were obtained by carrying out the same coating process without any coating solution or by spraying distilled water in place of coating solution.

3.2. Physicochemical characterization

3.2.1. Particle size and shape distributions

Laser diffraction (Mastersizer S, Malvern Instruments Ltd, Malvern, UK) was used to evaluate particle size with a 5 mW He-Ne laser operating at 632.8 nm wavelength and a 300 RF lens. Dry dispersion was carried out with an Aero S air disperser module (Malvern Instruments Ltd). The analytical conditions were adapted for each powder: air pressure was fixed at 2 bar, feed rate between 30 and 60 %, and hopper length between 2 and 3 mm. The volume-equivalent sphere diameter was chosen as size estimator. Classical granulometric parameters D_{10} , D_{50} , and D_{90} , where D_x designates the diameter for which x % of the particles have a smaller size, were used to characterize particle size distributions. The width of particle size distributions was estimated by the span, calculated with **Equation 11** (Grossman and Cline, 1957; Hogg, 2008).

$$span = \frac{D_{90} - D_{10}}{D_{50}} \quad \text{Equation 11}$$

Particle shape was evaluated by image analysis with a QICPIC apparatus (Sympatec Inc., Clausthal-Zellerfeld, Germany). The powder was dispersed by the RODOS dispersion unit at 1 bar air relative pressure and the feeder set at 35 %. Shape parameters were calculated by

the PAQXOS software. The software calculates the diameter of a circle of equal projection area (EQPC), which corresponds to the diameter of a circle with the same the projection area of the particle area. Sphericity is defined by the ratio between the perimeter of a perfect circle and the real perimeter of the particle. Convexity evaluates the compactness of the particle by the ratio of the projection area of the particle and the projection of the convex hull. Aspect ratio is calculated as the ratio between maximal and minimal Feret diameters of the particle (Irie et al., 2021; Witt et al., 2007; Yu et al., 2011; Yu and Hancock, 2008).

3.2.2. Aerated density

Aerated density was measured with a FT4 powder rheometer (Freeman Technology, Worcestershire, UK) using a custom test. The powder bed was conditioned once in a 25 mm × 10 mL cylindrical vessel by the gentle displacement of a 23.5 mm blade downward and upward through the powder bed. Then, the vessel was split, which allows removing the excess powder in order to weight a precise volume (10 mL) of powder bed. The aerated density was calculated as the mass-to-volume ratio of the powder bed.

3.2.3. Glass transition temperature transition

Glass transition temperature analysis was carried out by differential scanning calorimetry (DSC SC 250, TA Instruments, Waters, France). 10.0 ± 0.5 mg powder was filled in a Tzero (TA Instruments, Waters, France) hermetic aluminium pan and equilibrated at -50 °C. They were heated from -20 °C to 100 °C at 10 °C.min⁻¹ to eliminate the sample thermal history, then cooling down to -20 °C. Last, samples were heated up to 100 °C and glass transition temperature was automatically detected by the software TRIOS (TA Instruments, France).

3.2.4. Bulk chemical properties

The bulk chemical composition (i.e. contents in water, lactose, lipids, proteins, and mineral) was experimentally determined for whole and skim milk powders only. For all other powders, the contents in macrocomponents were deduced from the technical sheets supplied by producers (**Table 2**).

3.2.4.1. *Water content*

The water content was determined by the mass loss of 2.5 g powder after drying at 103 °C during at least 3 h until stabilization of the sample mass following ISO 5537:2004 (AFNOR, 2004a).

3.2.4.2. *Water activity*

Water activity (a_w) was determined with a HygroPalm23-AW portable water activity-meter (Rotronic, France) in quick mode based on the **Equation 12** in a temperature-controlled room at 20 °C using a 3 cm powder layer following ISO 21807:2004 (AFNOR, 2004b).

$$a_w = \frac{P}{p^{sat}} \quad \text{Equation 12}$$

With:

- $a_w(-)$, water activity;
- P (bar), water vapor pressure of the sample;
- P^{sat} (bar), pure water vapor pressure.

3.2.4.3. *Protein content*

Protein content was determined with the Kjeldahl method. The nitrogen present in organic form in the sample was mineralized with sulfuric acid to form mineral nitrogen, i.e. ammonium ion (NH_4^+). The mineral nitrogen was converted in gaseous ammonia (NH_3) by action of sodium hydroxide NaOH and the mixture was distilled. The ammonia fraction of the distillate was recovered using a refrigerant. Then, it was diluted in boric acid solution and titrated to calculate the quantity of nitrogen in the sample. The protein content was determined from nitrogen content using a general conversion coefficient (protein-to-nitrogen mass ratio of 6.25) (Bradstreet, 1954).

3.2.4.4. *Lipid content*

Total lipids were quantified with a method adapted from Folch et al. (1957). 5 g powder was dissolved into a 2:1 (v/v) chloroform/methanol mixture. The mixture was stirred at 700 rpm during 15 min. Then, the solvent was separated by filtration on a sintered glass filter of 10 – 16 μm porosity and recovered in a round-bottom boiling flask that was previously dried and weighed. The solvent containing the lipids was removed with a rotary vacuum evaporator (Heidolph Laborator 4000) at low stirring and 40 °C. The flask without residual solvent was dried at 103 °C for 15 min for complete solvent evaporation and finally weighed.

3.2.4.5. *Mineral content*

Mineral content was performed by calcination of 2 g sample at 550 °C during 12 h, following normalized methods (ADPI, 2002; Waiss et al., 2020).

3.2.4.6. *Content in carbohydrates*

3.2.4.6.1. *Carbohydrates content*

Content in carbohydrates was calculated by difference with other components (George and Latimer, 2019).

3.2.4.6.2. *Sugars content*

The determination of sugars content was carried out for coated powders in order to measure the amount of sugar added during the coating process. Coated powders and standard solutions of sugars (sucrose, lactose, galactose, glucose, and fructose) were quantified with an adapted dinitrosalicylic (DNS) acid method (Sumner and Graham, 1922). The DNS reagent was prepared following Garriga et al. (2017) by mixing 1 g of 3,5-dinitrosalicylic acid (Sigma-Aldrich, Germany) in 20 mL of 2 M NaOH (Fisher Scientific, Germany) with 30 g of sodium-potassium tartrate tetrahydrate (Sigma-Aldrich, Germany) in 50 mL distilled water, and completing the volume of the mixture up to reach 100 mL. The first step of the DNS method consisted in acid hydrolysis of 1 g sample or 0.05 g standard in a 50 mL volumetric flask completed with 0.25 N sulfuric acid during 1 h at 50 °C in a thermostated bath. Then, 1 mL hydrolyzed sample mixture was added into a 15 mL tube with 2 mL DNS reagent to proceed the reaction in a dry bath at 100 °C during 5 min. To stop the reaction, 7 mL distilled water was added, then absorbance was read at 540 nm with a UV/visible spectrophotometer (UV-1280, Shimadzu, Japan). Calibration was carried out for each analyzed sugar from 0.01 to 1 g/L.

3.2.5. *Surface characterization*

3.2.5.1. *Surface imaging*

3.2.5.1.1. *Electronic microscopies*

SEM was used to image the shape of particles and the appearance of their surface at 200, 1 500, and 5 000 × magnifications. SEM analyses were performed under partial vacuum with a scanning electron microscope (Hitachi S-4800, Japan) operating at 1.0 kV acceleration voltage. Samples were prepared by sprinkling powder on a double-sided carbon tape and fixed on SEM stubs, then the powder was coated with carbon in a sputter coater (Polaron SC7640, Thermo VG Scientific, East Grinstead, United Kingdom).

ESEM was used to image surface appearance of sample particles at 2 000 and 3 000 × magnifications. ESEM analyses were performed under partial vacuum with an environmental scanning electron microscope (Quanta 600F, FEI Company, USA) operating at 10.0 kV acceleration voltage, at 500 Pa water vapor, and using a GSED (gaseous secondary electron

detector). Sample were prepared by storage in humidity-controlled oven (Climacell, MMM Medcenter, Germany), at 20, 40, and 60 % relative humidities at 25 °C during 1 h.

3.2.5.1.2. Atomic force microscopy

Surface imaging was carried out by AFM (Flex-Axiom, Nanosurf, Liestal, Switzerland) with the Nanosurf C3000 controller software. Samples were fixed on a circular glass slide by sprinkling the powder on a thin and regular layer of epoxy glue. Surface imaging (topography) was realized in contact mode at 25 °C in air on a measurement area of 10 μm × 10 μm (1 024 points) with a Stat0.2LauD cantilever (Nanosurf) with a spring constant of 0.2 N.m⁻¹. Particle roughness was calculated as the average roughness of three areas of 0.1 μm x 0.1 μm located on different particles with **Equation 13**.

$$S_a = \frac{1}{n} \sum_{i=1}^n |y_i| \quad \text{Equation 13}$$

Where y_i is the height measured by the piezoelectric scanner for a given pixel (i), and n the number of analyzed pixels.

3.2.5.2. Surface properties

3.2.5.2.1. Nanoindentation

Particle surface elasticity was determined by AFM (Flex-Axiom, Nanosurf) in nanoindentation mode at 25 °C in air on a measurement area of 10 μm × 10 μm with 1 024 points with a Dyn190AI cantilever (Nanosurf). The spring constant was determined using the thermal calibration method and the deflection sensitivity was calibrated on a hard surface (glass or silicon).

Thanks to the previously calculated spring constant, the cantilever deflection can be converted into a force thanks to the Hooke's law (**Equation 14**):

$$F = -k_c \times d \quad \text{Equation 14}$$

Where F is the Force (N), k_c the cantilever spring constant (N/m) and d deflection distance (m).

The Hertz model (**Equation 15**) was used to calculate the Young's modulus (elasticity) of particle surface from the 1 024 force curves to create elasticity maps with the ANA software (Nanosurf) (Adam et al., 2022; Hertz, 1882).

$$F(\delta) = \frac{2E \tan \alpha}{\pi (1-\vartheta^2)} \delta$$

Equation 15

With:

- F , the force (N);
- α , the semi-top angle of the tip (°);
- E , Young's modulus (Pa);
- δ , indentation depth (m);
- ϑ , the Poisson coefficient (-).

The change in surface elasticity of particles upon water uptake was studied by performing the measures at native humidity and after 1 h storage at 25 °C in humidity-controlled oven (Climacell, MMM Medcenter, Deutschland) at 20, 40, and 60 % relative humidities.

3.2.5.2.2. Powder surface composition characterization

XPS measurements are performed in ultra-high vacuum (10^{-8} Pa). Powder surface is irradiated by X-rays, which causes a complete transfer of X-ray photon energy to atomic electrons of the sample. When the electron binding energy E_b is lower than the photon energy $h\nu$, where h designates the Planck constant (6.63×10^{-34} m².kg.s⁻¹) and ν the radiation frequency (s⁻¹), an electron is emitted from the atom with a typical kinetic energy E_k related to E_b through **Equation 16**:

$$E_b = h\nu - E_k$$

Equation 16

Analyses were realized with a Kratos Axis Ultra (Kratos Analytical, Manchester, UK) X-ray photoelectron spectrometer with a monochromatic Al X-ray source at 150 W. The analytical area was about 700 $\mu\text{m} \times 300 \mu\text{m}$ and the analytical depth 10 nm. Powder samples were attached to a sample holder with double-sided conductive tape. XPS spectra were then recorded and treated using the Kratos Vision software. Quantification was performed using the photoemission cross-sections and transmission coefficients given in the Kratos Vision package. The main elements (C, O, N, P, and Ca) detected at the powder surface were identified by means of their respective binding energy. Also, the carbon peak was deconvoluted into its main chemical bonds (C-(C, H); C-(O, N); C=O; and O-C=O).

For milk powders, it was assumed that nitrogen was present only in proteins; therefore, surface composition in milk components (i.e. lactose, proteins, and lipids) could be calculated

from the relative atomic concentrations of carbon, oxygen, and nitrogen measured by XPS and the theoretical atomic composition of main components (Fournaise et al., 2020; Gaiani, 2006; Nijdam and Langrish, 2006; Nikolova et al., 2015) using **equations 17, 18, and 19**.

$$I^C = \alpha_p \times I^{C.P} + \alpha_{La} \times I^{C.La} + \alpha_{Li} \times I^{C.Li} \quad \text{Equation 17}$$

$$I^O = \alpha_p \times I^{O.P} + \alpha_{La} \times I^{O.La} + \alpha_{Li} \times I^{O.Li} \quad \text{Equation 18}$$

$$I^N = \alpha_p \times I^{N.P} + \alpha_{La} \times I^{N.La} + \alpha_{Li} \times I^{N.Li} \quad \text{Equation 19}$$

Where:

- I^C, I^O, I^N are the mole fractions of carbon, oxygen and nitrogen at the sample surface (these values were directly obtained by XPS from the peak areas of the $C_{1s}, O_{1s},$ and N_{1s});

- $\alpha_p, \alpha_{La}, \alpha_{Li}$ are the surface proportion of proteins, lactose and lipids;

- $I^{C.P}, I^{C.La}, I^{C.Li}$ are the mole fractions of carbon in proteins (P), lactose (La), and lipids (Li);

- $I^{O.P}, I^{O.La}, I^{O.Li}$ are the mole fractions of oxygen in proteins (P), lactose (La), and lipids (Li);

- $I^{N.P}, I^{N.La}, I^{N.Li}$ are the mole fractions of nitrogen in proteins (P), lactose (La), and lipids (Li).

3.3. Powder reconstitution behavior

3.3.1. Wettability evaluation

3.3.1.1. *Normalized method*

Wettability measurement was adapted from the IDF (1987) method: wetting time was defined in the current study as the time in seconds taken by 1.00 ± 0.01 g powder to become wet when deposited at the surface of 10.0 ± 0.1 g distilled water at 25°C in a 20 mL beaker under magnetic stirring at 600 rpm.

3.3.1.2. *Sessile drop method*

For application of the sessile drop method, powder samples were prepared by two different ways, either by compaction into pellets or sputtering in fine layer on double-sided tape (**Figure 31**) (Angelopoulou et al., 2021a; Lazghab et al., 2005).

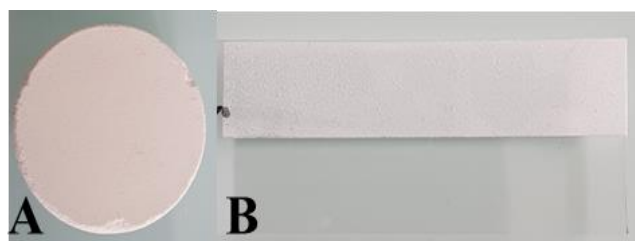


Figure 31. A- powder samples prepared by compaction into pellets and B- sputtering on double-sided tape.

Sessile drop measurements were performed with the experimental setup presented in **Figure 32**. A 1 μL drop of distilled water was deposited on the surface of the sample using a syringe. The drop was backlit and a CCD camera supplied with a zoom lens of 18 – 108 mm focal length permitted to capture images of the drop profile. Images were analyzed using the Optimas software (USA) in order to extract the coordinates of the drop profile. A software developed by Roques-Carmes et al. (2013) and based on Bashforth's equations allowed to calculate the apparent contact angle.

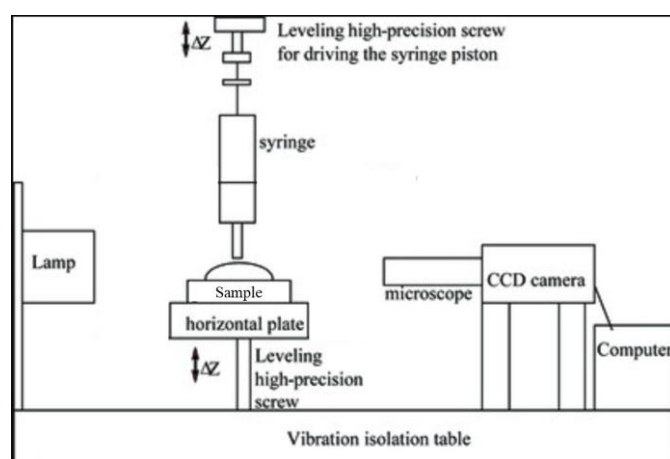


Figure 32. Experimental apparatus employed for the sessile drop method, adapted from Roques-Carmes et al., (2013).

3.3.1.3. *Capillary rise method*

Samples were prepared by pouring 500 ± 1 mg powder in a 1-cm diameter glass tube. The powder bed was tapped 200 times with a JEL STAV II jointing volumeter (J. Engelsmann AG, Germany) before evaluating the capillary rise with a tensiometer (K 100 tensiometer, Krüss GmbH, Germany) using ethanol at 25 °C. It would have been interesting to perform these analyses with distilled water as solvent, but measurements were prevented by the immediate filter clogging at the entrance of the glass tube. The wetting time corresponded to the time at

which the wetted sample mass measured by the tensiometer stabilized. The wetting velocity is the speed to wet the powder bed in the glass tube.

3.3.2. Monitoring of reconstitution kinetics

3.3.2.1. *Monitoring of reconstitution kinetics by conductimetry*

An experimental setup (**Figure 33**) was developed to follow powder reconstitution kinetics by conductimetry. It was constituted of a cylindrical jacketed glass 3 L reactor of 150 mm diameter (6010476, Grosseron, Germany) thermostated by a heated water bath (Eco Gold, Lauda, UK), a mechanical stirrer (ZR 2102 control, Heidolph, Germany), and a 5.08 cm diameter impeller (pitch blade turbine 2" 32Ra food grade finish, Fusion fluid equipment, USA). Powder reconstitution kinetics were followed by conductimetry (SevenCompact S230, Mettler Toledo, Switzerland) with a conductivity probe (InLab 731-ISM, Mettler Toledo, Switzerland) ranging from 0.01 to 1 000 mS.cm⁻¹. Powder was fed with a vibratory feeder (DR 100 Model, Retsch, France). Vessel design and reconstitution conditions were based on the literature, the objective was to mimic an industrial mixing tank (**Figure 33**) (Gaiani, 2006; Galet et al., 2004; Goalard et al., 2006; Mitchell et al., 2019, 2015; Schober and Fitzpatrick, 2005). Powder reconstitution experiments were performed with distilled water at 25.0 ± 0.2 °C in the following conditions: 10.0 % (w/w) powder/water mass ratios with a total mass (powder + water) fixed at 2.650 kg, 800 rpm stirring rate, and 3.6 g/s feed rate. Experiment duration ranged between 15 min and 2 h, depending on the time needed for conductivity stabilization for each powder.

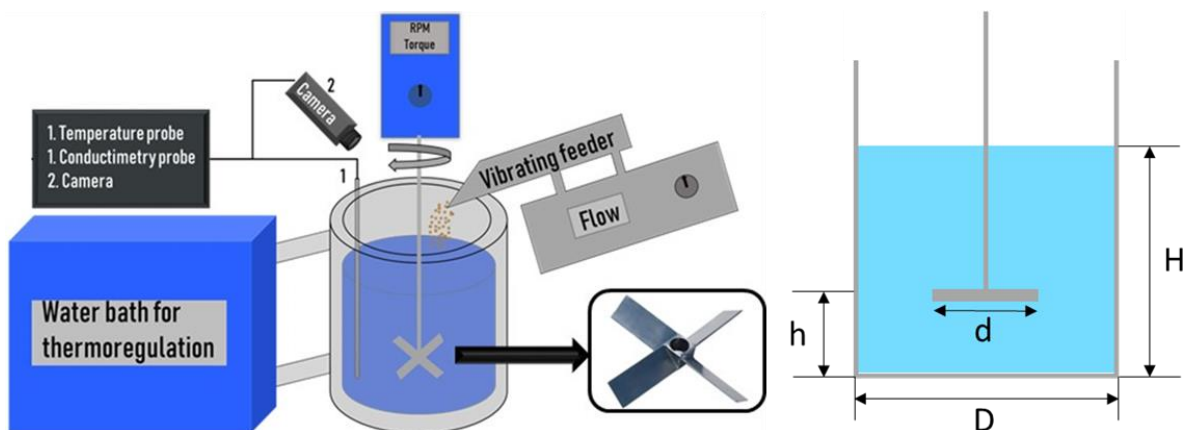


Figure 33. Experimental setup used for reconstitution experiments and schema of the geometrical characteristics of the A200 impeller and the cylindrical reactor (h:d:H:D of 1:1:3:3 with H = D = 150 mm and h = d = 50 mm) (Fournaise et al., 2021b).

3.3.1.1. Reconstitution kinetics monitoring by laser granulometry

The monitoring of food powder reconstitution kinetics was carried out with a laser diffraction granulometer (Mastersizer 3000, Malvern Instruments Ltd, UK) using wet dispersion. Reconstitution conditions were similar for all powders: 0.1 g powder was quickly poured into 125 mL distilled water at 25 °C in the Hydro MV module (Malvern Instruments Ltd, UK) stirred at 2 000 rpm. Powder reconstitution was followed until reaching D50 stability, i.e., for durations ranging from 15 min to 2 h depending on the investigated powder, by acquiring one measurement on both lasers every 5 s. The curve displaying the temporal evolution of the median particle size D50, called reconstitution curve hereafter, was built by averaging results obtained for three replicates of reconstitution assays. **Figure 34** displays the reconstitution curve obtained for instant mashed potatoes powder as an example.

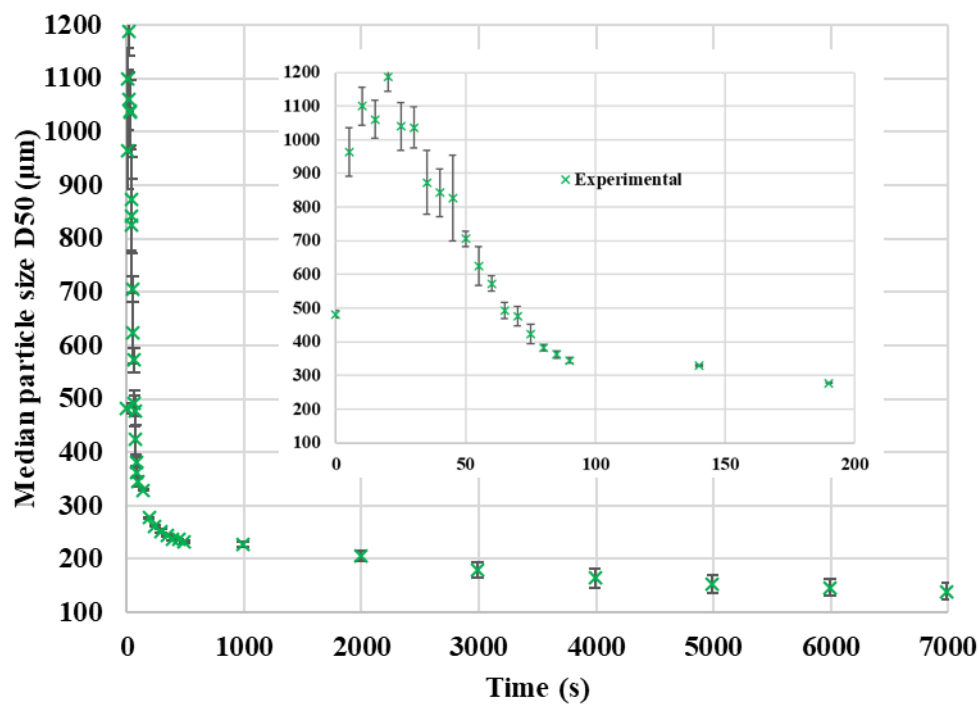


Figure 34. Example of reconstitution curve of instant mashed potatoes powder.

3.4. Modelling of powder reconstitution

3.4.1. Descriptive modelling of powder reconstitution kinetics

3.4.1.1. Descriptive modelling of reconstitution kinetics followed by conductivity

3.4.1.1.1. Conductivity normalization

Upon powder reconstitution, conductivity evolved from an initial value of 0 $\mu\text{S}/\text{cm}$ (real value inferior to the conductimeter sensitivity) to a final value that depended on powder nature (**Figure 35**).

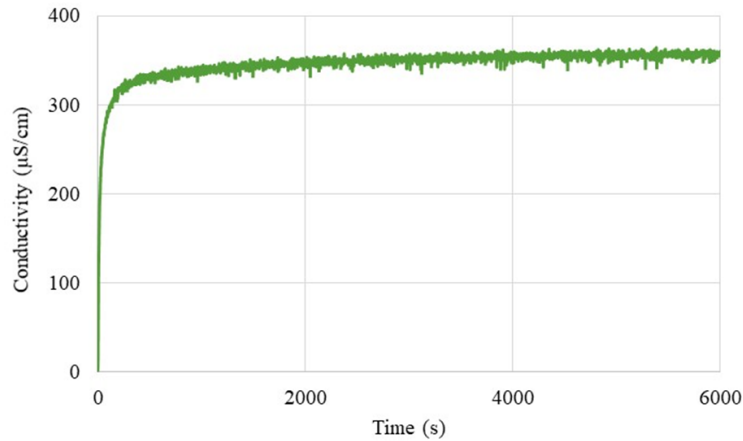


Figure 35. Raw conductivity curve of milk protein concentrate.

Therefore, to be able to fit conductivity curves and determine reconstitution times, conductivity values, averaged from the three experimental replicates, were normalized following **Equation 20**:

$$c(t) = \frac{\kappa(t) - \kappa_{ini}}{\kappa_{fin} - \kappa_{ini}} \quad \text{Equation 20}$$

Where:

- $c(t)$ designates normalized conductivity (-);
- $\kappa(t)$ stands for conductivity at time t ($\mu\text{S}\cdot\text{cm}^{-1}$);
- κ_{ini} represents the initial conductivity, i.e. distilled water conductivity (close to $0 \mu\text{S}\cdot\text{cm}^{-1}$);
- κ_{fin} corresponds to the final conductivity ($\mu\text{S}\cdot\text{cm}^{-1}$).

Consequently, all normalized conductivity curves started at 0 and ended at 1. These curves had a sigmoidal shape (**Figure 36**) which can be related to the different steps of powder reconstitution:

- first, upon powder wetting/swelling and sinking, very few powder components were solubilized and conductivity increased very slightly over a rather long time;
- then, powder dispersion and solubilization occurred, leading to a marked conductivity increase;
- finally, as the amount of powder to be solubilized became low, conductivity still increased but evolved more slowly, until reaching the final conductivity once all soluble powder material has solubilized.

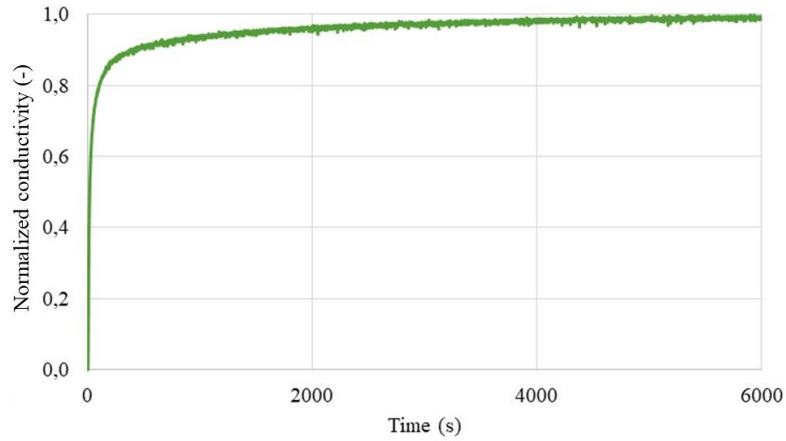


Figure 36. Normalized conductivity curves of milk protein concentrate.

3.4.1.1.2. Curve fitting

The normalized conductivity curves were fitted with the OriginPro 2019 software (OriginLab Corporation) using the least squares method solved by the Levenberg Marquardt iteration algorithm. It was found that the Hill model (**Equation 21**) was the most suitable and simple model to fit normalized conductivity curves of all powders (Hill, 1910):

$$c(t) = c_0 + (c_\infty - c_0) \frac{t^n}{k^n + t^n} \quad \text{Equation 21}$$

With:

- c_0 , initial normalized conductivity (-);
- c_∞ , final normalized conductivity (-);
- t , time (s);
- k (s) and n (-), Hill model time constant and power, respectively.

For all powders, initial and final normalized conductivity being equal to 0 and 100 %, respectively, the Hill model could simply be rewritten as (**Equation 22**):

$$c(t) = \frac{t^n}{k^n + t^n} \quad \text{Equation 22}$$

Model parameter k corresponds to the time needed to reach 50 % normalized conductivity. The slope of normalized conductivity curve at $t = k$ was found equal to $\frac{n}{4k}$, then it can be considered that the model parameter n gives an indication of the powder reconstitution rate once wetted, swelled, and sinked, i.e. in the dispersion and solubilization steps. Last, powder reconstitution time was deduced from obtained Hill model by taking the time needed to reach 95 % normalized conductivity, it was then noted $t_{95\%}$ and expressed in seconds.

3.4.1.2. *Descriptive modelling of reconstitution kinetics by laser granulometry*

The median particle size is expected to increase during the wetting and sinking/swelling steps (abbreviated in swelling step hereafter), then to decrease in the dispersion and solubilization steps at different kinetic rates, corresponding to a slope change in the reconstitution curve. For some investigated powders such as instant mashed potatoes powder (**Figure 37A**), the observation of reconstitution curves (with temporal axis in logarithmic scale for a better identification of times at which slope changes occurred) allowed to identify the successive predominance of the three main reconstitution steps. This reconstitution behavior was called the first reconstitution type and could be described by the model developed in this section.

Some powders, for instance T45 flour (**Figure 37B**), exhibited no particle size increase at the beginning of the reconstitution assay, because no swelling occurred, or it was too insignificant or too quick to be accurately monitored by laser granulometry. These powders were considered to belong to the group of second reconstitution type and their reconstitution could also be modelled using the approach of the present section.

For some powders like small couscous (**Figure 37C**), a swelling step was present in reconstitution curves, but no significant slope change was detected. This may happen with powders for which:

- one of the dispersion or solubilization steps was too quick to be accurately monitored by laser granulometry,
- one of the dispersion and solubilization steps overwhelmed the impact of the other step,
- or powders for which dispersion and solubilization steps had similar kinetics.

This reconstitution behavior was named the third reconstitution type and the model developed in the section 4.3.1. was also able to describe its kinetics.

For instant coffee (**Figure 37D**), reconstitution occurred too quickly to be accurately monitored by laser granulometry owing to acquisition frequency limitations. In this case, defined as the fourth reconstitution type, reconstitution steps could not be distinguished, and the modelling approach developed in the section 3.4.1.2.1. was not suitable to evaluate reconstitution kinetics.

The fifth reconstitution type was defined for powders leading to accurate reconstitution curves but too complex to be modelled by the descriptive modelling approach of the current section, which decouples the three main reconstitution steps but is not able to take into account multiple kinetics for a given step. Among investigated powders, this was the case for milk protein isolate (**Figure 37E**) for which the reconstitution curve exhibited a first increase, then a first decrease, followed by a second increase and a second decrease.

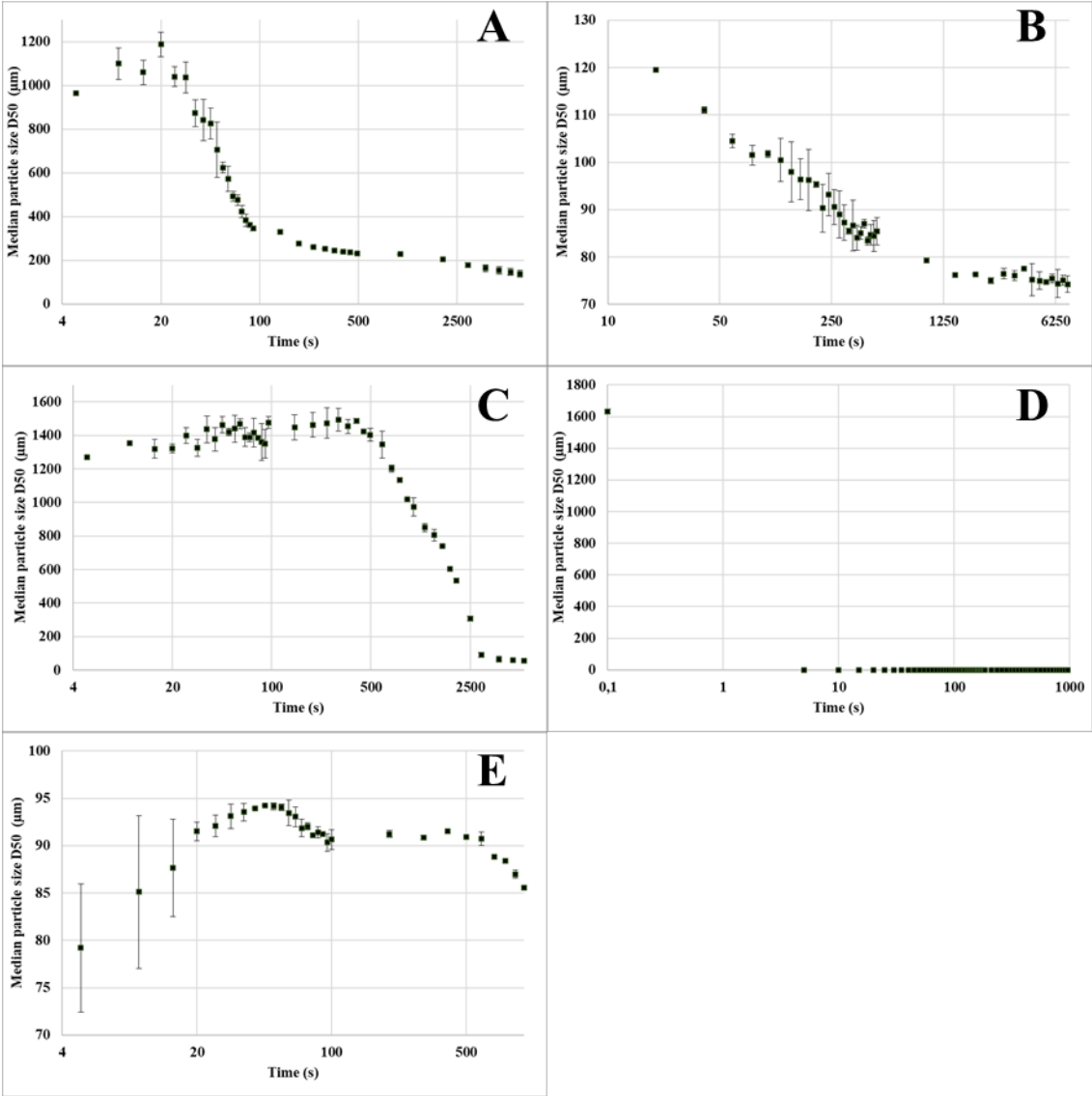


Figure 37. Reconstitution curves obtained by monitoring or reconstitution assays with laser granulometry, with temporal axis in logarithmic scale. (A) instant mashed potatoes powder (first reconstitution type); (B) T45 flour (second reconstitution type); (C) small couscous (third reconstitution type); (D) instant coffee (fourth reconstitution type); (E) MPI (fifth reconstitution

type). Error bars indicate standard deviations obtained with three replicates of reconstitution assays; some, inferior to the marker size, are not visible.

3.4.1.2.1. Descriptive model of particle size evolution upon reconstitution

The aim of the descriptive modelling approach developed in this study was to determine a single-equation model able to describe the temporal evolution of the median particle size D50 upon reconstitution. This model was intended to identify the kinetics of each of the three main reconstitution steps detected on reconstitution curves, namely swelling, dispersion, and solubilization steps. A sum of three first-order indicial responses (**Equation 23**) was employed with the objective to link each first-order indicial response to a single reconstitution step.

$$D50(t) = D50_0 + A_0 \left(1 - e^{-\frac{t}{\tau_0}}\right) - A_1 \left(1 - e^{-\frac{t}{\tau_1}}\right) - A_2 \left(1 - e^{-\frac{t}{\tau_2}}\right) \quad \text{Equation 23}$$

Where:

- $D50_0$ (μm): modelled initial median particle size at wet state;
- A_0 (μm): amplitude of the increasing first-order indicial response (swelling step);
- τ_0 (s): time-constant of the increasing first-order indicial response (swelling step);
- A_1 (μm): amplitude of the first decreasing first-order indicial response (dispersion step);
- τ_1 (s): time-constant of the first decreasing first-order indicial response (dispersion step);
- A_2 (μm): amplitude of the second decreasing first-order indicial response (solubilization step);
- τ_2 (s): time-constant of the second decreasing first-order indicial response (solubilization step).

For powders of the first reconstitution type, model parameters were expected to be all different from zero, whereas A_0 was fixed at 0 μm for powders of the second reconstitution type (then, the descriptive model led to a sum of two decreasing first-order indicial responses), and A_2 was fixed at 0 μm for powders of the third reconstitution type (then, the descriptive model led to a sum of two first-order indicial responses, the first one increasing and the other one decreasing).

The reconstitution curves of powders of first, second, and third reconstitution types were fitted with the Excel solver (Microsoft 365) using the least squares method solved by the generalized reduced gradient algorithm. Direct fitting of the whole reconstitution curve with **Equation 23** was judged unsatisfactory for many reasons:

- sometimes, the fitting method did not converge,
- when fitting was achieved, modelled initial median particle size at wet state $D50_0$ was often inferior to the median particle size at dry state, which was not physically sound,
- and/or calculated durations of each reconstitution step seemed to be unrelated to what could be deduced from the observation of reconstitution curves.

Thus, a descriptive modelling approach that was successful for all powders of first, second, and third reconstitution types and led to physically-sound and consistent estimations of initial median particle size at wet state and durations of each reconstitution step was developed. First, the increasing and decreasing parts of the reconstitution curves were separately fitted; then, the complete model was fitted by using the first estimation of model coefficients deduced by separate fittings for the initialization of model parameters.

For first and third reconstitution type powders, the increasing part of the temporal evolution of the median particle size from its initial value to its maximal value, corresponding to the predominance of the swelling step, was fitted with an increasing first-order indicial response (**Equation 24**) by specifying the constraint that the modelled initial median particle size $D50_0^*$ should be superior or equal to the median particle size at dry state. Indeed, at the beginning of reconstitution, it was considered that particles could have swelled or agglomerated (upon wetting and immersion) but their size could not be smaller to the dry median particle size, as no significant erosion or solubilization was expected in such a short water-contact time (few seconds). The fitting procedure performed with the Excel solver was initialized with the median particle size at dry state for $D50_0^*$, and rough graphical estimations of the extent of median particle size evolution and the time needed for this evolution for A_0 and τ_0 , respectively.

$$D50(t) = D50_0^* + A_0 \left(1 - e^{-\frac{t}{\tau_0}} \right) \quad \text{Equation 24}$$

Where $D50_0^*$ (μm) stands for the modelled initial median particle size D50 using **Equation 24** only.

For powders of the second reconstitution type, for which no swelling was observed, this part of the modelling approach was obviously not performed.

The decreasing part of the temporal evolution of the median particle size, from its maximal value to its final value, corresponding to the dispersion and solubilization steps, was modelled by the sum of two decreasing first-order indicial responses (**Equation 25**) for powders

of the first and second reconstitution types (for which a slope change was observed in the decreasing part of the reconstitution curve). The fitting procedure performed with the Excel solver was initialized with the experimental maximal median particle size for $D50_1$, and rough graphical estimations of the extents of median particle size evolution and the times needed for these evolutions during dispersion and solubilization steps for A_1 , τ_1 , A_2 , and τ_2 , respectively.

$$D50(t) = D50_1 - A_1 \left(1 - e^{-\frac{t}{\tau_1}}\right) - A_2 \left(1 - e^{-\frac{t}{\tau_2}}\right) \quad \text{Equation 25}$$

Where $D50_1$ (μm) designates the modelled initial median particle size $D50$ using **Equation 24** only.

The same equation was employed with A_2 fixed at $0 \mu\text{m}$ for third reconstitution type powders (for which no distinction could be made between dispersion and solubilization steps), leading to a single decreasing first-order indicial response.

Then, the whole reconstitution curve was fitted with **Equation 23** by using the model parameters obtained by separate fitting with **Equations 24 and 25** ($D50_0^*$, A_0 , τ_0 , A_1 , τ_1 , A_2 , and τ_2) to initiate the fitting procedure performed with the Excel solver. As previously indicated, A_0 was fixed at $0 \mu\text{m}$ for powders of the second reconstitution type and A_2 was fixed at $0 \mu\text{m}$ for powders of the third reconstitution type. Obtained model parameters ($D50_0$, A_0 , τ_0 , A_1 , τ_1 , A_2 , and τ_2) were then used to calculate characteristic swelling, dispersion, and reconstitution times, as well as swelling, dispersion, and solubilization rates.

3.4.1.2.2. Estimation of the duration and the particle size evolution rate of each reconstitution step

The swelling time t_{swelling} was defined as the time for which the predominance of the swelling mechanism ends. When applicable, it was calculated as the time at which modelled median particle size reached its maximal value $D50_{\text{max}}$. This was determined with the Excel solver as the lowest time value for which the first derivative of $D50(t)$ (**Equation 26**) was equal to zero.

$$\frac{dD50(t)}{dt} = \frac{A_0}{\tau_0} e^{-\frac{t}{\tau_0}} - \frac{A_1}{\tau_1} e^{-\frac{t}{\tau_1}} - \frac{A_2}{\tau_2} e^{-\frac{t}{\tau_2}} \quad \text{Equation 26}$$

Thus, the maximal median particle size $D50_{\text{max}}$ was equal to $D50(t_{\text{swelling}})$ and the duration of the swelling-dominated reconstitution phase $\Delta t_{\text{swelling}}$ was equal to t_{swelling} .

The dispersion time $t_{\text{dispersion}}$, when applicable, was calculated as the time for which the absolute difference between experimental values and the reconstitution model considering that the swelling step was completely ended (i.e., it has induced an increase in the median particle size up to $D50_0 + A_0$) and taking into account the influence of the dispersion step only $D50_0 + A_0 - A_1 \left(1 - e^{-\frac{t}{\tau_1}}\right)$ became superior to the absolute difference between experimental values and the reconstitution model considering that the swelling and dispersion steps were completely ended (i.e., they have induced an evolution of the median particle size up to $D50_0 + A_0 - A_1$) and taking into account the influence of the solubilization step only $D50_0 + A_0 - A_1 - A_2 \left(1 - e^{-\frac{t}{\tau_2}}\right)$. Thus, the duration of the dispersion-dominated reconstitution phase $\Delta t_{\text{dispersion}}$ was equal to the difference between the dispersion and swelling times ($t_{\text{dispersion}} - t_{\text{swelling}}$).

The final median particle size $D50_{\infty}$ was equal to the limit of $D50(t)$ when the time tends to the infinity, i.e., $D50_0 + A_0 - A_1 - A_2$. It was chosen to define the reconstitution time as the time needed to reach 95 % of the median particle size decrease in the dispersion and solubilization steps (**Equation 27**).

$$D50(t_{\text{reconstitution}}) = 95 \% \times D50_{\infty} + 5 \% \times D50_{\text{max}} \quad \text{Equation 27}$$

Hence, the duration of the solubilization-dominated reconstitution phase $\Delta t_{\text{solubilization}}$ was equal to the difference between the dispersion and swelling times ($t_{\text{solubilization}} - t_{\text{dispersion}}$).

Characteristic particle size evolution rates during swelling, dispersion, and solubilization steps were calculated as slopes at half height of the considered reconstitution step using the first derivative of $D50(t)$ (**Equation 26**) and the Excel solver for the determination of half-height times of each reconstitution step:

- the swelling rate (positive value) was defined as the value taken by first derivative of $D50(t)$ at the time (inferior to t_{swelling}) when modelled $D50$ reached $\frac{D50_0 + D50_{\text{max}}}{2}$,

- the dispersion rate (negative value) was calculated as the value taken by first derivative of $D50(t)$ at the time (comprised between t_{swelling} and $t_{\text{dispersion}}$) when modelled $D50$ reached $\frac{D50_{\text{max}} + D50(t_{\text{dispersion}})}{2}$,

- and the solubilization rate (negative value) was the value taken by first derivative of $D50(t)$ at the time (superior to $t_{\text{dispersion}}$) when modelled $D50$ reached $\frac{D50(t_{\text{dispersion}}) + D50_{\infty}}{2}$.

3.4.1.3. Predictive modelling of powder reconstitution time

This part deals with the development of an empirical model to predict the reconstitution time using the laboratory-scale mixing vessel and the reconstitution conditions used for monitoring of reconstitution kinetics by conductimetry (cf. section 3.4.1.1.1.). To this aim, predictors, i.e. input data in the model, were the main powder physicochemical properties influencing powder reconstitution (namely, median particle size, proximal composition, and surface hydrophobicity) identified from principal components analysis in section 4.1. and extra powder characteristics (particle sphericity, convexity, aspect ratio, and aerated density). All investigated powders were considered in this part of the PhD work with a view to obtain an empirical model able to apply to all kinds of food powders, regardless of their wetting and reconstitution behavior.

Several approaches were used with the purpose to predict the reconstitution time from experimental values calculated as $t_{95\%}$ from Hill model applied on conductivity curves obtained in reconstitution assays. Reconstitution times predicted from models were noted $t_{reconstitution}$.

As regards predictors taken as model input data (most influencing powder physicochemical properties and few extra characteristics), they were either considered unnormalized, i.e. numerical values of predictors expressed in their SI unit, or converted into normalized values where 0 % correspond to the minimal value of the considered predictor among investigated powders and 100 % to its maximal value. Normalization was expected to confer the same variation range to all predictors, which could facilitate modelling and help interpreting obtained models, as discussed later in section 4.4.

As regards models, five types were employed (Leube, 2013; Zheng and Lu, 2011) : a multilinear model (**Equation 28**), a monome model which consist in a product of power laws (**Equation 29**), an exponential model composed of a product of exponential laws (**Equation 30**), an hybrid model in the form of a product of power and exponentials laws, and partial least square regression.

Multilinear (**Equation 28**), monome (**Equation 29**), exponential (**Equation 30**) and hybrid (mixed power and exponential laws) models were determined with the Excel solver (Microsoft 365) using the generalized reduced gradient algorithm for solving the least squares method, consisting in the search for the collection of model weights permitting to minimize the sum of quadratic errors $\sum_{i=1}^n (t_{95\%,i} - t_{reconstitution,i})^2$ where n represents the number of

observations, i.e. the number of investigated powders, and i designates an integer varying from 1 to n .

$$t_{reconstitution,j} = w_0 + \sum_{j=1}^m w_j x_{i,j} \quad \text{Equation 28}$$

$$t_{reconstitution,j} = w_0 \times \prod_{j=1}^m (x_{i,j} + 10^{-4})^{w_j} \quad \text{Equation 29}$$

$$t_{reconstitution,j} = w_0 \times \prod_{j=1}^m \exp(w_j x_{i,j}) \quad \text{Equation 30}$$

With:

- m , the number of predictors,
- j , an integer varying from 1 to m ;
- w_0 and w_j , model weights;
- $x_{i,j}$, predictor variables, i.e. most influencing physicochemical properties and few extra characteristics, for the i^{th} observation, i.e. investigated powder.

To avoid obtaining a null value of predicted reconstitution times for powders having one of their physicochemical property equal to 0 (sugar content for instance), 10^{-4} (consisting in a very small value compared to numerical values of considered physicochemical parameters) was added to each $x_{i,j}$ in the monome model.

Partial least square regression was performed with the Galaxy software (ChemFlow 20.05) using the NIPALS regression algorithm. The method establishes correlations between predictors to reduce the set of model input data to a minimum number of latent variables which are independent, gather the maximum of predictor variability, and permit to make predictions of dependent variables while taking into account the maximum of their variability (**Equations 31 and 32**). In the case of the PhD work, the number of dependent variables was equal to 1 (as reconstitution time was the only variable to be predicted by investigated empirical models).

$$X = TP^T + E \quad \text{Equation 31}$$

$$Y = UQ^T + F \quad \text{Equation 32}$$

Where X , the matrix of predictor variables ($n \times m$); Y is the matrix of dependent variables ($n \times p$); m , the number of predictors; n , the number of observations; p , the number of dependent variables (equal to 1 in the current PhD work); T , the matrix of X scores ($n \times l$); P , the matrix

of X loadings ($1 \times m$); E, the residual matrix of X ($n \times m$); U the matrix of Y scores ($n \times 1$); Q the matrix of Y loadings ($1 \times m$); F the residual matrix of Y ($n \times p$); l, the number of latent variables (permitting to achieve the best model accuracy).

In the matrix of predictor variables X, columns correspond to the different predictors (most influencing powder physicochemical properties deduced in section 4.1. and few extra characteristics) and rows to the different observations, i.e. investigated powders. The matrix of dependent variable Y is constituted by a single column giving, for each observation (investigated powders), the reconstitution times deduced from reconstitution kinetics monitored by conductimetry. T and P matrices express the links between predictors and latent variables. In E, the matrix of X residuals, columns correspond to the part of predictor variability not taken into account by latent variables and rows to the different observations. U and Q matrices express the links between dependent and latent variables. In F, the matrix of Y residuals, columns correspond to the part of variability of dependent variables not taken into account by the model and rows to the different observations.

PLSR can be seen as a multilinear regression (**cf. Equation 28**), also called OLSR (ordinary least squares regression), for which the inputs are latent variables instead of predictor variables.

3.5. Statistical analysis

All analyzes were carried out on the thirty-six powders and performed in triplicate except for some XPS analysis ($n = 2$ or 1). PCA was used to link powder physicochemistry and manufacturing process to reconstitution behavior using Unscrambler (CAMO software AS, Norway). Reconstitution assays were triplicated to ensure good analytical repeatability and obtain good accuracy of descriptive reconstitution models. Some analyses were performed $n = 9$ for coated powders to ensure that there is no difference between the 3 batches produced by formulation ($n = 3$ per batch). The duration and the median particle size evolution rate of each reconstitution step were correlated with powder physicochemical properties by calculating Pearson's correlation coefficients with Microsoft 365 Excel ($p < 0.05$). Data were compared by one-way ANOVA performed with Microsoft 365 Excel and means were separated by Tukey's HSD test at Excel $p < 0.05$ significance level.

IV. Results and discussion

4.1. Main powder physicochemical characteristics influencing their reconstitution behavior

This part seeks to identify the main physicochemical properties (composition, structure, etc.) of food powders influencing their reconstitution and their impact on the different reconstitution steps.

Thirty-six food powders corresponding to a wide range of physicochemical characteristics (bulk and surface chemical composition, median particle size, span, and water activity) and manufacturing processes (grinding, freeze-drying, spray-drying, and crystallization) were investigated for their reconstitutability. Their reconstitution profiles were acquired by conductivity measurements and fitted with Hill model. Physicochemical characteristics of investigated powders were correlated to their wetting and reconstitution times by principal component analysis. Four powder categories were identified on the basis of wetting and reconstitution times; i.e. green group (good reconstitution); yellow (correct reconstitution), orange groups (mediocre reconstitution); red group (poor reconstitution). Long wetting times were associated with high particle surface hydrophobicity, small median particle size, as well as high protein and lipid contents in the powder bulk. Long reconstitution times were linked to the powder manufacturing process (ground powders), as well as to low sugar content in the powder bulk.

4.1.1. Impact of particle size distribution and lipid content on powder reconstitution

To highlight the impact of particle size distribution and lipids content on powder reconstitution behavior, a focus was carried out on instant coffee and milk powders.

4.1.1.1. *Powder physicochemical properties*

Raw and ground instant coffee powders presented similar chemical composition and differed in median particle size D_{50} (around 1 630 μm and 31 μm , respectively) (**Tables 2 & 3**). Raw instant coffee powder had a monomodal particle size distribution with a span around 1, which was consistent for an agglomerated powder, whereas the particle size distribution of ground instant coffee powder was bimodal with a span around 13. On the opposite, skim and whole milk powders differed in chemical composition and presented similar median particle sizes D_{50} (around 80 μm) and monomodal particle size distributions (**Tables 2 & 3**). Skim milk

powder presented a low lipid content (1.5 g/100 g on wet basis), whereas whole milk powder was rich in lipids (26 g/100 g on wet basis).

Table 3. Proteins, lipids, carbohydrates (fibers excluded), fibers, and minerals content ranges*, median particle size, as well as C/O and C-C/other C bonds ratios at the particle surface for investigated powders.

Powder sample name	Proteins content range (-)	Lipids content range (-)	Carbohydrates (fibers excluded) content range (-)	Fibers content range (-)	Minerals content range (-)	Median particle size D50 (μm)	C/O ratio	C-C/other C bonds ratio (-)
Polenta R (raw)	3	3	2	3	4	642 \pm 23	3.97 \pm 0.10	1.29 \pm 0.26
Polenta 1.0 mm	3	3	2	3	4	392 \pm 19	3.82 \pm 0.13	1.09 \pm 0.01
Polenta 0.08 mm	3	3	2	3	4	20 \pm 0	3.06 \pm 0.00	1.00 \pm 0.00
Instant coffee R (raw)	2	3	3	2	2	1 633 \pm 15	2.80 \pm 0.01	0.92 \pm 0.03
Ground instant coffee	2	3	3	2	2	31 \pm 0	2.62 \pm 0.01	0.93 \pm 0.02
Granulated sugar	4	4	1	4	4	583 \pm 16	1.61 \pm 0.08	0.21 \pm 0.02
Caster sugar	4	4	1	4	4	451 \pm 35	1.59 \pm 0.15	0.40 \pm 0.03
Icing sugar	4	4	1	4	4	23 \pm 1	1.60 \pm 0.01	0.27 \pm 0.02
Flour T45	3	3	3	2	4	83 \pm 0	4.17 \pm 0.06	1.47 \pm 0.02
Flour T55	3	3	3	2	4	76 \pm 0	4.19 \pm 0.09	1.54 \pm 0.06
Cocoa 12F A-	2	2	3	1	3	13 \pm 0	4.29 \pm 0.10	2.12 \pm 0.10
Cocoa 12F A+	2	2	3	1	3	12 \pm 0	4.51 \pm 0.09	2.31 \pm 0.23
Cocoa 12F A+++	2	2	3	1	3	11 \pm 0	4.68 \pm 0.53	2.34 \pm 0.31
Cocoa 23F A+	2	2	3	1	3	34 \pm 0	5.09 \pm 0.40	2.80 \pm 0.46
Pea fiber	2	3	3	3	3	56 \pm 0	3.04 \pm 0.09	0.99 \pm 0.01
SMP	2	3	3	4	2	77 \pm 0	2.52 \pm 0.05	0.70 \pm 0.08
SMP G	2	3	3	4	2	167 \pm 1	2.71**	0.67**
WMP	2	2	3	4	2	80 \pm 0	3.38 \pm 0.13	1.02 \pm 0.01
MPI	1	3	4	4	2	54 \pm 0	4.06**	1.08**
WPI	1	3	4	4	2	45 \pm 1	4.00**	0.90**
MCP	1	3	4	4	2	54 \pm 0	3.90**	1.41**
Hazelnut	3	1	3	2	4	512 \pm 19	6.65 \pm 0.31	4.02 \pm 0.06
Instant mash	3	3	2	2	4	614 \pm 11	3.44 \pm 0.31	1.11 \pm 0.24
Coarse salt	4	4	4	4	1	1 910 \pm 42	5.05 \pm 1.01	4.79 \pm 0.26

Fine salt	4	4	4	4	1	604 ± 12	4.98 ± 0.38	4.25 ± 0.54
Baking soda	4	4	4	4	1	183 ± 1	1.57 ± 0.19	1.67 ± 0.12
Couscous F	3	3	2	3	4	975 ± 5	4.97**	1.25**
Couscous M	3	3	2	3	4	1 830 ± 2	4.23**	1.34**
Acerola	4	4	2	4	4	38 ± 1	1.78**	0.35**
Xanthan gum	4	4	4	1	4	89 ± 0	1.33**	0.21**
Agar gum	4	4	4	1	4	108 ± 2	1.66**	0.18**
Pectin	4	4	4	1	4	142 ± 3	1.51**	0.25**
Yeast extract 1	1	4	4	4	2	554 ± 5	0.67**	2.74**
Yeast extract 2	1	4	4	4	2	119 ± 1	0.83**	3.14**
Onion	3	3	2	2	4	58 ± 1	2.91**	0.87**
Lactose	4	4	1	4	4	34 ± 0	1.60**	0.27**

* Ranges of macromponent contents were defined as follows: range 1 corresponded to contents between 0 and 25 g/100 g on wet basis, range 2 to 25 - 50 g/100 g, range 3 to 50 - 75 g/100 g, and range 4 to 75 - 100 g/100 g from powder data sheet.

**Analyses were carried out on a single area of 700 µm × 300 µm.

The water contents of coffee and milk powders were comprised between 1.6 and 2 g/100 g on wet basis and their water activity ranged between 0.16 and 0.34 (**Table 4**), which is favorable to their preservation (George and Latimer, 2019; Roos, 2002).

Table 4. Water activity, water content, wetting time, reconstitution time, and Hill model parameters (k and n) of investigated powders.

Powder sample name	Water activity a_w (-)	Water content (g/100 g on wet basis)	Wetting time (s)	Reconstitution time t_{95} (s)	Hill model time constant k (s)	Hill model power n (-)
Polenta R (raw)	0.59 ± 0.01	3.17 ± 0.03	127 ± 5	$2\ 107.7 \pm 223.2$	33.7 ± 2.4	0.72 ± 0.04
Polenta 1 mm	0.55 ± 0.00	3.04 ± 0.10	67 ± 3	$1\ 075.8 \pm 99.5$	17.6 ± 1.6	0.72 ± 0.01
Polenta 0.08 mm	0.47 ± 0.00	2.43 ± 0.11	352 ± 10	432.1 ± 14.7	45.9 ± 7.7	1.31 ± 0.09
Instant coffee R (raw)	0.16 ± 0.00	1.65 ± 0.18	22 ± 2	38.9 ± 2.3	12.8 ± 0.6	2.16 ± 0.08
Ground instant coffee	0.38 ± 0.00	2.05 ± 0.05	51 ± 4	106.5 ± 6.8	26.7 ± 3.7	2.15 ± 0.31
Granulated sugar	0.48 ± 0.00	0.02 ± 0.00	17 ± 1	34.7 ± 1.1	8.9 ± 0.2	1.15 ± 0.28
Caster sugar	0.48 ± 0.00	0.02 ± 0.00	8 ± 1	25.2 ± 3.8	3.7 ± 0.6	1.55 ± 0.21
Icing sugar	0.49 ± 0.00	0.10 ± 0.01	25 ± 3	47.5 ± 4.2	13.9 ± 0.7	2.66 ± 0.16
Flour T45	0.55 ± 0.00	3.35 ± 0.13	51 ± 4	777.1 ± 64.0	15.6 ± 1.3	0.74 ± 0.02
Flour T55	0.54 ± 0.00	3.05 ± 0.06	52 ± 4	683.8 ± 65.4	14.6 ± 1.1	0.78 ± 0.05
Cocoa 12F A-	0.27 ± 0.00	0.91 ± 0.00	207 ± 17	948.8 ± 103.9	99.5 ± 9.0	1.31 ± 0.02
Cocoa 12F A+	0.30 ± 0.00	1.10 ± 0.14	156 ± 7	516.2 ± 47.2	69.5 ± 4.4	1.47 ± 0.04
Cocoa 12F A+++	0.36 ± 0.00	1.41 ± 0.03	95 ± 7	197.5 ± 28.7	47.9 ± 6.4	2.15 ± 0.47
Cocoa 23F A+	0.18 ± 0.00	0.76 ± 0.03	115 ± 13	363.3 ± 62.3	38.0 ± 5.5	1.31 ± 0.13
Pea fiber	0.44 ± 0.00	2.16 ± 0.04	93 ± 8	197.6 ± 14.5	46.8 ± 7.5	2.06 ± 0.25
SMP	0.34 ± 0.00	1.46 ± 0.00	35 ± 4	75.4 ± 0.7	16.4 ± 1.1	2.08 ± 0.22
SMP G	0.34 ± 0.00	1.48 ± 0.03	6 ± 2	80.0 ± 10.0	27.3 ± 2.9	2.58 ± 0.20
WMP	0.23 ± 0.00	1.78 ± 0.02	68 ± 8	112.0 ± 10.4	36.2 ± 5.3	2.76 ± 0.13
MPI	0.25 ± 0.00	1.59 ± 0.01	1797 ± 66	$2\ 843.3 \pm 198.9$	133.6 ± 9.2	0.96 ± 0.01
WPI	0.10 ± 0.00	1.44 ± 0.14	1300 ± 56	307.3 ± 36.8	70.1 ± 3.8	2.01 ± 0.17
MCP	0.25 ± 0.00	1.56 ± 0.01	1226 ± 53	$1\ 315.0 \pm 168.2$	83.3 ± 10.7	1.24 ± 0.06
Hazelnut	0.58 ± 0.00	1.21 ± 0.02	154 ± 6	914.1 ± 44.8	52.4 ± 8.5	1.03 ± 0.05

Instant mash	0.37 ± 0.00	2.06 ± 0.03	23 ± 2	103.3 ± 3.6	8.6 ± 0.6	1.18 ± 0.10
Coarse salt	0.51 ± 0.00	0.02 ± 0.01	41 ± 7	93.2 ± 5.2	21.7 ± 0.6	2.02 ± 0.04
Fine salt	0.49 ± 0.00	0.02 ± 0.00	14 ± 2	26.3 ± 1.7	5.9 ± 1.0	2.00 ± 0.19
Baking soda	0.61 ± 0.00	9.46 ± 0.43	25 ± 4	103.4 ± 10.0	7.5 ± 1.2	1.13 ± 0.10
Couscous F	0.52 ± 0.00	2.58 ± 0.05	367 ± 30	1 619.4 ± 115.0	137.1 ± 5.2	1.19 ± 0.03
Couscous M	0.53 ± 0.00	2.77 ± 0.09	730 ± 39	2 575.1 ± 209.9	296.0 ± 17.1	1.36 ± 0.03
Acerola	0.23 ± 0.00	2.75 ± 0.06	102 ± 16	78.1 ± 7.1	18.5 ± 1.2	2.05 ± 0.12
Xanthan gum	0.25 ± 0.00	2.06 ± 0.07	14 ± 2	423.8 ± 16.3	49.3 ± 2.8	1.37 ± 0.05
Agar agar	0.25 ± 0.00	1.30 ± 0.06	9 ± 1	397.1 ± 50.1	33.8 ± 2.0	1.20 ± 0.08
Pectin	0.23 ± 0.00	0.75 ± 0.08	11 ± 2	335.9 ± 36.5	88.9 ± 8.6	2.22 ± 0.04
Yeast extract 1	0.15 ± 0.00	2.16 ± 0.11	58 ± 6	70.3 ± 4.9	5.5 ± 0.5	1.09 ± 0.07
Yeast extract 2	0.15 ± 0.00	2.22 ± 0.07	30 ± 3	58.2 ± 7.9	6.1 ± 0.8	1.25 ± 0.04
Onion	0.35 ± 0.00	0.11 ± 0.03	65 ± 12	167.7 ± 10.7	44.0 ± 1.9	2.20 ± 0.07
Lactose	0.05 ± 0.00	2.75 ± 0.11	2 ± 1	238.3 ± 24.4	19.2 ± 0.8	1.17 ± 0.03

4.1.1.2. Particle surface characterization

The surface atomic proportions of instant coffee and milk powders are displayed in **Figure 38 - left**. Carbon, oxygen, and nitrogen surface proportions were similar for all powders except for whole milk powder that had more surface carbon and less surface oxygen and nitrogen. Surface and bulk compositions of milk powders were compared in **Figure 39**. The bulk composition was measured by classical chemical analysis techniques whereas the surface composition was deduced from XPS analysis using **Equations 24, 25, and 26**. It appears that whole milk powder was mainly covered by lipids, whereas skim milk powder presented a surface overrepresentation mostly in lipids but also in proteins in a lesser extent similarly to Murrieta-Pazos et al. (2012) and Fournaise et al. (2020). These differences between bulk and surface compositions are known to strongly influence powder reconstitution behavior (Kim et al., 2002). For coffee powders, it was not possible to use the matrix method as nitrogen is also present in non-proteic compounds like caffeine (and not in proteins only as for milk powders). Nevertheless, the surface atomic composition was still informative. It was very close to that of skim milk powder for carbon and oxygen, but nitrogen contents were slightly lower (**Figure 38 - left**). Carbon bond ratios of the four powders are presented in **Figure 38 - right**. Again, only whole milk powder had a clearly more hydrophobic surface than the three other powders.

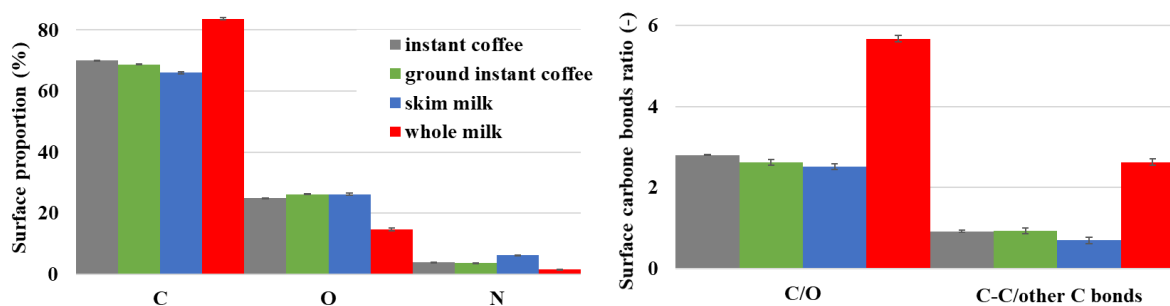


Figure 38. Surface atomic compositions (left) and carbon bond ratios (right) of instant coffee, ground instant coffee, skim milk, and whole milk powders.

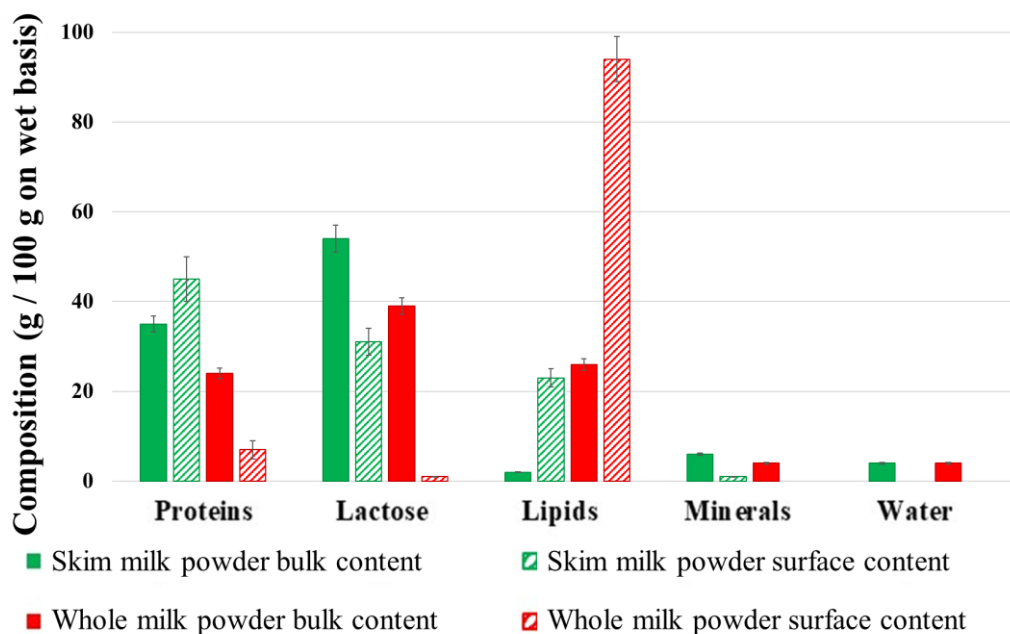


Figure 39. Bulk and surface compositions of skim and whole milk powders.

4.1.2. Powder reconstitution kinetics monitored by conductivity

4.1.2.1. *Impact of particle size on reconstitution*

The reconstitution behavior of raw and ground instant coffee powders, differing in median particle size, is detailed in **Table 5** and **Figure 40A**. The wetting step is known to be highly linked to the median particle size, as well as bulk and surface compositions. As previously shown, the bulk and surface compositions of instant coffee powders were identical (**Figure 38** and **Table 2**). It appeared that wettability was better for the raw instant coffee powder composed of larger particles (23 s wetting time) than for the ground instant coffee powder (52 s wetting time). Indeed, a high proportion of large and/or agglomerated particles is known to improve powder wettability (Hogekamp and Schubert, 2003; Schuck et al., 2012). The reconstitution time was also shorter for raw instant coffee powder probably owing to its shorter wetting step. Hill model parameters, time constant k and power n , were also informative about the reconstitution kinetics. k , corresponding to the time needed to reach half of the final conductivity, was doubled for the ground instant coffee powder, denoting slower reconstitution kinetics. Moreover, the slope of the normalized conductivity curve at half maximal normalized conductivity, equal to $\frac{n}{4k}$, could be viewed as an indicator of reconstitution rate; for instant coffee powders, $\frac{n}{4k}$ equaled 0.050 and 0.020 s⁻¹ for raw and ground samples, respectively. This confirms the slower reconstitution rate of ground instant coffee powder, likely due to its lower median particle size preventing its correct wetting and dispersion (Freudig et al., 1999;

O'Mahony and McSweeney, 2016); indeed, interparticular cohesive forces are expected to be stronger between small particles owing to their higher contact surface (Fu et al., 2012; Zhou et al., 2010).

Table 5. Wetting and reconstitution times, as well as Hill model parameters (time constant k and power n) and coefficient of determination (R^2) of normalized conductivity curve fitting by Hill model for investigated milk and coffee powders.

	Wetting time (s)	Reconstitution time $t_{95\%}$ (s)	Hill model time constant k (s)	Hill model power n (-)	Hill model coefficient of determination R^2
Skim milk powder	35 ± 4	75.4 ± 1.0	16.4 ± 1.1	2.08 ± 0.22	0.95
Whole milk powder	68 ± 8	112.0 ± 10.4	36.2 ± 5.3	2.76 ± 0.13	0.98
Instant coffee powder	22 ± 2	34.7 ± 1.1	12.8 ± 0.6	2.16 ± 0.08	0.98
Ground instant coffee powder	51 ± 4	106.5 ± 6.8	26.7 ± 3.7	2.15 ± 0.31	0.98

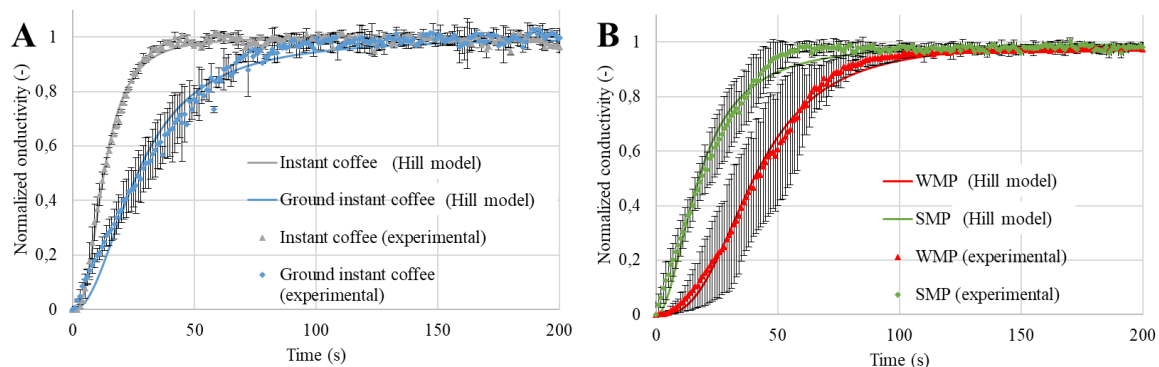


Figure 40. A- Effect of median particle size and B- fat content on powder reconstitution kinetics.

4.1.2.2. Impact of lipid content on reconstitution

Whole and skim milk powders presented similar median particle sizes but differed in chemical composition through their lipid content. Their reconstitution behavior is presented in **Table 5** and **Figure 40B**. The bulk and surface compositions of these powders markedly differed. Whole milk powder, having a well higher surface lipid content, had a well higher surface hydrophobicity (Hogekamp and Schubert, 2003; Murrieta-Pazos et al., 2012). This surely caused that whole milk powder had a wetting time (68 s) longer than skim milk powder (35 s), the latter having a more hydrophilic surface which is known to improve wettability. These results met literature regarding the negative influence of surface hydrophobicity on powder wetting (Gaiani et al., 2006; Ji et al., 2017; Kim et al., 2002; Wu et al., 2020). The reconstitution time ($t_{95\%}$) was shorter for the skim milk powder, confirming the deleterious

effect of surface lipids on reconstitution. This may be related to wettability that is well impaired at higher surface lipid content. Hill model parameters (time constant k and power n) were greater for skim milk powder, indicating a higher reconstitution rate and a shorter reconstitution time. This was confirmed by the calculation of the slope of the normalized conductivity curve at half-height (which is an indicator of reconstitution rate as previously mentioned): $\frac{n}{4k}$ equaled 0.029 and 0.018 s^{-1} for skim and whole milk powders, respectively. This confirms the slower reconstitution rate of whole milk powder.

4.1.3. Surface composition of the thirty-six food powders

On the best knowledge of the author, surface analysis by XPS has been performed only on few food powders, dairy or wheat powders for example (Kim et al., 2002; Mohamad Saad et al., 2009). For the first time, a large investigation was performed on thirty-six food powders in order to collect surface atomic proportions (in carbon, oxygen, and nitrogen), as well as C/O and C-C/(other carbon bonds) ratios as indicators of surface hydrophobicity (**Table 3**). It appears that surface chemical composition was highly variable for investigated powders. Three hypothesized powder groups were constituted on the basis of surface hydrophilicity/hydrophobicity (**Figure 41**). The most hydrophilic surface powders were associated with the lowest ranges of C/O and C-C/other C bonds ratios of 0 - 2 and 0 - 1, respectively. Intermediate (slightly hydrophobic) powders corresponded to ranges of C/O and C-C/other C bonds ratios of 2 - 4 and 1 - 2, respectively. The most hydrophobic surface powders were defined for the highest ranges of C/O and C-C/other C bonds ratios of 4 - 7 and 2 - 4, respectively. Sugar, acerola juice, lactose, agar, xanthan, pectin, and baking soda powders were then sorted as the powders with the most hydrophilic surface powders of the study. On the opposite, hazelnut, cocoas, milk protein concentrate, whole milk, and whey proteins powders were classified as the powders with the most hydrophobic surface of the study. Many investigated food powders (cereal powders, flours, coffee powders, couscous powders, instant mashed potatoes powder, etc.) fell into the intermediate category of slightly hydrophobic surface.

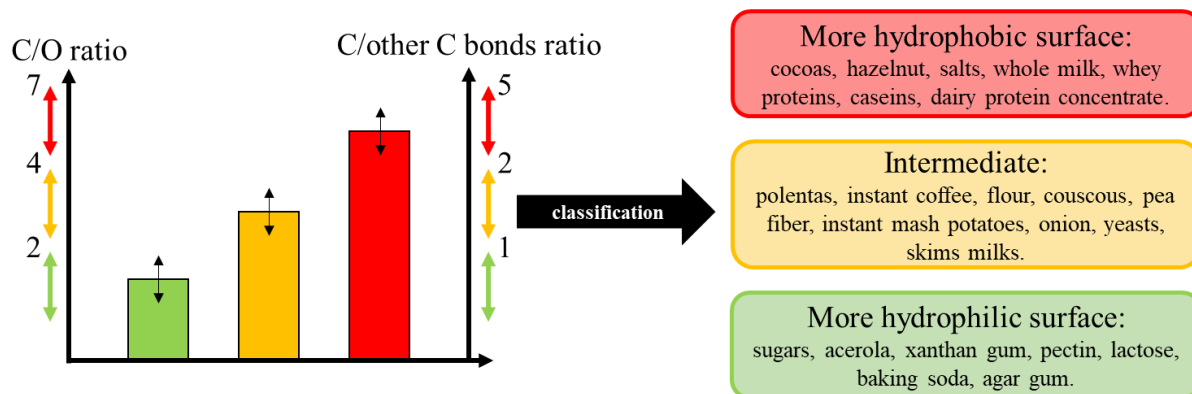


Figure 41. Classification of investigated powders into three groups (more hydrophobic, intermediate, and more hydrophilic) from C/O and C-C bonds/C-other atom bonds ratios at particle surface.

4.1.4. Principal component analysis linking physicochemical properties, manufacturing process, and reconstitution behavior of the thirty-six food powders

A PCA was performed to link powder physicochemical properties and their reconstitution behavior. The main objective was to capture the variability of data in a few principal components, which encompass the most variation of the dataset. The data taken into consideration in the PCA are related to powder bulk and surface composition, manufacturing process, median particle size, and reconstitution properties (wetting and reconstitution times, as well as Hill model parameters) (**Tables 2, 3, and 4**). The wetting time was measured by an empirical method (FIL method), while the reconstitution time was deduced from Hill model fitting of conductivity curves obtained from powder reconstitution in the stirred reactor (**Figure 33**). The process conditions employed for these analyses markedly differed, which explains why some powders (whey protein isolates or acerola for instance) presented a wetting time greater than their reconstitution time (**Table 4**).

The loading plot shows how strongly each powder physicochemical characteristic influences the variability amongst powders, represented according to the two principal components PC1 and PC2 (**Figure 42**), the bulk composition is unshown because the classification by ranges transforms the compositions into qualitative data. PC1, corresponding to the horizontal axis and representing 34 % of powder characteristics variability, was linked to reconstitution times ($t_{95\%}$, k , and n) and manufacturing process. PC2, associated with the vertical axis and corresponding to 27 % powder variability, was correlated to median particle size (D50), wetting time, and surface chemical composition. Hence, a long wetting time was related to a small median particle

size and an elevated surface hydrophobicity (Kim et al., 2002; Szulc and Lenart, 2013). The relationship between median particle size and wettability had already been demonstrated on milk powders (Chever et al., 2017), the current work thus makes it possible to generalize this relationship to food powders whatever their composition and manufacturing process. Hill model parameters logically appeared to be correlated with the reconstitution time: a high k value or a low n value (both inducing a low slope of the normalized conductivity curve at half maximal normalized conductivity $\frac{n}{4k}$ value) were related to a high reconstitution time, i.e. slow reconstitution kinetics. The score plot locates investigated powder samples on the PC1 \times PC2 plot (**Figure 43**). Powders situated on the bottom side (negative PC2) had long wetting times, whereas powders found in the right side (positive PC1) were linked to long reconstitution times. Therefore, four groups of powders were defined on the basis of their reconstitution behavior: short wetting and reconstitution times (green: good); long wetting time and short reconstitution time (yellow: correct); short wetting time and long reconstitution time (orange: mediocre); long wetting and reconstitution times (red: poor).

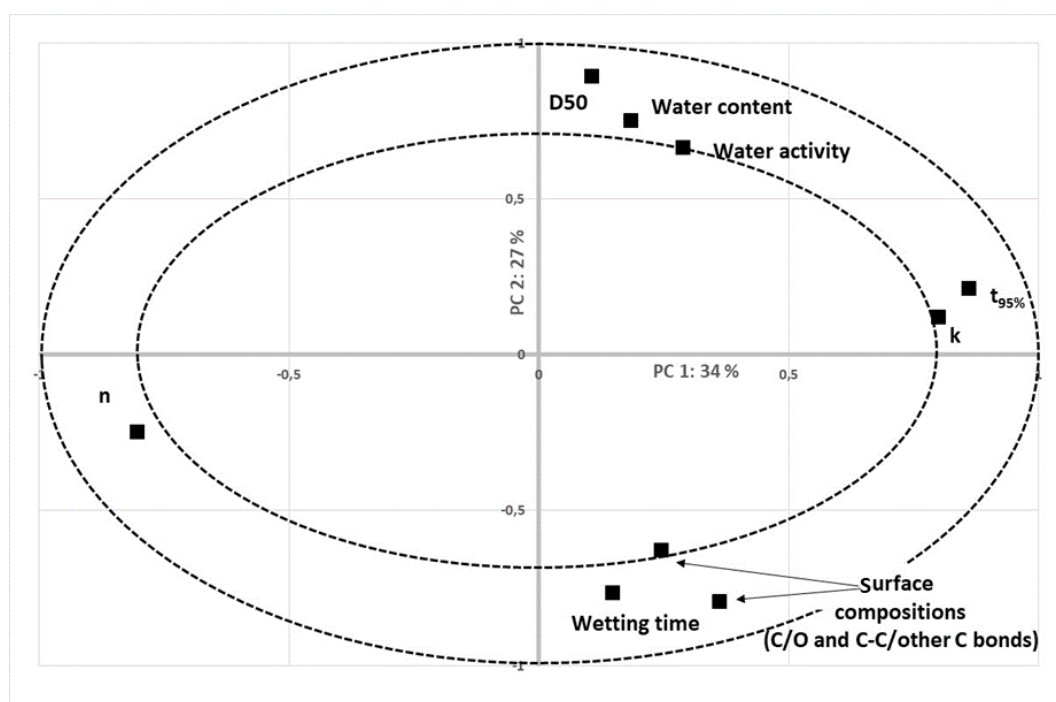


Figure 42. Correlation scores obtained from PCA for the thirty-six investigated powders.

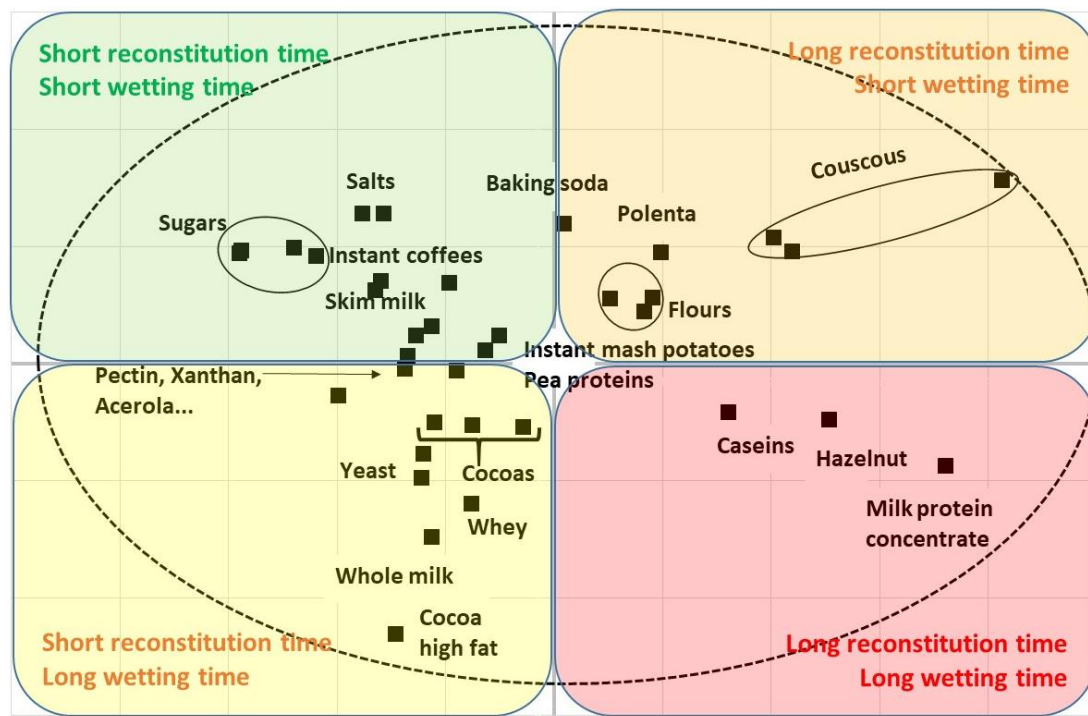


Figure 43. Classification of the thirty-six investigated powders deduced from PCA (loading scores).

The reconstitution behavior of milk powders has been extensively described in the literature contrarily to other food powders (Caric and Milanovic, 2002; Fang et al., 2011; Gaiani et al., 2006). For the first time, the main factors influencing the reconstitution are identified for a large variety of powders. Manufacturing processes, mainly grinding and spray-drying, were associated to long and short reconstitution times, respectively. Indeed, cereal powders (couscous powders, flours, semolina, wheat powders), obtained by grinding, had slow reconstitution kinetics. Besides, small particle and hydrophobic surface powders were correlated to long wetting times, whereas large particle and hydrophilic powders were associated with short wetting times. Finally, powder within each of red and green groups separately were also similar in terms of bulk composition (high lipids; high sugar or mineral contents, respectively).

4.1.5. Conclusion

For the first time, the main factors influencing powder reconstitution behavior (median particle size, bulk chemical composition, surface composition, and manufacturing process) have been identified for a large number of food powders. The current study permitted to confirm and generalize the knowledge developed so far on a limited number of powders and identify four reconstitution behaviors (**Figure 44**).

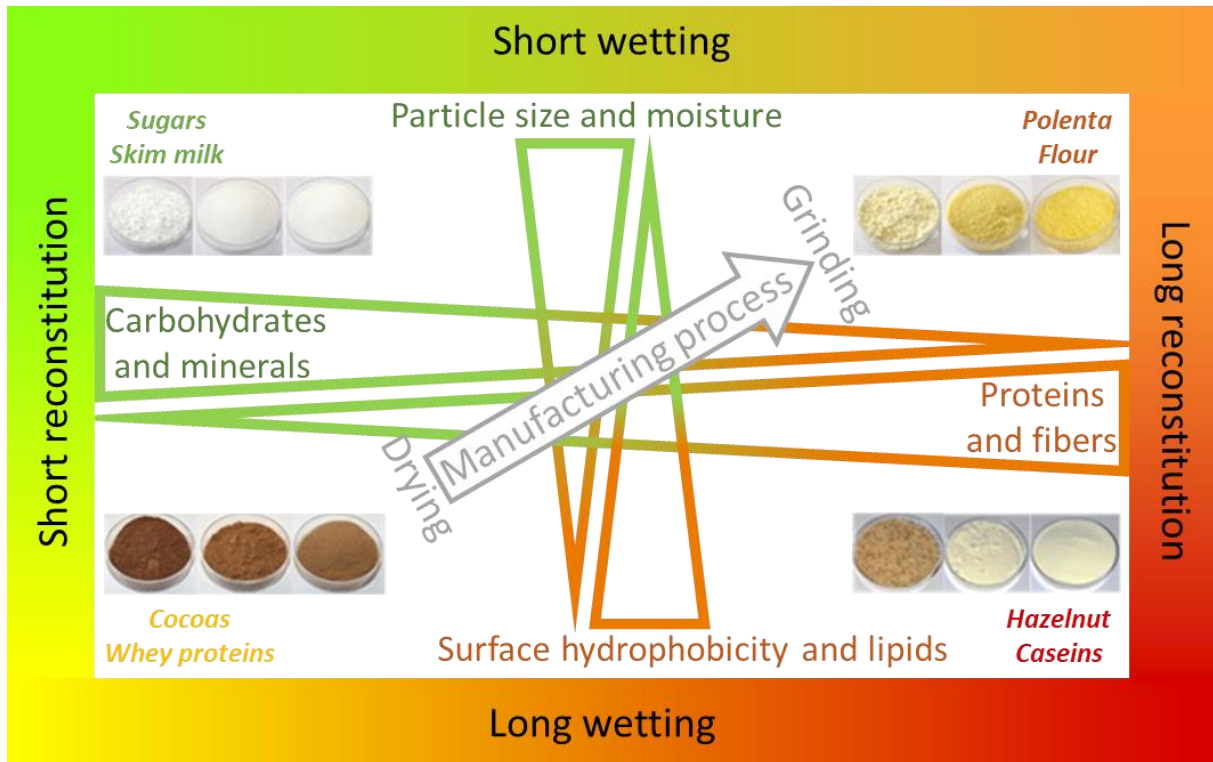


Figure 44. Overview of the main factors influencing powder reconstitution.

The industrial interest of the proposed classification resides in the fact that powder reconstitution properties can be modulated by changing powder formulation (particle size distribution, surface composition, bulk composition, etc.) without modifying the reconstitution conditions (stirring speed, temperature, etc.). It would be interesting to go one step further by linking powder physicochemical characteristics and manufacturing process to the different reconstitution steps.

4.2. Coating of whey protein isolate with sugars: surface modification and wettability

This part of the PhD investigated the influence of particle surface characteristics on wettability in relation with interactions between particle surface and water.

The coating of powders with sugars is a well-established technique to improve wettability. However, it seems that no study to date has focused on the molecular and atomic characterization of particle surface to understand its impact on wettability. In order to improve its wettability, a powder identified with PCA as having short reconstitution time but a slow wetting (whey protein isolate) was coated with a solution prepared with a powder having short reconstitution time and a quick wetting. This study is divided into three parts:

- first, it was intended to identify the minimum amount of sucrose required to coat whey protein isolate powder in order to significantly improve its wettability;

- then, the respective impact of different sugars (sucrose, lactose, glucose, fructose, and galactose) on wettability was evaluated.

- last, the mimicry of the beginning of wetting step of whey protein isolate coated with sucrose by air moisture uptake to understand how the mechanisms at play upon interaction of particle surface with water can be enhanced by coating.

4.2.1. Determination of coating duration

Firstly, the objective was to significantly improve whey protein isolate powder wettability by sucrose coating, while adding as few sucrose as possible. It was aimed resulting in a fine coating that should not change particle size too much. Keeping the initial particle size distribution of whey protein isolate powder was an important criterion in order to be able to unravel the single influence of surface modification change induced by sucrose coating. Indeed, the strong influence of particle size on wettability has often been reported (Lazghab et al., 2005; Schuck et al., 2012). A peculiar attention has been paid to avoid particle agglomeration, which changes the particle size distribution and generally induces a marked improvement of powder wettability (Chever et al., 2017; Ji et al., 2015; Szulc and Lenart, 2013). Indeed, the agglomeration of small particles at the surface of larger ones may occur, as reported in coating or multi-effect spray-drying processes (Chever et al., 2017; Lehmann, 1992; Schuck et al., 2012).

4.2.1.1. Physicochemical properties

Particle size distributions were monomodal with a D_{50} around 46 μm and a span around 2 (**Table 6 & Figure 45**). Differences between control and coated powders were not significant, except for the Sucrose-45 powder (i.e. coated 45 min with sucrose) which exhibited slightly smaller particle sizes. On the day of production of this sample, the environmental conditions were drier, therefore the fluidization and spraying air were drier, favoring attrition-induced particle size reduction in the fluidized bed (Wyszynski and Bridgwater, 1993). The coating time did not have any significant impact on particle size distribution, even though the coating process seemed to promote the adsorption of finer particles at the surface of larger ones, as reflected by the slight increase in D_{10} and D_{50} .

Table 6. Granulometric parameters of native, control, and sucrose-coated whey protein isolate powders obtained at different processing times in the fluid-bed coater.

	D_{10} (μm)	D_{50} (μm)	D_{90} (μm)	Span (-)
Native WPI	13.30 ^c \pm 0.10	45.13 ^d \pm 0.67	102.33 ^{bcd} \pm 0.58	1.97 ^{ab} \pm 0.02
Water-15	13.57 ^c \pm 0.06	47.27 ^{ab} \pm 0.15	108.00 ^a \pm 1.00	2.00 ^a \pm 0.01
Sucrose-15	14.13 ^{ab} \pm 0.06	48.25 ^a \pm 0.05	106.00 ^{ab} \pm 1.00	1.90 ^{bc} \pm 0.03
Water-30	14.43 ^{ab} \pm 0.21	46.63 ^b \pm 0.55	102.00 ^{cde} \pm 1.00	1.88 ^{cd} \pm 0.02
Sucrose-30	14.47 ^a \pm 0.15	46.97 ^b \pm 0.12	104.00 ^{bc} \pm 1.73	1.90 ^{bc} \pm 0.04
Water-45	14.47 ^a \pm 0.15	46.57 ^b \pm 0.50	101.00 ^{cde} \pm 2.65	1.86 ^{cd} \pm 0.04
Sucrose-45	12.93 ^d \pm 0.15	43.90 ^d \pm 0.26	101.33 ^{bcd} \pm 0.58	2.02 ^a \pm 0.02
Water-60	14.37 ^{ab} \pm 0.12	46.50 ^b \pm 0.17	99.53 ^{de} \pm 1.27	1.83 ^{cd} \pm 0.02
Sucrose-60	14.10 ^b \pm 0.00	46.90 ^b \pm 0.60	98.27 ^e \pm 1.03	1.81 ^d \pm 0.02

Native powder = unfluidized whey protein powder; Water-X (control powders) = whey protein powder fluidized with water during X min; Sucrose-X (coated powders) = whey protein powder coated with sucrose during X min. Means with different superscripted letters in the same column were significantly different according to Tukey's HSD test ($p < 0.05$; $n = 3$).

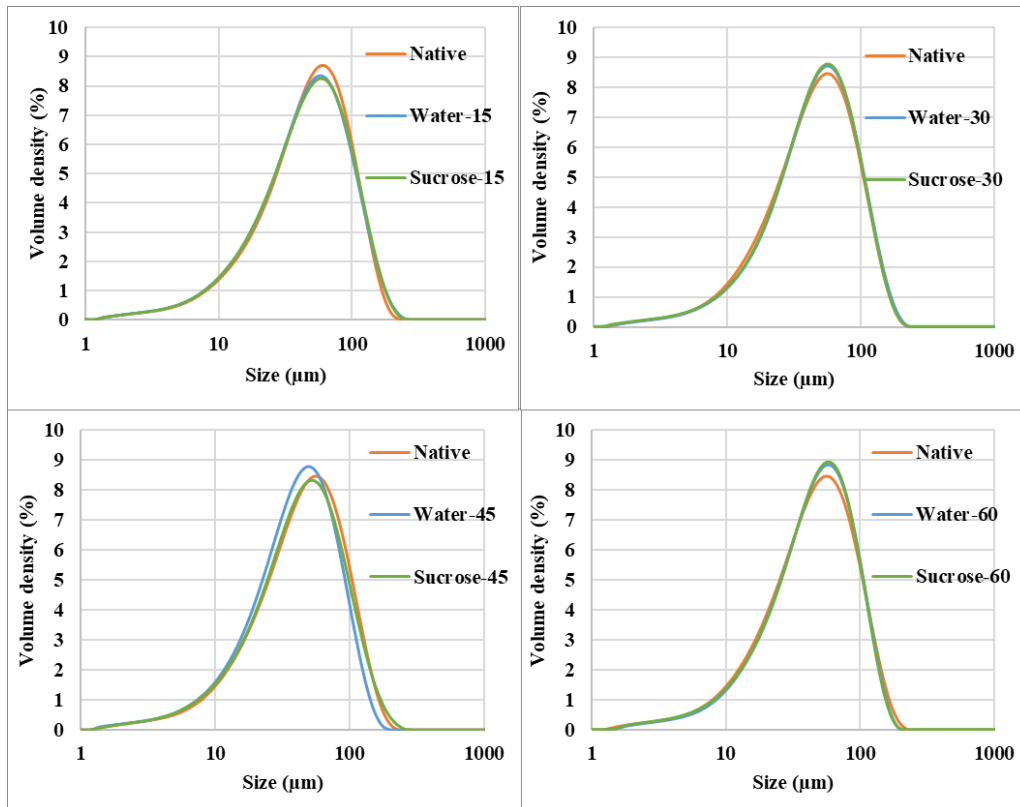


Figure 45. Particle size distributions (in volume) of native, control, and sucrose-coated whey protein isolate powders.

Control and sucrose-coated whey protein isolate powders had similar water activity and water content, regardless of the coating time. The coating process induced additional drying of the particles which resulted in a decrease in water activity and water content in comparison with the native whey protein isolate powder (**Table 7**). The amount of added sucrose varied between 0 and 3.6 g/100 g powder. It was logically found that sucrose content of coated whey protein isolate powders linearly increased with the coating time upon sucrose coating (**Table 2 & Figure 46**).

Table 7. Physicochemical properties of native sucrose and native, control, and sucrose-coated whey protein isolate powders.

	Water content (g/100 g on wet basis)	Water activity (-)	Added sucrose (g/100 g on wet basis)	C/O ratio (-)
Native sucrose	/	/	/	1.65 ^b ± 0.25
Native WPI	1.56 ^a ± 0.06	0.25 ^a ± 0.00	0.00 ^e	3.82 ^a ± 0.02
Water-15	1.25 ^b ± 0.06	0.11 ^b ± 0.00	0.00 ^e	/
Sucrose-15	1.24 ^b ± 0.03	0.10 ^b ± 0.00	0.62 ^d ± 0.14	3.79 ^a ± 0.01
Water-30	1.56 ^a ± 0.27	0.08 ^c ± 0.01	0.00 ^e	/
Sucrose-30	1.07 ^c ± 0.09	0.09 ^b ± 0.01	2.15 ^c ± 0.04	3.74 ^a ± 0.03
Water-45	1.44 ^a ± 0.10	0.10 ^b ± 0.00	0.00 ^e	/
Sucrose-45	1.24 ^b ± 0.01	0.10 ^b ± 0.00	2.89 ^b ± 0.02	3.77 ^a ± 0.05
Water-60	1.24 ^b ± 0.01	0.11 ^b ± 0.00	0.00 ^e	/
Sucrose-60	1.25 ^b ± 0.17	0.10 ^b ± 0.00	3.62 ^a ± 0.08	3.70 ^a ± 0.07

/: not performed.

Means with different superscripted letters in the same column were significantly different according to Tukey's HSD test ($p < 0.05$; $n = 3$).

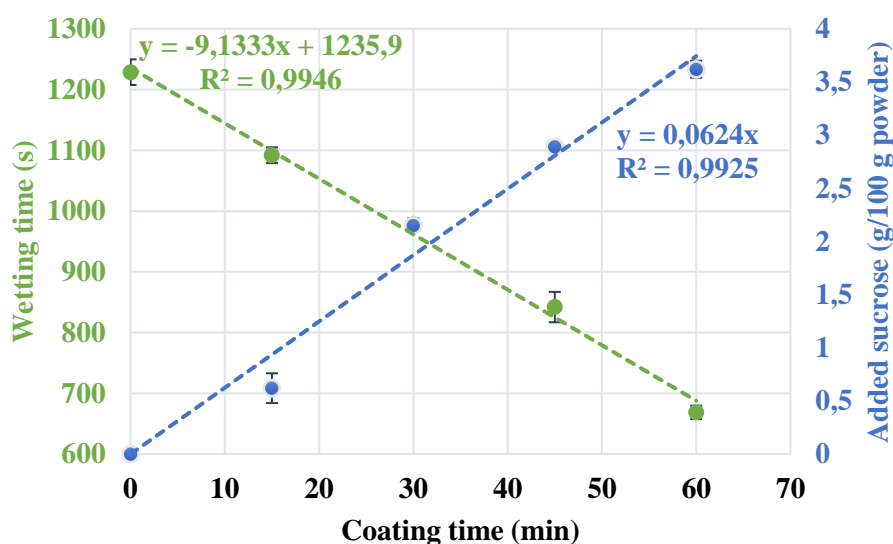


Figure 46. Evolution of wetting time and proportion of added sucrose of sucrose-coated whey protein isolate powders with the coating time.

4.2.1.2. Wettability

Wetting time of sucrose-coated whey protein isolate powders linearly decreased with the increase in coating time (**Table 8 & Figure 46**). For example, sucrose coating during 1 h allowed to decrease wetting time by around 46 %, which could be very useful for industrial applications. Wetting time also followed a linear decreasing trend when the amount of added sucrose was increased, as illustrated by the relationship obtained by linear regression in **Figure 47**. This evidenced the marked impact of sucrose coating on whey protein isolate powder wettability and establishes a predictive relationship of coated powder wettability.

Table 8. Wetting time of native sucrose and native, control, and sucrose-coated whey protein isolate powders, as well as native sucrose.

	Wetting time (s)
Native sucrose	8 ^g ± 1
Native WPI	1 229 ^a ± 21
Water-15	1 217 ^a ± 28
Sucrose-15	1 092 ^c ± 13
Water-30	1 158 ^b ± 8
Sucrose-30	978 ^d ± 10
Water-45	1 163 ^b ± 7
Sucrose-45	842 ^e ± 25
Water-60	1 157 ^b ± 9
Sucrose-60	669 ^f ± 11

Means with different superscripted letters in the same column were significantly different according to Tukey's HSD test ($p < 0.05$; $n = 9$).

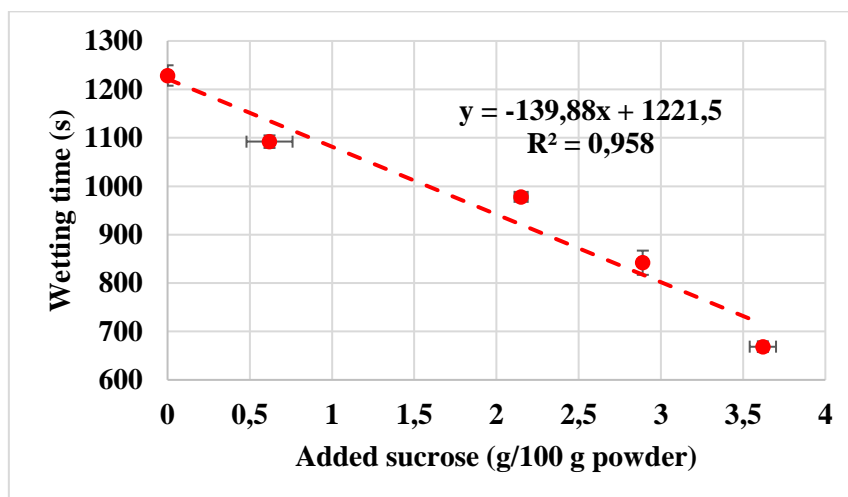


Figure 47. Influence of added sucrose on wetting time of sucrose-coated whey protein isolate powders.

It can be concluded that fluid-bed wet coating with sucrose permitted to markedly improve whey protein isolate powder wettability while limiting powder attrition and agglomeration. Then, the influence of the nature of sugar used for coating was studied in these suitable coating conditions.

4.2.2. Impact of sugar nature on wettability of coated whey protein isolate powders

4.2.2.1. Physicochemical properties

Particle size distributions of control and coated whey protein isolate powders were monomodal with a D_{50} around 46 μm and a span around 1.93 (Table 9 & Figure 48). Air-control whey protein isolate powder (fluidized during 60 min without water spraying) showed a decrease in median particle size that can be attributed to attrition upon fluidization in the

absence of sprayed liquid. All other control and coated powders had close granulometric characteristics, showing that powder agglomeration and coating-induced size increase were not significant in chosen coating conditions. According to SEM images (**Figure 48**), control and coated whey protein isolate powders had similar appearance. Sugar coating did not affect the particle size distribution and it was not possible to identify the location of coated areas. The results made it possible to formulate the following hypothesis that the small quantity of sugar added would induce the formation of a thin layer at particle surface which would be masked by the carbon layer coated at sample surface during their preparation for SEM analyses. SEM images confirm that the sugar-coating process induced only a slight agglomeration of small particles at the surface of larger ones, which is in line with particle size measurements (section 4.2.1.1. and **Table 9**). In the absence of sprayed solution (air-control), a slight attrition of particles (broken particles) was observed, due to fluidization-induced shocks between particles, which is a known effect of fluidization (Ray et al., 1987). Granulometric results presented in **Table 9** are in line with microscopic observations: no significant differences between control and coated powders were observed.

Table 9. Granulometric parameters of whey protein isolate powders in native state, fluidized without (Air-60) or with water (Water-60), and coated with different sugars for 60 min.

	D ₁₀ (µm)	D ₅₀ (µm)	D ₉₀ (µm)	Span (-)
Native WPI	13.30 ^d ± 0.10	45.13 ^b ± 0.67	102.33 ^b ± 0.58	1.97 ^a ± 0.02
Air-60	13.03 ^c ± 0.13	44.00 ^a ± 0.35	98.30 ^d ± 1.28	1.94 ^a ± 0.16
Water-60	14.37 ^{ab} ± 0.10	46.50 ^b ± 0.15	99.53 ^{cd} ± 1.10	1.83 ^b ± 0.19
Sucrose-60	14.32 ^{ab} ± 0.34	46.93 ^b ± 0.58	104.31 ^{bc} ± 5.22	1.91 ^a ± 0.10
Lactose-60	14.16 ^b ± 0.37	46.86 ^b ± 1.55	105.78 ^{ab} ± 3.38	1.96 ^a ± 0.05
Glucose-60	14.80 ^a ± 0.72	48.67 ^b ± 1.83	111.11 ^a ± 4.28	1.98 ^a ± 0.03
Fructose-60	14.18 ^b ± 0.53	46.22 ^b ± 0.89	105.44 ^b ± 5.66	1.97 ^a ± 0.12
Galactose-60	14.42 ^{ab} ± 0.21	47.46 ^b ± 0.38	106.56 ^{ab} ± 2.19	1.94 ^a ± 0.03

Means with different superscripted letters in the same column were significantly different according to Tukey's HSD test ($p < 0.05$; $n = 3$).

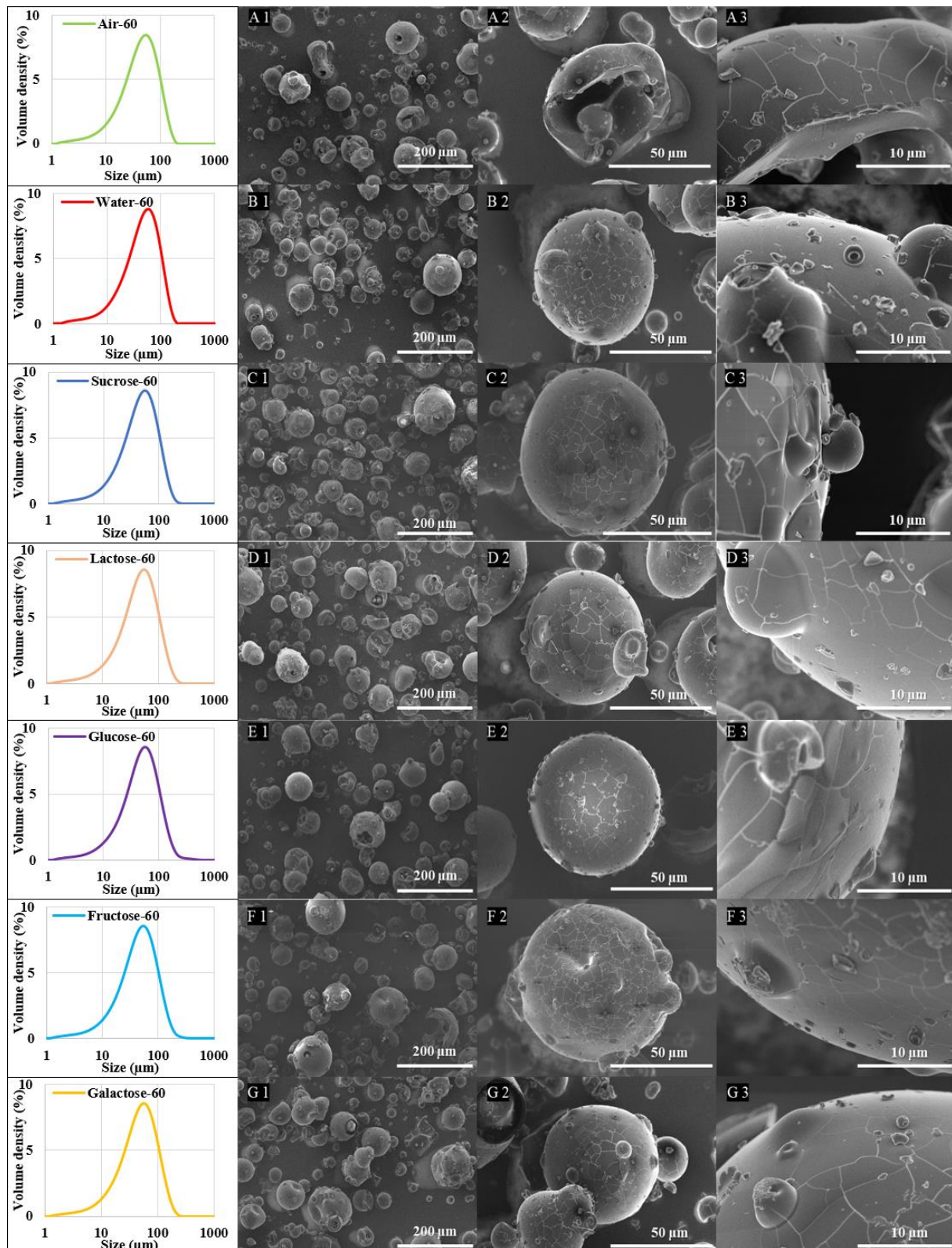


Figure 48. Particle size distributions (in volume) and SEM pictures of whey protein isolate powders fluidized without air A- Air-60, with water B- Water-60 and coated with different sugars for 60 min. C- Sucrose-60, D- Lactose-60, E- Glucose-60, F- Fructose-60, and G- Galactose-60. 1: $\times 200$ magnification, 2: $\times 1\,500$ magnification, and 3: $\times 5\,000$ magnification.

As for the section 4.2.1.1., water content and water activity were not significantly different for control and coated powders, except for the air-control powder that presented lower values due to the absence of sprayed liquid, leading to a further drying of whey protein isolate powder in this case (Table 10). The amount of added sugar showed no significant difference when using different sugars.

Table 10. Physicochemical properties of whey protein isolate powders fluidized without (Air-60) or with water (Water-60) and coated with different sugars for 60 min.

	Water content (g/100 g on wet basis)	Water activity (-)	Proportion of added sugars (g/100 g on wet basis)
Native	1.44 ^a ± 0.14	0.10 ^a ± 0.00	0.00 ^b ± 0.00
Air-60	0.11 ^c ± 0.00	0.05 ^b ± 0.00	0.00 ^b ± 0.00
Water-60	1.24 ^b ± 0.01	0.11 ^a ± 0.00	0.00 ^b ± 0.00
Sucrose-60	1.26 ^a ± 0.13	0.10 ^a ± 0.00	3.62 ^a ± 0.08
Lactose-60	1.34 ^a ± 0.35	0.11 ^a ± 0.00	3.56 ^a ± 0.09
Glucose-60	1.31 ^a ± 0.26	0.10 ^a ± 0.00	3.54 ^a ± 0.10
Fructose-60	1.47 ^a ± 0.43	0.11 ^a ± 0.00	3.59 ^a ± 0.12
Galactose-60	1.38 ^a ± 0.19	0.10 ^a ± 0.00	3.53 ^a ± 0.14

Means with different superscripted letters in the same column were significantly different according to Tukey's HSD test ($p < 0.05$; $n = 3$).

The surface atomic composition of the different native sugar powders (**Figure 49**) did not show any significant difference, which was unexpected because the atomic proportions of carbon, hydrogen, and nitrogen slightly different: monosaccharide ($C_6H_{12}O_6$) and disaccharide ($C_{12}H_{22}O_{11}$). The proportion of oxygen should be slightly lower for disaccharides (Horton et al., 1994; Tita-Goldstein, 2013). The surface atomic composition of control and sugar-coated whey protein isolate powders were similar. XPS measurements being carried out over a large area ($700 \mu\text{m} \times 300 \mu\text{m}$), the lack of significant difference between control and sugar-coated whey protein isolate powders could result from the location of coated sugar in small patches dispersed at the surface of the particles rather than in a fine continuous layer.

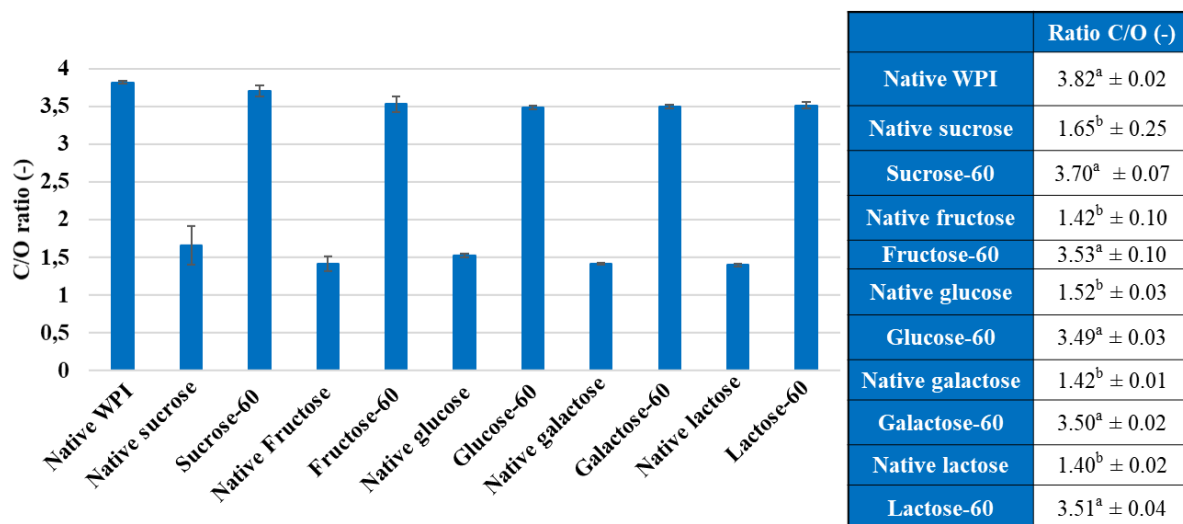


Figure 49. C/O ratio of whey protein isolate powders coated for 60 min with different sugars and native WPI and sugars. Means with different superscripted letters in the same column were significantly different according to Tukey's HSD test ($p < 0.05$; $n = 2$).

The DSC results did not allow to determine the glass transition temperature of whey protein isolate powders coated for 60 min with different sugars (**Figure 50**). Indeed, with such a small amount of added sugar (3.6 g/100 g powder), even if the glass transition of sample sugar occurred upon analysis, there is a high probability that corresponding enthalpy change remained under the detection limit of the device. However, it is very likely that the powders had already passed the glass transition temperature T_g (**Table 11**) during the coating operation performed at relatively high temperature (50 °C) and high relative humidity (Roos, 2013; Simperler et al., 2006), leading to crystallized sugars at particle surface at the end of the coating operation.

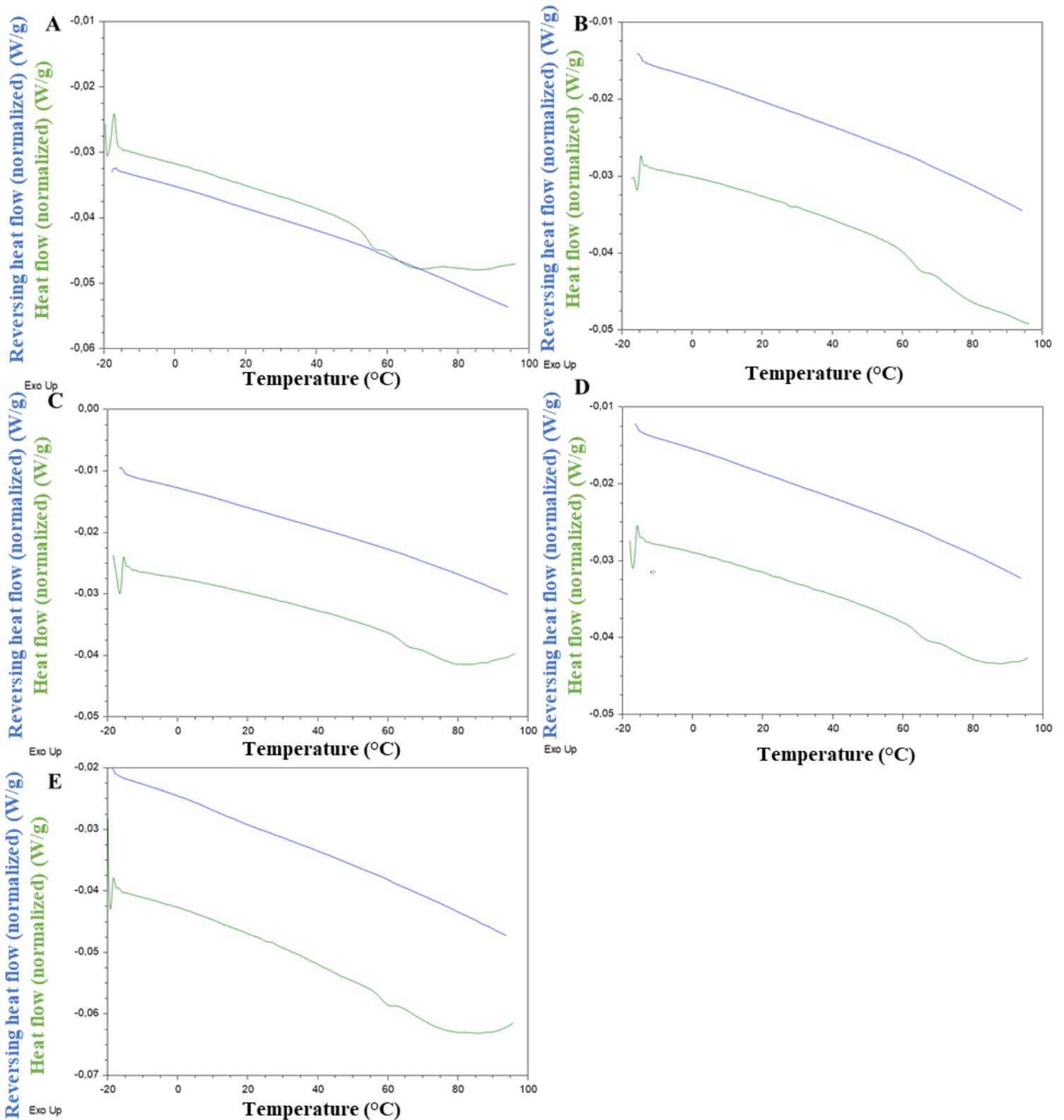


Figure 50. Differential scanning calorimetry spectra of whey protein isolate powders coated with different sugars for 60 min. A: Sucrose-60; B: Lactose-60; C: Glucose-60; D: Fructose-60; and E: Galactose-60).

Table 11. Glass transition temperature of sucrose, lactose, glucose, fructose, and galactose (Haque et al., 2006; Y. Roos, 1995; Tita-Goldstein, 2013).

Sugar	Glass transition temperature (°C)
Sucrose	57 - 79
Lactose	100
Glucose	31
Fructose	5
Galactose	30

XPS and SEM analyses did not show any modification of the surface of the particles despite sugar addition at 3.6 g/100 g on wet basis. This led to the hypothesis that particle coating was not homogeneous; instead of a fine continuous sugar layer, sugars may be found in small patches dispersed at particle surface.

4.2.2.2. *Wettability*

Wettability differences were observed between native, control, and coated whey protein isolate powders according to the sugar nature for coated powders (**Figure 51**). Control powders (Air-60 and Water-60) have a slightly better wettability than the native powder. This can be explained by the drying of particles (**cf. Table 10**) or the production of more spherical and/or smooth particles induced by the fluidization with warm air in the Wurster process (Schuck et al., 2012; Sharma et al., 2012). Air-60 control whey protein isolate powder had the worst wetting behavior among fluidized powders due to its smaller median particle size and its lower sphericity (as evidenced by the presence of broken particles on SEM images, **cf. Figure 48**), both being known to be deleterious for the wetting mechanism (Roos et al., 2020). Water-control whey protein isolate powder had a slightly better wettability, showing a small positive influence of the coating operation even by spraying water only, as particle attrition was limited in this wet environment and a very little occurrence of agglomeration of small particles on larger particles was denoted (Dhanalakshmi et al., 2011; Turchiuli et al., 2013). Sugar-coating permitted to highly improve whey protein isolate powder wettability: the addition of some sugars (sucrose and glucose) even permitted to reduce wetting time almost by half. All sugars did not have the same positive influence on whey protein isolate powder wettability; their influence can be sorted according to the following increasing order (**Figure 51**): lactose < galactose \approx fructose < glucose \approx sucrose. As wetting of native sugars is rather an instant phenomenon, wetting time measured by the FIL method cannot be more discriminating between sugars. Wettability of sugar-coated whey protein isolate powders seemed rather independent from sugar glass transition temperature (a low Pearson's correlation coefficient of 0.25 was

found, corresponding to an absence of correlation) and solubility (Pearson's correlation coefficient of 0.16, also denoting the absence of correlation) (**Table 12**). Wettability improvement may be mainly influenced by the chemical structure of sugars while not being linked to the chain length (mono- or di-saccharide) (Brown and Pickering, 1897; Preedy, 2012).

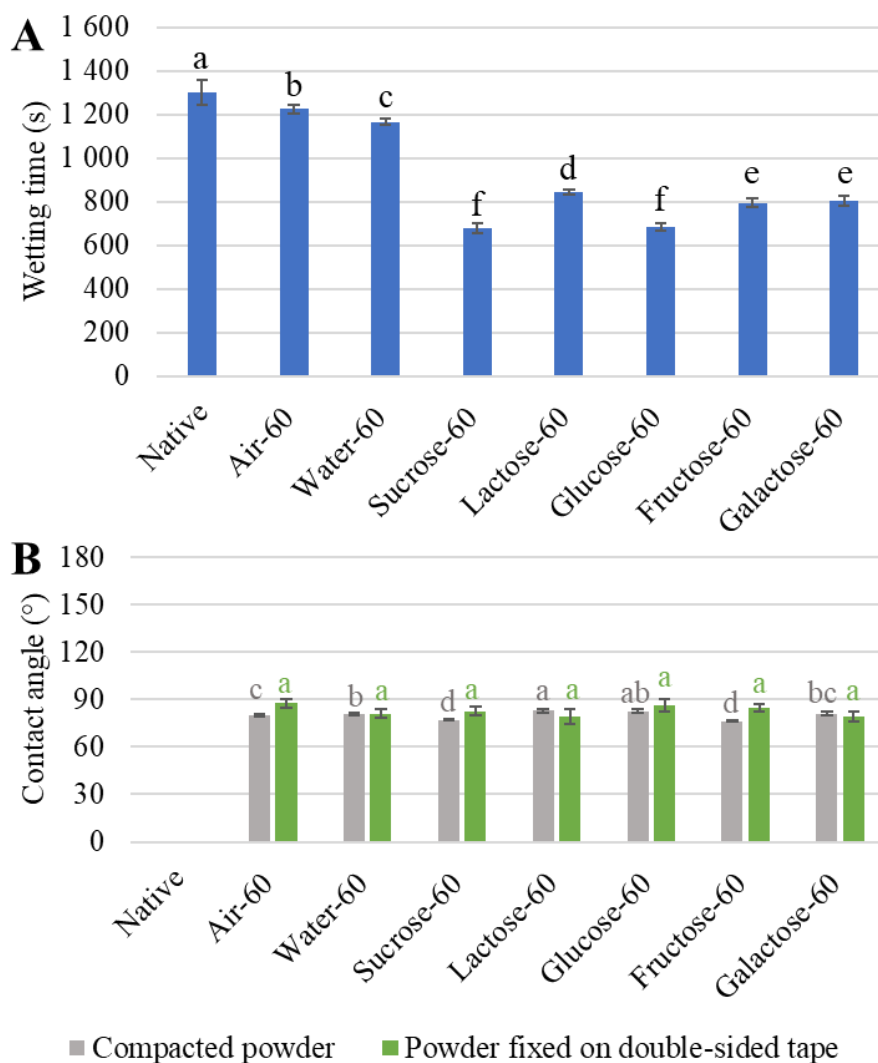


Figure 51. A- Wetting time by FIL method, B- contact angle of whey protein isolate powders fluidized without (Air-60) or with water (Water-60) and coated with different sugars for 60 min. Letters in the same column were significantly different according to Tukey's HSD test ($p < 0.05$; $n = 9$).

Table 12. Solubility of sucrose, lactose, glucose, fructose, and galactose (Haque et al., 2006; Roos, 1995; Tita-Goldstein, 2013).

	Solubility (g/mL)
Sucrose	2.02
Lactose	0.22
Glucose	0.90
Fructose	3.75
Galactose	0.68

Contact angle and capillary rise analyses have been carried out to try to understand why wettability improvement of sugar-coated whey protein isolate powders depended on the sugar nature (**Figure 51 & 13**).

Contact angle measurement performed on powder compacts or particles fixed on double-sided tape did not permit to evidence differences in surface properties of sugar-coated whey protein isolate powders according to the nature of coated sugar. The slight variations in contact angles between sugar-coated samples may be explained by the lack of repeatability regarding the roughness of the powder compact or layer (Hideo Nakae et al., 1998), not from the influence of the nature of sugars. Indeed, the variation trends between coated powders were totally different for the two preparation methods.

As for capillary rise analysis, high standard errors were associated with obtained wetting times and velocities, revealing that capillary rise measurements had poor repeatability, resulting in variations that probably overwhelmed the possible differences coming from the nature of coated sugar. Due to the low repeatability making the results unusable, all powders have not been analyzed. High variability of capillary rise results may be the consequence of the use of vibration to compact the sample powder bed; mechanical methods such as application of normal stress with a vented piston could solve this problem. Capillary rise measurement of the contact angle of coated powders with mixtures of two liquids in different proportions (Raux et al., 2013) and the compaction of the powder bed before the measurement could help discriminating the different whey protein powders coated by sugars.

Table 13. Wetting properties of whey protein isolate powders fluidized with water (Water-60) and coated with different sugars for 60 min determined by capillary rise.

	Capillary rise wetting time (s)	Wetting velocity ($\mu\text{m/s}$)
Water-60	395 ± 151	3.1 ± 1.4
Sucrose-60	331 ± 140	3.7 ± 1.5
Lactose-60	553 ± 238	2.5 ± 1.3
Galactose-60	529 ± 298	2.9 ± 1.6

4.2.2.3. Surface characterization

AFM measurements made it possible to quickly identify the presence of coated areas at whey protein isolate powder surface (**Figure 52 and Table 14**). Indeed, uncoated and coated areas markedly differ in roughness: 5 – 6 nm and over 86 nm, respectively. AFM analysis thus allowed to validate the previous hypothesis on the location of coating sugar in small patches distributed at the surface of whey protein isolate powder. However, the differences of coated layer roughness according to the nature of coated sugar cannot explain the observed wettability variations of coated whey protein isolate powders (Pearson’s correlation coefficient of 0.33 showing an insignificant correlation).

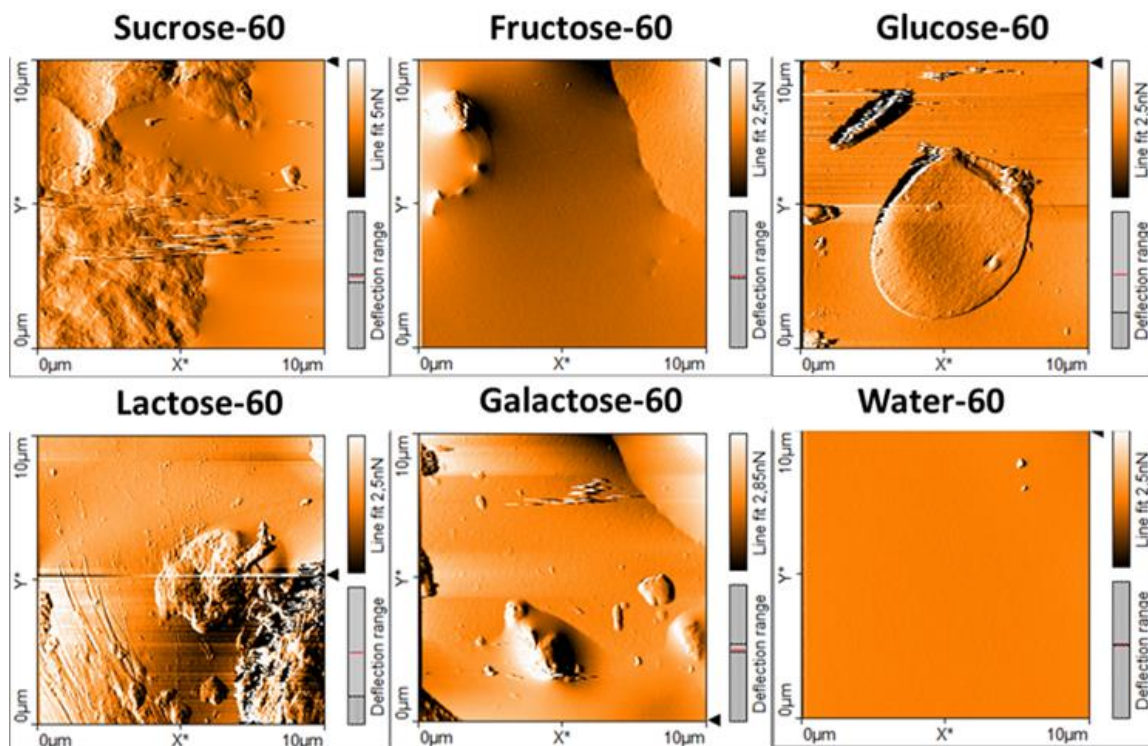


Figure 52. Surface topography of whey protein isolate powders fluidized with water (Water-60) and coated with different sugars for 60 min.

Table 14. Particle and coated layer roughnesses of whey protein isolate powders fluidized with water (Water-60) and coated with different sugars for 60 min.

	Particle roughness (nm)	Coated layer roughness (nm)
Water-60	5.1 ± 0.3	/
Sucrose-60	5.8 ± 1.5	122.2 ± 38.6
Lactose-60	6.6 ± 0.5	168.0 ± 47.8
Glucose-60	6.5 ± 1.1	86.4 ± 8.9
Fructose-60	5.2 ± 0.1	246.7 ± 84.9
Galactose-60	5.1 ± 0.6	124.2 ± 17.0

Coating thickness was evaluated (**Figure 53 and Table 15**) and showed no significant difference between the different sugar-coated whey protein isolate powders. Patch thickness was considered to equal the height difference between the maximum patch height and the height of the baseline, corresponding to particle surface located under the patch (cf. Figure 53). It was highly heterogeneous (coating thickness ranged between 0.15 and 0.55 μm in the various observations on the same sugar-coated whey protein isolate powder) and the average coating thickness was about 0.30 μm .

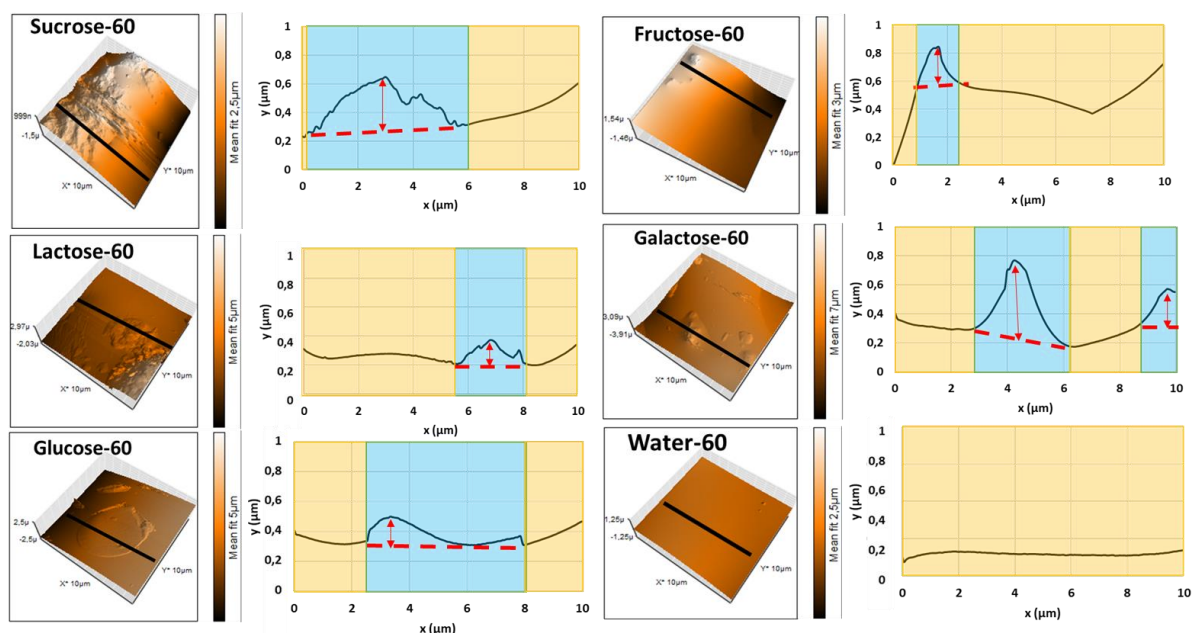


Figure 53. Measurement principle of coating thickness of whey protein isolate powders fluidized with water (Water-60) and coated with different sugars for 60 min. Three dimensional images show the black line where thickness was measured. Yellow parts of the diagrams correspond to uncoated (smooth) areas, and blue parts to coated (rough) areas.

Table 15. Coating thickness of whey protein isolate powders coated for 60 min with different sugars.

	Thickness (μm)
Sucrose-60	$0.30^a \pm 0.12$
Lactose-60	$0.27^a \pm 0.11$
Glucose-60	$0.31^a \pm 0.13$
Fructose-60	$0.30^a \pm 0.16$
Galactose-60	$0.28^a \pm 0.12$

Means with different superscripted letters in the same column were significantly different according to Tukey's HSD test ($p < 0.05$; $n = 9$).

It was not possible to link wettability of sugar-coated whey protein isolate powders to the nature of the sugars in relation with their physicochemical properties (solubility, glass transition temperature, and chain length), nor with coating roughness and thickness. The main hypothesis to explain the absence of observable differences in physicochemical properties of coated whey protein isolate powders in spite of their significant differences in wettability, it should be the difficulty to observe differences in sugars hydrophilicity. Sugars are known to be highly hydrophilic, so there are only slight differences between sugars hydrophilicity, not enough to easily identify a significant trend.

4.2.3. Impact of a humid environment on sucrose-coated whey protein isolate powder

Whey protein isolate powder coated with sucrose for 60 min (initially equilibrated with air at 10 % relative humidity as shown by its water activity of 0.10) was stored for 1 h in an oven at 25° C at 20, 40, or 60 % relative humidities in order to evaluate the evolution of its physicochemical properties and wettability upon water uptake. This study was intended to evaluate bulk and surface modifications of coated powders upon interaction with waters with a view to better understand the mechanisms at play in the very first moments of its reconstitution.

4.2.3.1. Physicochemical properties and wettability

The increase in air relative humidity resulted in a significant increase in water content from 3.13 g/100 g on wet basis at 10 % of relative humidity (RH) to 8.78 g/100 g on wet basis at 60 % RH (**Table 16**). Water uptake upon equilibration with humid air also induced particle swelling, as reflected by an increase in particle size as already reported (Crouter and Briens, 2014; Rosenberg et al., 1985).

Interaction with humid air also affected wettability, which was impaired at higher relative humidity (10 % increase in wetting time was observed for relative humidity increase from 10 to 60 %) according to a linear trend (**Table 16** and **Figures 54 & 55**). This result goes against what has been highlighted in section 4.1.4. and in the literature for the impact of the water content (Fournaise et al., 2021b; Hammes et al., 2015; Hołysz et al., 2010). This decrease in wettability upon surface equilibration with humid air could result from the formation of a viscous and sticky layer at the surface of sucrose-coated whey protein isolate powder (Teunou and Fitzpatrick, 1999; Wallack and King, 1988) which would be deleterious for powder wettability by reducing the ability of water penetration into particles.

Table 16. Granulometric characteristics, water content, and wettability of whey protein isolate powders coated with sucrose for 60 min under various conditions of air relative humidity from 10 to 60 %.

	D10 (µm)	D50 (µm)	D90 (µm)	Span (-)	Water content (g/100 g on wet basis)	Wettability (s)
Sucrose-60, 10 % RH	14.10 ^a ± 0.00	46.40 ^c ± 0.17	98.27 ^b ± 1.03	1.81 ^c ± 0.02	3.13 ^d ± 0.10	720 ^c ± 4
Sucrose-60, 20 % RH	14.73 ^b ± 0.23	48.13 ^b ± 0.92	107.33 ^a ± 2.52	1.92 ^b ± 0.03	5.07 ^c ± 0.11	737 ^{bc} ± 6
Sucrose-60, 40 % RH	14.60 ^{bc} ± 0.10	47.60 ^{bc} ± 0.56	109.33 ^a ± 0.58	1.99 ^a ± 0.02	6.09 ^b ± 0.20	751 ^b ± 10
Sucrose-60, 60 % RH	15.47 ^a ± 0.29	49.70 ^a ± 0.44	110.67 ^a ± 0.58	1.92 ^b ± 0.02	8.78 ^a ± 0.28	795 ^a ± 16

Means with different superscripted letters in the same column were significantly different according to Tukey's HSD test ($p < 0.05$; $n = 3$).

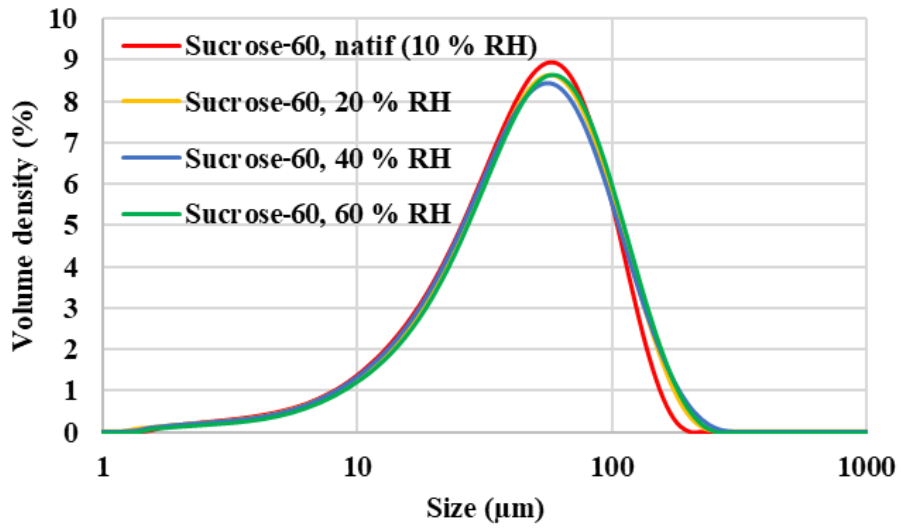


Figure 54. Particle size distributions of whey protein isolate powders coated with sucrose for 60 min at relative humidities between 10 and 60 %.

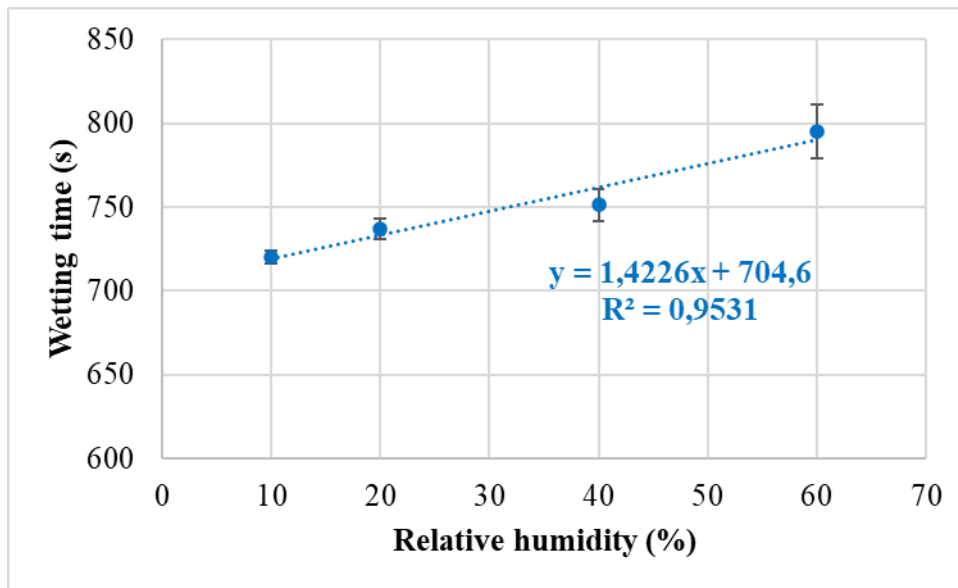


Figure 55. Evolution of the wetting time with the increase in relative humidity.

4.2.3.2. *Surface characterization*

Surface nanomechanics probed by AFM made it possible to identify coated areas (sucrose) on whey protein isolate powder coated with sucrose for 60 min (**Figure 56A**) due to their high Young's modulus above 5 GPa. Indeed, this range of Young's modulus is in line with the literature for crystalized sugars (Perkins et al., 2007). Uncoated areas (whey proteins isolate) had a lower Young's modulus around 2 GPa, which is consistent with what was measured by Gaiani et al., (2021) on β -lactoglobulin powder. Equilibration of sucrose-coated whey protein isolate powder led to a decrease in Young's modulus of the whole coated powder surface under 2 GPa (**Figures 56A and 56B**). This suggests that sucrose patches were plasticized upon water uptake by the coated powder, which can be explained by the structural transformation of sucrose from crystalline to amorphous upon water uptake, already highlighted by Palzer (2007). Uncoated areas also get softer probably because the whole surface became wet upon equilibration at 60 % relative humidity (**Figures 56C and 56D**).

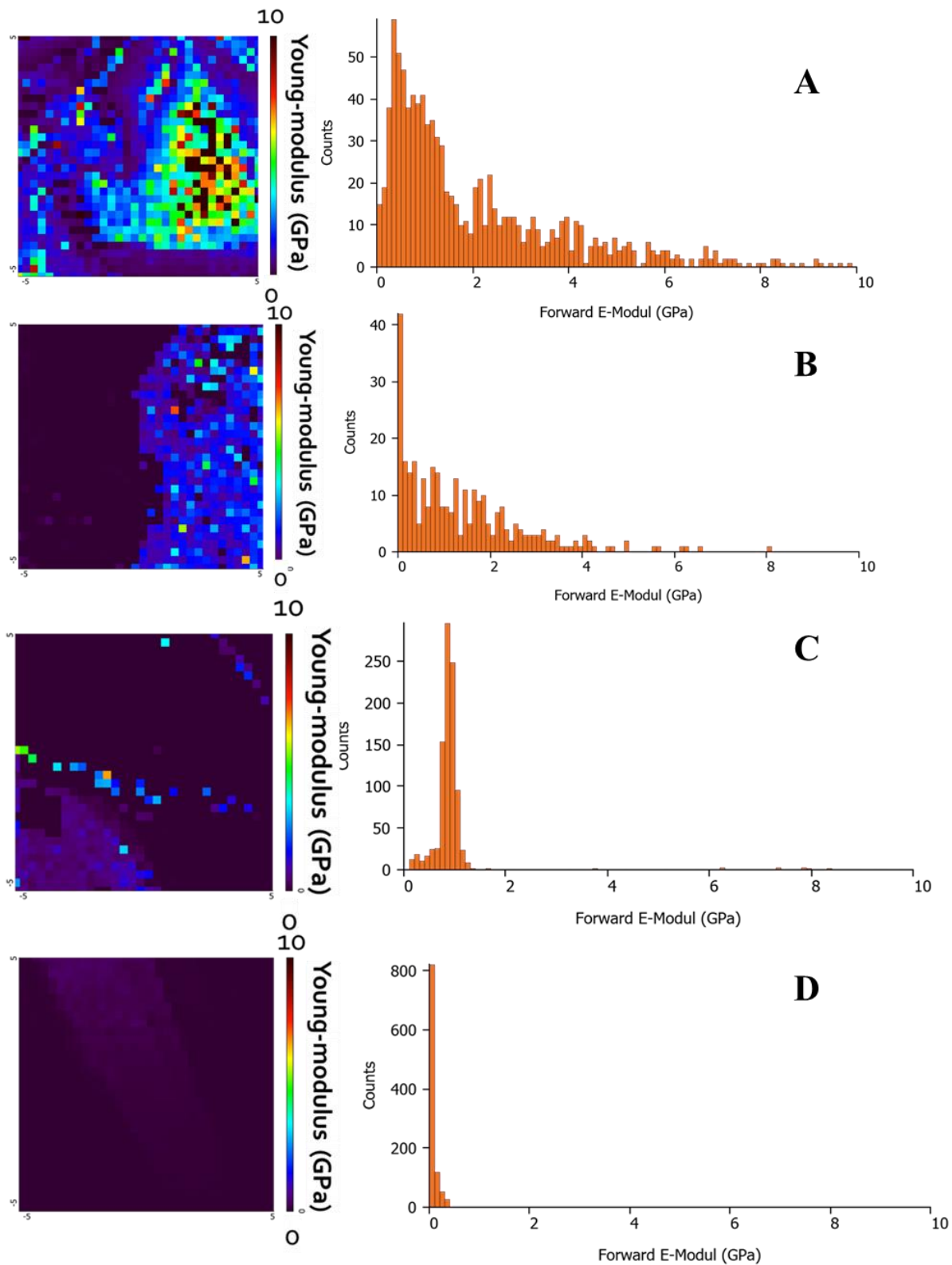


Figure 56. Young's modulus maps and diagrams of sucrose-coated whey protein isolate powders (sucrose-60) equilibrated at various relative humidities, A- 10 % RH, B- 20 % RH, C- 40 % RH, and D- 60 % RH.

ESEM observation seemed to confirm the hypothesis put forward from AFM results. Indeed, the crystalline (polygonal) appearance of sucrose patches at 10 % RH (**Figure 57A**) was lost at higher relative humidities (**Figures 57B, C, and D**), suggesting a structural transformation into amorphous sucrose in accordance with nanoindentation results and literature (Palzer, 2007). Also, upon equilibration at relative humidities over 40 %, the surface of the uncoated area around and under patches seemed to sink (**Figures 57C and D**). This last phenomenon may be interpreted as local plasticization of whey protein isolate, probably owing to a higher local water content.

AFM and ESEM results permit to hypothesize a mechanism explaining wettability improvement of whey protein isolate powder upon sugar-coating. Upon contact with water, sugar patches may quickly absorb water due to their hydrophilicity, leading to their plasticization and the decrease in their Young's modulus. Then, upon water diffusion through sugar patches, the contact between water and whey protein isolate powder surface would be facilitated, accelerating the water absorption by whey protein isolate powder surface, leading to its plasticization in the proximity of sugar patches, in accordance with ESEM observations at higher relative humidity. This may improve the wetting of whey protein isolate surface and the access of water to its potential open pores.

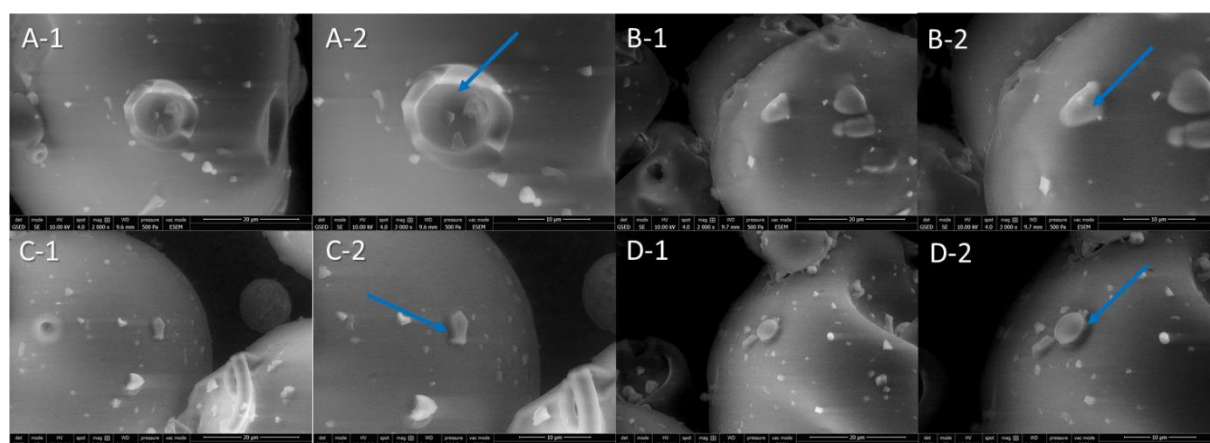
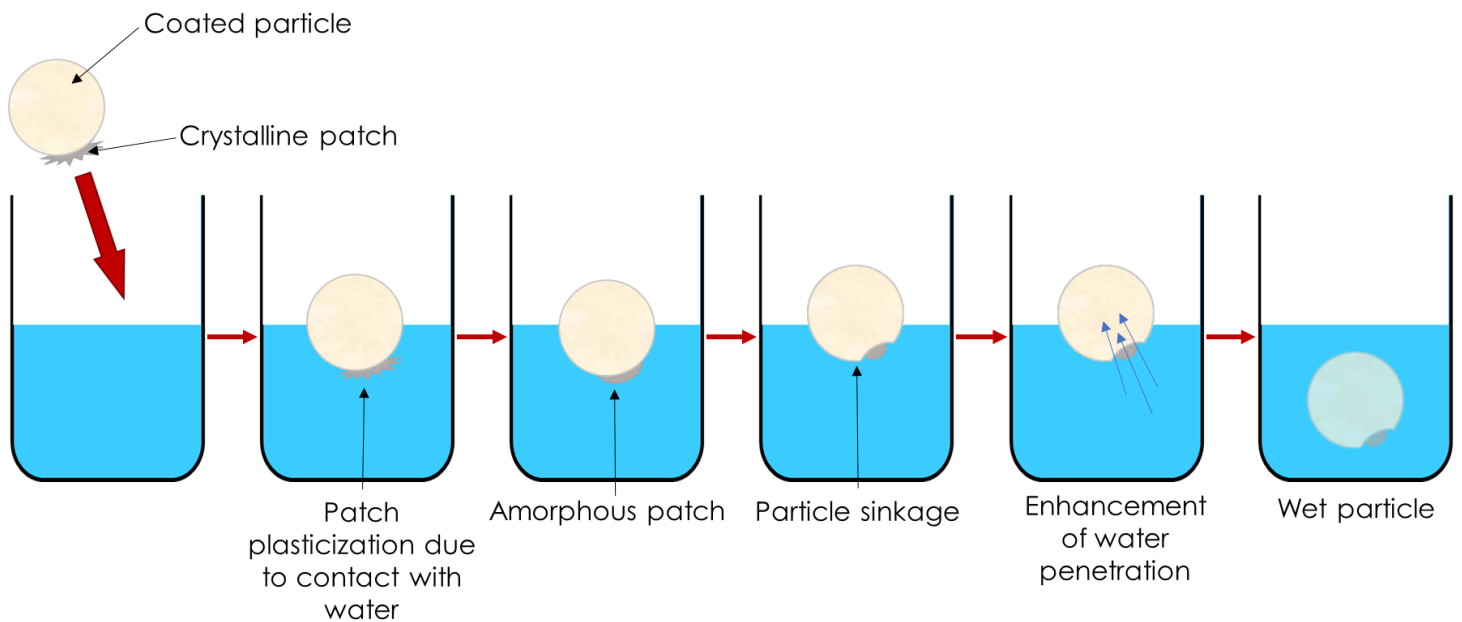


Figure 57. Evolution of the surface appearance with the increase of the relative humidity, A- sucrose-60 10 % RH, B- sucrose-60 20 % RH, C- sucrose-60 40 % RH, D- sucrose-60 60 % RH, 1: $\times 2\,000$ magnification, and 2: $\times 3\,000$ magnification. Blue arrows indicate the location of patches.

4.2.4. Conclusion

Modifying the surface of the whey protein isolate powder by sugar coating has allowed to improve the wetting time to be halved without inducing agglomeration, meaning that the improved wetting is only due to the coated operation. This demonstrates that a small amount of sugar can greatly improve the wetting of the powder, so coating with more sugar and/or agglomeration seems not necessary to greatly improve the wetting step. On the other hand, it was not possible to find an explanation for the wettability differences between formulations with different sugars. This may be due to the high level of hydrophilicity of the sugars and the low difference in hydrophilicity between sugars which would make it difficult to explain wettability differences. Despite the inability to identify the differences between the sugars, it was possible to hypothesize the mechanism of wetting improvement due to coated sugars. The sugar patches present at the powder surface could quickly interact with water and put water in contact with whey protein isolate powder surface, especially with potential open pores, thus enhancing its wetting (**Figure 58**). It would be necessary to perform topography and nanoindentation AFM analyses on the same area of coated particle surface during the increase in relative humidity to be able to check the hypothesis of improved contact with water induced by the presence of sugar patches.

Figure 58. Hypothesis about the mechanism of wetting for whey protein powder coated with sugar.



4.3. Descriptive modelling of food powders reconstitution kinetics followed by laser granulometry

This part of the PhD work was dedicated to the investigation of reconstitution kinetics with descriptive models with the objective to determine characteristic kinetic parameters for the whole reconstitution and its steps.

Reconstitution kinetics of various food powders in fixed mixing conditions were followed by laser granulometry. Obtained reconstitution profiles were fitted using a sum of first-order indicial responses. This descriptive modelling approach allowed linking each of the main reconstitution steps (swelling, dispersion, and solubilization) to a single first-order indicial response and characterizing their kinetics. Initial, maximal, and final median particle sizes; swelling, dispersion, and solubilization durations and rates; as well as an overall reconstitution time, were calculated from model parameters (section 3.4.1.2.). This descriptive modelling approach was not successful for instant powders (their reconstitution being too quick to be followed by laser granulometry) or powders composed of several major components having well different kinetics for the same reconstitution steps. The durations and rates of reconstitution steps were successfully correlated with physicochemical properties of investigated powders in order to evidence the most influencing properties on the reconstitution kinetics of food powders.

4.3.1. Application of the two-step fitting approach of the descriptive reconstitution model: example of instant mash

Reconstitution curve of instant mash (**Figure 37A**) was of first type (distinguishable swelling, dispersion, and solubilization steps). The experimental median particle size first increased from 481 μm to 1 188 μm between time zero and about 20 s, corresponding to the swelling step. Then, it decreased from 1 188 μm to 109 μm from about 20 s to the end of the reconstitution assay, which was associated with the dispersion and solubilization steps. The slope change in the decreasing part of the reconstitution curve indicated that dispersion took place between 20 and 100 s approximately, and solubilization was the dominant reconstitution mechanism above circa 100 s.

Thus, the separate fitting of increasing and decreasing parts of the reconstitution curve was carried out following the procedure described in the subsection 4.1.2 of material and methods. The swelling-dominated reconstitution phase only (increasing part) was modelled with **Equation 24** with $D50_0^* = 482 \mu\text{m}$, $A_0 = 623 \mu\text{m}$, $\tau_0 = 3.2 \text{ s}$, and $R^2 = 95.8 \%$ (**Figure 59**).

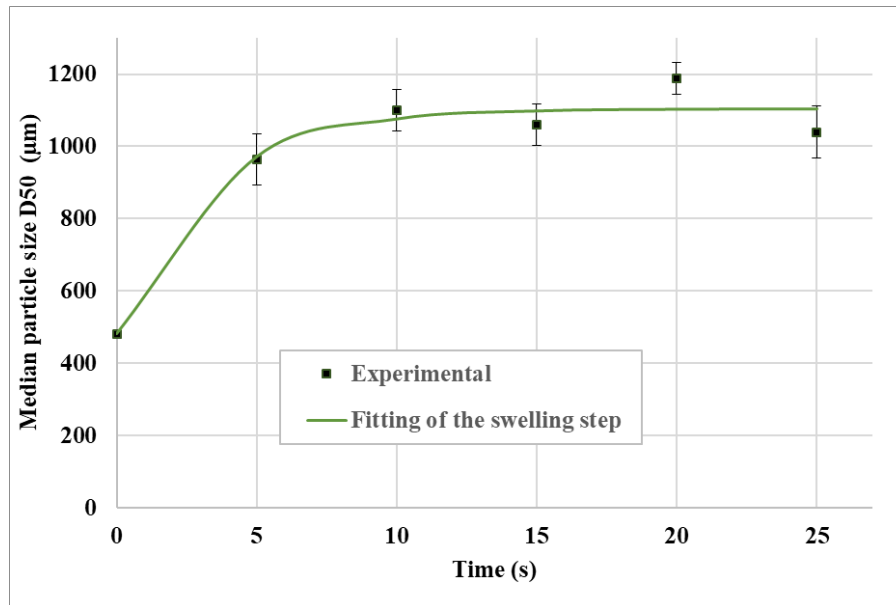


Figure 59. Separate fitting of the swelling step of the (first type) reconstitution profile of instant mash using **Equation 24**. Error bars indicate standard deviations obtained with three replicates of reconstitution assays; some, inferior to the marker size, are not visible.

The dispersion- and solubilization-dominated reconstitution phases only (decreasing part) were modelled with **Equation 25** with $D50_1 = 1\,939 \mu\text{m}$, $A_1 = 1\,687 \mu\text{m}$, $\tau_1 = 35.9 \text{ s}$, $A_2 = 153 \mu\text{m}$, $\tau_2 = 4\,990 \text{ s}$, and $R^2 = 98.9 \%$ (**Figure 60**).

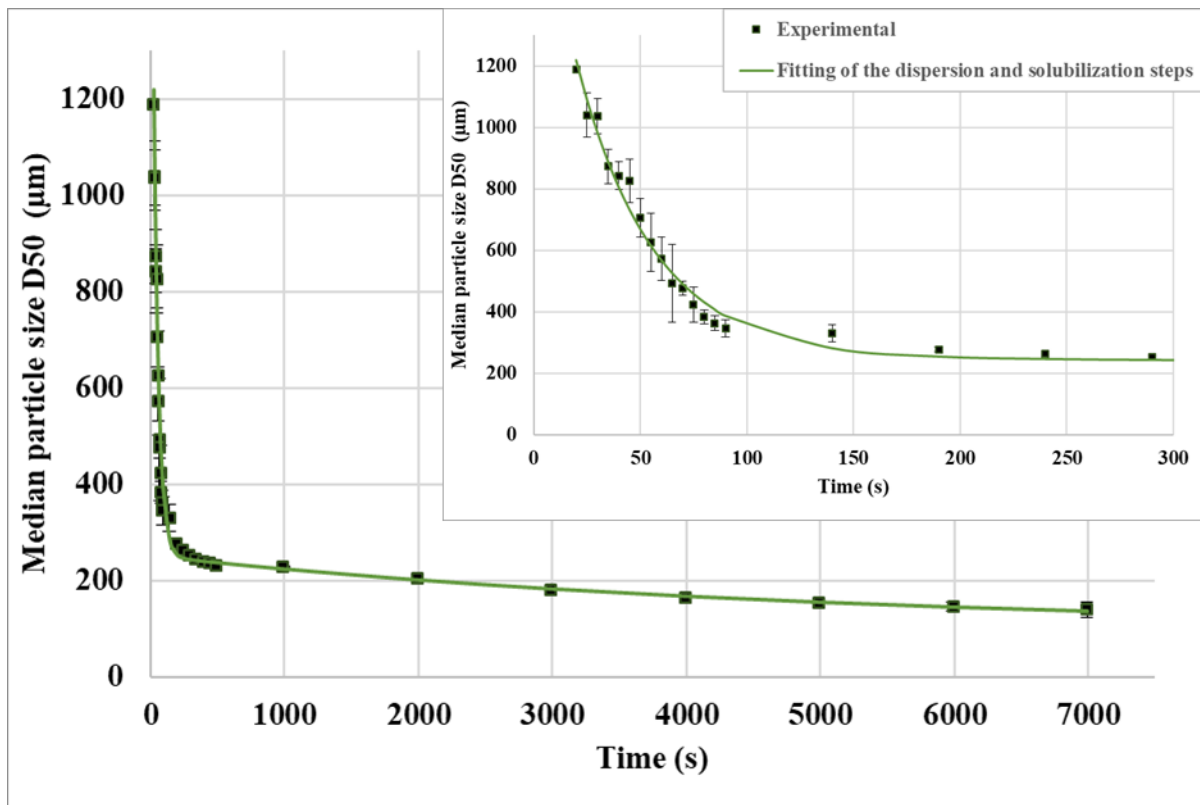


Figure 60. Separate fitting of the dispersion and solubilization steps of the (first type) reconstitution profile of instant mash using **Equation 25**.

Error bars indicate standard deviations obtained with three replicates of reconstitution assays; some, inferior to the marker size, are not visible.

The last step of the fitting approach consisted in modelling the whole reconstitution curve using **Equation 23** following the procedure described in section 4.2.1. of material and methods, resulting in $D50_0 = 653 \mu\text{m}$, $A_0 = 4\,297 \mu\text{m}$, $\tau_0 = 16.0 \text{ s}$, $A_1 = 4\,695 \mu\text{m}$, $\tau_1 = 24.8 \text{ s}$, $A_2 = 153 \mu\text{m}$, $\tau_2 = 4\,990 \mu\text{m}$, and $R^2 = 99.3 \%$. The obtained descriptive model was in great accordance with the reconstitution curve (**Figure 61**), as denoted by the elevated coefficient of determination R^2 .

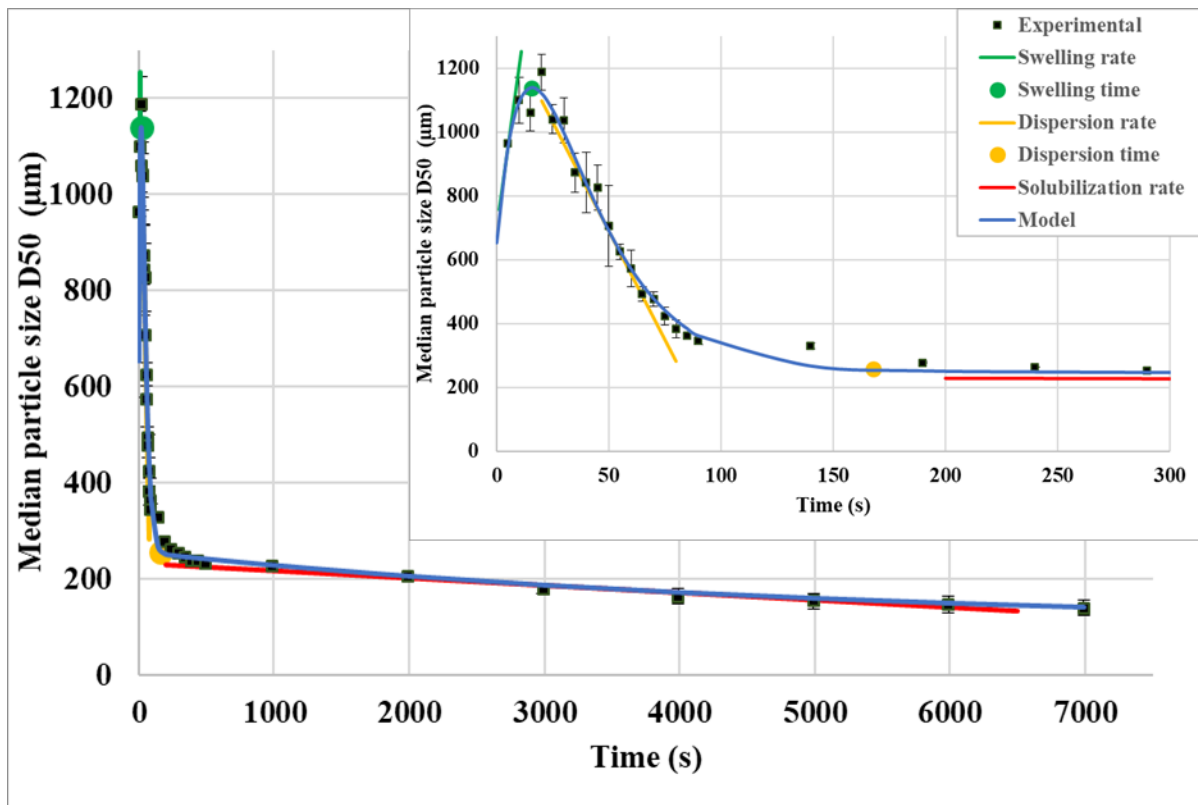


Figure 61. Descriptive reconstitution model for instant mash obtained by fitting with **Equation 23**; swelling and dispersion times; swelling, dispersion, and solubilization rates.

Error bars indicate standard deviations obtained with three replicates of reconstitution assays; some, inferior to the marker size, are not visible.

Following the procedure described in the section 4.2.1. of material and methods, the complete reconstitution model was used to calculate modelled initial, maximal, and final median particle sizes; swelling, dispersion, and solubilization durations and rates; as well as reconstitution time: $D50_0 = 653 \mu\text{m}$, $D50_{\text{max}} = 1139 \mu\text{m}$, $D50_{\infty} = 103 \mu\text{m}$, $\Delta t_{\text{swelling}} = 15.7 \text{ s}$, $\Delta t_{\text{dispersion}} = 152 \text{ s}$, $\Delta t_{\text{solubilization}} = 5222 \text{ s}$, $t_{\text{reconstitution}} = 5390 \text{ s}$, $+49.6 \mu\text{m}\cdot\text{s}^{-1}$ swelling rate, $-13.6 \mu\text{m}\cdot\text{s}^{-1}$ dispersion rate, and $-0.015 \mu\text{m}\cdot\text{s}^{-1}$ solubilization rate.

4.3.2. Influence of physicochemical properties on powder reconstitution steps

The modelling approach following the procedure described in section 3.4.1.2. permitted to obtain the descriptive reconstitution models displayed in **Figures 62, 63, and 64** when applied to the first, second, and third types of reconstitution curves of investigated powders. Model parameters; initial, maximal, and final median particle sizes; swelling, dispersion, and solubilization durations and rates; as well as reconstitution times are listed in **Table 17**.

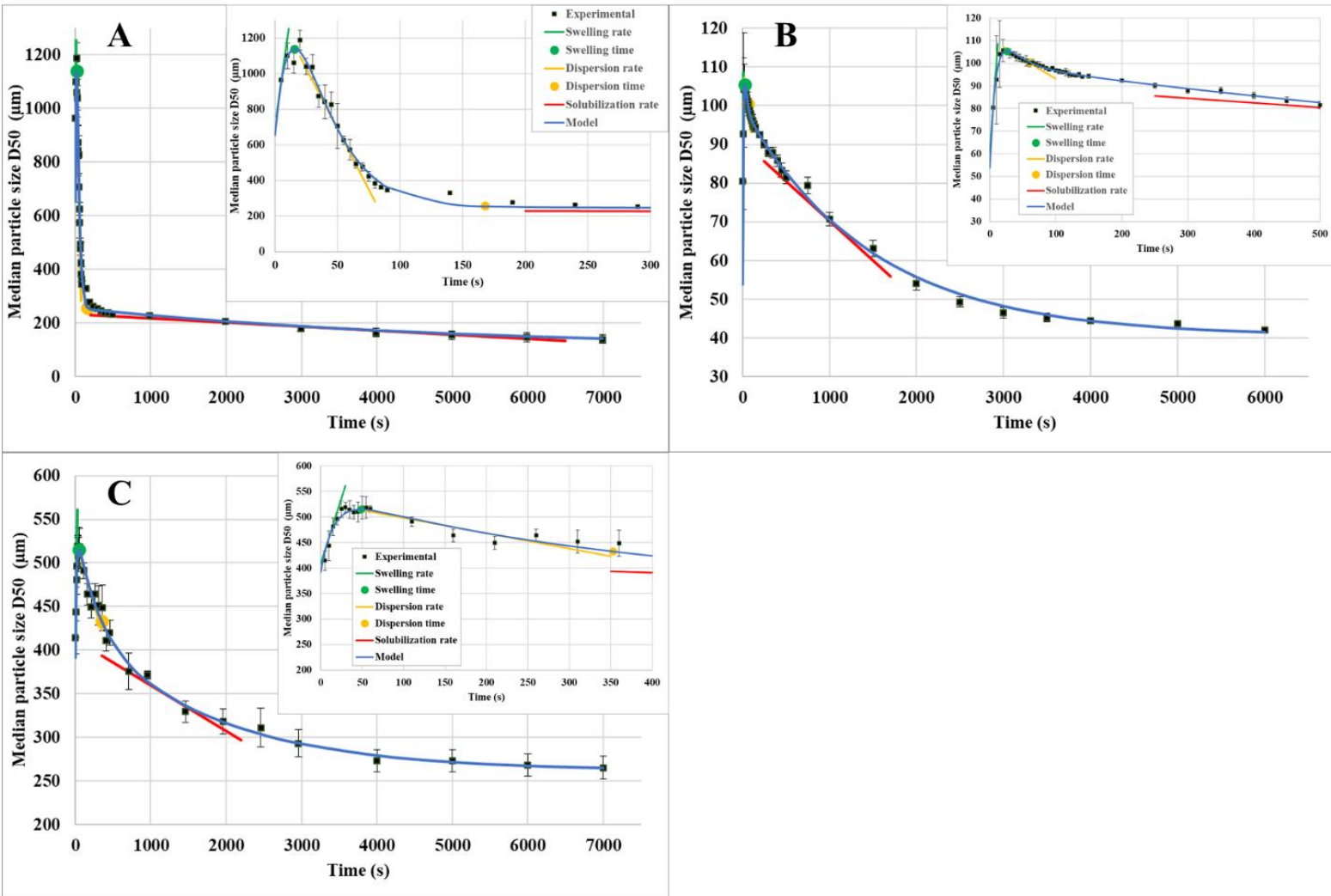


Figure 62. Descriptive reconstitution model, swelling, dispersion, and solubilization times and rates of powders of the first reconstitution type: (A) instant mash, (B) casein, and (C) polenta 1.0 mm.

Error bars indicate standard deviations obtained with three replicates of reconstitution assays; some, inferior to the marker size, are not visible.

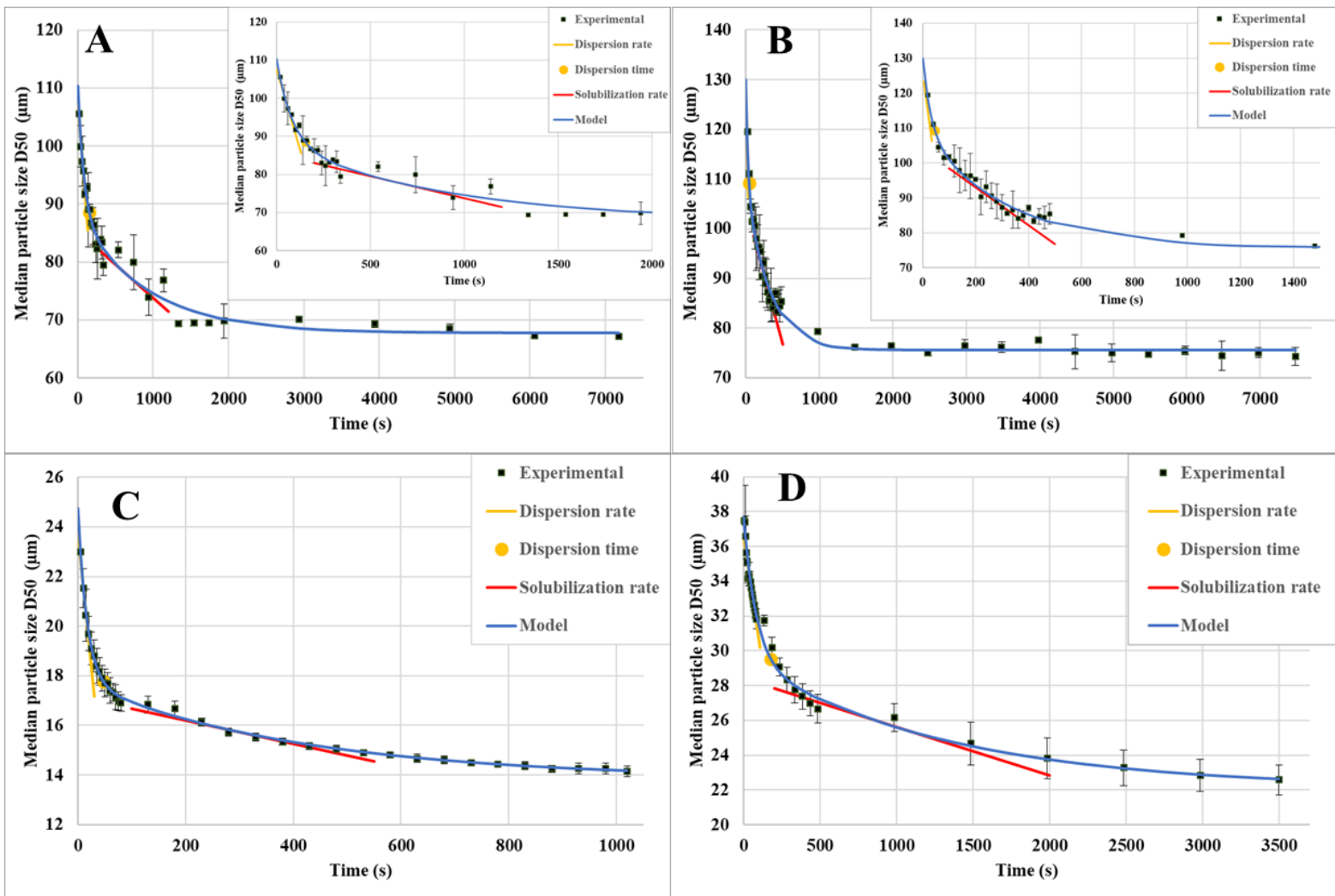


Figure 63. Descriptive reconstitution model, dispersion time, as well as dispersion and solubilization rates of powders of the second reconstitution type: (A) T55 flour, (B) T45 flour, (C) cocoa fat- alka-, and (D) cocoa fat+ alka+.

Error bars indicate standard deviations obtained with three replicates of reconstitution assays; some, inferior to the marker size, are not visible.

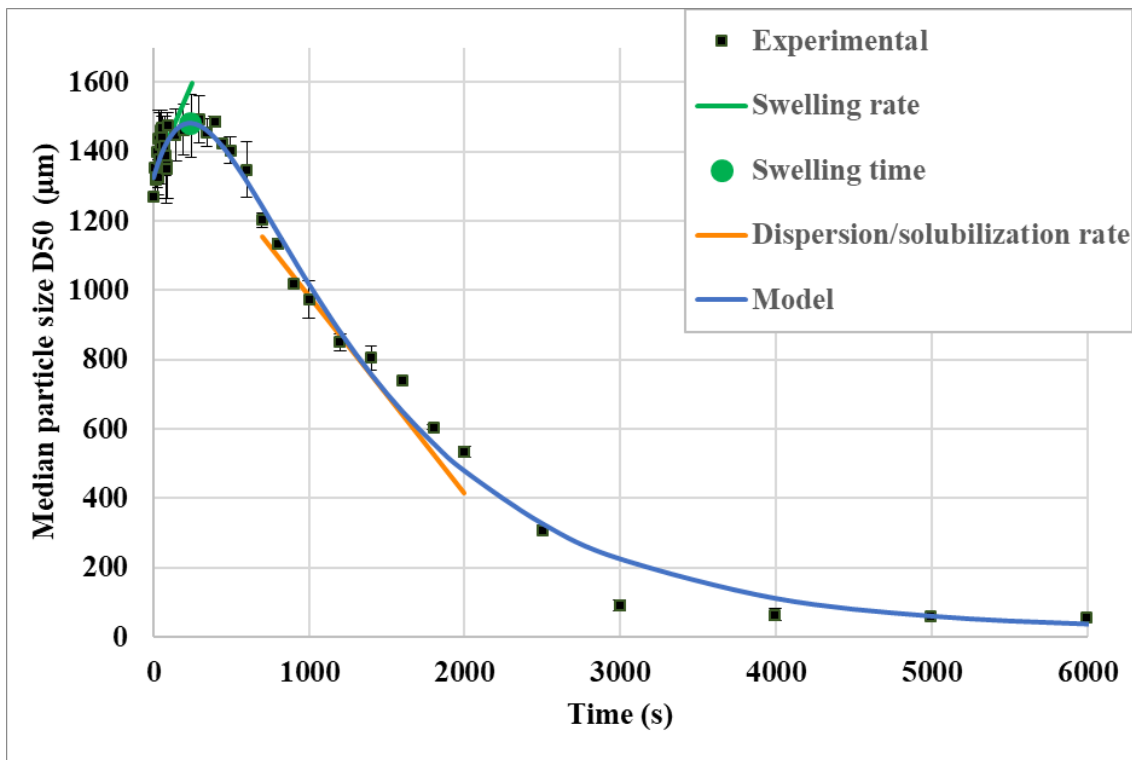


Figure 64. Descriptive reconstitution model, swelling, dispersion/solubilization times and rates of small couscous (third reconstitution type).

Error bars indicate standard deviations obtained with three replicates of reconstitution assays; some, inferior to the marker size, are not visible.

Table 17. Modelled initial, maximal, and final median particle sizes; model parameters and coefficient of determination; swelling, dispersion, and solubilization durations and rates; reconstitution time of investigated powders of the first (instant mash, casein, and polenta 1.0 mm), second (T55 flour, T45 flour, cocoa fat- alka-, and cocoa fat+ alka+), and third reconstitution types (small couscous).

		Sample	D50 ₀ (µm)	D50 _{max} (µm)	D50 _∞ (µm)	A ₀ (µm)	τ ₀ (s)	A ₁ (µm)	τ ₁ (s)	A ₂ (µm)	τ ₂ (s)	R ² (%)	Swelling duration (s)	Dispersion duration (s)	Solubilization duration (s)	Reconstitution time (s)	Swelling rate (µm/s)	Dispersion rate (µm/s)	Solubilization rate (µm/s)
Type of reconstitution curve (cf. material and methods 3.4.1.2.1.)	1 st	Instant mash	653	1 139	103	4 297	16.0	4 695	24.8	153	4 990	99.3	15.7	152	5 222	5 390	+49.6	-13.6	-1.5 × 10 ⁻²
		Casein	53.8	105	40.4	69.4	8.5	23.5	30.3	59.2	1 473	99.8	26.2	35.1	4 216	4 278	+4.0	-0.17	-2.0 × 10 ⁻²
		Polenta 1.0 mm	392	515	262	153	15.6	113	274	170	1 752	99.0	48.6	304	4 204	4 556	+5.1	-0.30	-5.2 × 10 ⁻²
	2 nd	T55 flour	110	110	67.8	/	/	21.9	80.9	20.7	903	97.7	/	155	1 897	2 052	/	-0.17	-1.1 × 10 ⁻²
		T45 flour	130	130	75.6	/	/	20.9	30.6	33.5	320	98.6	/	46,6	756	803	/	-0.57	-5.4 × 10 ⁻²
		Cocoa fat- alka-	24.7	24.7	13.8	/	/	7.0	17.2	3.9	412.6	99.8	/	48.0	765	813	/	-0.22	-4.7 × 10 ⁻³
		Cocoa fat+ alka+	37.7	37.7	22.1	/	/	8.2	82.5	7.4	1 334	99.1	/	179	2 824	3 004	/	-5.8 × 10 ⁻²	-2.7 × 10 ⁻³
	3 rd	Small couscous	1 324	1 481	17.4	993	288	2 299	1 244	/	/	99.1	234	/	4 054	4 288	1.0	-0.57*	

/: not applicable.

*: dispersion/solubilization rate.

With the modelling approach developed in this study, the information about reconstitution kinetics of food powders was gathered in the characteristic parameters calculated from the descriptive reconstitution model (**Table 17**), each parameter being associated with one reconstitution step only. The obtained descriptive model was not built to predict the durations and rates of reconstitution steps from powder physicochemical properties (bulk and surface chemical compositions, granulometric characteristics) and reconstitution conditions (e.g., stirring speed, impeller type, volume and geometry of the reconstitution reactor, powder/water mass ratio, water temperature), but the characteristic parameters of each reconstitution step calculated from the descriptive model can still be used to establish correlations with powder physicochemistry and reconstitution conditions. However, in this study, the latter were fixed and their influence on reconstitution steps could therefore not be evaluated. Thus, only powder physicochemical parameters that had the most influence on powder reconstitution kinetics were identified by calculating Pearson's correlation coefficients (**Table 18**).

Table 18. Pearson’s correlation coefficients between powder physicochemical properties (bulk and surface chemical compositions, granulometric characteristics) and reconstitution characteristic parameters (swelling, dispersion, and solubilization durations and rates; reconstitution time issued from the descriptive modelling approach).

Pearson’s correlation coefficients (R)	Protein content	Lipid content	Content in carbohydrates, sugars and fibers excluded	Sugar content	Fiber content	Mineral content	Water activity	Water content	C/O ratio	C-C/other C bonds ratio	Dry median particle size
Swelling rate	-0.35	-0.96	0.31	-0.64	0.92	-0.31	-0.16	-0.26	-0.70	-0.81	-0.04
Swelling duration	-0.30	0.56	0.31	-0.74	-0.22	-0.36	0.55	0.38	0.96	-0.02	0.87
Dispersion rate	0.28	0.29	-0.38	0.10	0.16	0.25	0.02	0.01	0.64	0.45	-0.74
Dispersion duration	-0.54	0.06	0.51	-0.35	-0.15	0.04	0.34	0.32	0.03	-0.08	0.61
Solubilization rate	0.20	0.55	-0.55	-0.07	0.61	0.22	-0.72	-0.74	0.30	0.52	-0.34
Solubilization duration	0.19	-0.23	0.09	0.42	-0.45	0.23	-0.13	0.01	-0.51	-0.45	0.72
Reconstitution time	0.11	-0.26	0.17	0.44	-0.49	0.13	-0.02	0.07	-0.27	-0.48	0.59

Green: highly significant correlations; orange: significant correlations; red: insignificant correlations.

As for powder swelling, both the dry median particle size and particle surface hydrophobicity (C/O ratio) were positively correlated with the swelling duration. This influence of median particle size on the time needed for powder swelling was expected as the prior mechanism of water uptake should be slower for large particles owing to their lower specific surface area. Besides, surface hydrophobicity may delay powder wetting and sinking, resulting in larger swelling duration (as wetting and sinking were considered as included in swelling step in the descriptive modelling approach developed in the present study). The swelling duration was also decreased at higher sugar content, which was logical as sugars quickly disperse and solubilize without observable swelling. Swelling was also significantly influenced by lipid and fiber contents along with particle surface hydrophobicity (C-C/other C bonds ratio): the presence of fibers increased the swelling rate owing to their hydrophilic nature (Bonacucina et al., 2009; Conti et al., 2006; Cuq et al., 2011; Kravtchenko et al., 1999). On the contrary, the presence of lipids and a higher surface hydrophobicity (denoted by a greater C-C/other C bonds ratio) tend to decrease the swelling rate due to limitation of surface wetting and water transfer into the particle (Fournaise et al., 2021b, 2020; Gaiani et al., 2007; Kim et al., 2002; Murrieta-Pazos et al., 2012).

Then, a positive correlation was found between the dispersion rate and particle surface hydrophobicity evaluated by the C/O ratio, which means that an increase in surface hydrophobicity led to a slower dispersion (as dispersion rates are negative values). This can be explained by the low degree of interaction of water with hydrophobic particle surface that is detrimental to the breaking of intraparticle hydrogen bonds and van der Waals interactions involved in powder dispersion (Cuq et al., 2011; Fournaise et al., 2021b; Freudig et al., 1999). On the opposite, a negative correlation was obtained between the dispersion rate and the median particle size, which means that a larger median particle size enhanced powder dispersion. This may be due to the lower cohesion of large particles, facilitating their dispersion by water (Enferad et al., 2021; Gnagne et al., 2017; Salameh et al., 2016).

Solubilization was slowed by the presence of insoluble components such as fibers, as denoted by the positive correlation between the solubilization rate (negative values) and fiber content. Water retention by insoluble fibers may explain this slowing of solubilization in the presence of insoluble components. On the contrary, water content was negatively correlated with the solubilization rate (negative values), showing that a higher water content tended to enhance solubilization. The same observation was made for water activity. The improvement of solubilization for powders richer in water may be explained by their probable higher

hydrophilily. Also, it was noticed by calculation of Pearson's correlation coefficients between water content and lipid or fiber contents (respectively equal to -0.68 and -0.63) that powders richer in water contained less lipids and fibers. Thus, the enhancement of solubilization at higher water content may also be indirectly viewed as the consequence of the reduced presence of compounds deleterious for powder solubilization. Last, solubilization duration was increased for larger particles, which can be explained by the fact that their specific surface area than for smaller particles, the release of soluble compounds from larger particles takes longer (Dokoumetzidis and Macheras, 2006; Fournaise et al., 2021b; Lamberti et al., 2004; Nernst, 1904).

In this study, the powder physicochemical property that exhibited the higher degree of correlation with reconstitution time was the dry median particle size ($R = 0.59$), showing that powder composed of larger particles may generally take more time to reach complete reconstitution. Indeed, an increase in particle size is known to favor powder wetting and dispersion, but large particles lead to longer swelling and solubilization steps (Dokoumetzidis and Macheras, 2006; Nernst, 1904).

4.3.3. Conclusion

This study presents a new descriptive modelling approach for food powder reconstitution. The proposed model permits to describe the temporal evolution of median particle size upon reconstitution and characterize the kinetics of the main steps of powder reconstitution, namely swelling, dispersion, and solubilization. This approach made it possible to determine swelling, dispersion, and solubilization durations and rates, as well as reconstitution time. This descriptive modelling approach was not successful for instant powders (their reconstitution being too quick to be followed by laser granulometry) or powders composed of several major components having well different kinetics for the same reconstitution steps. The kinetic data obtained from this descriptive modelling approach were linked to powder physicochemistry (median particle size, span, bulk chemical composition, surface hydrophobicity) in order to identify the main physicochemical properties influencing each reconstitution step. Swelling lasted longer for powders composed of large particles and/or particles with a hydrophobic surface but it was shorter in the presence of sugars, whereas the swelling rate was enhanced in the presence of fibers and decreased in the presence of lipids. Dispersion was facilitated for large particles, whereas it was impaired by particle surface hydrophobicity. Solubilization was slowed down in the presence of fibers, and for large particles due to their lower specific surface area. Overall, these trends were consistent with

literature knowledge, showing the relevancy of the developed descriptive modelling approach. The identification of the most influent powder physicochemical properties and reconstitution conditions is a necessary step for the future development of empirical models able to predict reconstitution times but also durations of each reconstitution steps, which would be useful for optimizing industrial applications of food powders.

4.4. Development of an empirical predictive model for powder reconstitution time

This last part of the PhD work concerns the development of an empirical model for the prediction of reconstitution times (t_{95} calculated with the Hill model) obtained by conductimetry in reconstitution assays from the most influential physicochemical properties of powders.

Various forms of classical multivariate mathematical models were tested, and the set of employed physicochemical parameters as predictors variables (inputs) was restricted to those identified as the most influent on powder reconstitution in the study presented in section 4.1.4, namely median particle size, shape factors (sphericity, aspect ratio, and convexity), aerated density, bulk chemical composition, and XPS ratios used for the characterization of surface hydrophobicity (x_1 : content in proteins (g/g on dry basis), x_2 : content in lipids g/g on dry basis), x_3 : content in carbohydrates* (g/g on dry basis), x_4 : content in fibers (g/g on dry basis), x_5 : content in minerals (g/g on dry basis), x_6 : water activity (-), x_7 : content in water g/g on dry basis), x_8 : C/O ratio (-), x_9 : C-C/C-other ratio (-), x_{10} : D50 (μm), x_{11} : content in sugars (g/g on dry basis), x_{12} : span (-), x_{13} : aerated density (-), x_{14} : sphericity (-), x_{15} : convexity (-), and x_{16} : aspect ratio (-)).

*Carbohydrates include sugars but exclude fibers, except in the section 4.4.2.2. where sugars are also excluded.

4.4.1. First approaches

4.4.1.1. Approaches with unnormalized data

The first predictive modelling approach, a multilinear model using unnormalized physicochemical properties (**Tables 2 and 3**) as input data (**Equation 28**), was used to link reconstitution times $t_{reconstitution,i}$ to physicochemical properties of powders, noted $x_{i,j}$ (with i ranging from 1 to n and j ranging from 1 to m , where n and m respectively designate the number of powders (36) and physicochemical properties taken as model inputs (10) (**Table 4**)

$$t_{reconstitution,i} = w_0 + \sum_{j=1}^m w_j x_{i,j} \quad \text{Equation 28}$$

With:

- m , the number of predictors (equal to 10 here),
- j , an integer varying from 1 to m ;

- w_0 and w_j , model weights;

- $x_{i,j}$, predictor variables, i.e. most influencing physicochemical properties and few extra characteristics, for the i^{th} observation, i.e. investigated powder.

The following model weights were obtained: $w_0 = 44.2$ s, $w_1 = 114$ s, $w_2 = -2.96$ s, $w_3 = -0.82$ s, $w_4 = 1.47 \times 10^{-2}$ s, $w_5 = -0.23$ s, $w_6 = 1.91$ s, $w_7 = 193$ s, $w_8 = -0.33$ s, $w_9 = -0.86$ s, $w_{10} = 0.53$ s/ μm . Prediction accuracy was insufficient as denoted by the weak coefficient of determination R^2 of 0.56 (**Figure 65**). The prediction was not at all satisfactory for powders with a short reconstitution time (green and yellow), whereas the trend was better for those with the longer reconstitution times (orange and red).

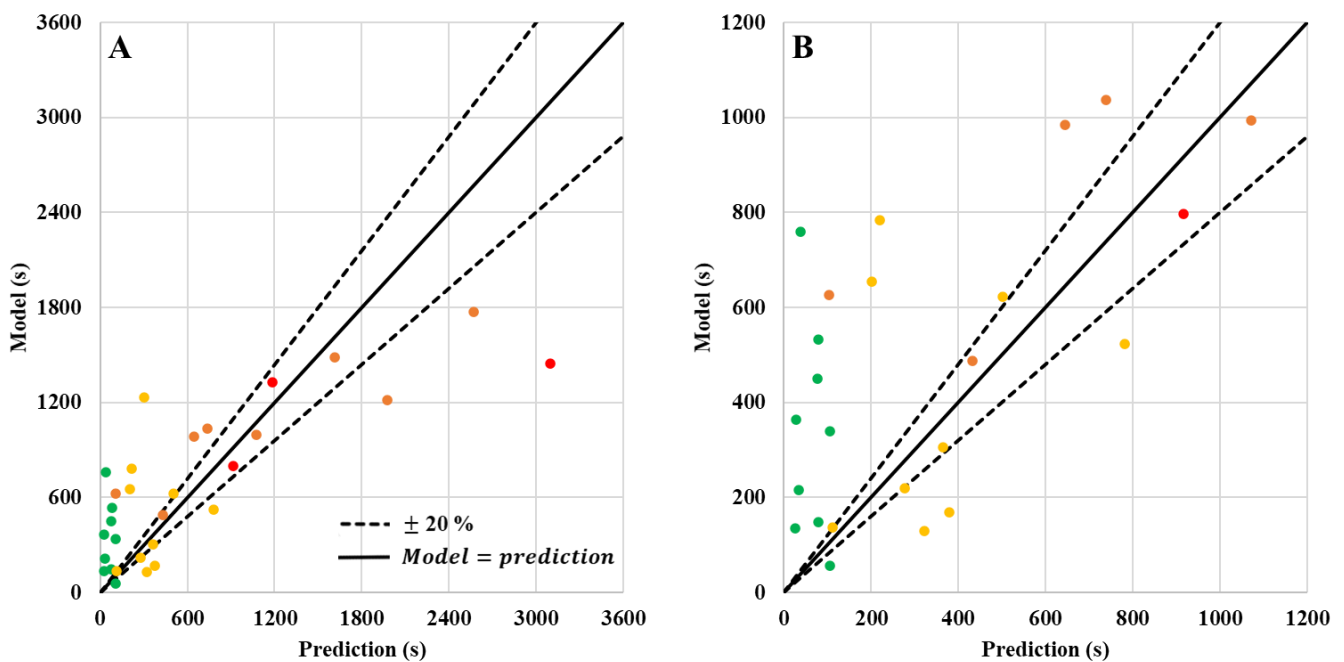


Figure 65. A- Comparison of predicted and experimental values of reconstitution times for the multilinear model obtained with unnormalized physicochemical parameters using **Equation 28**. B- focus on reconstitution times between 0 and 1 200 s. Colors correspond to the powder classification according to wetting and reconstitution behavior deduced from section 4.1.4.: green, good behavior (short wetting and short reconstitution), yellow: decent behavior (long wetting and short reconstitution), orange: mediocre behavior (short wetting and long reconstitution), and red: poor behavior (long wetting and long reconstitution).

After that, a monome model (**Equation 29**) was used to link physicochemical properties of powders and reconstitution times. The first try of monome model using raw (unnormalized)

values of physicochemical parameters was not satisfactory in spite of the good coefficient of determination $R^2 = 0.91$ (**Figure 66**). The monome model made it possible to improve prediction accuracy: powders with a short reconstitution time were better predicted even if the results remain insufficient.

$$t_{reconstitution,i} = w_0 \times \prod_{j=1}^m (x_{i,j} + 10^{-4})^{w_j} \quad \text{Equation 29}$$

With $w_0 = 1.36$ s, $w_1 = 1.47$, $w_2 = -0.41$, $w_3 = -0.93$, $w_4 = -0.15$, $w_5 = -0.62$, $w_6 = 0.78$, $w_7 = 3.28$, $w_8 = 1.01$, $w_9 = 0.68$, $w_{10} = 0.48$.

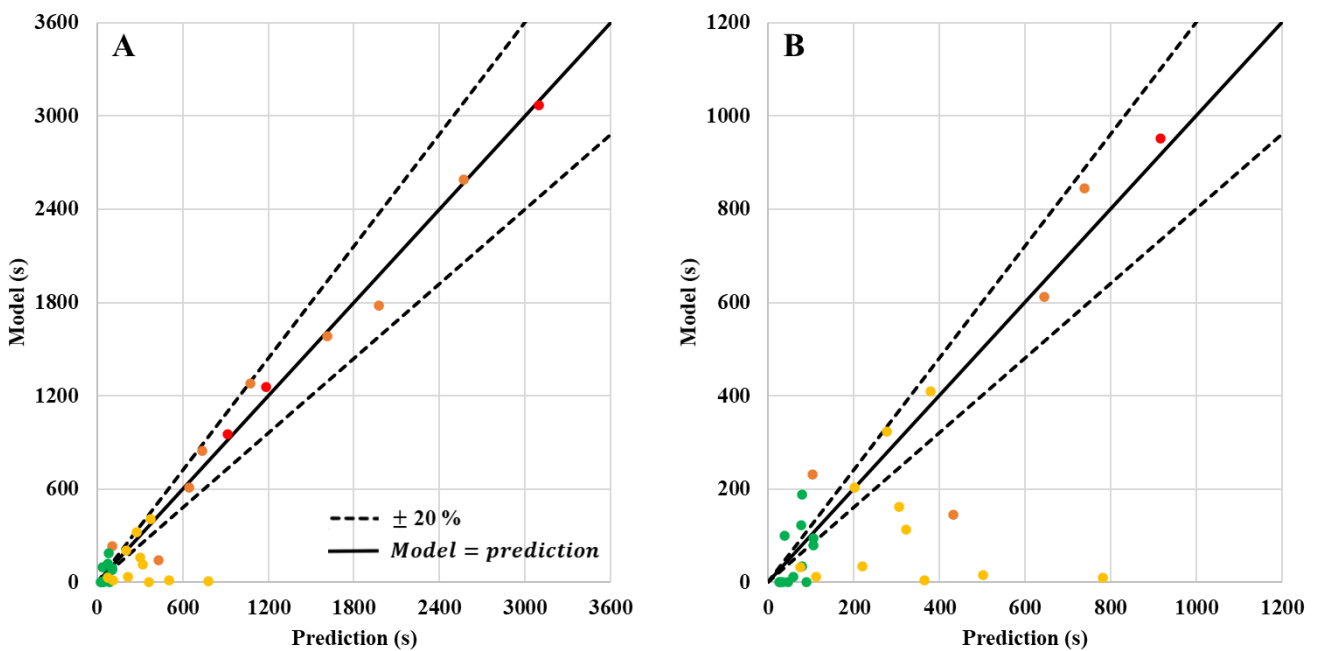


Figure 66. A- Comparison of predicted and experimental values of reconstitution times for the monome model obtained with unnormalized physicochemical parameters using **Equation 29**. B- focus on reconstitution times between 0 and 1 200 s. Colors correspond to the powder classification according to wetting and reconstitution behavior deduced from section 4.1.4.: green, good behavior (short wetting and short reconstitution), yellow: decent behavior (long wetting and short reconstitution), orange: mediocre behavior (short wetting and long reconstitution), and red: poor behavior (long wetting and long reconstitution).

It was then tried to use an exponential model (**Equation 30**) to link physicochemical properties of powders and reconstitution times. The first try of exponential model using raw (unnormalized) values of physicochemical parameters was not satisfactory in spite of the good coefficient of determination $R^2 = 0.90$ (**Figure 67**). The exponential model made it possible to improve prediction accuracy compared to the multilinear model but it was slightly less accurate than the monome model.

$$t_{reconstitution,i} = w_0 \times \prod_{j=1}^m \exp (w_j x_{i,j}) \quad \text{Equation 30}$$

With $w_0 = 11.11$ s, $w_1 = 2.87 \times 10^{-2}$, $w_2 = 4.7 \times 10^{-3}$, $w_3 = -5.48 \times 10^{-2}$, $w_4 = -1.81 \times 10^{-2}$, $w_5 = -8.79 \times 10^{-2}$, $w_6 = 14.98$, $w_7 = 0.38$, $w_8 = 0.34$, $w_9 = -1.91$, $w_{10} = 8.63 \times 10^{-4} \mu\text{m}^{-1}$.

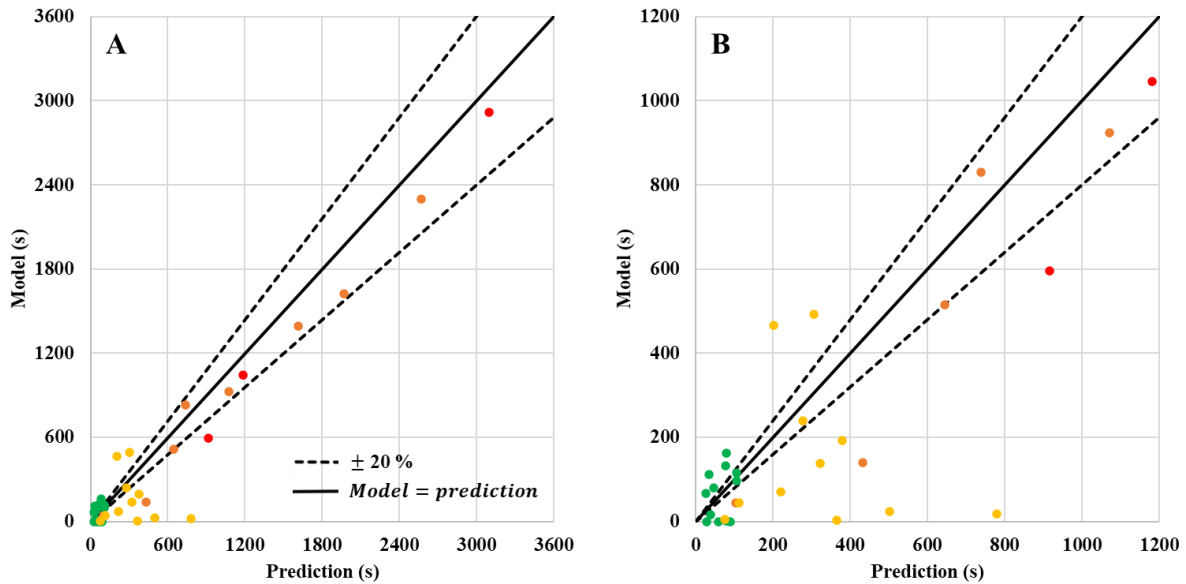


Figure 67. A- Comparison of predicted and experimental values of reconstitution times for the exponential model obtained with unnormalized physicochemical parameters using **Equation 30**. B- focus on reconstitution times between 0 and 1 200 s. Colors correspond to the powder classification according to wetting and reconstitution behavior deduced from section 4.1.4.: green, good behavior (short wetting and short reconstitution), yellow: decent behavior (long wetting and short reconstitution), orange: mediocre behavior (short wetting and long reconstitution), and red: poor behavior (long wetting and long reconstitution).

4.4.1.2. *Approaches with normalized data*

The great difference in model accuracy for long and short reconstitution times and the large differences in powder physicochemical properties may be an obstacle for the development of models, as the physicochemical parameters evaluated with the larger numerical values and/or those having the larger variation range may have a too important mathematical impact on the determination of models. Thus, it was tried to use normalized physicochemical parameters and reconstitution times with the **Equation 20** in predictive models in the fourth approach, in order to confer the same variation ranges (from 0 to 100 %) to input data (**Table 19**).

Table 19. Normalized input data (predictors) and reconstitution time (dependent variable) used for the determination of predictive models.

Powder sample name	Normalized proteins content (%)	Normalized lipids content (%)	Normalized carbohydrates content, sugars and fibers excluded (%)	Normalized sugars content (%)	Normalized fibers content (%)	Normalized mineral content (%)	Normalized water activity (%)	Normalized water content (%)	Normalized median particle size (%)	Normalized reconstitution time (%)
Polenta R (raw)	9	3	99	7	3	0	96	33	33	63
Polenta 1.0 mm	9	3	99	7	3	0	89	32	20	34
Polenta 0.08 mm	9	3	100	7	3	0	74	26	0	13
Instant coffee R (raw)	24	9	54	0	8	9	20	17	85	0
Ground instant coffee	24	9	54	0	8	9	59	22	1	3
Granulated sugar	0	0	0	100	0	0	77	0	30	0
Caster sugar	0	0	0	100	0	0	76	0	23	0
Icing sugar	0	0	0	100	0	0	79	1	1	1
Flour T45	15	2	89	7	6	0	90	35	4	23
Flour T55	15	2	89	7	6	0	87	32	3	20
Cocoa 12F A-	29	18	26	1	39	2	39	9	0	25
Cocoa 12F A+	28	18	26	1	39	2	45	12	0	16
Cocoa 12F A+++	24	38	22	0	33	2	24	8	1	11
Cocoa 23F A+	28	18	26	1	39	2	56	15	0	6
Pea fiber	11	0	39	5	51	3	69	23	2	6
SMP	38	2	0	55	0	8	52	15	3	2
SMP G	38	2	0	55	0	8	52	15	3	2
WMP	36	36	0	38	0	6	32	8	19	3
MPI	100	2	0	2	0	7	35	16	2	100

WPI	100	2	0	6	0	3	10	15	2	9
MCP	96	2	0	2	0	9	35	16	2	38
Hazelnut	15	100	2	8	9	0	95	13	19	29
Instant mash	9	1	100	2	9	0	57	22	25	3
Coarse salt	0	0	0	0	0	100	83	85	100	2
Fine salt	0	0	0	0	0	100	79	76	25	0
Baking soda	0	0	0	0	0	91	100	100	2	3
Couscous F	15	3	97	3	3	0	84	27	51	9
Couscous M	15	3	97	3	3	0	85	29	95	2
Acerola	18	0	21	49	17	1	19	13	1	2
Xanthan gum	0	0	0	0	99	0	32	29	4	12
Agar gum	0	0	0	0	99	0	36	22	5	8
Pectin	0	0	0	0	100	0	35	14	7	10
Yeast extract 1	66	1	23	2	0	19	18	8	29	2
Yeast extract 2	66	1	23	2	0	19	17	8	6	1
Onion	12	2	51	40	6	0	54	23	2	5
Lactose	0	0	0	100	0	0	0	1	1	7

The multilinear model was applied to normalized input data and reconstitution time (**Table 19**). The prediction was slightly improved compared to unnormalized data (section 4.4.1.1.) but the accuracy was still insufficient due to a weak coefficient of determination ($R^2 = 0.57$) (**Figure 68**). Obtained model weights were: $w_0 = -4.94 \times 10^{-2}$, $w_1 = 0.20$, $w_2 = -0.37$, $w_3 = -0.26$, $w_4 = -9.56 \times 10^{-2}$, $w_5 = -0.56$, $w_6 = 0.25$, $w_7 = 0.23$, $w_8 = 0.43$, $w_9 = -5.65 \times 10^{-2}$, $w_{10} = 0.26$.

As the prediction of the multilinear model was worse than for the monome model when using unnormalized data, it was tried to apply the monome model to normalized data.

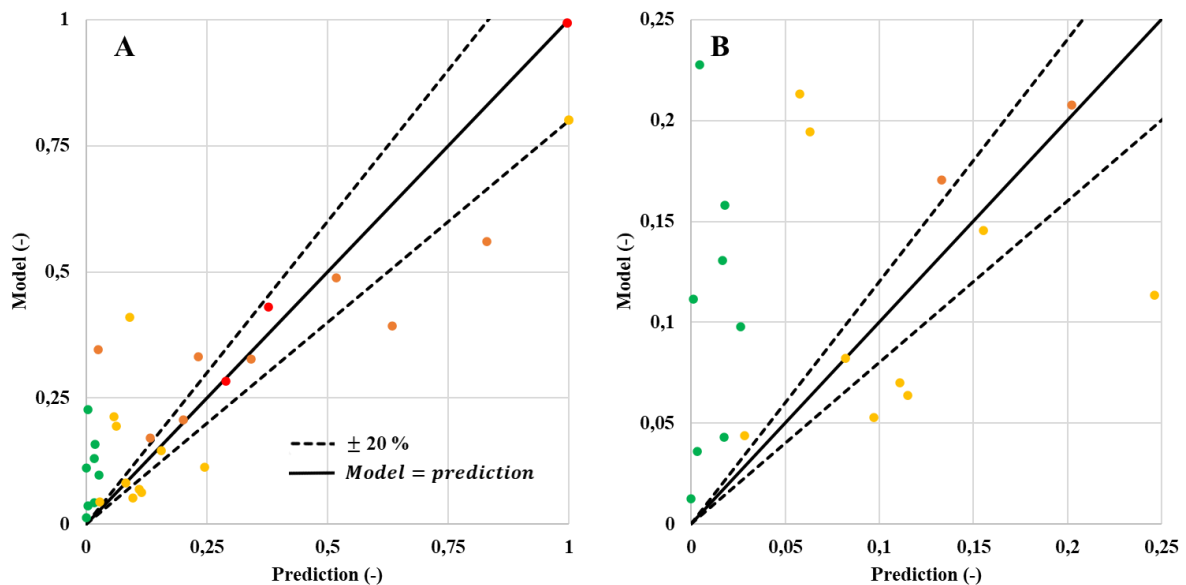


Figure 68. A- Comparison of predicted and experimental values of reconstitutions times for the multilinear model obtained with normalized physicochemical parameters using **Equation 28**. B- focus on normalized reconstitution times between 0 and 25 %. Colors correspond to the powder classification according to wetting and reconstitution behavior deduced from section 4.1.4.: green, good behavior (short wetting and short reconstitution), yellow: decent behavior (long wetting and short reconstitution), orange: mediocre behavior (short wetting and long reconstitution), and red: poor behavior (long wetting and long reconstitution).

The monome model was applied to normalized data (**Tables 2 and 20**), which led to: $R^2 = 0.93$. Obtained model weights were: $w_0 = 1.36$, $w_1 = 1.47$, $w_2 = -0.41$, $w_3 = -0.93$, $w_4 = -0.15$, $w_5 = -0.62$, $w_6 = 0.78$, $w_7 = 2.28$, $w_8 = 1.01$, $w_9 = -2.29 \times 10^{-4}$, $w_{10} = 0.68$.

This permitted to improve modelling accuracy for all powders even if predictions for powders of the green group were still particularly unsatisfactory (**Figure 69**).

The model underestimates the reconstitution time for powders for short reconstitution times (green and yellow), especially because it is not suitable to handle null values of physicochemical parameters, in spite of the attempt to get around this problem by adding 10^{-4} to all values of physicochemical parameters. The interest of this kind of model resides in the fact that the sign of model weights is informative of the type of influence of concerned predictor on the dependent variable: positive (resp., negative) influence in case of positive sign (resp., negative). Also, the use of normalized data confers to the order of magnitude of model weights the ability to identify predictors having the most influence on the dependent variable: as normalized predictors all range between 0 and 100 %, the higher the absolute value of the model weight, the greater the influence of associated predictor. For example, the model weight associated with C-C/ C-other ratio was equal to -2.29×10^{-4} , its impact was very low (low absolute value in comparison with other model weights). On the contrary, the water content led to a marked positive influence, showing that water content tended to increase the reconstitution time.

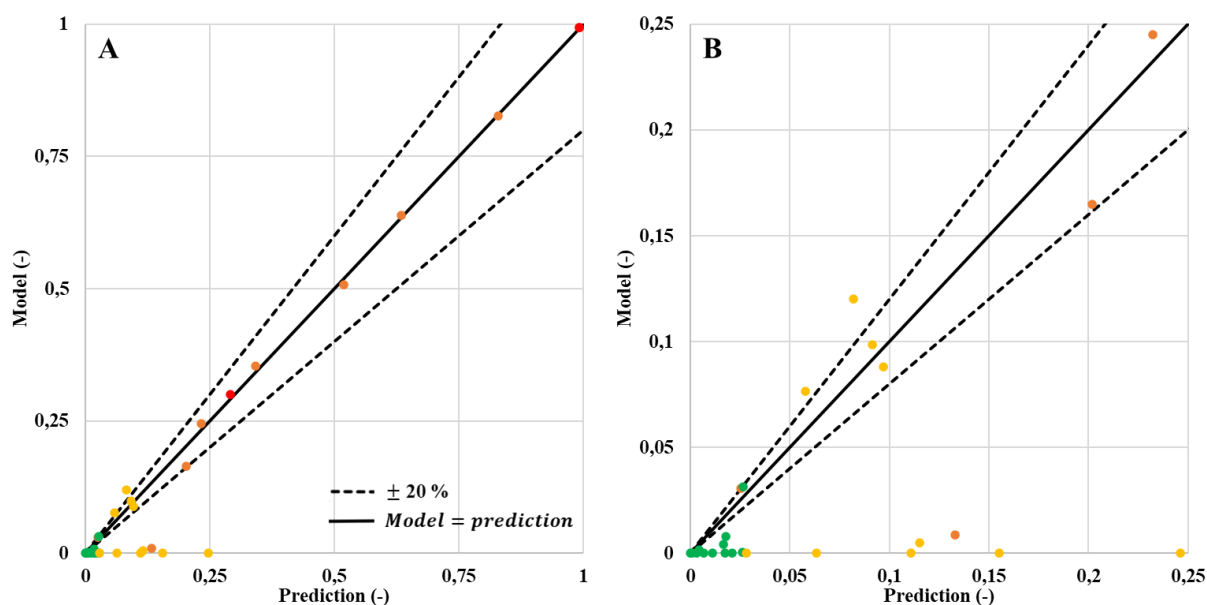


Figure 69. A- Comparison of predicted and experimental values of reconstitutions times for the monome model obtained with normalized physicochemical parameters using **Equation 29**. B- focus on normalized reconstitution times between 0 and 25 %. Colors correspond to the powder classification according to wetting and reconstitution behavior deduced from section 4.1.4.: green, good behavior (short wetting and short reconstitution), yellow: decent behavior

(long wetting and short reconstitution), orange: mediocre behavior (short wetting and long reconstitution), and red: poor behavior (long wetting and long reconstitution).

The exponential model was applied to normalized data (**Tables 2 and 19**), which led to $R^2 = 0.92$, showing that model accuracy was similar for monome and exponential models. Obtained model weights were: $w_0 = 1.01 \times 10^{-4}$, $w_1 = 6.29$, $w_2 = 3.29$, $w_3 = -1.72$, $w_4 = 2.04$, $w_5 = -5.24$, $w_6 = 8.85$, $w_7 = 4.24$, $w_8 = 2.15$, $w_9 = -9.07$, $w_{10} = 1.68$.

The model underestimates the reconstitution time for powders for short reconstitution times (yellow group) and overvalued the reconstitution time for powders with very short reconstitution times (green group) (**Figure 70**).

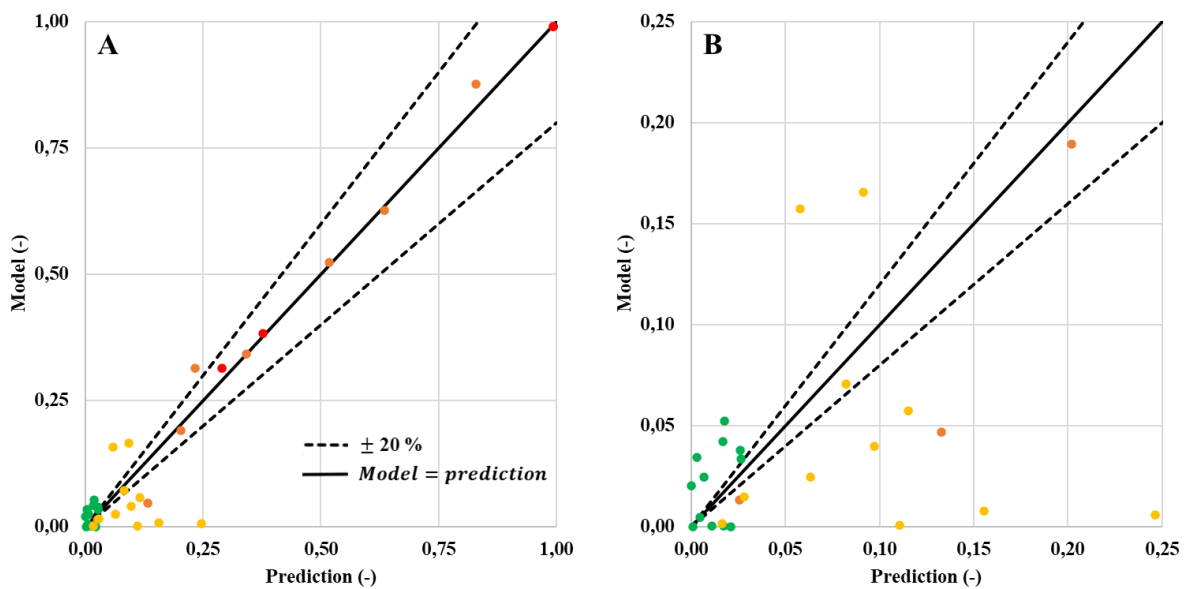


Figure 70. A- Comparison of predicted and experimental values of reconstitutions times for the exponential model obtained with normalized physicochemical parameters using **Equation 30**. B- focus on normalized reconstitution times between 0 and 25 %. Colors correspond to the powder classification according to wetting and reconstitution behavior deduced from section 4.1.4.: green, good behavior (short wetting and short reconstitution), yellow: decent behavior (long wetting and short reconstitution), orange: mediocre behavior (short wetting and long reconstitution), and red: poor behavior (long wetting and long reconstitution).

Partial least squares regression (PLSR), another multilinear modelling technique (**Equations 31 and 32**), was performed with normalized input data (**Table 19**). The results were not satisfying with a poor R^2 of 0.61 (**Figure 71**). The PLSR model led to a worse prediction than the monome model (section 4.4.1.1.) for long reconstitution times (orange and red) and short reconstitution times with fast wetting (green), however the prediction of short times with slow wetting (yellow) was slightly improved.

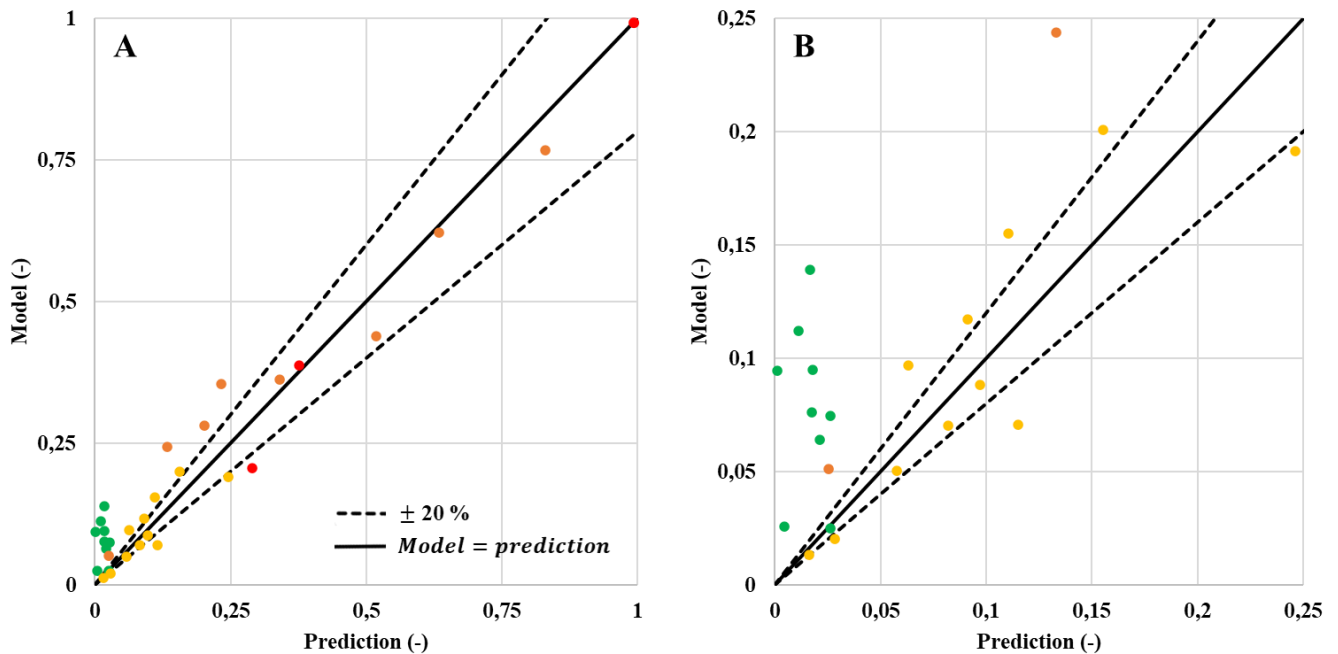


Figure 71. A- Comparison of predicted and experimental values of reconstitutions time for the PLSR model obtained with normalized physicochemical parameters. B- focus on normalized reconstitution times between 0 and 25 %. Colors correspond to the powder classification according to wetting and reconstitution behavior deduced from section 4.1.4.: green, good behavior (short wetting and short reconstitution), yellow: decent behavior (long wetting and short reconstitution), orange: mediocre behavior (short wetting and long reconstitution), and red: poor behavior (long wetting and long reconstitution).

So far, the monome model applied to normalized data allowed the best prediction of the reconstitution time, however an improvement of the prediction accuracy for short reconstitution times (under 10 min) was still required. Modifying the monome model appeared to be the most suitable approach to this aim.

4.4.2. Improvement of prediction accuracy

4.4.2.1. *Modification of the monome model*

In view to improve modelling accuracy of monome model applied to normalized data, some power laws were changed to exponentials (**Equations 29 and 30**), as exponentials seemed more adapted than power laws to describe the individual impact of some physicochemical properties, such as C/O ratio for example (**Figure 72 and Table 20**). The general trend of reconstitution time dependency to some physicochemical properties was still better described by power laws than exponentials, cf. D50 for instance (**Figure 72**).

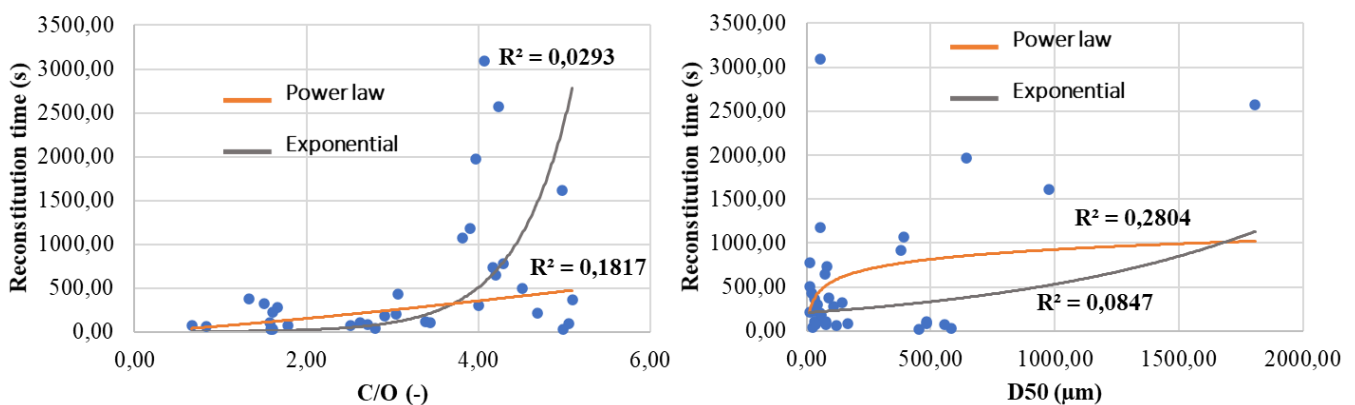


Figure 72. Comparison of exponential and power laws for the dependency of reconstitution times to the physicochemical parameters to be used in the predictive model; examples of the C/O ratio and D50.

Table 20. Coefficients of determinations of exponential and power law regressions for the dependency of reconstitution times to the physicochemical parameters to be used in the predictive model (green: higher R², red: lower R²).

	Coefficient of determination R ² of exponential regression	Coefficient of determination R ² of power law regression
Proteins content	1.02×10^{-2}	1.04×10^{-1}
Lipids content	4.80×10^{-3}	1.22×10^{-1}
Carbohydrates content, fibers excluded	1.18×10^{-1}	2.31×10^{-2}
Fibers content	1.90×10^{-2}	2.48×10^{-2}
Minerals content	5.27×10^{-2}	1.24×10^{-2}
Water activity	4.89×10^{-2}	7.36×10^{-2}
Water content	1.09×10^{-1}	9.77×10^{-2}
D50	8.47×10^{-2}	2.80×10^{-1}
C/O ratio	1.76×10^{-1}	1.06×10^{-1}
C-C/other C bonds ratio	2.43×10^{-2}	5.00×10^{-6}

Modifying the monome model by adding exponential terms slightly improved the prediction (R² from 0.93 to 0.95) (**Figure 73**), mainly for powders of the yellow group, but the reconstitution times of powders of the green group were still hardly estimated by the model, remaining mostly underestimated. This hybrid model was still not applicable for reconstitution times of less than 5 min. Obtained model weights were: $w_0 = 0.11$, $w_1 = -0.65$, $w_2 = 0.91$, $w_3 = -0.96$, $w_4 = -0.44$, $w_5 = -28.33$, $w_6 = 0.64$, $w_7 = 16.06$, $w_8 = -1.91$, $w_9 = -6.71$, and $w_{10} = 0.22$.

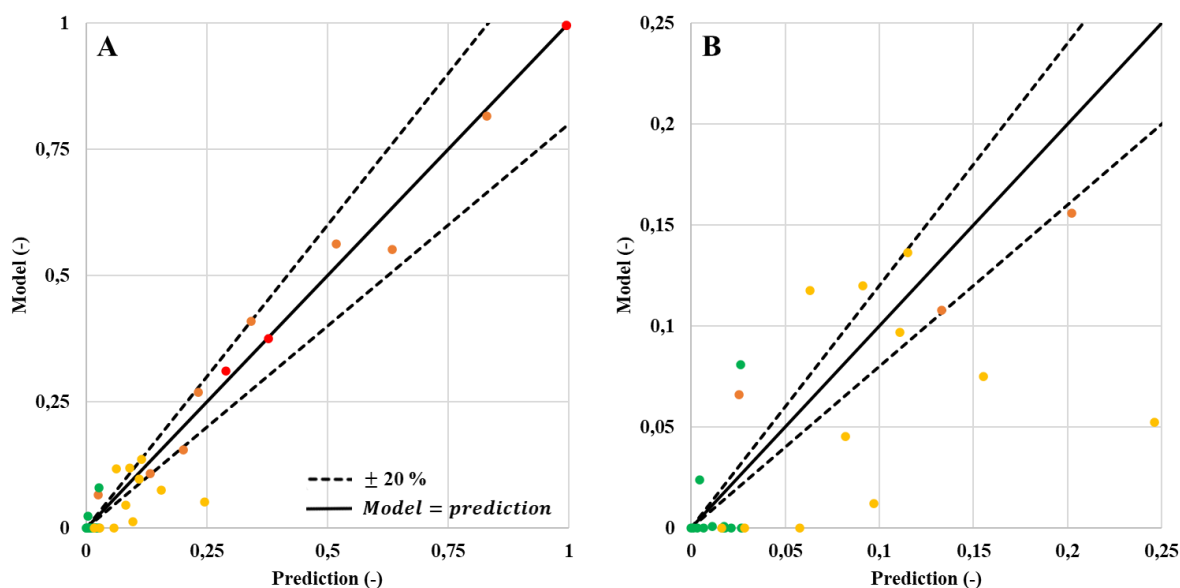


Figure 73. A- Comparison of predicted and experimental values of reconstitutions times for the model combining power laws and exponentials obtained with normalized physicochemical parameters using **Equations 29 and 30**. B- focus on normalized reconstitution times between 0 and 25 %. Colors correspond to the powder classification according to wetting and reconstitution behavior deduced from section 4.1.4.: green, good behavior (short wetting and short reconstitution), yellow: decent behavior (long wetting and short reconstitution), orange: mediocre behavior (short wetting and long reconstitution), and red: poor behavior (long wetting and long reconstitution).

4.4.2.2. *Addition of physicochemical parameters as input data*

It was tried to improve the accuracy of this hybrid model by adding extra predictors, i.e. physicochemical parameters, as input data: sugars content, span (width of particle size distribution), particle shape parameters (sphericity, convexity, and aspect ratio), and powder aerated density (**Tables 21 and 22**). The hybrid model was enriched with power laws or exponentials based on these new predictors (**Equations 29 and 30**), according to those more adapted to describe the individual impact of these extra physicochemical properties (**Table 23**).

Table 21. Extra powder physicochemical properties used for predictive modelling.

Powder sample name	Carbohydrates content, sugars and fibers excluded (g/100g)	Sugars content (g/100g)	Span (-)	Aerated density (-)	Sphericity (-)	Convexity (-)	Aspect ratio (-)
Polenta R (raw)	77.54	6.84	1.13	0.67	0.79	0.92	0.67
Polenta 1.0 mm	77.64	6.85	1.56	0.65	0.81	0.93	0.71
Polenta 0.08 mm	78.142	6.89	2.05	0.46	0.72	0.76	0.68
Instant coffee R (raw)	42.60	0.00	1.00	0.25	0.78	0.94	0.7
Ground instant coffee	42.60	0.00	12.88	0.36	0.77	0.84	0.71
Granulated sugar	0.00	99.98	1.36	0.86	0.84	0.94	0.68
Caster sugar	0.00	99.98	1.42	0.87	0.85	0.94	0.68
Icing sugar	0.00	99.90	8.66	0.43	0.34	0.53	0.65
Flour T45	69.62	6.63	2.6	0.54	0.75	0.84	0.69
Flour T55	69.83	6.65	2.19	0.56	0.79	0.86	0.69
Cocoa 12F A-	20.55	0.56	2.51	0.34	0.47	0.5	0.66
Cocoa 12F A+	20.51	0.56	2.66	0.4	0.24	0.46	0.61
Cocoa 12F A+++	17.53	0.44	1.13	0.5	0.78	0.81	0.72
Cocoa 23F A+	20.45	0.55	2.43	0.36	0.67	0.71	0.65
Pea fiber	30.16	4.78	2.06	0.39	0.79	0.85	0.69
SMP	0.00	55.18	1.63	0.56	0.81	0.8	0.74
WMP	0.00	37.67	1.69	0.49	0.76	0.85	0.7
Hazelnut	1.80	8.05	2.6	0.35	0.69	0.89	0.69
Instant mash	78.27	2.49	2.04	0.41	0.72	0.89	0.63
Coarse salt	0.00	0.00	2.04	1.15	0.80	0.95	0.69
Fine salt	0.00	0.00	0.73	1.05	0.82	0.94	0.65
Baking soda	0.00	0.00	1.63	1.06	0.82	0.92	0.65
MCP	0.00	2.07	1.8	0.38	0.82	0.86	0.76
Couscous F	76.27	3.23	0.64	0.8	0.82	0.94	0.75
Couscous M	76.11	3.22	0.81	0.74	0.8	0.94	0.75
MPI	0.00	1.04	1.51	0.37	0.85	0.88	0.78
Whey	0.00	5.74	1.98	0.41	0.86	0.89	0.8
SMP G	0.00	55.18	1.52	0.54	0.76	0.87	0.71
Acerola	16.35	49.05	1.76	0.54	0.84	0.86	0.8
Xanthan gum	0.00	0.00	1.49	0.71	0.83	0.9	0.65
Agar gum	0.00	0.00	1.95	0.54	0.81	0.9	0.64
Pectin	0.00	0.00	2.31	0.84	0.84	0.92	0.65
Yeast extract 1	17.93	2.32	1.63	0.42	0.83	0.89	0.77
Yeast extract 2	17.93	2.32	1.9	0.41	0.79	0.89	0.73
Onion	39.99	39.78	3.23	0.69	0.84	0.89	0.7
Lactose	0.00	99.89	2.67	0.48	0.62	0.72	0.66

Table 22. Extra normalized powder physicochemical properties used for predictive modelling.

Powder sample name	Normalized carbohydrates content, sugars and fibers excluded (%)	Normalized sugars content (%)	Normalized span (%)	Normalized aerated density (%)	Normalized sphericity (%)	Normalized convexity (%)	Normalized aspect ratio (%)
Polenta R (raw)	99	7	4	47	88	94	29
Polenta 1.0 mm	99	7	8	45	92	95	49
Polenta 0.08 mm	100	7	12	23	77	60	37
Instant coffee R (raw)	54	0	3	0	87	96	45
Ground instant coffee	54	0	100	12	85	77	52
Granulated sugar	0	100	6	68	96	96	35
Caster sugar	0	100	6	69	98	98	35
Icing sugar	0	100	66	20	16	14	22
Flour T45	89	7	13	33	82	77	38
Flour T55	89	7	13	35	87	81	39
Cocoa 12F A-	26	1	15	10	37	26	26
Cocoa 12F A+	26	1	17	17	0	0	0
Cocoa 12F A+++	22	0	4	28	87	70	56
Cocoa 23F A+	26	1	15	13	68	50	19
Pea fiber	39	5	12	16	88	79	38
SMP	0	55	8	35	91	85	65
WMP	0	38	9	27	83	78	48
Hazelnut	2	8	16	11	72	87	40
Instant mash	100	2	11	17	76	87	11
Coarse salt	0	0	11	100	90	100	39
Fine salt	0	0	1	88	92	97	21
Baking soda	0	0	8	90	93	92	19
MCP	0	2	9	14	93	81	77
Couscous F	97	3	0	61	93	97	70
Couscous M	97	3	1	54	89	96	69
MPI	0	1	7	13	98	85	89
Whey	0	6	11	18	100	87	99
SMP G	0	55	7	32	83	84	52
Acerola	21	49	9	32	96	80	100
Xanthan gum	0	0	7	51	94	88	22
Agar gum	0	0	11	32	91	88	12
Pectin	0	0	14	66	96	92	17
Yeast extract 1	23	2	8	20	94	87	81
Yeast extract 2	23	2	10	18	88	86	64
Onion	51	40	21	49	97	86	47
Lactose	0	100	17	26	61	52	23

Table 23. Coefficients of determinations of exponential and power law regressions for the dependency of reconstitution times to the additional physicochemical parameters to be used in the predictive model (green: higher R², red: lower R²).

	Coefficient of determination R ² of exponential regression	Coefficient of determination R ² of power law regression
Carbohydrates content, sugars and fibers excluded	1.18 × 10 ⁻¹	2.31 × 10 ⁻²
Sugars content	8.97 × 10 ⁻²	3.57 × 10 ⁻²
Span	8.41 × 10 ⁻²	7.19 × 10 ⁻²
Aerated density	9.90 × 10 ⁻³	7.00 × 10 ⁻³
Sphericity	2.00 × 10 ⁻⁴	1.19 × 10 ⁻²
Convexity	2.00 × 10 ⁻³	2.16 × 10 ⁻²
Aspect ratio	1.80 × 10 ⁻³	9.33 × 10 ⁻²

Model parameters were: $w_0 = 0.97$, $w_1 = 0.60$, $w_2 = 0.40$, $w_3 = -7.48$, $w_4 = 0.11$, $w_5 = -28.87$, $w_6 = 2.56$, $w_7 = 5.79$, $w_8 = -5.79$, $w_9 = -5.28$, $w_{10} = 0.32$, $w_{11} = -13.11$, $w_{12} = -3.11$, $w_{13} = 4.34$, $w_{14} = 2.72$, $w_{15} = -2.19$, and $w_{16} = -0.59$.

Prediction accuracy was enhanced by addition of extra physicochemical parameters (R² was raised from 0.95 to 0.99), but the model unfortunately remained imprecise for powders having a reconstitution time inferior to 5 min (**Figure 74**). The predictions of reconstitution time remained underestimated for most powders of the green group, which highlighted that some physicochemical parameters that are very influent on reconstitution time may be missing in this study. Moreover, investigated powders did not permit to have sufficiently intermediate values of predictors, impairing the ability of models to correctly evaluate their individual influence such as carbohydrates, sugars, and minerals content. Last, the number of input parameters (16) is too large for the number of total powders included in the study (36). Despite these limits it was possible to build the model following **Equation 33**.

$$t_{reconstitution} = 0.97 \times x_1^{0.60} \times x_2^{0.40} \times e^{x_3 \times -7.48} \times e^{x_4 \times -13.11} \times x_5^{0.11} \times e^{x_6 \times -28.87} \times x_7^{2.56} \times e^{x_8 \times 5.79} \times e^{x_9 \times -5.79} \times e^{x_{10} \times -5.28} \times x_{11}^{0.32} \times e^{x_{12} \times -3.11} \times e^{x_{13} \times 4.34} \times x_{14}^{2.72} \times x_{15}^{-2.19} \times x_{16}^{-0.59}$$

Equation 33

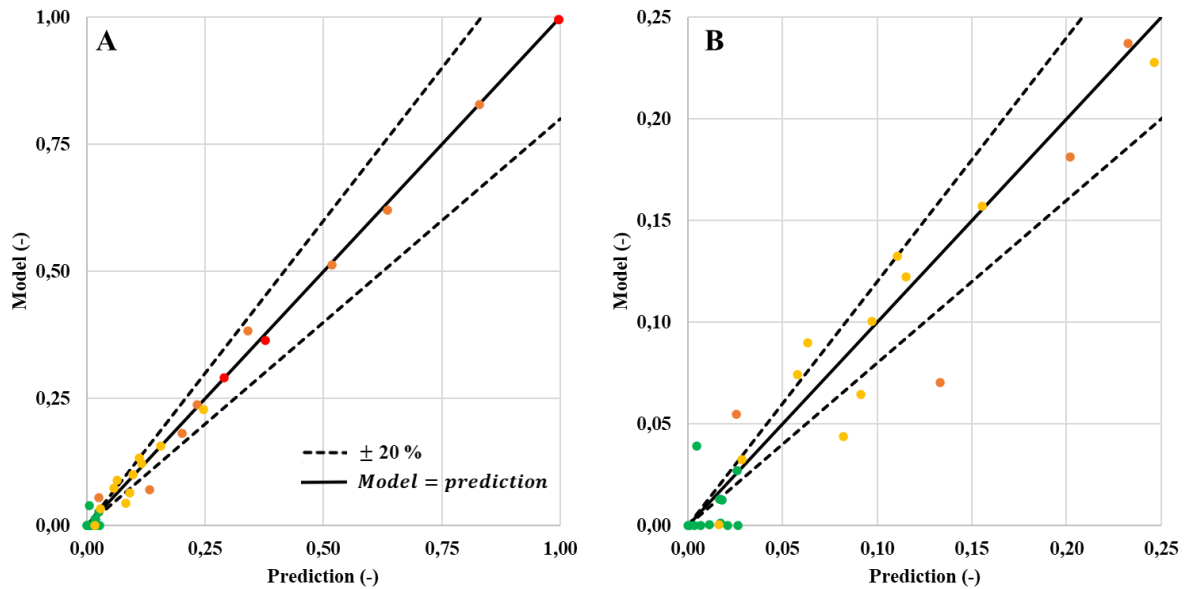


Figure 74. A- Comparison of predicted and experimental values of reconstitutions times for the model combining power laws and exponentials obtained with the extended set of normalized physicochemical parameters using **Equations 33**. B- focus on normalized reconstitution times between 0 and 25 %. Color corresponds to the powder classification according to wetting and reconstitution behavior deduced from chapter 4.1.4.: green, good behavior (short wetting and short reconstitution), yellow: decent behavior (long wetting and short reconstitution), orange: mediocre behavior (short wetting and long reconstitution), and red: poor behavior (long wetting and long reconstitution).

4.4.3. Conclusions of the predictive modelling of the reconstitution time

The predictive modelling approach developed for the reconstitution time, using the extended set of normalized powder physicochemical properties and a hybrid model mixing power and exponential laws was satisfactory for short, intermediate, and long reconstitution times, but the prediction failed for powders with very short reconstitution times (less than 5 min). The limitations of this kind of empirical models seem to have been reached. Indeed, some powder physicochemical properties that may have an important influence on powder reconstitutability (presumably, porosity and bulk-surface composition differences for instance) were missing from the set of input data. Also, considering a larger number of powders with

more varied chemical composition seems necessary to make this kind of empirical predictive model more efficient. Last, it was not possible to proceed to cross-validation. Indeed, it was chosen to employ the results obtained for all investigated powders to build the predictive model, as the number of powders (36) powders was not sufficiently high in comparison to the number of predictor variables (16 in the most accurate model).

V. Conclusion and perspectives

5.1. Conclusion

Pour la première fois, les principaux facteurs influençant le comportement de reconstitution des poudres (taille des particules, composition chimique, composition de surface, procédé de fabrication, etc.) ont été identifiés par analyse en composantes principales pour un grand nombre de poudres alimentaires dans les mêmes conditions d'analyses (**Figure 44**), contrairement aux études précédentes réalisées classiquement sur un nombre limité de poudres. Il en ressort que l'étape de mouillage est favorisée par une grande taille de particules (supérieure à 90 μm) et/ou une forte teneur en eau, alors que les poudres riches en lipides et/ou à surface hydrophobe ont de mauvaises propriétés de mouillage. Une reconstitution rapide des poudres est associée à une forte teneur en glucides et/ou en minéraux alors qu'une forte teneur en protéines et/ou en fibres induit une reconstitution lente. L'effet du procédé est plus nuancé : en général, les poudres produites par séchage ont un temps de reconstitution plus rapide que celles produites par broyage. Cette tendance pourrait être expliquée par la composition des poudres, les poudres issues de séchage sont composées de plus de composés solubles (ex : les sucres) contrairement aux poudres produites par broyage riche en composés insolubles (ex : les fibres). De plus, l'étude a permis de confirmer et de généraliser les connaissances développées jusqu'à présent sur un nombre de poudres limité et de classer les poudres issues d'agroressources en quatre catégories selon leurs aptitudes au mouillage et à la reconstitution. L'intérêt industriel de cette étude réside dans le fait que les propriétés physicochimiques principales influençant la reconstitution ont été identifiées, et pourront être utilisées pour moduler le temps de reconstitution en modifiant la formulation des poudres (distribution granulométrique, composition surfacique, composition globale, etc.).

Les essais de reconstitution par suivi conductimétrique et les analyses physicochimiques et fonctionnelles des poudres issues d'agroressources ont permis d'identifier des poudres dont la reconstitution est limitée par l'étape de mouillage, qu'il pourrait être intéressant, afin d'améliorer leur aptitude à la reconstitution, d'enrober par des constituants qui se mouillent et se reconstituent facilement. A ce titre, il a été décidé d'enrober la poudre d'isolat de protéines de lactosérum par des sucres. Les conditions d'enrobage choisies ont permis l'ajout d'une petite quantité de sucres (seulement 3,6 g/100 g), sans induire d'agglomération des particules, afin que l'amélioration du mouillage soit uniquement due à la modification de composition chimique de surface résultant de l'enrobage. Dans ces conditions, le temps de mouillage d'une poudre d'isolat de protéines de lactosérum a été divisé par deux par enrobage avec du saccharose.

Il a été observé que l'amélioration de la mouillabilité de la poudre de protéines du lactosérum dépendait assez nettement du type de sucre utilisé, mais il n'a pas été possible de trouver une explication physicochimique à l'impact du type de sucre, vraisemblablement à cause de la faible différence d'hydrophilie entre les sucres ainsi qu'à la faible quantité de sucres ajoutés. Il a toutefois été possible d'émettre des hypothèses sur le mécanisme d'amélioration de l'aptitude au mouillage induit par l'enrobage par une investigation biophysique plus poussée de la poudre enrobée de saccharose. Il a été mis en évidence par des méthodes de microscopie que la surface de la poudre enrobée n'était pas recouverte de saccharose de manière uniforme, mais plutôt sous forme de patches cristallisés. L'équilibrage de la poudre enrobée en atmosphère humide a permis de montrer que les patches de saccharose interagissent rapidement avec l'eau de l'air, ce qui conduit à leur plastification et à l'affaissement de la surface sous les patches. Ceci a permis d'élaborer l'hypothèse d'amélioration de la mouillabilité des poudres par l'enrobage avec des sucres suivante : les patches de sucre, se mouillant facilement, captent l'eau, ce qui favorise le contact de la surface des particules avec l'eau et permet ainsi une entrée plus rapide d'eau dans les éventuels pores de surface des particules (**Figure 58**).

Une approche semi-empirique de modélisation descriptive pour la reconstitution des poudres alimentaires a été développée. Le modèle proposé permet de décrire l'évolution temporelle de la taille médiane des particules lors de la reconstitution et de caractériser la cinétique de trois des principales étapes de reconstitution de la poudre, à savoir le gonflement, la dispersion et la solubilisation. Cette approche a permis de déterminer les durées et vitesses moyennes de gonflement, de dispersion et de solubilisation, ainsi qu'un temps de reconstitution. Cette approche de modélisation descriptive n'est pas adaptée pour les poudres instantanées (leur reconstitution étant trop rapide pour être suivie par granulométrie laser) ou les poudres composées de plusieurs composants majeurs ayant des cinétiques bien différentes pour les mêmes étapes de reconstitution. Les données cinétiques issues de cette approche de modélisation descriptive ont été corrélées aux propriétés physicochimiques des poudres (taille médiane des particules, span, composition chimique, hydrophobicité de surface) pour identifier celles influençant majoritairement chaque étape de reconstitution. Il en ressort que le gonflement dure plus longtemps pour les poudres composées de grandes tailles de particules et/ou de particules à la surface hydrophobe, mais il est plus court en présence de sucres. L'aptitude au gonflement est plus importante en présence de fibres et plus faible en présence de lipides. La dispersion était facilitée pour les grandes tailles de particules, alors qu'elle était ralentie par l'hydrophobicité de la surface des particules. La solubilisation est plus lente en

présence de fibres et pour les grandes tailles de particules du fait de leur plus faible surface spécifique. Dans l'ensemble, ces tendances étaient cohérentes avec les connaissances de la littérature et les paramètres physicochimiques les plus influents sur la reconstitution des poudres mis en évidence analyse statistique par ACP des résultats de caractérisation des cinétiques de reconstitution suivies par conductimétrie, confirmant la pertinence de l'approche de modélisation descriptive développée.

Ces travaux ont permis d'envisager la possibilité d'utiliser les paramètres physicochimiques des poudres pour prédire empiriquement le temps de reconstitution dans les conditions de reconstitution mises en œuvre lors du travail de thèse. Le meilleur modèle prédictif développé est basé sur les valeurs numériques normalisées des propriétés physicochimiques les plus influentes et sa forme mathématique correspond à un produit de lois puissance et exponentielles, dérivées d'un modèle monôme classique. Les prédictions sont satisfaisantes pour les temps de reconstitution courts, intermédiaires et longs, mais mauvaises pour les poudres avec des temps de reconstitution très courts (moins de cinq minutes). Le nombre de poudres utilisées lors de l'étude ne semble pas suffisant au regard du nombre de paramètres physicochimiques influents à prendre en compte dans le modèle. De plus, les gammes de variation de certains paramètres physicochimiques des poudres étudiées semblent trop restreintes pour permettre de capter précisément l'effet de ces paramètres par le modèle. Le manque de précision du modèle a également pu résulter de l'absence de prise en compte de certaines propriétés physicochimiques des poudres exerçant potentiellement une influence importante sur l'aptitude à la reconstitution, telles que la porosité, la densité apparente, l'état structural (amorphe ou cristallin), les propriétés mécaniques de surface, etc.

5.2. Perspectives

Les résultats très intéressants de criblage des poudres par ACP nécessitent toutefois des études plus approfondies concernant différents aspects de la thèse qui pourraient permettre d'approfondir les connaissances sur la reconstitution des poudres. Il pourrait être judicieux d'étendre la caractérisation des propriétés physicochimiques des poudres à d'autres paramètres potentiellement très influents sur l'aptitude à la reconstitution tels que la densité, la porosité, la forme, l'état structural (cristallin ou amorphe), la température de transition vitreuse éventuelle, la composition chimique de surface, etc. Ces paramètres physicochimiques supplémentaires permettraient de mieux comprendre les phénomènes impliqués dans la reconstitution des poudres et ainsi permettre de mieux maîtriser cette opération unitaire cruciale pour la mise en œuvre industrielle des poudres.

Il semble également nécessaire de s'intéresser à l'impact des conditions opératoires de reconstitution des poudres qui influencent également fortement le temps de reconstitution comme par exemple la vitesse d'agitation, la température, la géométrie de la cuve de mélange, etc. Les conditions de reconstitution sont en effet un levier important pour moduler le comportement de reconstitution des poudres. De plus, en ajoutant des instruments de mesure dans la cuve de mélange pour suivre les cinétiques de reconstitution des poudres permettraient l'accès à plus d'informations. L'ajout d'une sonde permettant l'analyse in situ de la taille et forme des particules et d'un couplemètre de précision sur l'agitateur permettrait d'obtenir plus d'informations sur les étapes de reconstitution de la poudre ainsi que l'évolution de la forme des particules au cours des différentes étapes de la reconstitution. A partir de ces nouvelles informations, il serait possible à l'aide de modèles descriptifs comme celui développé dans cette thèse pour le suivi granulométrique des cinétiques de reconstitution de déterminer le temps et la vitesse de chaque étape de la reconstitution. Des travaux ultérieurs sur les modèles descriptifs des cinétiques de reconstitution pourraient avantageusement être réalisés avec un plus grand nombre de poudres afin de bénéficier de gammes de variation plus importantes des propriétés physicochimiques des poudres et ainsi mieux cerner leur rôle dans les différentes étapes de la reconstitution. Il serait également très important pour la compréhension des phénomènes et pour la maîtrise de la reconstitution des poudres à l'échelle industrielle d'étudier l'influence des conditions d'agitation (nature de l'agitateur, fréquence d'agitation, géométrie de la cuve, rapport massique poudre/eau, etc.). En effet, l'identification des propriétés physicochimiques et des conditions d'agitation ayant le plus d'influence sur la reconstitution des poudres est une étape nécessaire pour le développement de modèles empiriques capables de prédire les temps de reconstitution, mais aussi les durées de chaque étape de reconstitution, ce qui serait utile pour optimiser les applications industrielles des poudres alimentaires. Il pourrait être intéressant de produire des poudres en modulant leur composition en protéines, lipides, glucides, sucres, fibres et minéraux à partir du même procédé pour mieux saisir l'impact de la composition sur le temps de reconstitution ou en modifiant la distribution de taille des particules par tamisage pour récupérer différentes classes de taille. Toutefois, ces propriétés physicochimiques ne sont pas les seules qui pourraient permettre d'améliorer la prédiction du temps de reconstitution : en modifiant des conditions de production, il serait possible de moduler la forme, la porosité ou encore le gradient de composition des particules.

Malgré le développement des connaissances sur le mouillage des poudres enrobées, le mécanisme exact du mouillage n'est pas connu. L'approche biophysique menée dans ce travail

de thèse pour identifier les modifications de surface induites par l'interaction avec l'humidité de l'air a eu pour inconvénient de ne pouvoir suivre l'évolution d'une même zone de la surface d'une particule lors de la modification de l'humidité de l'air en équilibre avec la poudre. Ceci pourrait être possible par AFM par des approches couplées de topographie et de nanoindentation à condition d'utiliser une cellule d'analyse à température et hygrométrie régulée. Enfin, il serait pertinent d'étudier l'impact de très fortes humidités relatives de l'air sur la forme, la porosité, l'élasticité de la surface des particules, en allant même jusqu'à dépasser le point de rosée pour étudier le mouillage des particules par condensation de l'eau de l'air sur celles-ci. Une étude sur l'effet de l'enrobage sur la cinétique de reconstitution avec les méthodes employées dans la section 4.1. pourrait permettre d'améliorer la compréhension de l'impact de l'enrobage durant la reconstitution. Il serait intéressant d'étudier l'effet de différents types d'enrobages pouvant améliorer le mouillage avec des composés permettant un bon mouillage comme des minéraux (par exemple, le chlorure de sodium), le lait écrémé, etc. Afin de mieux comprendre les interactions eau/surface durant le mouillage, l'utilisation d'enrobage riche en protéines hydrophobes ou en lipides pourrait permettre une meilleure compréhension de l'étape du mouillage. Durant cette thèse, il a été observé un enrobage par patches, il serait donc intéressant de déterminer l'effet d'un enrobage uniforme avec une épaisseur plus ou moins grande à la surface d'une poudre sur le mouillage et la reconstitution.

VI. References

- Adam, A., Jasniewski, J., Vuillemin, M.E., Simard, B., Burgain, J., Badin, R., Muniglia, L., Michaux, F., 2022. Enzymatic mediated modification of gum Arabic by curcumin oxidation products: Physicochemical and self-assembly study. *Food Hydrocolloids* 126, 107451. <https://doi.org/10.1016/j.foodhyd.2021.107451>
- ADPI, 2002. Determination of total ash in standards for grades of dry milks including methods of analysis. (American Dry Product Institute, Elmhurst, IL 40–41.
- AFNOR, 2005. Dried milk and dried milk products - Determination of insolubility index. ISO 8156:2005.
- AFNOR, 2004a. Microbiology of food and animal feeding stuffs - Determination of water activity. ISO 21807:2004.
- AFNOR, 2004b. Dried milk - Determination of moisture content (Reference method). ISO 5537:2004.
- Aguilera, J.M., 2005. Why food microstructure? *Journal of Food Engineering*, IV Iberoamerican Congress of Food Engineering (CIBIA IV) 67, 3–11. <https://doi.org/10.1016/j.jfoodeng.2004.05.050>
- Ajayi, O.M., Amin, S., 2021. Flow and performance effects of talc alternatives on powder cosmetic formulations. *International Journal of Cosmetic Science* 43, 588–600. <https://doi.org/10.1111/ics.12733>
- Allen, T., Roux, N., 1988. *Granulométrie. Techniques de l'Ingénieur*.
- Amagliani, L., Schmitt, C., 2017. Globular plant protein aggregates for stabilization of food foams and emulsions. *Trends in Food Science & Technology* 67, 248–259. <https://doi.org/10.1016/j.tifs.2017.07.013>
- Andre, G., Kulakauskas, S., Chapot-Chartier, M.-P., Navet, B., Deghorain, M., Bernard, E., Hols, P., Dufrêne, Y.F., 2010. Imaging the nanoscale organization of peptidoglycan in living *Lactococcus lactis* cells. *Nat Commun* 1, 27. <https://doi.org/10.1038/ncomms1027>
- Andueza, S., de Peña, M.P., Cid, C., 2003. Chemical and Sensorial Characteristics of Espresso Coffee As Affected by Grinding and Torrefacto Roast. *J. Agric. Food Chem.* 51, 7034–7039. <https://doi.org/10.1021/jf034628f>
- Angelopoulou, D., Meunier, V., Forny, L., Niederreiter, G., Palzer, S., Salman, A.D., 2021a. Influence of localized thermal effects on the reconstitution kinetics of lactose-coated

- whole milk powder. *Food Research International* 150, 110774.
<https://doi.org/10.1016/j.foodres.2021.110774>
- Angelopoulou, D., Meunier, V., Forny, L., Niederreiter, G., Palzer, S., Salman, A.D., 2021b. Particle surface design for enhanced reconstitution of fat-based food powders. *Powder Technology* 393, 397–404. <https://doi.org/10.1016/j.powtec.2021.07.054>
- Atalar, I., Yazici, F., 2019. Effect of different binders on reconstitution behaviors and physical, structural, and morphological properties of fluidized bed agglomerated yoghurt powder. *Drying Technology* 37, 1656–1664. <https://doi.org/10.1080/07373937.2018.1529038>
- Barbosa, F.S., Farage, M.C.R., Beaucour, A.-L., Ortola, S., 2012. Evaluation of aggregate gradation in lightweight concrete via image processing. *Construction and Building Materials* 29, 7–11. <https://doi.org/10.1016/j.conbuildmat.2011.08.081>
- Barbosa-Cánovas, G.V., Juliano, P., 2005. Physical and Chemical Properties of Food Powders, in: *Encapsulated and Powdered Foods*. CRC Press.
- Becker, L., Zaiter, A., Petit, J., Zimmer, D., Karam, M.-C., Baudelaire, E., Scher, J., Dicko, A., 2016. Improvement of antioxidant activity and polyphenol content of *Hypericum perforatum* and *Achillea millefolium* powders using successive grinding and sieving. *Industrial Crops and Products* 87, 116–123. <https://doi.org/10.1016/j.indcrop.2016.04.036>
- Ben Abdelaziz, I., Sahli, A., Bornaz, S., Scher, J., Gaiani, C., 2014. Dynamic method to characterize rehydration of powdered cocoa beverage: Influence of sugar nature, quantity and size. *Powder Technology* 264, 184–189. <https://doi.org/10.1016/j.powtec.2014.05.031>
- Benjakul, S., Karnjanapratum, S., 2018. Characteristics and nutritional value of whole wheat cracker fortified with tuna bone bio-calcium powder. *Food Chemistry* 259, 181–187. <https://doi.org/10.1016/j.foodchem.2018.03.124>
- Bhandari, B., 2013. 1 - Introduction to food powders, in: Bhandari, Bhesh, Bansal, N., Zhang, M., Schuck, P. (Eds.), *Handbook of Food Powders*, Woodhead Publishing Series in Food Science, Technology and Nutrition. Woodhead Publishing, pp. 1–25. <https://doi.org/10.1533/9780857098672.1>
- Bhandari, B.R., Senoussi, A., Dumoulin, E.D., Lebert, A., 1993. Spray Drying of Concentrated Fruit Juices. *Drying Technology* 11, 1081–1092. <https://doi.org/10.1080/07373939308916884>
- Biscans, B., 2013. Cristallisation en solution. *Techniques de l'Ingénieur*.
- Blazy, P., Jdid, E., Yvon, J., 2006. Fragmentation - Technologie. *Techniques de l'Ingénieur*.

- Bonacucina, G., Cespi, M., Palmieri, G.F., 2009. Evaluation of dissolution kinetics of hydrophilic polymers by use of acoustic spectroscopy. *International Journal of Pharmaceutics* 377, 153–158. <https://doi.org/10.1016/j.ijpharm.2009.04.043>
- Boucheham, N., Galet, L., Patry, S., Zidoune, M.N., 2019. Physicochemical and hydration properties of different cereal and legume gluten-free powders. *Food Science & Nutrition* 7, 3081–3092. <https://doi.org/10.1002/fsn3.1170>
- Bradstreet, R.B., 1954. Kjeldahl Method for Organic Nitrogen. *Anal. Chem.* 26, 185–187. <https://doi.org/10.1021/ac60085a028>
- Brown, H.T., Pickering, S.U., 1897. LXXIII.—Thermal phenomena attending the change in rotatory power of freshly prepared solutions of certain carbohydrates, with some remarks on the cause of multirotation. *J. Chem. Soc., Trans.* 71, 756–783. <https://doi.org/10.1039/CT8977100756>
- Burgain, J., 2013. Microencapsulation de bactéries probiotiques dans des matrices laitières : études des mécanismes de formation par une approche multi-échelle (These de doctorat). Université de Lorraine.
- Burgain, J., El Zein, R., Scher, J., Petit, J., Norwood, E.-A., Francius, G., Gaiani, C., 2016a. Local modifications of whey protein isolate powder surface during high temperature storage. *Journal of Food Engineering* 178, 39–46. <https://doi.org/10.1016/j.jfoodeng.2016.01.005>
- Burgain, J., Petit, J., Scher, J., Rasch, R., Bhandari, B., Gaiani, C., 2017. Surface chemistry and microscopy of food powders. *Progress in Surface Science* 92, 409–429. <https://doi.org/10.1016/j.progsurf.2017.07.002>
- Burgain, J., Scher, J., Petit, J., Francius, G., Gaiani, C., 2016b. Links between particle surface hardening and rehydration impairment during micellar casein powder storage. *Food Hydrocolloids* 61, 277–285. <https://doi.org/10.1016/j.foodhyd.2016.05.021>
- Cabré, X., Roquejoffre, J.-M., 2009. Propagation de fronts dans les équations de Fisher–KPP avec diffusion fractionnaire. *Comptes Rendus Mathématique* 347, 1361–1366. <https://doi.org/10.1016/j.crma.2009.10.012>
- Caliskan, G., Nur Dirim, S., 2013. The effects of the different drying conditions and the amounts of maltodextrin addition during spray drying of sumac extract. *Food and Bioproducts Processing* 91, 539–548. <https://doi.org/10.1016/j.fbp.2013.06.004>
- Camire, M., Dougherty, M., Briggs, J., 2007. Functionality of fruit powders in extruded corn breakfast cereals. *Food Chemistry* 101, 765–770.

- Cannova, F., Davidson, M., Forte, L., Sadler, B., 2018. Influence of Crushing Technology and Particle Shape on the Bulk Density of Anode Grade Petroleum Coke, in: Martin, O. (Ed.), *Light Metals 2018, The Minerals, Metals & Materials Series*. Springer International Publishing, Cham, pp. 1169–1177. https://doi.org/10.1007/978-3-319-72284-9_153
- Caparino, O.A., Tang, J., Nindo, C.I., Sablani, S.S., Powers, J.R., Fellman, J.K., 2012. Effect of drying methods on the physical properties and microstructures of mango (Philippine ‘Carabao’ var.) powder. *Journal of Food Engineering* 111, 135–148. <https://doi.org/10.1016/j.jfoodeng.2012.01.010>
- Caric, M., Milanovic, S., 2002. Milk powders, *Physical and Functional Properties of Milk Powders*. Encyclopedia of Dairy Sciences 1874–1880.
- Cayot, P., Lorient, D., 1997. Structures et technofonctions des protéines du lait [Texte imprimé]. Paris : Londres : New York : Tec & doc-Lavoisier.; [s.l.] : Arilait Recherches. DL 1997.
- Chandrapala, J., Martin, G.J.O., Zisu, B., Kentish, S.E., Ashokkumar, M., 2012. The effect of ultrasound on casein micelle integrity. *Journal of Dairy Science* 95, 6882–6890. <https://doi.org/10.3168/jds.2012-5318>
- Chandrapala, J., Zisu, B., Palmer, M., Kentish, S., Ashokkumar, M., 2011. Effects of ultrasound on the thermal and structural characteristics of proteins in reconstituted whey protein concentrate. *Ultrason. Sonochem.* 18, 951–957. <https://doi.org/10.1016/j.ultsonch.2010.12.016>
- Chandrapala, J., Zisu, B., Palmer, M., Kentish, S.E., Ashokkumar, M., 2014. Sonication of milk protein solutions prior to spray drying and the subsequent effects on powders during storage. *Journal of Food Engineering* 141, 122–127. <https://doi.org/10.1016/j.jfoodeng.2014.05.017>
- Chever, S., Méjean, S., Dolivet, A., Mei, F., Den Boer, C.M., Le Barzic, G., Jeantet, R., Schuck, P., 2017. Agglomeration during spray drying: Physical and rehydration properties of whole milk/sugar mixture powders. *LWT - Food Science and Technology* 83, 33–41. <https://doi.org/10.1016/j.lwt.2017.05.002>
- Conti, S., Gaisford, S., Buckton, G., Conte, U., 2006. Solution calorimetry to monitor swelling and dissolution of polymers and polymer blends. *Thermochimica Acta, Second Symposium on Calorimetry and Chemical Thermodynamics in Campinas, Brazil* 450, 56–60. <https://doi.org/10.1016/j.tca.2006.07.017>

- Courtois, F., 2013. 4 - Roller and drum drying for food powder production, in: Bhandari, B., Bansal, N., Zhang, M., Schuck, P. (Eds.), *Handbook of Food Powders*, Woodhead Publishing Series in Food Science, Technology and Nutrition. Woodhead Publishing, pp. 85–104. <https://doi.org/10.1533/9780857098672.1.85>
- Crouter, A., Briens, L., 2014. The Effect of Moisture on the Flowability of Pharmaceutical Excipients. *AAPS PharmSciTech* 15, 65–74. <https://doi.org/10.1208/s12249-013-0036-0>
- Crowley, S.V., 2016. Physicochemical characterisation of protein ingredients prepared from milk by ultrafiltration or microfiltration for application in formulated nutritional products (Doctoral thesis). University College Cork.
- Crowley, S.V., Gazi, I., Kelly, A.L., Huppertz, T., O'Mahony, J.A., 2014. Influence of protein concentration on the physical characteristics and flow properties of milk protein concentrate powders. *Journal of Food Engineering* 135, 31–38. <https://doi.org/10.1016/j.jfoodeng.2014.03.005>
- Cuq, B., Mandato, S., Jeantet, R., Saleh, K., Ruiz, T., 2013. 7 - Agglomeration/granulation in food powder production, in: Bhandari, B., Bansal, N., Zhang, M., Schuck, P. (Eds.), *Handbook of Food Powders*, Woodhead Publishing Series in Food Science, Technology and Nutrition. Woodhead Publishing, pp. 150–177. <https://doi.org/10.1533/9780857098672.1.150>
- Cuq, B., Rondet, E., Abecassis, J., 2011. Food powders engineering, between knowhow and science: Constraints, stakes and opportunities. *Powder Technology, Special Issue: Papers presented to the Symposium STPMF 2009, Science and Technology of Powders and Sintered Materials* 208, 244–251. <https://doi.org/10.1016/j.powtec.2010.08.012>
- Dankar, I., Haddarah, A., Omar, F.E.L., Pujolà, M., Sepulcre, F., 2018. Characterization of food additive-potato starch complexes by FTIR and X-ray diffraction. *Food Chemistry* 260, 7–12. <https://doi.org/10.1016/j.foodchem.2018.03.138>
- Deli, M., Petit, J., Nguimbou, R.M., Beaudelaire Djantou, E., Njintang Yanou, N., Scher, J., 2019. Effect of sieved fractionation on the physical, flow and hydration properties of *Boscia senegalensis* Lam., *Dichostachys glomerata* Forssk. and *Hibiscus sabdariffa* L. powders. *Food Sci Biotechnol* 28, 1375–1389. <https://doi.org/10.1007/s10068-019-00597-6>
- Deotale, Dutta, S., Moses, J., Balasubramaniam, V., Anandharamakrishnan, C., 2020. Foaming Characteristics of Beverages and Its Relevance to Food Processing. *Food Engineering Reviews* 12, 229–250.

- Dewettinck, K., Huyghebaert, A., 1999. Fluidized bed coating in food technology. *Trends in Food Science & Technology* 10, 163–168. [https://doi.org/10.1016/S0924-2244\(99\)00041-2](https://doi.org/10.1016/S0924-2244(99)00041-2)
- Dewettinck, K., Huyghebaert, A., 1998. Top-Spray Fluidized Bed Coating: Effect of Process Variables on Coating Efficiency. *LWT - Food Science and Technology* 31, 568–575. <https://doi.org/10.1006/fstl.1998.0417>
- Dhanalakshmi, K., Ghosal, S., Bhattacharya, S., 2011. Agglomeration of Food Powder and Applications. *Critical Reviews in Food Science and Nutrition* 51, 432–441. <https://doi.org/10.1080/10408391003646270>
- Di Battista, C.A., Constenla, D., Ramírez-Rigo, M.V., Piña, J., 2015. The use of arabic gum, maltodextrin and surfactants in the microencapsulation of phytosterols by spray drying. *Powder Technology* 286, 193–201. <https://doi.org/10.1016/j.powtec.2015.08.016>
- Dickinson, E., 2010. Food emulsions and foams: Stabilization by particles. *Current Opinion in Colloid & Interface Science* 15, 40–49. <https://doi.org/10.1016/j.cocis.2009.11.001>
- Diersch, H.-J.G., Clausnitzer, V., Myrnyy, V., Rosati, R., Schmidt, M., Beruda, H., Ehrnsperger, B.J., Virgilio, R., 2011. Modeling Unsaturated Flow in Absorbent Swelling Porous Media: Part 2. Numerical Simulation. *Transp Porous Med* 86, 753–776. <https://doi.org/10.1007/s11242-010-9650-4>
- Diersch, H.-J.G., Clausnitzer, V., Myrnyy, V., Rosati, R., Schmidt, M., Beruda, H., Ehrnsperger, B.J., Virgilio, R., 2010. Modeling Unsaturated Flow in Absorbent Swelling Porous Media: Part 1. Theory. *Transp Porous Med* 83, 437–464. <https://doi.org/10.1007/s11242-009-9454-6>
- Doesthale, Y., Devara, S., Rao, S., Belavady, B., 1979. Effect of milling on mineral and trace element composition of raw and parboiled rice, Yeshwant G; Devara, S; Rao, Shankar; Belavady, Bhavani. *Journal of the science of food and agriculture* 30, 40–46. <https://doi.org/10.1002/jsfa.2740300108>
- Dokoumetzidis, A., Macheras, P., 2006. A century of dissolution research: From Noyes and Whitney to the Biopharmaceutics Classification System. *International Journal of Pharmaceutics* 321, 1–11. <https://doi.org/10.1016/j.ijpharm.2006.07.011>
- Donald, A.M., He, C., Royall, C.P., Sferrazza, M., Stelmashenko, N.A., Thiel, B.L., 2000. Applications of environmental scanning electron microscopy to colloidal aggregation and film formation. *Colloids and Surfaces A: Physicochemical and Engineering Aspects* 174, 37–53. [https://doi.org/10.1016/S0927-7757\(00\)00520-3](https://doi.org/10.1016/S0927-7757(00)00520-3)

- Duarte, C.R., Olazar, M., Murata, V.V., Barrozo, M.A.S., 2009. Numerical simulation and experimental study of fluid–particle flows in a spouted bed. *Powder Technology* 188, 195–205. <https://doi.org/10.1016/j.powtec.2008.04.077>
- Eastman, J.E., Moore, C.O., 1984. Cold-water-soluble granular starch for gelled food compositions. US4465702A.
- Enferad, S., Petit, J., Gaiani, C., Falk, V., Burgain, J., Kiesgen De Richter, S., Jenny, M., 2021. Effect of particle size and formulation on powder rheology. *Particulate Science and Technology* 39, 362–370. <https://doi.org/10.1080/02726351.2020.1738605>
- English, A., 1981. Future uses of skimmed milk-texturizing processes. *International Journal of Dairy Technology* 34, 70–73. <https://doi.org/10.1111/j.1471-0307.1981.tb01503.x>
- Ennis, M.P., O’Sullivan, M.M., Mulvihill, D.M., 1998. The hydration behaviour of rennet caseins in calcium chelating salt solution as determined using a rheological approach. *Food Hydrocolloids* 12, 451–457. [https://doi.org/10.1016/S0268-005X\(98\)00063-0](https://doi.org/10.1016/S0268-005X(98)00063-0)
- Fäldt, P., Bergenståhl, B., Carlsson, G., 1993. The surface coverage of fat on food powders analyzed by ESCA (electron spectroscopy for chemical analysis). *Food Structure* 225–234.
- Fang, Y., Rogers, S., Selomulya, C., Chen, X.D., 2012. Functionality of milk protein concentrate: Effect of spray drying temperature. *Biochemical Engineering Journal* 62, 101–105. <https://doi.org/10.1016/j.bej.2011.05.007>
- Fang, Y., Selomulya, C., Ainsworth, S., Palmer, M., Chen, X.D., 2011. On quantifying the dissolution behaviour of milk protein concentrate. *Food Hydrocolloids* 25, 503–510. <https://doi.org/10.1016/j.foodhyd.2010.07.030>
- Fang, Y., Selomulya, C., Chen, X.D., 2010. Characterization of milk protein concentrate solubility using focused beam reflectance measurement. *Dairy Sci. Technol.* 90, 253–270. <https://doi.org/10.1051/dst/2009050>
- Fitzpatrick, J.J., van Lauwe, A., Coursol, M., O’Brien, A., Fitzpatrick, K.L., Ji, J., Miao, S., 2016. Investigation of the rehydration behaviour of food powders by comparing the behaviour of twelve powders with different properties. *Powder Technology* 297, 340–348. <https://doi.org/10.1016/j.powtec.2016.04.036>
- Folch, J., Lees, M., Stanley, G.H.S., 1957. A Simple Method for the Isolation and Purification of Total Lipides from Animal Tissues. *J. Biol. Chem.* 226, 497–509.
- Forbes, R.T., Davis, K.G., Hindle, M., Clarke, J.G., Maas, J., 1998. Water vapor sorption studies on the physical stability of a series of spray-dried protein/sugar powders for

- inhalation. *Journal of Pharmaceutical Sciences* 87, 1316–1321.
<https://doi.org/10.1021/js9800811>
- Forny, L., Marabi, A., Palzer, S., 2011. Wetting, disintegration and dissolution of agglomerated water soluble powders. *Powder Technology*, 9th International Symposium on Agglomeration and 4th International Granulation Workshop, 2009 206, 72–78.
<https://doi.org/10.1016/j.powtec.2010.07.022>
- Fournaise, T., Burgain, J., Perroud, C., Scher, J., Gaiani, C., Petit, J., 2020. Impact of formulation on reconstitution and flowability of spray-dried milk powders. *Powder Technology* 372, 107–116. <https://doi.org/10.1016/j.powtec.2020.05.085>
- Fournaise, T., Burgain, J., Perroud-Thomassin, C., Petit, J., 2021a. Impact of the whey protein/casein ratio on the reconstitution and flow properties of spray-dried dairy protein powders. *Powder Technology*. <https://doi.org/10.1016/j.powtec.2021.06.026>
- Fournaise, T., Petit, J., Gaiani, C., 2021b. Main powder physicochemical characteristics influencing their reconstitution behavior. *Powder Technology* 383, 65–73.
<https://doi.org/10.1016/j.powtec.2021.01.056>
- Frančišković-Bilinski, S., Bilinski, H., Vdović, N., Balagurunathan, Y., Dougherty, E.R., 2003. Application of image-based granulometry to siliceous and calcareous estuarine and marine sediments. *Estuarine, Coastal and Shelf Science* 58, 227–239.
[https://doi.org/10.1016/S0272-7714\(03\)00074-X](https://doi.org/10.1016/S0272-7714(03)00074-X)
- Freudig, B., Hogeekamp, S., Schubert, H., 1999. Dispersion of powders in liquids in a stirred vessel. *Chemical Engineering and Processing: Process Intensification* 38, 525–532.
[https://doi.org/10.1016/S0255-2701\(99\)00049-5](https://doi.org/10.1016/S0255-2701(99)00049-5)
- Fu, X., Huck, D., Makein, L., Armstrong, B., Willen, U., Freeman, T., 2012. Effect of particle shape and size on flow properties of lactose powders. *Particuology, Advances in Characterization and Modeling of Particulate Processes* 10, 203–208.
<https://doi.org/10.1016/j.partic.2011.11.003>
- Gaboriaud, F., Dufrière, Y.F., 2007. Atomic force microscopy of microbial cells: Application to nanomechanical properties, surface forces and molecular recognition forces. *Colloids and Surfaces B: Biointerfaces* 54, 10–19. <https://doi.org/10.1016/j.colsurfb.2006.09.014>
- Gaiani, C., 2006. Étude des mécanismes de réhydratation des poudres laitières [Ressource électronique] : influence de la structure et de la composition des poudres (Mémoire de thèse de doctorat soutenu le 5 juillet 2006). Vandoeuvre-les-Nancy : INPL. 2006.

- Gaiani, C., Mullet, M., Arab-Tehrany, E., Jacquot, M., Perroud, C., Renard, A., Scher, J., 2011. Milk proteins differentiation and competitive adsorption during spray-drying. *Food Hydrocolloids* 25, 983–990. <https://doi.org/10.1016/j.foodhyd.2010.09.013>
- Gaiani, C., Omar, R., El-Kirat-Chatel, S., Cvetkovska, L., Alexander, M., Ray, C., Burgain, J., Francius, G., 2021. Atomic force microscopy nanoscale analysis: Impact of storage conditions on surface properties of whey protein powders. *Food Hydrocolloids* 118, 106801. <https://doi.org/10.1016/j.foodhyd.2021.106801>
- Gaiani, Schuck, P., Scher, J., Desobry, S., Banon, S., 2007. Dairy Powder Rehydration: Influence of Protein State, Incorporation Mode, and Agglomeration. *Journal of Dairy Science* 90, 570–581. [https://doi.org/10.3168/jds.S0022-0302\(07\)71540-0](https://doi.org/10.3168/jds.S0022-0302(07)71540-0)
- Galet, L., Goalard, C., Dodds, J.A., 2009. The importance of surface energy in the dispersion behaviour of talc particles in aqueous media. *Powder Technology, Selection of Papers from the Symposium Powder Science and Technology - Powders and Sintered Material STP-PMF 2007* 190, 242–246. <https://doi.org/10.1016/j.powtec.2008.04.086>
- Galet, L., Patry, S., Dodds, J., 2010. Determination of the wettability of powders by the Washburn capillary rise method with bed preparation by a centrifugal packing technique. *Journal of Colloid and Interface Science* 346, 470–475. <https://doi.org/10.1016/j.jcis.2010.02.051>
- Galet, L., Vu, T.O., Oulahna, D., Fages, J., 2004. The Wetting Behaviour and Dispersion Rate of Cocoa Powder in Water. *Food and Bioproducts Processing* 82, 298–303. <https://doi.org/10.1205/fbio.82.4.298.56399>
- Gao, W., Chen, F., Wang, X., Meng, Q., 2020. Recent advances in processing food powders by using superfine grinding techniques: A review. *Comprehensive Reviews in Food Science and Food Safety* 19, 2222–2255. <https://doi.org/10.1111/1541-4337.12580>
- Garriga, M., Almaraz, M., Marchiaro, A., 2017. Determination of reducing sugars in extracts of *Undaria pinnatifida* (harvey) algae by UV-visible spectrophotometry (DNS method), in: *Determination of reducing sugars in extracts of Undaria pinnatifida* (harvey) algae by UV-visible spectrophotometry (DNS method). pp. 444–445.
- Gaudel, N., Gaiani, C., Harshe, Y.M., Kammerhofer, J., Pouzot, M., Desobry, S., Burgain, J., 2022. Reconstitution of fruit powders: A process – structure – function approach. *Journal of Food Engineering* 315, 110800. <https://doi.org/10.1016/j.jfoodeng.2021.110800>
- Geladi, P., Linderholm, J., 2020. *Principal Component Analysis* ☆. Elsevier.

- George, W., Latimer, J., 2019. Official Methods of Analysis of AOAC International - 20th Edition, 2016, 21st ed, AOAC International.
- Gianfrancesco, A., 2009. Séchage par atomisation : propriétés de collage des particules en relation avec l'agglomération (Mémoire de thèse de doctorat soutenu le 19 juin 2009). AgroParisTech.
- Gnagne, E., 2017. Optimisation d'un procédé de production de farines stabilisées de foutou et fofou à base de banane plantain. université Nangui Abrogoua, République de Côte d'Ivoire.
- Goalard, C., Samimi, A., Galet, L., Dodds, J.A., Ghadiri, M., 2006. Characterization of the Dispersion Behavior of Powders in Liquids. *Particle & Particle Systems Characterization* 23, 154–158. <https://doi.org/10.1002/ppsc.200601024>
- Goldszal, A., Bousquet, J., 2001. Wet agglomeration of powders: from physics toward process optimization. *Powder Technology* 117, 221–231. [https://doi.org/10.1016/S0032-5910\(00\)00369-7](https://doi.org/10.1016/S0032-5910(00)00369-7)
- Gong, Z., Zhang, M., Mujumdar, A.S., Sun, J., 2007. Spray Drying and Agglomeration of Instant Bayberry Powder. *Drying Technology* 26, 116–121. <https://doi.org/10.1080/07373930701781751>
- Grossman, R.B., Cline, M.G., 1957. Relationships between Rigidity and Particle Size Distribution. *Soil Science Society of America Journal* 21, 322–325. <https://doi.org/10.2136/sssaj1957.03615995002100030019x>
- Hammes, M.V., Englert, A.H., Noreña, C.P.Z., Cardozo, N.S.M., 2015. Study of the influence of soy lecithin addition on the wettability of buffalo milk powder obtained by spray drying. *Powder Technology* 277, 237–243. <https://doi.org/10.1016/j.powtec.2015.02.047>
- Haque, Md.K., Kawai, K., Suzuki, T., 2006. Glass transition and enthalpy relaxation of amorphous lactose glass. *Carbohydrate Research* 341, 1884–1889. <https://doi.org/10.1016/j.carres.2006.04.040>
- Henry, J., 2013. *Advances in Food and Nutrition Research*, - 1st Edition, Advances in Food and Nutrition Research. ed. Elsevier.
- Herri, J.M., Gruy, F., Pic, J.S., Cournil, M., Cingotti, B., Sinquin, A., 1999. Interest of in situ turbidimetry for the characterization of methane hydrate crystallization: Application to the study of kinetic inhibitors. *Chemical Engineering Science* 54, 1849–1858. [https://doi.org/10.1016/S0009-2509\(98\)00433-3](https://doi.org/10.1016/S0009-2509(98)00433-3)

- Hertz, H., 1882. Ueber die Berührung fester elastischer Körper (On Contact Between Elastic Bodies). *Journal für die reine und angewandte Mathematik (Crelles Journal)* 156.
- Hideo Nakae, Ryuichi Inui, Yosuke Hirata, Hiroyuki Saito, 1998. Effects of surface roughness on wettability. *Acta Materialia* 46, 2313–2318. [https://doi.org/10.1016/S1359-6454\(98\)80012-8](https://doi.org/10.1016/S1359-6454(98)80012-8)
- Higuchi, T., 1961. Rate of Release of Medicaments from Ointment Bases Containing Drugs in Suspension. *Journal of Pharmaceutical Sciences* 50, 874–875. <https://doi.org/10.1002/jps.2600501018>
- Hill, A.V., 1910. The possible effects of the aggregation of the molecules of haemoglobin on its dissociation curves. *J. Physiol.(Lond.)* iv–vii.
- Hixon, A., Crowell, J., 1931. Dependence of reaction velocity upon surface and agitation. 923–931.
- Hla, P.K., Hogekamp, S., 1999. Wetting behaviour of instantized cocoa beverage powders. *International Journal of Food Science & Technology* 34, 335–342. <https://doi.org/10.1046/j.1365-2621.1999.00275.x>
- Hobbs, L., 2009. Chapter 21 - Sweeteners from Starch: Production, Properties and Uses, in: BeMiller, J., Whistler, R. (Eds.), *Starch (Third Edition)*, Food Science and Technology. Academic Press, San Diego, pp. 797–832. <https://doi.org/10.1016/B978-0-12-746275-2.00021-5>
- Hogekamp, S., Schubert, H., 2003. Rehydration of Food Powders. *Food sci. technol. int.* 9, 223–235. <https://doi.org/10.1177/1082013203034938>
- Hogg, G., 2008. Issues in particle size analysis. *Kona Powder and Particle Journal* 26, 81–93.
- Hołysz, L., Mirosław, M., Terpiłowski, K., Szcześ, A., 2010. Influence of relative humidity on the wettability of silicon wafer surfaces. *Appl. Phys. Lett.*
- Hopfenberg, H.B., 1976. Controlled Release from Erodible Slabs, Cylinders, and Spheres, in: *Controlled Release Polymeric Formulations*, ACS Symposium Series. AMERICAN CHEMICAL SOCIETY, pp. 26–32. <https://doi.org/10.1021/bk-1976-0033.ch003>
- Höpfner, T., Bluma, A., Rudolph, G., Lindner, P., Scheper, T., 2010. A review of non-invasive optical-based image analysis systems for continuous bioprocess monitoring. *Bioprocess Biosyst Eng* 33, 247–256. <https://doi.org/10.1007/s00449-009-0319-8>
- Horton, H.R., Moran, L.A., Ochs, R.S., Rawn, D., Scrimgeour, K.G., 1994. *Principes de biochimie*, De Boeck. ed.
- Huffel, S. van, Lemmerling, P., 2013. *Total Least Squares and Errors-in-Variables Modeling: Analysis, Algorithms and Applications*. Springer Science & Business Media.

- Hussain, R., Gaiani, C., Scher, J., 2012. From high milk protein powders to the rehydrated dispersions in variable ionic environments: A review. *Journal of Food Engineering* 113, 486–503. <https://doi.org/10.1016/j.jfoodeng.2012.06.011>
- IDF, 1987. Détermination de la dispersibilité et de la mouillabilité. International Dairy Federation, Brussels, Belgium.
- Illy, E., Navarini, L., 2011. Neglected Food Bubbles: The Espresso Coffee Foam. *Food Biophysics* 6, 335–348. <https://doi.org/10.1007/s11483-011-9220-5>
- Iordache, M., Jelen, P., 2003. High pressure microfluidization treatment of heat denatured whey proteins for improved functionality. *Innovative Food Science & Emerging Technologies* 4, 367–376. [https://doi.org/10.1016/S1466-8564\(03\)00061-4](https://doi.org/10.1016/S1466-8564(03)00061-4)
- Irie, K.R., Petit, J., Gnagne, E.H., Kouadio, O.K., Gaiani, C., Scher, J., Amani, G.N., 2021. Effect of particle size on flow behaviour and physical properties of semi-ripe plantain (AAB Musa spp) powders. *International Journal of Food Science & Technology* 56, 205–214. <https://doi.org/10.1111/ijfs.14620>
- Jacquot, C., Petit, J., Michaux, F., Chávez Montes, E., Dupas, J., Girard, V., Gianfrancesco, A., Scher, J., Gaiani, C., 2016. Cocoa powder surface composition during aging: A focus on fat. *Powder Technology* 292, 195–202. <https://doi.org/10.1016/j.powtec.2016.01.032>
- Janssen, D., De Palma, R., Verlaak, S., Heremans, P., Dehaen, W., 2006. Static solvent contact angle measurements, surface free energy and wettability determination of various self-assembled monolayers on silicon dioxide. *Thin Solid Films* 515, 1433–1438. <https://doi.org/10.1016/j.tsf.2006.04.006>
- Jeanet, R., Schuck, P., Six, T., Andre, C., Delaplace, G., 2010. The influence of stirring speed, temperature and solid concentration on the rehydration time of micellar casein powder. *Dairy Sci. Technol.* 90, 225–236. <https://doi.org/10.1051/dst/2009043>
- Jensen, H., Soloviev, A., Li, Z., Søggaard, E.G., 2005. XPS and FTIR investigation of the surface properties of different prepared titania nano-powders. *Applied Surface Science* 246, 239–249. <https://doi.org/10.1016/j.apsusc.2004.11.015>
- Ji, J., Cronin, K., Fitzpatrick, J., Fenelon, M., Miao, S., 2015. Effects of fluid bed agglomeration on the structure modification and reconstitution behaviour of milk protein isolate powders. *Journal of Food Engineering, Food Structure Design: Innovation in Food Structure-Properties Relationships* 167, 175–182. <https://doi.org/10.1016/j.jfoodeng.2015.01.012>

- Ji, J., Cronin, K., Fitzpatrick, J., Miao, S., 2017. Enhanced wetting behaviours of whey protein isolate powder: The different effects of lecithin addition by fluidised bed agglomeration and coating processes. *Food Hydrocolloids* 71, 94–101. <https://doi.org/10.1016/j.foodhyd.2017.05.005>
- Jiang, H., Zhang, M., Adhikari, B., 2013. 21 - Fruit and vegetable powders, in: Bhandari, B., Bansal, N., Zhang, Min, Schuck, P. (Eds.), *Handbook of Food Powders*, Woodhead Publishing Series in Food Science, Technology and Nutrition. Woodhead Publishing, pp. 532–552. <https://doi.org/10.1533/9780857098672.3.532>
- Jolliffe, I., 2005. Principal Component Analysis, in: *Encyclopedia of Statistics in Behavioral Science*. American Cancer Society. <https://doi.org/10.1002/0470013192.bsa501>
- Jones, D.M., 1988. Controlling Particle Size and Release Properties, in: *Flavor Encapsulation*, ACS Symposium Series. American Chemical Society, pp. 158–176. <https://doi.org/10.1021/bk-1988-0370.ch017>
- Kail, N., Briesen, H., Marquardt, W., 2008. Analysis of FBRM measurements by means of a 3D optical model. *Powder Technology* 185, 211–222. <https://doi.org/10.1016/j.powtec.2007.10.015>
- Kalogianni, E.P., Xynogalos, V.A., Karapantsios, T.D., Kostoglou, M., 2002. Effect of Feed Concentration on the Production of Pregelatinized Starch in a Double Drum Dryer. *LWT - Food Science and Technology* 35, 703–714. <https://doi.org/10.1006/fstl.2002.0925>
- Karam, M.C., Hosri, C., Hussain, R., Barbar, R., Gaiani, C., Scher, J., 2017. Effect of whey powder rehydration and dry-denaturation state on acid milk gels characteristics. *Journal of Food Processing and Preservation* 41, e13200. <https://doi.org/10.1111/jfpp.13200>
- Karam, M.C., Petit, J., Zimmer, D., Baudelaire Djantou, E., Scher, J., 2016. Effects of drying and grinding in production of fruit and vegetable powders: A review. *Journal of Food Engineering* 188, 32–49. <https://doi.org/10.1016/j.jfoodeng.2016.05.001>
- Karlsson, A.O., Ipsen, R., Ardö, Y., 2007. Observations of casein micelles in skim milk concentrate by transmission electron microscopy. *LWT - Food Science and Technology* 40, 1102–1107. <https://doi.org/10.1016/j.lwt.2006.05.012>
- Karthik, P., Chhanwal, N., Anandharamakrishnan, C., 2017. Drum Drying, in: *Handbook of Drying for Dairy Products*. John Wiley & Sons, Ltd, pp. 43–56. <https://doi.org/10.1002/9781118930526.ch4>

- Kasas, S., Longo, G., Dietler, G., 2013. Mechanical properties of biological specimens explored by atomic force microscopy. *J. Phys. D: Appl. Phys.* 46, 133001. <https://doi.org/10.1088/0022-3727/46/13/133001>
- Kelly, G.M., O'Mahony, J.A., Kelly, A.L., Huppertz, T., Kennedy, D., O'Callaghan, D.J., 2015. Influence of protein concentration on surface composition and physico-chemical properties of spray-dried milk protein concentrate powders. *International Dairy Journal* 51, 34–40. <https://doi.org/10.1016/j.idairyj.2015.07.001>
- Kerwin, B.A., 2008. Polysorbates 20 and 80 Used in the Formulation of Protein Biotherapeutics: Structure and Degradation Pathways. *Journal of Pharmaceutical Sciences* 97, 2924–2935. <https://doi.org/10.1002/jps.21190>
- Kim, E.H., 2008. Surface composition of industrial spray-dried dairy powders and its formation mechanisms.
- Kim, E.H., Chen, X.D., Pearce, D., 2003. On the Mechanisms of Surface Formation and the Surface Compositions of Industrial Milk Powders. *Drying Technology* 21, 265–278. <https://doi.org/10.1081/DRT-120017747>
- Kim, E.H., Chen, X.D., Pearce, D., 2002. Surface characterization of four industrial spray-dried dairy powders in relation to chemical composition, structure and wetting property. *COLLOIDS AND SURFACES B BIOINTERFACES* 197.
- Kim, E.H.-J., Chen, X.D., Pearce, D., 2005. Effect of surface composition on the flowability of industrial spray-dried dairy powders. *Colloids and Surfaces B: Biointerfaces* 46, 182–187. <https://doi.org/10.1016/j.colsurfb.2005.11.005>
- Klang, V., Valenta, C., Matsko, N.B., 2013. Electron microscopy of pharmaceutical systems. *Micron* 44, 45–74. <https://doi.org/10.1016/j.micron.2012.07.008>
- Knudsen, J.C., Skibsted, L.H., 2010. High pressure effects on the structure of casein micelles in milk as studied by cryo-transmission electron microscopy. *Food Chemistry* 119, 202–208. <https://doi.org/10.1016/j.foodchem.2009.06.017>
- Kosasih, L., Bhandari, B., Prakash, S., Bansal, N., Gaiani, C., 2016. Effect of whole milk concentrate carbonation on functional, physicochemical and structural properties of the resultant spray dried powder during storage. *Journal of Food Engineering* 179, 68–77. <https://doi.org/10.1016/j.jfoodeng.2016.02.005>
- Kravtchenko, T.P., Renoir, J., Parker, A., Brigand, G., 1999. A novel method for determining the dissolution kinetics of hydrocolloid powders. *Food Hydrocolloids* 13, 219–225. [https://doi.org/10.1016/S0268-005X\(99\)00002-8](https://doi.org/10.1016/S0268-005X(99)00002-8)

- Kumar, P.M., Badrinarayanan, S., Sastry, M., 2000. Nanocrystalline TiO₂ studied by optical, FTIR and X-ray photoelectron spectroscopy: correlation to presence of surface states. *Thin Solid Films* 358, 122–130. [https://doi.org/10.1016/S0040-6090\(99\)00722-1](https://doi.org/10.1016/S0040-6090(99)00722-1)
- Laguna, A., Ouattara, A., Gonzalez, R.O., Baron, O., Famá, G., El Mamouni, R., Guiot, S., Monroy, O., Macarie, H., 1999. A Simple and Low Cost Technique for Determining the Granulometry of Upflow Anaerobic Sludge Blanket Reactor Sludge. *Water Science and Technology* 40, 1–8. <https://doi.org/10.2166/wst.1999.0371>
- Lallbeeharry, P., Tian, Y., Fu, N., Wu, W.D., Woo, M.W., Selomulya, C., Chen, X.D., 2014. Effects of ionic and nonionic surfactants on milk shell wettability during co-spray-drying of whole milk particles. *Journal of Dairy Science* 97, 5303–5314. <https://doi.org/10.3168/jds.2013-7772>
- Lamberti, M., Geiselman, A., Conde-Petit, B., Escher, F., 2004. Starch transformation and structure development in production and reconstitution of potato flakes. *LWT - Food Science and Technology* 37, 417–427. <https://doi.org/10.1016/j.lwt.2003.10.015>
- Lankveld, J., 1984. Texturizing milk proteins. Presented at the PROCEEDINGS OF THE INTERNATIONAL CONGRESS ON MILK PROTEINS, Pudoc Wageningen, LUXEMBURG, pp. 129–135.
- Lazghab, M., Saleh, K., Pezron, I., Guigon, P., Komunjer, L., 2005. Wettability assessment of finely divided solids. *Powder Technology*, 4th French Meeting on Powder Science and Technology 157, 79–91. <https://doi.org/10.1016/j.powtec.2005.05.014>
- Lee, W., Clark, S., Swanson, B.G., 2006. Functional Properties of High Hydrostatic Pressure-Treated Whey Protein. *Journal of Food Processing and Preservation* 30, 488–501. <https://doi.org/10.1111/j.1745-4549.2005.00081.x>
- Lehmann, K., 1992. Fluid-Bed Spray Coating, in: *Microcapsules and Nanoparticles in Medicine and Pharmacy*. CRC Press.
- Leube, P.C., 2013. Methods for physically-based model reduction in time: analysis, comparison of methods and application.
- Li, K., Woo, M.W., Patel, H., Metzger, L., Selomulya, C., 2018. Improvement of rheological and functional properties of milk protein concentrate by hydrodynamic cavitation. *Journal of Food Engineering* 221, 106–113. <https://doi.org/10.1016/j.jfoodeng.2017.10.005>
- Li, R., Roos, Y.H., Miao, S., 2017. Characterization of mechanical and encapsulation properties of lactose/maltodextrin/WPI matrix. *Food Hydrocolloids* 63, 149–159. <https://doi.org/10.1016/j.foodhyd.2016.08.033>

- Liao, C.-C., Hsiao, S.-S., Wu, C.-S., 2012. Experimental study on the effect of surface roughness of the intruder on the Brazil nut problem in a vertically vibrated bed. *Phys. Rev. E* 86, 061316. <https://doi.org/10.1103/PhysRevE.86.061316>
- Lie-Piang, A., Leeman, M., Castro, A., Börjesson, E., Nilsson, L., 2021. Investigating the effect of powder manufacturing and reconstitution on casein micelles using asymmetric flow field-flow fractionation (AF4) and transmission electron microscopy. *Food Research International* 139, 109939. <https://doi.org/10.1016/j.foodres.2020.109939>
- Linden, G., Lorient, D., 1999. *New Ingredients in Food Processing: Biochemistry and Agriculture*. CRC Press.
- Liu, Y., Guo, X., Lu, H., Gong, X., 2015. An Investigation of the Effect of Particle Size on the Flow Behavior of Pulverized Coal. *Procedia Engineering, New Paradigm of Particle Science and Technology Proceedings of The 7th World Congress on Particle Technology* 102, 698–713. <https://doi.org/10.1016/j.proeng.2015.01.170>
- Lowell, S., Shields, J.E., 1991. *Powder Surface Area and Porosity*. Springer Science & Business Media.
- Lu, X., Lu, Q., Zhu, Z., Yin, J., Wang, Z., 2003. Laser induced periodic structure on lecithin-doped polyimide film surface and its ability to align liquid crystal molecules. *Polymer* 44, 4501–4507. [https://doi.org/10.1016/S0032-3861\(03\)00433-6](https://doi.org/10.1016/S0032-3861(03)00433-6)
- Ma, Y., Evans, T.M., Philips, N., Cunningham, N., 2019. Modeling the effect of moisture on the flowability of a granular material. *Meccanica* 54, 667–681. <https://doi.org/10.1007/s11012-018-0901-8>
- Makower, B., Dye, W.B., 1956. Sugar Crystallization, Equilibrium Moisture Content and Crystallization of Amorphous Sucrose and Glucose. *J. Agric. Food Chem.* 4, 72–77. <https://doi.org/10.1021/jf60059a010>
- Mandato, S., Rondet, E., Delaplace, G., Barkouti, A., Galet, L., Accart, P., Ruiz, T., Cuq, B., 2012. Liquids' atomization with two different nozzles: Modeling of the effects of some processing and formulation conditions by dimensional analysis. *Powder Technology* 224, 323–330. <https://doi.org/10.1016/j.powtec.2012.03.014>
- Marabi, A., Mayor, G., Burbidge, A., Wallach, R., Saguy, I.S., 2008. Assessing dissolution kinetics of powders by a single particle approach. *Chemical Engineering Journal* 139, 118–127. <https://doi.org/10.1016/j.cej.2007.07.081>
- Marella, C., Salunke, P., Biswas, A.C., Kommineni, A., Metzger, L.E., 2015. Manufacture of modified milk protein concentrate utilizing injection of carbon dioxide. *Journal of Dairy Science* 98, 3577–3589. <https://doi.org/10.3168/jds.2014-8946>

- Martins, L.S., Monticelli, F.M., Mulinari, D.R., 2020. Influence of the granulometry and fiber content of palm residues on the diesel S-10 oil sorption in polyurethane /palm fiber biocomposites. *Results in Materials* 8, 100143. <https://doi.org/10.1016/j.rinma.2020.100143>
- Mathlouthi, M., Genotelle, J., 1998. Role of water in sucrose crystallization1Presented at the Second International Meeting of the Portuguese Carbohydrate Chemistry Group.1. *Carbohydrate Polymers* 37, 335–342. [https://doi.org/10.1016/S0144-8617\(98\)00079-4](https://doi.org/10.1016/S0144-8617(98)00079-4)
- McKENNA, A.B., 1997. Examination of whole milk powder by confocal laser scanning microscopy. *Journal of Dairy Research* 64, 423–432. <https://doi.org/10.1017/S0022029997002331>
- Mehta, M., Jones, M., 1985. Coated pellets under the microscope. *Pharmaceutical Technology*.
- Merkus, H.G., 2009. *Particle Size Measurements: Fundamentals, Practice, Quality*. Springer Science & Business Media.
- Mevik, B.-H., Cederkvist, H.R., 2004. Mean squared error of prediction (MSEP) estimates for principal component regression (PCR) and partial least squares regression (PLSR). *Journal of Chemometrics* 18, 422–429. <https://doi.org/10.1002/cem.887>
- Meyer, S., Rajendram, V.S., Povey, M.J. w., 2006. Characterization of Reconstituted Milk Powder by Ultrasound Spectroscopy. *Journal of Food Quality* 29, 405–418. <https://doi.org/10.1111/j.1745-4557.2006.00082.x>
- Miller-Livney, T., Hartel, R.W., 1997. Ice Recrystallization in Ice Cream: Interactions Between Sweeteners and Stabilizers. *Journal of Dairy Science* 80, 447–456. [https://doi.org/10.3168/jds.S0022-0302\(97\)75956-3](https://doi.org/10.3168/jds.S0022-0302(97)75956-3)
- Mimouni, A., Deeth, H.C., Whittaker, A.K., Gidley, M.J., Bhandari, B.R., 2010. Investigation of the microstructure of milk protein concentrate powders during rehydration: Alterations during storage. *Journal of Dairy Science* 93, 463–472. <https://doi.org/10.3168/jds.2009-2369>
- Mimouni, A., Deeth, H.C., Whittaker, A.K., Gidley, M.J., Bhandari, B.R., 2009. Rehydration process of milk protein concentrate powder monitored by static light scattering. *Food Hydrocolloids* 23, 1958–1965. <https://doi.org/10.1016/j.foodhyd.2009.01.010>
- Miñarro, B., Albanell, E., Aguilar, N., Guamis, B., Capellas, M., 2012. Effect of legume flours on baking characteristics of gluten-free bread. *Journal of Cereal Science* 56, 476–481. <https://doi.org/10.1016/j.jcs.2012.04.012>
- Mitchell, W.R., Forny, L., Althaus, T., Niederreiter, G., Palzer, S., Hounslow, M.J., Salman, A.D., 2020. Tracking of powder lump formation and dispersion with the use of FBRM

- technology and video recordings. *Powder Technology* 367, 10–19. <https://doi.org/10.1016/j.powtec.2020.03.035>
- Mitchell, W.R., Forny, L., Althaus, T., Niederreiter, G., Palzer, S., Hounslow, M.J., Salman, A.D., 2019. Surface tension-driven effects in the reconstitution of food powders. *Chemical Engineering Research and Design* 146, 464–469. <https://doi.org/10.1016/j.cherd.2019.04.015>
- Mitchell, W.R., Forny, L., Althaus, T.O., Niederreiter, G., Palzer, S., Hounslow, M.J., Salman, A.D., 2015. Mapping the rate-limiting regimes of food powder reconstitution in a standard mixing vessel. *Powder Technology, 6th International Workshop on Granulation: Granulation across the length scales* 270, 520–527. <https://doi.org/10.1016/j.powtec.2014.08.014>
- Mohamad Saad, M., Gaiani, C., Scher, J., Cuq, B., Ehrhardt, J.J., Desobry, S., 2009. Impact of re-grinding on hydration properties and surface composition of wheat flour. *Journal of Cereal Science* 49, 134–140. <https://doi.org/10.1016/j.jcs.2008.08.001>
- Mohanan, A., Nickerson, M.T., Ghosh, S., 2020. Utilization of pulse protein-xanthan gum complexes for foam stabilization: The effect of protein concentrate and isolate at various pH. *Food Chemistry* 316, 126282. <https://doi.org/10.1016/j.foodchem.2020.126282>
- Moore, J.G., 1995. Drum Dryers, in: *Handbook of Industrial Drying*. CRC Press.
- Mori, Y., Yoshida, H., Masuda, H., 2007. Characterization of Reference Particles of Transparent Glass by Laser Diffraction Method. *Particle & Particle Systems Characterization* 24, 91–96. <https://doi.org/10.1002/ppsc.200601048>
- Murrieta-Pazos, I., Gaiani, C., Galet, L., Scher, J., 2012. Composition gradient from surface to core in dairy powders: Agglomeration effect. *Food Hydrocolloids* 26, 149–158. <https://doi.org/10.1016/j.foodhyd.2011.05.003>
- Muzaffar, K., Nayik, G.A., Kumar, P., 2015. Stickiness Problem Associated with Spray Drying of Sugar and Acid Rich Foods: A Mini Review. *Journal of Nutrition & Food Sciences*.
- Naini, V., Byron, P.R., Phillips, E.M., 1998. Physicochemical Stability of Crystalline Sugars and Their Spray-Dried Forms: Dependence upon Relative Humidity and Suitability for Use in Powder Inhalers. *Drug Development and Industrial Pharmacy* 24, 895–909. <https://doi.org/10.3109/03639049809097269>
- Nakai, Y., Fukuoka, E., Nakajima, S., Hasegawa, J., 1977. Crystallinity and Physical Characteristics of Microcrystalline Cellulose. *Chemical & Pharmaceutical Bulletin* 25, 96–101. <https://doi.org/10.1248/cpb.25.96>

- Nawaz, M.A., Gaiani, C., Fukai, S., Bhandari, B., 2016. X-ray photoelectron spectroscopic analysis of rice kernels and flours: Measurement of surface chemical composition. *Food Chemistry* 212, 349–357. <https://doi.org/10.1016/j.foodchem.2016.05.188>
- Ndangui, C.B., Kimbonguila, A., Nzikou, J., Matos, L., Pambou-Tobi, N., Abena, A., Silou, T., Scher, J., Desobry, S., 2010. Nutritive Composition and Properties Physico-chemical of Gumbo (*Abelmoschus esculentus* L.) Seed and Oil. undefined.
- Nernst, W., 1904. Theorie der Reaktionsgeschwindigkeit in heterogenen Systemen. *Zeitschrift für Physikalische Chemie* 47U, 52–55. <https://doi.org/10.1515/zpch-1904-4704>
- Neves, M.I.L., Desobry-Banon, S., Perrone, I.T., Desobry, S., Petit, J., 2019. Encapsulation of curcumin in milk powders by spray-drying: Physicochemistry, rehydration properties, and stability during storage. *Powder Technology* 345, 601–607. <https://doi.org/10.1016/j.powtec.2019.01.049>
- Nicholas, M., Josefson, M., Fransson, M., Wilbs, J., Roos, C., Boissier, C., Thalberg, K., 2020. Quantification of surface composition and surface structure of inhalation powders using TOF-SIMS. *International Journal of Pharmaceutics* 587, 119666. <https://doi.org/10.1016/j.ijpharm.2020.119666>
- Nijdam, J.J., Langrish, T.A.G., 2006. The effect of surface composition on the functional properties of milk powders. *Journal of Food Engineering* 77, 919–925. <https://doi.org/10.1016/j.jfoodeng.2005.08.020>
- Nikolova, Y., Petit, J., Gianfrancesco, A., Sanders, C.F.W., Scher, J., Gaiani, C., 2015. Impact of Spray-Drying Process Parameters on Dairy Powder Surface Composition and Properties. *Drying Technology* 33, 1654–1661. <https://doi.org/10.1080/07373937.2015.1060494>
- Nindo, C.I., Tang, J., 2007. Refractance Window Dehydration Technology: A Novel Contact Drying Method. *Drying Technology* 25, 37–48. <https://doi.org/10.1080/07373930601152673>
- Noy, A., Vezenov, D., Lieber, C., 1997. CHEMICAL FORCE MICROSCOPY. *Annual Review of Materials Science* 27, 381–421. <https://doi.org/10.1146/annurev.matsci.27.1.381>
- Noyes, A.A., Whitney, W.R., 1897. THE RATE OF SOLUTION OF SOLID SUBSTANCES IN THEIR OWN SOLUTIONS. [WWW Document]. <https://doi.org/10.1021/ja02086a003>
- Nurhadi, B., Roos, Y.H., Maidannyk, V., 2016. Physical properties of maltodextrin DE 10: Water sorption, water plasticization and enthalpy relaxation. *Journal of Food Engineering* 174, 68–74. <https://doi.org/10.1016/j.jfoodeng.2015.11.018>

- Oestergaard, B., 2016. Hydrodynamic cavitation helps dairy powder processing.
- O'Mahony, J.A., McSweeney, P.L.H., 2016. Advanced dairy chemistry. Volume 1B: Proteins: Applied aspects. Fourth Edition. Springer.
- Omobuwajo, T.O., Busari, O.T., Osemwegie, A.A., 2000. Thermal agglomeration of chocolate drink powder. *Journal of Food Engineering* 46, 73–81. [https://doi.org/10.1016/S0260-8774\(00\)00067-4](https://doi.org/10.1016/S0260-8774(00)00067-4)
- Ong, X.Y., Taylor, S.E., Ramaioli, M., 2021. On the formation of dry granular jets at a liquid surface. *Chemical Engineering Science* 245, 116958. <https://doi.org/10.1016/j.ces.2021.116958>
- Ong, X.Y., Taylor, S.E., Ramaioli, M., 2019. Pouring of Grains onto Liquid Surfaces: Dispersion or Lump Formation? *Langmuir* 35, 11150–11156. <https://doi.org/10.1021/acs.langmuir.9b01277>
- Onwulata, C., 2005. Encapsulated and Powdered Foods. CRC Press.
- Otsuka, M., Ofusa, T., Matsuda, Y., 1999. Effect of environmental humidity on the transformation pathway of carbamazepine polymorphic modifications during grinding. *Colloids and Surfaces B: Biointerfaces* 13, 263–273. [https://doi.org/10.1016/S0927-7765\(99\)00014-4](https://doi.org/10.1016/S0927-7765(99)00014-4)
- Özisik, M.N., Orlande, H.R.B., 2021. Inverse Heat Transfer: Fundamentals and Applications, 2nd ed. CRC Press, Boca Raton. <https://doi.org/10.1201/9781003155157>
- Palamanit, A., Prachayawarakorn, S., Tungtrakul, P., Soponronnarit, S., 2016. Performance Evaluation of Top-Spray Fluidized Bed Coating for Healthy Coated Rice Production. *Food Bioprocess Technol* 9, 1317–1326. <https://doi.org/10.1007/s11947-016-1720-3>
- Palzer, S., 2007. Chapter 13 Agglomeration of dehydrated consumer foods, in: Salman, A.D., Hounslow, M.J., Seville, J.P.K. (Eds.), *Handbook of Powder Technology, Granulation*. Elsevier Science B.V., pp. 591–671. [https://doi.org/10.1016/S0167-3785\(07\)80048-0](https://doi.org/10.1016/S0167-3785(07)80048-0)
- Paramita, V., Lida, K., Furuta, T., 2010. Effect of Additives on the Morphology of Spray-Dried Powder. *Drying Technology* 323–329.
- Park, H., Chung, H., 2014. Influence of the addition of aronia powder on the quality and antioxidant activity of muffins. *Korean Journal of Food Preservation* 21, 668–675.
- Parker, A., Vigouroux, F., Reed, W.F., 2000. Dissolution kinetics of polymer powders. *AIChE Journal* 46, 1290–1299. <https://doi.org/10.1002/aic.690460703>
- Pearson, K., 1901. LIII. On lines and planes of closest fit to systems of points in space. *The London, Edinburgh, and Dublin Philosophical Magazine and Journal of Science* 2, 559–572. <https://doi.org/10.1080/14786440109462720>

- Perez, M., Décaudin, B., Maiguy-Foinard, A., Barthélémy, C., Lebuffe, G., Storme, L., Odou, P., 2017. Dynamic Image Analysis To Evaluate Subvisible Particles During Continuous Drug Infusion In a Neonatal Intensive Care Unit. *Sci Rep* 7, 9404. <https://doi.org/10.1038/s41598-017-10073-y>
- Perkins, M., Ebbens, S.J., Hayes, S., Roberts, C.J., Madden, C.E., Luk, S.Y., Patel, N., 2007. Elastic modulus measurements from individual lactose particles using atomic force microscopy. *International Journal of Pharmaceutics* 332, 168–175. <https://doi.org/10.1016/j.ijpharm.2006.09.032>
- Petit, J., Méjean, S., Accart, P., Galet, L., Schuck, P., Le Floch-Fouéré, C., Delaplace, G., Jeantet, R., 2015. A dimensional analysis approach for modelling the size of droplets formed by bi-fluid atomisation. *Journal of Food Engineering* 149, 237–247. <https://doi.org/10.1016/j.jfoodeng.2014.10.022>
- Petit, J., Michaux, F., Jacquot, C., Chávez Montes, E., Dupas, J., Girard, V., Gianfrancesco, A., Scher, J., Gaiani, C., 2017. Storage-induced caking of cocoa powder. *Journal of Food Engineering* 199, 42–53. <https://doi.org/10.1016/j.jfoodeng.2016.12.005>
- Phisut, N., 2012. Spray drying technique of fruit juice powder: some factors influencing the properties of product.
- Potes, N., Kerry, J.P., Roos, Y.H., 2012. Additivity of water sorption, alpha-relaxations and crystallization inhibition in lactose–maltodextrin systems. *Carbohydrate Polymers* 89, 1050–1059. <https://doi.org/10.1016/j.carbpol.2012.03.061>
- Povey, M.J.W., Watson, N., Parker, N.G., 2013. 7 - Ultrasonic and acoustic microscopy: principles and applications to food microstructures, in: Morris, V.J., Groves, K. (Eds.), *Food Microstructures*, Woodhead Publishing Series in Food Science, Technology and Nutrition. Woodhead Publishing, pp. 192–222. <https://doi.org/10.1533/9780857098894.1.192>
- Preedy, V.R., 2012. *Dietary Sugars: Chemistry, Analysis, Function and Effects*. Royal Society of Chemistry.
- Pugh, R.J., 2016. *Bubble and Foam Chemistry*. Cambridge University Press.
- Puri, V., Dantuluri, A.K., Kumar, M., Karar, N., Bansal, A.K., 2010. Wettability and surface chemistry of crystalline and amorphous forms of a poorly water soluble drug. *European Journal of Pharmaceutical Sciences* 40, 84–93. <https://doi.org/10.1016/j.ejps.2010.03.003>

- Qiu, Z., Stowell, J.G., Cao, W., Morris, K.R., Byrn, S.R., Carvajal, M.T., 2005. Effect of Milling and Compression on the Solid-State Maillard Reaction. *Journal of Pharmaceutical Sciences* 94, 2568–2580. <https://doi.org/10.1002/jps.20448>
- Ramos, K.J., Bahr, D.F., 2007. Mechanical behavior assessment of sucrose using nanoindentation. *Journal of Materials Research* 22, 2037–2045. <https://doi.org/10.1557/jmr.2007.0249>
- Rao, M.A.A., 2010. *Rheology of Fluid and Semisolid Foods: Principles and Applications*. Springer Science & Business Media.
- Ratti, C., 2013. 3 - Freeze drying for food powder production, in: Bhandari, B., Bansal, N., Zhang, M., Schuck, P. (Eds.), *Handbook of Food Powders*, Woodhead Publishing Series in Food Science, Technology and Nutrition. Woodhead Publishing, pp. 57–84. <https://doi.org/10.1533/9780857098672.1.57>
- Ratti, C., 2008. *Advances in Food Dehydration*. CRC Press. ISBN 978-1-4200-5253-4.
- Raux, P.S., Cockenpot, H., Ramaioli, M., Quéré, D., Clanet, C., 2013. Wicking in a Powder. *Langmuir* 29, 3636–3644. <https://doi.org/10.1021/la400015v>
- Ray, Y.-C., Jiang, T.-S., Wen, C.Y., 1987. Particle attrition phenomena in a fluidized bed. *Powder Technology* 49, 193–206. [https://doi.org/10.1016/0032-5910\(87\)80128-6](https://doi.org/10.1016/0032-5910(87)80128-6)
- Richard, B., 2012. *Influence de la physico-chimie des poudres laitières et des conditions opératoires de dispersion sur la dynamique de réhydratation* (thesis). <http://www.theses.fr>. Lille 1.
- Richard, B., Toubal, M., Le Page, J.-F., Nassar, G., Radziszewski, E., Nongaillard, B., Debreyne, P., Schuck, P., Jeantet, R., Delaplace, G., 2012. Ultrasound tests in a stirred vessel to evaluate the reconstitution ability of dairy powders. *Innovative Food Science & Emerging Technologies* 16, 233–242. <https://doi.org/10.1016/j.ifset.2012.06.007>
- Roos, Y., 1995. Characterization of food polymers using state diagrams. *Journal of Food Engineering* 24, 339–360. [https://doi.org/10.1016/0260-8774\(95\)90050-L](https://doi.org/10.1016/0260-8774(95)90050-L)
- Roos, Y., Karel, M., 1991. Phase Transitions of Mixtures of Amorphous Polysaccharides and Sugars. *Biotechnology Progress* 7, 49–53. <https://doi.org/10.1021/bp00007a008>
- Roos, Y.H., 2013. Relaxations, Glass Transition and Engineering Properties of Food Solids, in: Yanniotis, S., Taoukis, P., Stoforos, N.G., Karathanos, V.T. (Eds.), *Advances in Food Process Engineering Research and Applications*, Food Engineering Series. Springer US, Boston, MA, pp. 79–90. https://doi.org/10.1007/978-1-4614-7906-2_4
- Roos, Y.H., 2002. Importance of glass transition and water activity to spray drying and stability of dairy powders. *Lait* 82, 475–484. <https://doi.org/10.1051/lait:2002025>

- Roos, Y.H., Afrassiabian, Z., Saleh, K., Famelart, M.-H., Audebert, A., Gulzar, M., Croguennec, T., Burgain, J., Fournaise, T., Gaiani, C., Scher, J., Petit, J., Martins, E., Rodrigues, R.C., Schuck, P., Perrone, Í.T., Machado, S.G., Carvalho, A.F. de, Roos, Y.H., Roos, Y.H., 2020. Powder properties and influencing factors, in: *Drying in the Dairy Industry*. CRC Press.
- Roques-Carmes, T., Babak, V., Mathieu, V., Gigante, A., 2013. Influence of Drop Volume and Surfactant Concentration on the Marangoni Flow and Contact Line Instabilities during the Spreading of Surfactant Solutions on Hydrophilic Surface. *Journal of Dispersion Science and Technology* 34, 1053–1066. <https://doi.org/10.1080/01932691.2012.735947>
- Rosenberg, M., Kopelman, I.J., Talmon, Y., 1985. A Scanning Electron Microscopy Study of Microencapsulation. *Journal of Food Science* 50, 139–144. <https://doi.org/10.1111/j.1365-2621.1985.tb13295.x>
- Rydhag, L., Wilton, I., 1981. The function of phospholipids of soybean lecithin in emulsions. *J Am Oil Chem Soc* 58, 830–837. <https://doi.org/10.1007/BF02665591>
- Salameh, C., Scher, J., Petit, J., Gaiani, C., Hosri, C., Banon, S., 2016. Physico-chemical and rheological properties of Lebanese kishk powder, a dried fermented milk-cereal mixture. *Powder Technology* 292, 307–313. <https://doi.org/10.1016/j.powtec.2016.01.040>
- Salehi, F., Aghajanzadeh, S., 2020. Effect of dried fruits and vegetables powder on cakes quality: A review. *Trends in Food Science & Technology* 95, 162–172. <https://doi.org/10.1016/j.tifs.2019.11.011>
- Santos, D., Maurício, A.C., Sencadas, V., Santos, J.D., Fernandes, M.H., Gomes, P.S., 2017. *Spray Drying: An Overview, Biomaterials - Physics and Chemistry - New Edition*. IntechOpen. <https://doi.org/10.5772/intechopen.72247>
- Sauer, D., Cerea, M., DiNunzio, J., McGinity, J., 2013. Dry powder coating of pharmaceuticals: A review. *International Journal of Pharmaceutics, Progress in Film Coating* 457, 488–502. <https://doi.org/10.1016/j.ijpharm.2013.02.032>
- Scheidegger, D., Radici, P.M., Vergara-Roig, V.A., Bosio, N.S., Pesce, S.F., Pecora, R.P., Romano, J.C.P., Kivatinitz, S.C., 2013. Evaluation of milk powder quality by protein oxidative modifications. *J. Dairy Sci.* 96, 3414–3423. <https://doi.org/10.3168/jds.2012-5774>

- Schober, C., Fitzpatrick, J.J., 2005. Effect of vortex formation on powder sinkability for reconstituting milk powders in water to high solids content in a stirred-tank. *Journal of Food Engineering* 71, 1–8. <https://doi.org/10.1016/j.jfoodeng.2004.09.027>
- Scholfield, C.R., 1981. Composition of soybean lecithin. *Journal of the American Oil Chemists' Society* 58, 889–892. <https://doi.org/10.1007/BF02659652>
- Schuck, P., Jeantet, R., Dolivet, A., 2012. *Analytical Methods for Food and Dairy Powders*. John Wiley & Sons.
- Sharma, A., Jana, A.H., Chavan, R.S., 2012. Functionality of Milk Powders and Milk-Based Powders for End Use Applications—A Review. *Comprehensive Reviews in Food Science and Food Safety* 11, 518–528. <https://doi.org/10.1111/j.1541-4337.2012.00199.x>
- Shein, E.V., Milanovskii, E.Yu., Molov, A.Z., 2006. The effect of organic matter on the difference between particle-size distribution data obtained by the sedimentometric and laser diffraction methods. *Eurasian Soil Sc.* 39, S84–S90. <https://doi.org/10.1134/S106422930613014X>
- Shetty, A.K., Shivani, S., 2020. Quantitative assessment of enamel remineralization after treatment with chicken eggshell powder: A scanning electron microscope (SEM) and energy-dispersive x-ray spectroscopy (EDX) study. *AIP Conference Proceedings* 2274, 050008. <https://doi.org/10.1063/5.0022513>
- Shi, C., He, Y., Ding, M., Wang, Y., Zhong, J., 2019. Nanoimaging of food proteins by atomic force microscopy. Part II: Application for food proteins from different sources. *Trends in Food Science & Technology, Application of Atomic Force Microscopy in Food Science* 87, 14–25. <https://doi.org/10.1016/j.tifs.2018.11.027>
- Shrestha, A.K., Howes, T., Adhikari, B.P., Wood, B.J., Bhandari, B.R., 2007a. Effect of protein concentration on the surface composition, water sorption and glass transition temperature of spray-dried skim milk powders. *Food Chemistry* 104, 1436–1444. <https://doi.org/10.1016/j.foodchem.2007.02.015>
- Shrestha, A.K., Ua-arak, T., Adhikari, B.P., Howes, T., Bhandari, B.R., 2007b. Glass Transition Behavior of Spray Dried Orange Juice Powder Measured by Differential Scanning Calorimetry (DSC) and Thermal Mechanical Compression Test (TMCT). *International Journal of Food Properties* 10, 661–673. <https://doi.org/10.1080/10942910601109218>
- Siepmann, J., Peppas, N.A., 2001. Modeling of drug release from delivery systems based on hydroxypropyl methylcellulose (HPMC). *Advanced Drug Delivery Reviews* 48, 139–157. <https://doi.org/10.1016/j.addr.2012.09.028>

- Sikand, V., Tong, P.S., Walker, J., 2013. Effect of adding salt during the diafiltration step of milk protein concentrate powder manufacture on mineral and soluble protein composition. *Dairy Sci. & Technol.* 93, 401–413. <https://doi.org/10.1007/s13594-013-0110-0>
- Silva, G., Rouau, X., Guilbert, S., 2011. Successive centrifugal grinding and sieving of wheat straw. *Powder Technology, Special Issue: Papers presented to the Symposium STPMF 2009, Science and Technology of Powders and Sintered Materials* 208, 266–270. <https://doi.org/10.1016/j.powtec.2010.08.015>
- Silva, J.V.C., O'Mahony, J.A., 2017. Flowability and wetting behaviour of milk protein ingredients as influenced by powder composition, particle size and microstructure. *International Journal of Dairy Technology* 70, 277–286. <https://doi.org/10.1111/1471-0307.12368>
- Simperler, A., Kornherr, A., Chopra, R., Bonnet, P.A., Jones, W., Motherwell, W.D.S., Zifferer, G., 2006. Glass Transition Temperature of Glucose, Sucrose, and Trehalose: An Experimental and in Silico Study. *J. Phys. Chem. B* 110, 19678–19684. <https://doi.org/10.1021/jp063134t>
- Sing, K.S.W., Williams, R.T., 2012. Historical aspects of capillarity and capillary condensation. *Microporous and Mesoporous Materials, Special Issue: Characterisation of Porous Solids IX* 154, 16–18. <https://doi.org/10.1016/j.micromeso.2011.09.022>
- Snow, R., Allen, T., Ennis, B., Litster, J., 1999. Size reduction and size enlargement, in: *Chemical Engineering Handbook*. pp. 20–89.
- Stancovski, V., Badilescu, S., 2014. In situ Raman spectroscopic–electrochemical studies of lithium-ion battery materials: a historical overview. *J Appl Electrochem* 44, 23–43. <https://doi.org/10.1007/s10800-013-0628-0>
- Stocco, G., Cipolat-Gotet, C., Cecchinato, A., Calamari, L., Bittante, G., 2015. Milk skimming, heating, acidification, lysozyme, and rennet affect the pattern, repeatability, and predictability of milk coagulation properties and of curd-firming model parameters: A case study of Grana Padano. *Journal of Dairy Science* 98, 5052–5067. <https://doi.org/10.3168/jds.2014-9146>
- Stokes, D.J., Thiel, B.L., Donald, A.M., 1998. Direct Observation of Water–Oil Emulsion Systems in the Liquid State by Environmental Scanning Electron Microscopy. *Langmuir* 14, 4402–4408. <https://doi.org/10.1021/la980281c>

- Sumner, J.B., Graham, V.A., 1922. Dinitrosalicylic acid as a reagent for blood sugar. *Proceedings of the Society for Experimental Biology and Medicine* 20, 96–96. <https://doi.org/10.3181/00379727-20-47>
- Sun, Y., Cai, Z., Fu, J., 2019. Particle morphomics by high-throughput dynamic image analysis. *Sci Rep* 9, 9591. <https://doi.org/10.1038/s41598-019-46062-6>
- Sweijen, T., Chareyre, B., Hassanzadeh, S.M., Karadimitriou, N.K., 2017. Grain-scale modelling of swelling granular materials; application to super absorbent polymers. *Powder Technology* 318, 411–422. <https://doi.org/10.1016/j.powtec.2017.06.015>
- Szakonyi, G., Zelkó, R., 2012. The effect of water on the solid state characteristics of pharmaceutical excipients: Molecular mechanisms, measurement techniques, and quality aspects of final dosage form. *Int J Pharm Investig* 2, 18–25. <https://doi.org/10.4103/2230-973X.96922>
- Szulc, K., Lenart, A., 2013. Surface modification of dairy powders: Effects of fluid-bed agglomeration and coating. *International Dairy Journal* 33, 55–61. <https://doi.org/10.1016/j.idairyj.2013.05.021>
- Taisne, L., 1997. Echanges d'huile entre gouttes d'emulsion (These de doctorat). Paris 6.
- Teunou, E., Fitzpatrick, J.J., 1999. Effect of relative humidity and temperature on food powder flowability. *Journal of Food Engineering* 42, 109–116. [https://doi.org/10.1016/S0260-8774\(99\)00087-4](https://doi.org/10.1016/S0260-8774(99)00087-4)
- Thierry, V., Denis, P., Pascale, S.-P., 2007. *Microencapsulation : des sciences aux technologies*. Lavoisier.
- Tita-Goldstein, A., 2013. *Mise en forme des poudres par compression: influence du procédé et de la formulation pour la maîtrise des propriétés d'usage*.
- Torres-Martinez, J.L., Mújica-Paz, H., Valdez-Fragoso, A., Ortega-Rivas, E., 2007. Coating of Puffed Wheat by a Tumbling Method a Fluidized Bed Technique. *Food Science and Technology* 25, 549–554. <https://doi.org/10.1080/02726350701492819>
- Turchiuli, C., Smail, R., Dumoulin, E., 2013. Fluidized bed agglomeration of skim milk powder: Analysis of sampling for the follow-up of agglomerate growth. *Powder Technology, Special Issue: 5th International Granulation Workshop Granulation across the length scale 2011* 238, 161–168. <https://doi.org/10.1016/j.powtec.2012.02.030>
- Van Huffel, S., Vandevallé, J., 1991. *The total least squares problem: computational aspects and analysis*, SIAM. ed. Philadelphia.

- Van Nieuwenhuyzen, W., 1976. Lecithin production and properties. *J Am Oil Chem Soc* 53, 425–427. <https://doi.org/10.1007/BF02605737>
- Vignolles, M.-L., Jeantet, R., Lopez, C., Schuck, P., 2007. Free fat, surface fat and dairy powders: interactions between process and product. A review. *Lait* 87, 187–236. <https://doi.org/10.1051/lait:2007010>
- Waghmare, R., 2020. Encapsulation Techniques For Delivery Of Bioactive Compounds In Milk And Dairy Products- A Review. *Journal of Dairy Research & Technology* 3, 1–9. <https://doi.org/10.24966/DRT-9315/100017>
- Waiss, I.M., Kimbonguila, A., Abdoul-Latif, F.M., Nkeletela, L.B., Matos, L., Scher, J., Petit, J., 2020. Effect of milling and sieving processes on the physicochemical properties of okra seed powders. *International Journal of Food Science & Technology*. <https://doi.org/10.1111/ijfs.14503>
- Wallack, D.A., King, C.J., 1988. Sticking and agglomeration of hygroscopic, amorphous carbohydrate and food powders. *Biotechnology progress (USA)*.
- Wan, L.S.C., Heng, P.W.S., Chia, C.G.H., 1992. Spray Drying as a Process for Microencapsulation and the Effect of Different Coating Polymers. *Drug Development and Industrial Pharmacy* 18, 997–1011. <https://doi.org/10.3109/03639049209069311>
- Wang, H., Liu, Y., Chen, L., Li, X., Wang, J., Xie, F., 2018. Insights into the multi-scale structure and digestibility of heat-moisture treated rice starch. *Food Chemistry* 242, 323–329. <https://doi.org/10.1016/j.foodchem.2017.09.014>
- Wang, J., Flanagan, D.R., 2002. General solution for diffusion-controlled dissolution of spherical particles. 2. Evaluation of experimental data. *Journal of Pharmaceutical Sciences* 91, 534–542. <https://doi.org/10.1002/jps.10039>
- Wang, J., Flanagan, D.R., 1999. General solution for diffusion-controlled dissolution of spherical particles. 1. Theory. *Journal of Pharmaceutical Sciences* 88, 731–738. <https://doi.org/10.1021/js980236p>
- Weaire, D., Phelan, R., 1996. The physics of foam. *J. Phys.: Condens. Matter* 8, 9519–9524. <https://doi.org/10.1088/0953-8984/8/47/055>
- Wee, J.J.Y., Chan, R.X., Seow, Y.-X., Viton, F., Zhou, W., 2020. Influence of sucrose reduction on powder and reconstitution properties of powdered cocoa malted beverage. *Powder Technology* 360, 221–230. <https://doi.org/10.1016/j.powtec.2019.09.051>
- Wendel, A., 2000. Lecithin, in: *Kirk-Othmer Encyclopedia of Chemical Technology*. John Wiley & Sons, Ltd. <https://doi.org/10.1002/0471238961.1205030923051404.a01>

- Werner, I., 1952. The identification of small amounts of sugars by means of X-ray diffraction patterns. *Mikrochim Acta* 39, 133–146. <https://doi.org/10.1007/BF01425011>
- Windhab, E.J., 1999. New Developments in Crystallization Processing. *Journal of Thermal Analysis and Calorimetry* 57, 171–180. <https://doi.org/10.1023/A:1010103105425>
- Witt, W., Köhler, U., List, J., 2007. CURRENT LIMITS OF PARTICLE SIZE AND SHAPE ANALYSIS WITH HIGH SPEED IMAGE ANALYSIS.
- Wold, S., Trygg, J., Berglund, A., Antti, H., 2001. Some recent developments in PLS modeling. *Chemometrics and Intelligent Laboratory Systems, PLS Methods* 58, 131–150. [https://doi.org/10.1016/S0169-7439\(01\)00156-3](https://doi.org/10.1016/S0169-7439(01)00156-3)
- Woodbury, K.A. (Ed.), 2002. *Inverse Engineering Handbook*. CRC Press, Boca Raton. <https://doi.org/10.1201/9781420041613>
- Wyszynski, M.L., Bridgwater, J., 1993. The effect of solid lubricants on powder attrition and breakage. *Tribology International* 26, 311–317. [https://doi.org/10.1016/0301-679X\(93\)90067-B](https://doi.org/10.1016/0301-679X(93)90067-B)
- Young, T., 1805. III. An essay on the cohesion of fluids. *Philosophical Transactions of the Royal Society of London* 95, 65–87. <https://doi.org/10.1098/rstl.1805.0005>
- Yousefi, S., Emam-Djomeh, Z., Mousavi, S.M., 2011. Effect of carrier type and spray drying on the physicochemical properties of powdered and reconstituted pomegranate juice (*Punica Granatum L.*). *J Food Sci Technol* 48, 677–684. <https://doi.org/10.1007/s13197-010-0195-x>
- Yu, W., Hancock, B.C., 2008. Evaluation of dynamic image analysis for characterizing pharmaceutical excipient particles. *International Journal of Pharmaceutics* 361, 150–157. <https://doi.org/10.1016/j.ijpharm.2008.05.025>
- Yu, W., Muteki, K., Zhang, L., Kim, G., 2011. Prediction of Bulk Powder Flow Performance Using Comprehensive Particle Size and Particle Shape Distributions. *Journal of Pharmaceutical Sciences* 100, 284–293. <https://doi.org/10.1002/jps.22254>
- Yuan, C., Xu, D., Cui, B., Wang, Y., 2019. Gelation of κ -carrageenan/Konjac glucomannan compound gel: Effect of cyclodextrins. *Food Hydrocolloids* 87, 158–164. <https://doi.org/10.1016/j.foodhyd.2018.07.037>
- Zaiter, A., Becker, L., Petit, J., Zimmer, D., Karam, M.-C., Baudelaire, É., Scher, J., Dicko, A., 2016. Antioxidant and antiacetylcholinesterase activities of different granulometric classes of *Salix alba* (L.) bark powders. *Powder Technology* 301, 649–656. <https://doi.org/10.1016/j.powtec.2016.07.014>

- Zheng, H., Lu, H., 2011. Use of kinetic, Weibull and PLSR models to predict the retention of ascorbic acid, total phenols and antioxidant activity during storage of pasteurized pineapple juice. *LWT - Food Science and Technology* 44, 1273–1281. <https://doi.org/10.1016/j.lwt.2010.12.023>
- Zhou, Q., Armstrong, B., Larson, I., Stewart, P.J., Morton, D.A.V., 2010. Effect of host particle size on the modification of powder flow behaviours for lactose monohydrate following dry coating. *Dairy Sci. Technol.* 90, 237–251. <https://doi.org/10.1051/dst/2009046>